Inflammation and mechanical loading in osteoarthritis: An integrative multi-scale approach

Juntong Lai

A thesis submitted in partial fulfilment of the requirements for the degree of *Doctor of Philosophy*

The University of Sheffield
Faculty of Engineering
School of Mechanical, Aerospace and Civil Engineering

Submission Date
February 2026

Cogito, ergo sum

— René Descartes

Declaration

I, the author, confirm that the Thesis is my own work. I am aware of the University's Guidance on the Use of Unfair Means (www.sheffield.ac.uk/ssid/unfair-means). This work has not been previously presented for an award at this, or any other, university.

Publications

- **J. Lai**, J. Tomlinson, L. Breakwell, and D. Lacroix, "A finite element study of the effect of cross-link stabilisation in a lumbar spine tumour model", Proc Inst Mech Eng H, p. 09544119251348279, Jul. 2025, doi: 10.1177/09544119251348279.
- **J. Lai** and D. Lacroix, "Mathematical modelling of inflammatory process and obesity in osteoarthritis", PLOS ONE, vol. 20, no. 6, p. e0323258, Jun. 2025, doi: 10.1371/journal.pone.0323258.
- **J. Lai** and D. Lacroix, "A computational study of adiposity-associated factors in the inflammatory process of osteoarthritis", Journal of Theoretical Biology, vol. 625, p. 112429, May 2026, doi: 10.1016/j.jtbi.2026.112429.
- **J. Lai** and D. Lacroix, "A novel integrative multi-scale framework of inflammation and mechanical loading in knee osteoarthritis", Biomechanics and Modeling in Mechanobiology, Apr. 2026, doi: 10.1007/s10237-026-02072-8.
- **J. Lai** and D. Lacroix, "Subject-specific multi-scale modelling of obesity-driven cartilage degeneration in knee osteoarthritis", In preparation.

Featured conference abstracts

- **J. Lai** and D. Lacroix, "Development of an integrative multi-scale framework of knee osteoarthritis in inflammation and mechanics," Oral abstract, 30th Congress of the European Society of Biomechanics (ESB), Zürich, Switzerland, 2025.
- **J. Lai** and D. Lacroix, "A computational study of the effects of obesity on the inflammatory process in osteoarthritis," Poster abstract, British Orthopaedic Research Society (BORS) Meeting 2024, Sheffield, UK, 2024.
- **J. Lai** and D. Lacroix, "Development of a computational inflammation model of osteoarthritis including obesity," Oral abstract, Virtual Physiological Human (VPH) Conference 2024, Stuttgart, Germany, 2024.
- **J. Lai** and D. Lacroix, "Mathematical modelling of inflammatory process and obesity in osteoarthritis," Oral abstract, 29th Congress of the European Society of Biomechanics (ESB), Edinburgh, UK, 2024.
- **J. Lai** and D. Lacroix, "Mathematical modelling of the inflammation process in osteoarthritis," Poster abstract, 70th Orthopaedic Research Society (ORS) Annual Meeting, California, USA, 2024.
- **J. Lai** and D. Lacroix, "A finite element study of the effect of cross-link stabilisation in a lumbar spine tumour model," Oral abstract, 35th SIMULIA EuroNorth Regional User Meeting, Manchester, UK, 2022.

Abstract

There are approximately 350 thousand new cases of osteoarthritis (OA) diagnosed annually in the UK. To date, there is a lack of criteria for early OA identification and for the prescription of disease-modifying osteoarthritis drugs (DMOADs), due to the limited understanding of OA phenotypes and endotypes. This directly affects over 600 million OA patients worldwide, with a higher risk of developing disability among ageing and obese individuals. Emerging research in computational approaches attempted to unravel OA mechanisms driven by both systemic and local factors. However, few computational tools have incorporated both inflammatory and mechanical regulations of obesity in OA. The overall aim of this thesis was to investigate the mechanobiological effects of obesity on OA by developing a novel multi-scale computational approach that integrates obesity-associated inflammation and mechanical loading in OA. A mathematical model of inflammation and obesity in OA was for the first time established and parameterised. The dynamics of inflammatory activities regulated by adipokines was numerically analysed, and the roles of tissue injury, body mass index (BMI) and physical activity level (PAL) in OA inflammation were examined. Based on this novel mathematical model, an integrative multi-scale modelling framework was developed for simulating subject-specific cartilage degeneration in obesity-associated OA. Parameter sensitivity analysis and simulations of cartilage degeneration demonstrated the common and subject-specific variations in degeneration patterns regulated by the mechanobiological effects of obesity. The integrative multi-scale approach developed in this thesis identified critical parameters that could contribute to discovering therapeutic targets in obesity-associated OA phenotypes and endotypes. In addition, it is a potential computational tool that can be individualised to assess the subject-specific heterogeneity of OA and predict cartilage degeneration in the context of obesity.

Acknowledgements

First and foremost, I express my deepest and most sincere gratitude to my primary supervisor, Professor Damien Lacroix, whose intellectual rigour, patience, and unwavering support have shaped not only this research but also the way I think as a researcher. I could never complete the exciting milestones during my PhD without his supportive supervision. His supervision extends far beyond technical discussions and always gives me encouragement. I am inspired a lot by my primary supervisor on pursuing my career in the wide field of in silico medicine.

Also, I would like to thank the time and efforts that my viva panel dedicates to the insightful discussions on my PhD research.

I would like to thank all of the members in my research group, both those who have moved on and those still in the group, Integrated Musculo-Skeletal Biomechanics Research (IMSB) Group, where I have been offered with a supportive academic environment. Their collaborations and willingness to share their knowledge have been invaluable. In particular, I am grateful that Dr Pinaki Bhattacharya has been my second supervisor, and I appreciate the insightful advice from him on thinking about both my Doctoral Development Plan (DDP) and career when I started my PhD journey. I would also like to thank Professor Claire Brockett, Professor Gwendolen Reilly and Dr Vee San Cheong for their kind and insightful conversations, which greatly inspired and encouraged me. I appreciate Professor Enrico Dall'Ara for his handwritten notes that helped me reflect on my presentations and for chairing USFD Digital Twin in Healthcare Network meetings (DT4HT), I greatly enjoyed the enthusiastic discussions I had within this network.

In addition, I am profoundly thankful to those excellent researchers whom I have met at conferences, Insigneo Institute and Virtual Physiological Human Institute (VPHi). Their knowledge, generosity, and intellectual exchange have greatly influenced my growth. Particularly,

I want to thank Insigneo Early Career Researcher (ECR) Committee and VPHi Young Scientist Committee (YSC) for supporting ECRs with a focus on networking and career development opportunities. As a member of both Insigneo ECR committee and VPHi YSC, I deeply appreciate the inclusive environment, mentorship, and collaborative spirit that these communities foster, which have enriched both my professional and personal development.

I am grateful for all generous supports in the University of Sheffield throughout my PhD period. The completion of this milestone would not have been possible without those supports. Particularly, I acknowledge IT Services at The University of Sheffield for the provision of services for High Performance Computing. Additionally, I would like to express my gratitude to Professor Shuisheng He for his encouragement and general advice at the start of my PhD journey, and to Dr Cassandra Terry for her invaluable mentoring through the Career Mentoring Programme.

I would like to thank my university studentship from UKRI EPSRC (grant number: EP/W524360/1/2747654) that has made my PhD thesis possible and thank Professor Damien Lacroix again for being my primary supervisor with this studentship. Also, I appreciate the Postgraduate Research Student Publication Scholarship for supporting my potential publications from this thesis.

Last but not least, I want to say thank you to my family and my life long partner, my wife, Ziyou Fang (I shall also refer her as Dr Fang). Her conversations, our long walks, warm hugs and our philosophical discussions have been a profound spiritual support throughout these days, and I know they will remain so for the rest of my life.

Again, I thank everyone, named and unnamed, who contributed to this journey in ways big and small. Every conversation, suggestion, challenge, and act of kindness helped shape this work and the person I have become.

"A splendid day is only once; and the morning in a day never comes again"

To my past and future

Contents

Declaration ii

Abstract iv

Acknowledgements v

List of Tables xi

List of Figures xiii

Nomenclature xxiv

1 Introduction 1

1.1 Research background 1

1.2 Aim and objectives 3

1.3 Thesis outline 4

2 Literature review 6

2.1 Anatomy of the knee joint 6

2.1.1 Articular cartilage 7

2.1.2 Subchondral bone 8

2.1.3 Infrapatellar fat pad 8

2.1.4 Meniscus 10

2.1.5 Ligaments 10

2.2 Pathological changes of articular cartilage and subchondral bone . . 10

2.2.1 Degeneration of articular cartilage 12

2.2.2 Grading assessment of OA severity 12

2.2.3 Degeneration of subchondral bone 13

2.3 The mechanism of inflammation in molecular and cellular levels . . . 16

2.3.1 Inflammatory cytokines 19

2.3.2 Adipokines 19
2.3.3 Matrix metalloproteinases (MMPs) 20
2.4 Mathematical modelling of inflammation in OA 24
2.4.1 ODE-based model 25
2.4.2 PDE-based model 31
2.4.3 Agent-based model 32
2.4.4 Data-driven modelling strategy in OA 33
2.5 Finite element modelling of the knee joint in OA 33
2.6 Effects of obesity on the joint biomechanics in knee OA 35
2.7 Multi-scale modelling of the cartilage degeneration in knee OA 37

3 Mathematical modelling of inflammatory process and obesity in osteoarthritis 42
3.1 Introduction 43
3.2 Methods 46
3.2.1 Regulatory network of inflammation 46
3.2.2 Enzyme kinetics 46
3.2.3 Mathematical formulation 47
3.2.4 Model nondimensionalisation and parameter estimation . . . 50
3.2.5 Sensitivity analysis 51
3.2.6 Simulation of inflammatory activities 53
3.3 Results 55
3.3.1 Model verification 55
3.3.2 Dynamics of the adipokine-mediated inflammation model . . 57
3.3.3 Evolution of inflammatory activities 62
3.4 Discussion 65
3.5 Conclusion 68
Appendix A: The formula of parameter nondimensionalisation 70
Appendix B: The description of dimensional parameters in the adipokine-mediated inflammation model in OA 71
Appendix C: The simultaneous equations when production rates are at equilibrium for the calculation of fixed points 73
Appendix D: Phase plane and bifurcation diagrams of the inflammation system 74

4 A computational study of adiposity-associated factors in the inflammatory process of osteoarthritis 79
4.1 Introduction . . . 80
4.2 Methods . . . 82
4.2.1 Governing equations . . . 82
4.2.2 Parameterisation . . . 85
4.2.3 Sensitivity analysis of inflammation and obesity . . . 90
4.2.4 Computational configurations of the inflammatory process . . . 91
4.3 Results . . . 92
4.3.1 Parameter sensitivity . . . 92
4.3.2 Effects of physical activity intervention . . . 95
4.3.3 Window period of physical activity intervention . . . 101
4.4 Discussion . . . 102
4.5 Conclusion . . . 106
Appendix E: Bifurcation diagram . . . 108
Appendix F: Simulations of OA inflammation with physical activity intervention and sensitivity of window period . . . 109

5 A novel integrative multi-scale framework of inflammation and mechanical loading in knee osteoarthritis 111
5.1 Introduction . . . 112
5.2 Materials and methods . . . 114
5.2.1 Finite element modelling strategy . . . 114
5.2.2 The multi-scale algorithm of cartilage degeneration . . . 116
5.2.3 Integrative multi-scale computational framework . . . 118
5.2.4 Computational analysis of cartilage degeneration . . . 119
5.3 Results . . . 122
5.3.1 Sensitivity of mechanical damage accumulation and boundary of cartilage integrity . . . 122
5.3.2 Sensitivity of the stress threshold leading to cartilage damage and degeneration . . . 123
5.3.3 Effects of obesity-associated inflammation and mechanics during cartilage degeneration . . . 127
5.4 Discussion . . . 131
5.5 Conclusion . . . 136

Appendix G: Sensitivity analysis of material properties and time increment for the knee joint (LTKN8941) . . . 137
Appendix H: The parameterisation of the obesity-associated inflammation model . . . 139

6 Subject-specific multi-scale modelling of obesity-driven cartilage degeneration in knee osteoarthritis 141
6.1 Introduction . . . 142
6.2 Materials and methods . . . 143
6.2.1 Subject-specific tibiofemoral joints . . . 143
6.2.2 Modification of finite element models . . . 145
6.2.3 Computational algorithm of cartilage degeneration . . . 146
6.2.4 Quantification of variations in cartilage degeneration . . . 148
6.3 Results . . . 149
6.3.1 Mechanical responses of three subjects in degeneration . . . 149
6.3.2 Comparison of obesity-dependent mechanical distributions in subject-specific joints . . . 150
6.3.3 Effects of obesity on the cartilage degeneration of three subject-specific knee joints . . . 154
6.4 Discussion . . . 159
6.5 Conclusion . . . 162
Appendix I: Sensitivity analysis of material properties for the knee joints (LTKN1468 and RTKN0668) . . . 163
Appendix J: Simulations of biomechanical responses in cartilage degeneration . . . 165

7 Discussion and conclusions 172
7.1 General discussion . . . 172
7.2 Limitations and future work . . . 176
7.3 Conclusion . . . 179

References 181

List of Tables

2.1 Inflammatory mediators and molecules in the course of OA, summarised from [83, 87, 89, 91, 92, 97-102, 104]. Interleukin (IL); Tumour necrosis factor (TNF); Inducible nitric oxide synthase (iNOS); Prostaglandin E (PGE); Cyclooxygenase (COX); Fibroblast-like synoviocytes (FLS); Vascular endothelial growth factor (VEGF); Phospholipase A2 (PLA2). 21
2.2 ODE-based models of different inflammation systems. 30
2.3 PDE-based and multi-scale models of OA. Reactive oxygen species (ROS); Erythropoietin (EPO); Erythropoietin receptor (EPOR). 32

3.1 The classification of the obesity level using BMI [39]. 49
3.2 The category of PAL [212]. 49
3.3 The estimated dimensionless parameters of the inflammation model. 51
3.4 The types of dynamics presented in bifurcations. 57

4.1 Descriptions of the estimated parameters in the production of PICs. 87
4.2 Descriptions of the estimated parameters in the production of AICs. 87
4.3 Descriptions of the estimated parameters in the production of MMPs. 88
4.4 Descriptions of the estimated parameters in the production of adipokines. 88
4.5 Descriptions of the estimated parameters in the production of Fn-fs. 89
4.6 The categories and ranges of BMI and PAL. 91
4.7 The system states resulting from physical activity intervention when varying the mechanical damage level, BMI and PAL. 101

5.1 The baseline parameters of tissue material in the FE model. 115
5.2 The parameters implemented in the multi-scale algorithm of cartilage degeneration 119

5.3 States of degenerative process over the accumulation of mechanical damage. 122

6.1 Material properties of the subject-specific FE models. 145
6.2 Parameters implemented to the multi-scale modelling framework of cartilage degeneration. 148
6.3 WRMSE quantification of differences between the frequency distributions of maximum principal stress. 154
6.4 WRMSE quantification of differences between the frequency distributions of minimum principal stress. 154

List of Figures

2.1 Schematic knee joint, modified from Betts et al. [48] under CC BY-NC-SA 4.0. Access for free at openstax.org. (a): Sagittal section; (b): Superior plane; (c) Anterior view. 7

2.2 Schematic representation of articular cartilage, reused from Oliveira et al. [51] under CC BY 4.0. 8

2.3 The geometry of subchondral bone, modified from Yamada et al. [53] with permission. 9

2.4 The effects of IFP on the inflammation of OA, modified from Zhou et al. [57] under CC BY 4.0. Immune cells leak into IFP from vessels. The mutual activation between immune cells and adipocytes upregulates the pro-inflammatory and catabolic molecules. Adipokines secreted from adipocytes also activate the production of inflammatory molecules but may have both catabolic and anabolic effects on cartilage. The increase of inflammation due to immune cells and adipocytes results in the progressive degradation of cartilage, though mesenchymal stromal cells (MSCs) from IFP and synovium are signalled to compensate the damage of cartilage. 9

2.5 The pathological variations of the knee joint in OA, modified from Glyn-Jones et al. [7] and Robinson et al. [16] with permissions. 11

2.6 The evolution of cartilage degenerative changes in OA. 13

2.7 The histology grading of cartilage in OA, reused from Palmer et al. [71] with permission. 14

2.8 The evolution of subchondral bone degenerative changes in OA. . . . 15

2.9 The local inflammatory mechanism in the knee OA progression, modified from Robinson et al. [16] and Sokolove et al. [83] with permissions. Due to the trauma or overuse of the knee joint, damage occurs and induces the production of DAMPs. DAMPs instruct cells, such as macrophages and chondrocytes, to secret a variety of inflammatory mediators. Similarly, inflammation-induced vascular leak can also signal cells to increase inflammation within the knee joint. The interactive cycle of chronic inflammation, tissue damage and tissue repair induces massive proteolytic enzymes so that the joint degeneration is progressively aggravated. 18
2.10 A mechanistic modelling framework of inflammation, reproduced from Scheff, Kamisoglu and Androulakis [113] with permission. 25
2.11 The schematic depiction of mathematical alternatives used in mechanistic models, reused from Eftimie et al. [130] under CC BY 4.0. . . . 26
2.12 The workflow of FE model development. 34
2.13 The schematic multi-scale modelling framework of cartilage degeneration, reused from Halloran et al. [172] with permission. 39

3.1 Schematic inflammatory network of cartilage including the concentrations of PICs, AICs, MMPs, adipokines and Fn-fs. Adipokines stimulate the production of PICs and MMPs as a source mediator of which concentration is regulated by adiposity. Adiposity can be varied by the system status including PAL, BMI and nutrition. Each mediator group has a rate of natural decay and the rate of production consists of the production from background, stimuli and inhibitors. Since Fn-fs are only released due to the deconstruction of tissue, the production is determined by mechanical damage and the catabolism of MMPs. Although other damaging products exist, Fn-fs are included in the network as a group of inflammatory mediators that directly regulate cytokine production. 46

3.2 The sensitivity of (a) nex and (b) θ_{A_d} to the adipokine concentration at equilibrium. nex is numerically correlated to obesity level so it measures the sensitivity of adipokine reduction due to different PALs at a certain level of obesity (EO: Extreme obesity; O: Obesity; OW: Overweight; NW: Normal weight; ND: Nutritional deficiency). θ_{A_d} is the dimensionless coefficient that determines the amount of adipokine reduction due to PAL (S: Sedentary; LA: Low active; A: Active; VA: Very active). 54
3.3 The equilibrium adipokine concentration against PAL and BMI. 54
3.4 The boxplots of the LSA for dimensionless parameters in (a) Baker's model [119] and (b) the adipokine-mediated inflammation model. The values of datasets represent the percentages of change in the measured responses from the system outputs perturbed by 1 percent change of a specified parameter at the inflamed limit cycle and the healthy state. Parameters that result in output changes over 1 percent are highlighted in blue for (a) and in red for (b). P_{bp}: The background production rate of PICs; P_{pp}: The production rate of PICs driven by PICs; P_{fp}: The production rate of PICs driven by Fn-fs; A_{pp}: The production rate of AICs driven by PICs; A_{ph}: The concentration of AICs at which the production rate of AICs driven by PICs is half of the maximum; A_{fp}: The production rate of AICs driven by Fn-fs; A_{fh}: The concentration of AICs at which the production rate of AICs driven by Fn-fs is half of the maximum; M_{bp}: The background production rate of MMPs; M_{pp}: The production rate of MMPs driven by PICs; M_{ph}: The concentration of MMPs at which the production rate of MMPs driven by PICs is half of the maximum; F_{dam}: Mechanical damage parameter; γ_p: Decay rate of PICs; γ_m: Decay rate of MMPs; γ_f: Decay rate of Fn-fs. 56

3.5 Bifurcation diagrams of parameters in the production of PICs and MMPs: (a) Production rate of PICs driven by adipokines; (b) Production rate of MMPs driven by adipokines; (c) Saturation rate in the stimulation of MMPs by adipokines; (d) Saturation rate in the inhibition of MMPs by AICs. Solid black lines where the pro-inflammatory is at a higher level represent the inflamed states; solid black lines where the pro-inflammatory is at a lower level represent the healthy states; dash blue lines represent the unstable states; solid blue lines represent unstable states; The scatter of blue points represents the average maximum and minimum concentration in the oscillated limit cycle. 58
3.6 Bifurcation diagrams of parameters in the production of adipokines: (a) Production rate of adipokines due to the number of adipocytes; (b) Production rate of adipokines due to the size of adipocytes; (c) Decay rate of adipokines. 59
3.7 Bifurcation diagrams of BMI^{meas} where (a) $\mu_{NA_d} = 0.01$, $\mu_{SA_d} = 0.01$; (b) $\mu_{NA_d} = 0.04$, $\mu_{SA_d} = 0.01$, and codimension-2 bifurcations of (c) μ_{NA_d} and BMI^{meas}; (d) μ_{SA_d} and BMI^{meas}. 60
3.8 Bifurcation diagrams of PAL when (a) $BMI^{meas} = 25$; (b) $BMI^{meas} = 35$ in the production of adipokines, and (c) Codimension-2 bifurcation of BMI^{meas} and PAL. 61
3.9 Bifurcation diagrams of $Damage$ under different physical activity interventions when (a) $BMI^{meas} = 25$; (b) $BMI^{meas} = 35$; (c) $BMI^{meas} = 45$ in the adipokine-mediated inflammation model. The dynamics transition is presented when $PAL = 2$ as an example. . . . 62
3.10 The sensitivity of the minimum damage leading to inflammation in the evolution of inflammatory activities. 63
3.11 The evolution of inflammatory activities under different strategies of physical activity intervention in the non-dimensionalised model. . . . 64
D.1 The phase plane of the inflammation system under the baseline parameters: (a) Intersections of nullclines; (b) Trajectories in the phase plane. 74
D.2 The comparison of bifurcation diagrams in the production of PICs between (a) Baker's model and (b) the adipokine-mediated inflammation model. 75

D.3 The comparison of bifurcation diagrams in the production of AICs between (a) Baker's model and (b) the adipokine-mediated inflammation model. 76
D.4 The comparison of bifurcation diagrams in the production of MMPs between (a) Baker's model and (b) the adipokine-mediated inflammation model. 77
D.5 The comparison of bifurcation diagrams in the production of Fn-fs between (a) Baker's model and (b) the adipokine-mediated inflammation model. 78

4.1 The regulatory network of the PICs, AICs, MMPs, adipokines and Fn-fs in OA inflammation. Reproduced from Lai and Lacroix (2025) under CC BY 4.0 [237]. PICs, AICs, MMPs, adipokines and Fn-fs interact to mediate the inflammatory process of OA. Damage is an external source to stimulate the production of Fn-fs due to the tissue injury resulting from mechanics. The production of adipokines is associated with the level of adiposity. PAL, BMI and nutrition are three modifiable system attributes that measure the adiposity level to govern the adipokine production. 83
4.2 The calibration of boundaries for the coefficients governing the decrease of adiposity: (a) nex; (b) C_{20}. The level of BMI includes extreme obesity (EO), obesity (O), overweight (OW), normal weight (NW) and nutritional deficiency (ND). The level of physical activity includes sedentary (S), low active (LA), active (A) and very active (VA). The BMI and PAL ranges are presented in Table 4.6. 90
4.3 The strategies of physical activity intervention in the inflammatory process for four representative cases (NW: Normal weight; OW: Overweight; LO: Low obesity; HO: High obesity). 92
4.4 PRCC analysis of the parameters in the inflammatory process. The correlations between parameters and (a) the level of PICs, (b) the level of AICs, (c) the level of MMPs (d) the level of adipokines, and (e) the level of Fn-fs are measured by PRCC values. The significance of correlation is denoted by (**) when p-value is less than 0.01, and PRCC varies from -1 to 1, implying negative and positive correlations between changes in parameters and mediator level. 94

4.5 The sensitivity of the mechanical damage threshold leading to inflammation: (a) The distribution of damage threshold (C_{22}) when PAL is from sedentary to very active and BMI is from nutritional deficiency to extreme obesity; (b) The representative relation between damage threshold and BMI at different sedentary PALs, where the red line represents the inflammation state without damage ($C_{22} = 0$). . . 96
4.6 Physical activity interventions in the inflammatory process when BMI level is normal weight: (a)– (c) Only before damage; (d) – (f) Only after damage; (g) – (i) Mixed strategy. The durations of physical activity intervention that are highlighted in red signify the transition from a healthy consequence to an inflamed result due to missing a time window after damage. 98
4.7 Physical activity interventions in the inflammatory process when BMI level is overweight: (a)– (c) Only before damage; (d) – (f) Only after damage; (g) – (i) Mixed strategy. The durations of physical activity intervention that are highlighted in red signify the transition from a healthy consequence to an inflamed result due to missing a time window after damage. 99
4.8 Physical activity interventions in the inflammatory process when BMI level is low obesity: (a)– (c) Only before damage; (d) – (f) Only after damage; (g) – (i) Mixed strategy. The durations of physical activity intervention that are highlighted in red signify no transition from a healthy consequence to an inflamed result after damage. 100
4.9 The variations of the window period for effective physical activity interventions in the evolution of the inflammatory process: (a) Sensitivity to the mechanical damage level when BMI = 25 and PAL = 1.5; (b) Sensitivity to the level of BMI when the mechanical damage level = 1.2 and PAL = 1.5; (c) Sensitivity to PAL when the mechanical damage level = 1.2 and BMI = 25. 102
E.1 The bifurcation of the adipokine production parameter (C_{19}) governed by BMI. 108
F.1 Physical activity interventions in the inflammatory process when BMI level is high obesity: (a)– (c) Only before damage; (d) – (f) Only after damage; (g) – (i) Mixed strategy. The durations of physical activity intervention that are highlighted in red signify no transition from a healthy consequence to an inflamed result after damage. 109

F.2 The sensitivity of the window period to the mechanical damage level when (a) BMI = 20 and PAL = 1.5, (b) BMI = 30 and PAL = 1.5, (c) BMI = 25 and PAL = 2, (d) BMI = 30 and PAL = 2. 110

5.1 The integrative multi-scale framework of the knee joint degeneration in mechanics and inflammation. Physical activity level (PAL) is defined by the ratio of total daily energy expenditure (TEE) to basal metabolic rate (BMR) [212], and daily nutrition is measured by the ratio of daily calorie intake to BMR. Controlling the values of the two attributes (PAL and daily nutrition) at 1 represents no physical activity and dietary interventions [237]. 120

5.2 Simulations of cartilage degeneration for three health profiles (low BMI, normal BMI and high BMI). 121

5.3 Sensitivity of r_d and F_{max} to the degenerative process resulted from the accumulation of mechanical damage. 123

5.4 Temporal variations in the percentage of nondegenerative cartilage volume when $S_{threshold} = \{0.1, 0.2, 0.3, 0.4, 0.5\}$ for different BMI levels: (a) low BMI, (b) normal BMI, and (c) high BMI. 125

5.5 The overall degeneration level of the degenerated elements in (a) femoral cartilage, (b) lateral tibial cartilage and (c) medial tibial cartilage when $S_{threshold} = \{0.1, 0.2, 0.3, 0.4, 0.5\}$ for different BMI levels. In the box chart, the median, interquartile range, and whiskers that extend to the minimum and maximum degeneration levels are indicated. 126

5.6 Distribution of mechanical damage level and total degeneration level on the femoral cartilage for a low BMI (a) & (d), a normal BMI (b) & (e), and a high BMI (c) & (f). The damage level leading to 1% degeneration (g) illustrates the relative mechanical and inflammatory contributions to cartilage degeneration. The mechanical damage tends to contribute more with a lower value of this metric compared to inflammation. The width of the KDE curves indicate the density of element distribution. Wider regions correspond to a larger number of cartilage elements, whereas narrower regions represent sparse distributions. 128

5.7 Distribution of mechanical damage level and total degeneration level on the lateral tibial cartilage for a low BMI (a) & (d), a normal BMI (b) & (e), and a high BMI (c) & (f). The damage level leading to 1% degeneration (g) illustrates the relative mechanical and inflammatory contributions to cartilage degeneration. The mechanical damage tends to contribute more with a lower value of this metric compared to inflammation. The width of the KDE curves indicate the density of element distribution. Wider regions correspond to a larger number of cartilage elements, whereas narrower regions represent sparse distributions. 129
5.8 Distribution of mechanical damage level and total degeneration level on the medial tibial cartilage for a low BMI (a) & (d), a normal BMI (b) & (e), and a high BMI (c) & (f). The damage level leading to 1% degeneration (g) illustrates the relative mechanical and inflammatory contributions to cartilage degeneration. The mechanical damage tends to contribute more with a lower value of this metric compared to inflammation. The width of the KDE curves indicate the density of element distribution. Wider regions correspond to a larger number of cartilage elements, whereas narrower regions represent sparse distributions. 130
G.1 The sensitivity analysis of the material properties for the knee joint (LTKN8941). 137
G.2 The sensitivity analysis of the minimum time increment for different BMI levels: (a) low BMI, (b) normal BMI, and (c) high BMI. The simulation was not converged when the minimum time increment was 0.1 month due to a relatively fast degeneration. 138

6.1 Subject-specific profiles of the knee joints, summarised based on the dataset developed by Cooper et al. under CC BY 4.0 [249]. 144
6.2 The multi-scale modelling workflow of cartilage degeneration. 147
6.3 Comparison of variations in maximum principal stress for subject-specific joints during cartilage degeneration. The frequency distributions of maximum principal stress are plotted for (a) - (b) femoral cartilage, (d) - (e) lateral tibial cartilage, (g) - (h) medial tibial cartilage. The corresponding peak values are highlighted in (c), (f) and (i) respectively. 151

6.4 Comparison of variations in minimum principal stress for subject-specific joints during cartilage degeneration. The frequency distributions of minimum principal stress are plotted for (a) - (b) femoral cartilage, (d) - (e) lateral tibial cartilage, (g) - (h) medial tibial cartilage. The corresponding peak values are highlighted in (c), (f) and (i) respectively. 152
6.5 Comparison of variations in maximum principal strain for subject-specific joints during cartilage degeneration. The frequency distributions of maximum principal strain are plotted for (a) - (b) femoral cartilage, (d) - (e) lateral tibial cartilage, (g) - (h) medial tibial cartilage. The corresponding peak values are highlighted in (c), (f) and (i) respectively. 153
6.6 Degeneration of the femoral cartilage in the three subject-specific joints with different BMI levels: (a) Box chart of overall degeneration level, (b) Distribution of degeneration level at a low BMI, (c) Distribution of degeneration level at a normal BMI, (d) Distribution of degeneration level at a high BMI. The median and interquartile range are displayed with whiskers that represent the minimum and maximum degeneration levels. 156
6.7 Degeneration of the lateral tibial cartilage in the three subject-specific joints with different BMI levels: (a) Box chart of overall degeneration level, (b) Distribution of degeneration level at a low BMI, (c) Distribution of degeneration level at a normal BMI, (d) Distribution of degeneration level at a high BMI. The median and interquartile range are displayed with whiskers that represent the minimum and maximum degeneration levels. 157
6.8 Degeneration of the medial tibial cartilage in the three subject-specific joints with different BMI levels: (a) Box chart of overall degeneration level, (b) Distribution of degeneration level at a low BMI, (c) Distribution of degeneration level at a normal BMI, (d) Distribution of degeneration level at a high BMI. The median and interquartile range are displayed with whiskers that represent the minimum and maximum degeneration levels. 158
I.1 The sensitivity analysis of the material properties for the knee joint (LTKN1468). 163

I.2 The sensitivity analysis of the material properties for the knee joint (RTKN0668). 164
J.1 Comparison of variations in maximum principal stress for LTKN8941 across different BMI levels during cartilage degeneration. The frequency distributions of maximum principal strain are plotted for (a) - (b) femoral cartilage, (d) - (e) lateral tibial cartilage, (g) - (h) medial tibial cartilage. The corresponding peak values are highlighted in (c), (f) and (i) respectively. 165
J.2 Comparison of variations in minimum principal stress for LTKN8941 across different BMI levels during cartilage degeneration. The frequency distributions of maximum principal strain are plotted for (a) - (b) femoral cartilage, (d) - (e) lateral tibial cartilage, (g) - (h) medial tibial cartilage. The corresponding peak values are highlighted in (c), (f) and (i) respectively. 166
J.3 Comparison of variations in maximum principal stress for LTKN1468 across different BMI levels during cartilage degeneration. The frequency distributions of maximum principal strain are plotted for (a) - (b) femoral cartilage, (d) - (e) lateral tibial cartilage, (g) - (h) medial tibial cartilage. The corresponding peak values are highlighted in (c), (f) and (i) respectively. 167
J.4 Comparison of variations in minimum principal stress for LTKN1468 across different BMI levels during cartilage degeneration. The frequency distributions of maximum principal strain are plotted for (a) - (b) femoral cartilage, (d) - (e) lateral tibial cartilage, (g) - (h) medial tibial cartilage. The corresponding peak values are highlighted in (c), (f) and (i) respectively. 168
J.5 Comparison of variations in maximum principal stress for RTKN0668 across different BMI levels during cartilage degeneration. The frequency distributions of maximum principal strain are plotted for (a) - (b) femoral cartilage, (d) - (e) lateral tibial cartilage, (g) - (h) medial tibial cartilage. The corresponding peak values are highlighted in (c), (f) and (i) respectively. 169

J.6 Comparison of variations in minimum principal stress for RTKN0668 across different BMI levels during cartilage degeneration. The frequency distributions of maximum principal strain are plotted for (a) - (b) femoral cartilage, (d) - (e) lateral tibial cartilage, (g) - (h) medial tibial cartilage. The corresponding peak values are highlighted in (c), (f) and (i) respectively. 170
J.7 Cartilage degeneration level and distribution in LTKN1468 and RTKN0668 after five-year simulations when a flexion of 10° was applied with an axial force of 1058N. 171

Nomenclature

ABM	Agent-based model
ACL	Anterior cruciate ligament
AI	Artificial intelligence
AIC	Anti-inflammatory cytokine
BMI	Body mass index
BMR	Basal metabolic rate
COX	Cyclooxygenase
CT	Computed tomography
DAMPs	Damage-associated molecular patterns
DL	Deep learning
DoF	Degree of freedom
ECM	Extracellular matrix
EPO	Erythropoietin
EPOR	Erythropoietin receptor
FE	Finite Element
FFQs	Food frequency questionnaires
FLS	Fibroblast-like synoviocytes
Fn-fs	Fibronectin fragments
GNP	Gross national product

IFP	Infrapatellar fat pad
IL	Interleukin
iNOS	Inducible nitric oxide synthase
IQR	Interquartile Range
KDE	Kernel density estimate
KL	Kellgren-Lawrence
LCL	Lateral collateral ligament
LDLs	Low density lipoproteins
LSA	Local Sensitivity Analysis
MCL	Medial collateral ligament
ML	Machine learning
MMPs	Matrix metalloproteinases
MRI	Magnetic resonance imaging
MSCs	Mesenchymal stromal cells
OA	Osteoarthritis
OARSI	Osteoarthritis Research Society International
ODE	Ordinary differential equation
PAL	Physical activity level
PCL	Posterior cruciate ligament
PDE	Partial differential equation
PGE	Prostaglandin E
PIC	Pro-inflammatory cytokine
PLA2	Phospholipase A2
PRRs	Pattern-recognition receptors

PTOA	Post-traumatic osteoarthritis
RA	Rheumatoid arthritis
ROS	Reactive oxygen species
TAK1	Transforming growth factor- -activated kinase 1
TEE	Total daily energy expenditure
TNF	Tumour necrosis factor
WRMSE	Weighted root-mean-square error

Chapter 1

Introduction

This chapter introduces the general research background and identifies existing gaps. It also presents the overall aim and objectives of the thesis and concludes with an overview of the thesis structure.

1.1 Research background

Osteoarthritis (OA) is recognised as a serious progressive disease of synovial joints [1] that can lead to disability and comorbidities [2]. It most commonly affects the knees, compared with other joints such as hands, hips, feet, and spine. Approximately 80% of worldwide burden in OA results from the knee disorder [3–5]. By 2020, there were around 600 million reported cases of OA globally [5], and it is estimated that the number of knee OA cases over the age of 45 will reach nearly 8.5 million in UK by 2035 [6].

The primary characteristics of osteoarthritic joints include the progressive degradation of articular cartilage and subchondral bone [7]. Over the last century, the wear and tear of cartilage was regarded as the main pathogenic factor of OA [8]. The appreciation of OA was limited by this oversimplified theory that narrowly focused on cartilage lesions passively driven by mechanics. In fact, running is not associated with an increased risk of knee OA in spite of the higher mechanical loading involved [9, 10], which could not be explained by mechanical factors alone. Improvements in molecular and imaging technologies have facilitated investigations into the molecular mechanisms and tissue-level changes in OA progression. The active degenerative process of tissue matrix was early revealed when cells within the joint were found to release matrix proteases [11]. Thereafter, accumulating modern research has revealed the pivotal role of inflammation in OA pathogenesis through systematic studies of plasma, synovial fluid, articular cartilage and

surrounding tissues [7, 12–18]. The association between synovitis and symptoms and progression of OA has been confirmed through advanced imaging techniques [19]. Inflammatory mediators secreted from chondrocytes, synovial cells and other joint cells can stimulate the production of proteolytic enzymes that degrade tissue matrix to disrupt the homeostasis within the joint environment [16]. However, inflammation is not an isolated process in OA pathology. OA inflammation is chronic and low-grade, which also interacts with innate immune responses [20, 21] and cellular mechanotransduction [22]. The mechanisms of these complex interactions may explain the observed correlation between obesity and the increased risk of OA in the joints without primary weight-bearing function [23].

At present, it is acknowledged that both low-grade inflammation and mechanical loadings play central roles in the heterogeneous degeneration of the knee joint in the context of various OA risk factor, such as age, obesity, genetics, gender, nutrition and abnormal morphology of the knee joint [24]. Despite the better understanding of OA, there is no effective treatment on modifying OA progression and its diagnosis at an early stage remains a challenge [25–29]. This is due to the limited understanding of the complex interactions between local and systemic factors, including biomechanics of arthritic tissues, immune responses and metabolic mechanisms. It is essential for the exploration of disease-modifying therapies to identify early OA and classify corresponding phenotypes and endotypes [30–33]. In the narrowed research scope of OA, phenotypes refer to the observable disease presentations in clinics while endotypes correspond to the underlying pathomechanisms [34]. So far, a unified standard for OA classification has not yet been established, leading to a research question of how obesity-associated OA phenotypes and endotypes can be identified. Investigating the inflammatory and mechanical effects of obesity is of great significance for addressing this research question.

Age and obesity are the most predominant risk factors in population, corresponding to different subtypes of OA. The increasing age may result in less capability of tissue regeneration and more underlying chronic age-related diseases that can increase the risk of OA [35, 36]. Compared to ageing, obesity is a manageable factor. The number of global OA incident cases associated with obesity is projected to be over 128 million by 2050 [5]. Nevertheless, current guidelines lack tailored recommendations for the management of OA in patients with obesity [37]. Obesity is defined as the deposition of adipose tissue and commonly measured by body mass index (BMI) [38]. In general, individuals with a BMI over 30 kg/m_2 are considered as obese [39]. Modern perspectives view OA as a systemic disease [40], where

obesity-associated disruptions of biomechanical responses, metabolic regulations and chronic inflammation play a pivotal role [41–43]. Specifically, the accumulation of adipose tissue is accompanied by mechanical overloading of weight-bearing joints, metabolic syndrome and the low-grade inflammation [44]. In 2020, Collins et al. [42] first confirmed the direct effect of adipose tissue in OA by using murine preclinical model of lipodystrophy where adipose tissue and adipokine signalling did not exist. This study indicates the role of adipose tissue and adipokines in regulating OA independent of mechanical loading and metabolic effects. In addition to obesity-induced inflammation, tissue injury resulting from overloading can activate local inflammatory responses within the joint, interacting with obesity-associated disruptions in metabolic and inflammatory activities. However, the exact regulating mechanisms of adiposity-associated factors are not yet fully elucidated as they interact simultaneously in OA pathology. This gives rise to another research question on how adipokine-mediated inflammation interrelates with tissue damage in the context of OA.

It is important to note that adipokine signalling generally involve multiple pathways in OA [45], thereby, it is difficult to either examine the complex adipokine-mediated inflammatory network or distinguish different obesity-driven degenerative pathways of joint tissues in experiments. As a non-invasive alternative, in silico approaches are powerful to both explore the complex OA mechanisms and predict tissue degeneration at different spatial and temporal scales [46]. Nevertheless, most existing computational approaches of studying obesity in OA focus primarily on the biomechanical effects. It has not been ascertained yet whether mechanical factors are a direct cause of the disease, whereas it is well known that the obesity-induced abnormal mechanical loading within the joint regulates OA pathogenesis [47]. Meanwhile, emerging evidence on the inflammatory role of obesity in OA underscores the need to develop computational approaches capable of capturing its mechanobiological effects. Therefore, this thesis focuses on the integration of obesity-associated inflammation and mechanical loading in OA by developing novel computational models.

1.2 Aim and objectives

Motivated by the disease impact and aforementioned research questions in the research on OA, the overall aim of this thesis was to develop an integrative multi-scale computational approach for the investigation of obesity-associated inflammation

and mechanics in OA. This was to be approached by the following research objectives:

- To develop a mathematical model of adipokine-mediated OA inflammation.
- To analyse the inflammatory dynamics regulated by obesity-associated factors.
- To parameterise the adipokine-mediated inflammatory responses in a time dimension.
- To study the sensitivity of adiposity factors and mechanical damage in the inflammatory activities of OA.
- To evaluate the interactions of BMI, time-dependent physical activity strategies and mechanical damage in the regulation of OA inflammation.
- To establish a multi-scale modelling framework that integrates the mechanobiological regulations of obesity in OA.
- To study the sensitivity of the critical parameters in the obesity-associated cartilage degeneration algorithm of the multi-scale approach.
- To assess the effects of inflammation and mechanical loading on cartilage degeneration at different BMI levels.
- To implement the integrative multi-scale approach for three subject-specific knee joints
- To investigate the subject-specific cartilage degeneration in the context of obesity-related OA by quantifying biomechanical responses and tissue degeneration.

1.3 Thesis outline

This thesis is organised into seven chapters, contributing to the development of computational tools and the advancement of knowledge in obesity-associated inflammation and mechanics in OA.

Chapter 1 introduces the research background and motivations of this thesis. The aim and objectives are summarised and the thesis structure is outlined in this chapter.

Chapter 2 reviews the fundamental anatomy of the knee joint, consensus and gaps in the pathological changes of cartilage and subchondral bone during OA, the mechanism of OA inflammation and roles of primary inflammatory mediators. Thereafter, computational modelling approaches are critically discussed in the research scope of OA inflammation, cartilage degeneration and joint biomechanics in OA.

Chapter 3 presents the development of the mathematical model of inflammation and obesity in OA, corresponding to the first main research objective. In this chapter, model parameter sensitivity is analysed with the examination of adipokine-mediated inflammation dynamics, and the effects of obesity are discussed.

Chapter 4 details the parameterisation of the adipokine-mediated OA inflammation model for the study of adiposity-associated factors, corresponding to the second main research objective. A global sensitivity analysis is performed in the estimated parameter space. The effects of BMI, physical activity intervention and mechanical damage are studied through simulations of the inflammatory process in OA.

Chapter 5 demonstrates the development of the integrative multi-scale approach for simulating cartilage degeneration regulated by obesity-related inflammation and mechanical loading, corresponding to the third main research objective. In this chapter, a cartilage degeneration algorithm is formulated by coupling the obesity-associated biomechanics and inflammatory responses. Parameter analysis in this algorithm is conducted and the obesity-driven degenerative process is analysed. Additionally, the inflammatory and mechanical contributions of obesity in cartilage degeneration are evaluated.

Chapter 6 applies the multi-scale modelling approach to three validated subject-specific knee joints to simulate the cartilage degeneration driven by obesity, corresponding to the fourth main research objective. The subject-specific patterns of cartilage degeneration driven by obesity are compared, and the significance of anatomical subject specificities is highlighted with the evaluation of obesity effects.

Chapter 7 discusses the overall contributions of this thesis in the research scope of OA. Limitations and future research directions are evaluated, and main findings are concluded.

Chapter 2

Literature review

This chapter provides a literature review on the present research landscape in the fundamental structures of the knee joint, the pathology of cartilage and subchondral bone degradation in osteoarthritis (OA) and the inflammation mechanism of OA with primary inflammatory mediators, aiming to summarise the prior knowledge in the critical characteristics of OA onset and progression. The degenerative processes of articular cartilage and subchondral bone are reviewed. In addition, the existing literature relevant to OA inflammation is evaluated, highlighting the critical role of obesity in the inflammatory process of OA. Prior knowledge in the scope of osteoarthritis provides evidence on the development of computational models. Following on that, mainstream computational modelling strategies are examined in the context of OA, including mechanistic and data-driven approaches. Continuum dynamical systems are generally built based on differential equations to simulate the regulatory network of inflammation, thereby recent ODE- and PDE-based models are summarised to evaluate the knowledge gaps and research limitations. Although agent-based and data-driven modelling approaches are emerging, their applications are still relatively limited. By the end of this chapter, FE method and multi-scale modelling approaches are discussed along with the general workflow of model development and applications in the knee OA. In particular, the effects of obesity on the OA joint are evaluated, highlighting the lack of computational study on the mechano-bio-chemical regulations of obesity across different scales during OA.

2.1 Anatomy of the knee joint

The human knee joint is a synovial joint mainly comprised of articular cartilage, bones (patella, femur, tibia and subchondral bone), fat pad, meniscus, ligaments

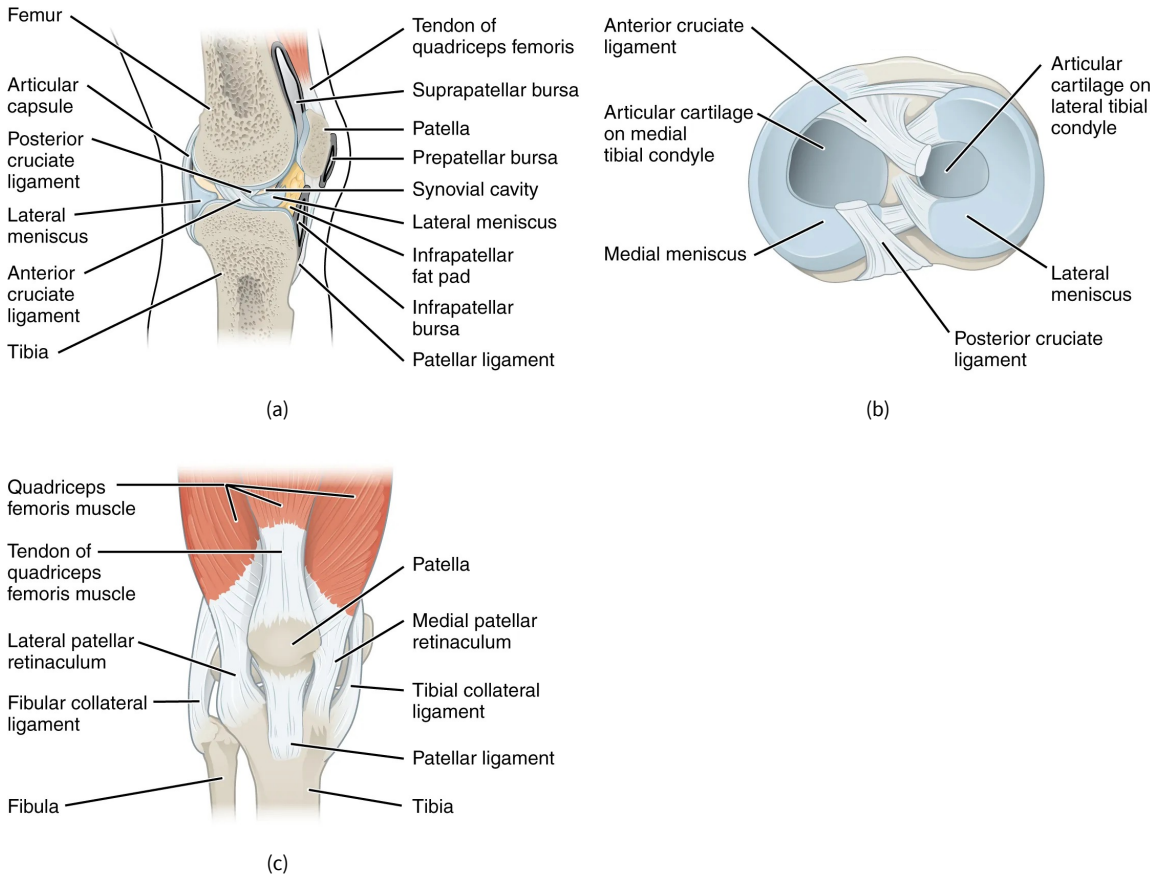

Figure 2.1: *Schematic knee joint, modified from Betts et al. [48] under CC BY-NC-SA 4.0. Access for free at openstax.org. (a): Sagittal section; (b): Superior plane; (c) Anterior view.*

and synovium. A schematic representation of the knee joint is shown in Figure 2.1. Whilst the anatomical structure of each constituent altogether provides the stability and motion behaviours under complex physiological loadings, the subchondral bone and articular cartilage are predominantly involved in the joint degradation. In addition, the inflammation within synovium, meniscus and infrapatellar fat pad can also accelerate the articular degeneration.

2.1.1 Articular cartilage

Cartilage is a functional unit that smoothly articulates bones and buffers physiological loadings resulting from joint physical motions. The cartilaginous tissue can be classified into four featured layers (Figure 2.2) where the extracellular matrix (ECM) densely distributes and chondrocytes sparsely exist across all layers [49]. In particular, the compositions of ECM are mainly water content, collagen formed by fibrils and proteins such as proteoglycans so as to possess viscoelasticity. The material of

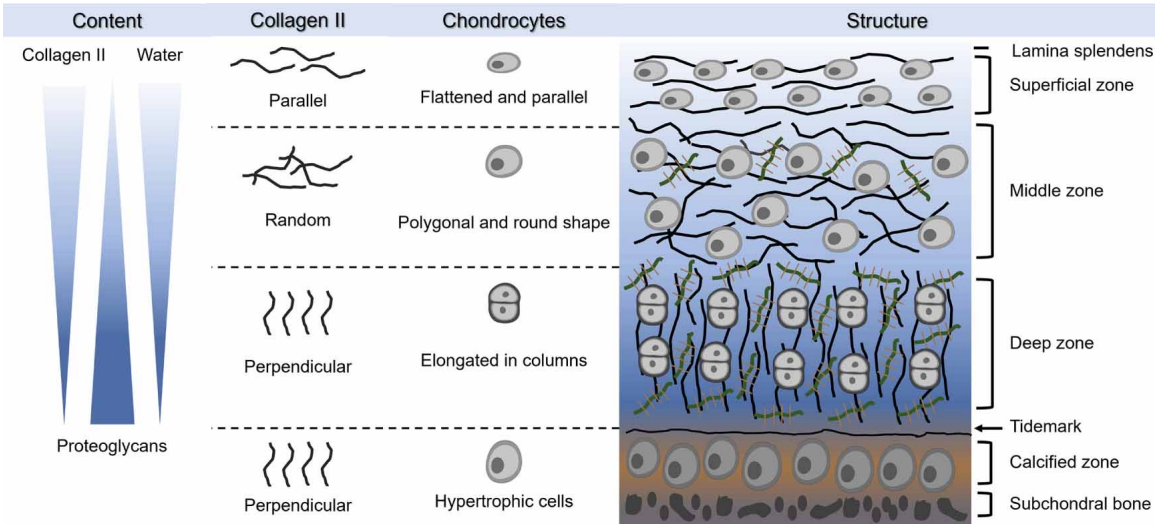

Figure 2.2: *Schematic representation of articular cartilage, reused from Oliveira et al. [51] under CC BY 4.0.*

cartilage expresses biphasic or triphasic behaviours, which has been summarised by Henak et al. [50]. Consequently, the heterogeneity of ECM provides both considerable compressive and tensile resistance and chondrocytes are responsible for the metabolism of cartilage.

2.1.2 Subchondral bone

Subchondral bone is the bony tissue connected to calcified cartilage and comprised of the porous structures, subchondral bone plate and subarticular spongiosa, where the vasculature and nerves cross. The difference of stress distribution in the subchondral bone varies its anatomical structure (Figure 2.3) including the fluctuant thickness of subchondral bone (0.2-0.4mm) [52]. As a dynamic bony component, subchondral bone possesses high stiffness and strength in order to absorb impact loadings transmitted from diaphyseal bones.

2.1.3 Infrapatellar fat pad

The structural adipose tissue, infrapatellar fat pad (IFP), plays significant roles in biological metabolism [41, 54] and biomechanics [55] of the knee OA. The contribution of IFP on the mechanical response might be protective, such as the stabilisation of the patella and patellar cushion [56]. However, the inflammatory interactions of IFP and articular tissues have been increasingly reported [42, 57]. As a local source of

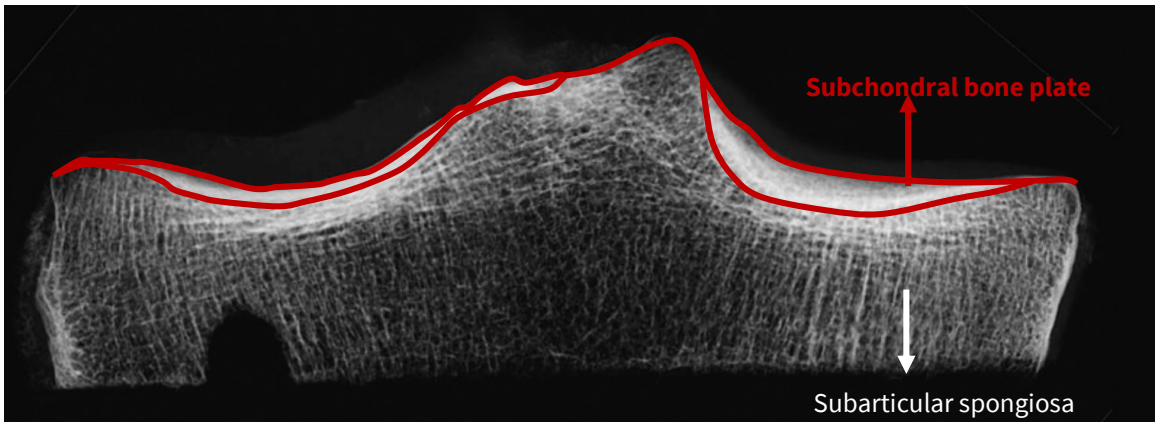

Figure 2.3: *The geometry of subchondral bone, modified from Yamada et al. [53] with permission.*

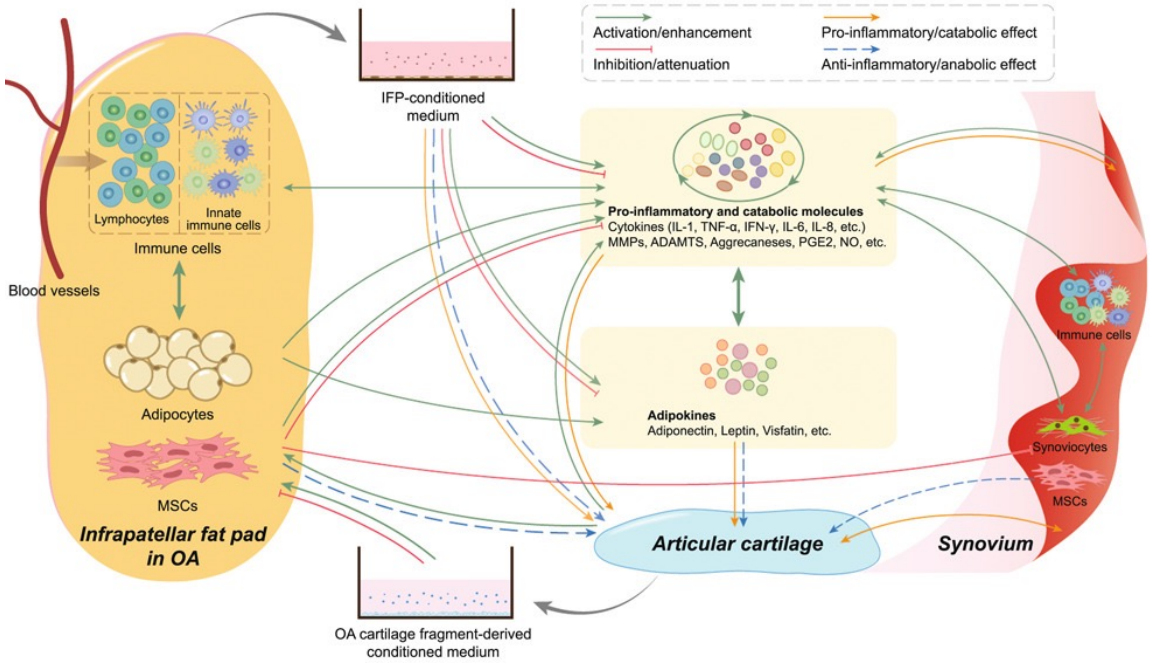

Figure 2.4: *The effects of IFP on the inflammation of OA, modified from Zhou et al. [57] under CC BY 4.0. Immune cells leak into IFP from vessels. The mutual activation between immune cells and adipocytes upregulates the pro-inflammatory and catabolic molecules. Adipokines secreted from adipocytes also activate the production of inflammatory molecules but may have both catabolic and anabolic effects on cartilage. The increase of inflammation due to immune cells and adipocytes results in the progressive degradation of cartilage, though mesenchymal stromal cells (MSCs) from IFP and synovium are signalled to compensate the damage of cartilage.*

adipocytes, IFP might have more involvement in the biological regulation during OA, as shown in Figure 2.4.

2.1.4 Meniscus

Menisci locate between the tibia and femur and are responsible for the loading transfer within the joint. Due to the characteristics of the fibrocartilaginous structure, the meniscus can evenly distribute the shock loads and stabilise the whole joint during physical motions [58]. As a consequence of meniscus tear, the biomechanics of the joint could be disturbed and the risk of OA is accordingly elevated. Whilst the degenerative cartilage and subchondral bone directly induce OA progression, the roles of meniscus defects in OA onset have been an emerging focus [59].

2.1.5 Ligaments

Ligaments include lateral collateral ligament (LCL), medial collateral ligament (MCL), anterior cruciate ligament (ACL) and posterior cruciate ligament (PCL), which can passively provide the kinetic knee joint with stability and constraints. Injuries of ligaments can lead to abnormal contact mechanics so that the shear force may be excessive within the joint [60], which thereby increases the risk of OA.

2.2 Pathological changes of articular cartilage and subchondral bone

There has been a controversy on the constituent that first starts the abnormities causative of joint degeneration in the early stage of OA. Regardless of the earliest sign (synovitis) during OA [18], abnormities of the human knee joint can be generally observed in articular cartilage and subchondral bone (Figure 2.5). Casper-Taylor et al. [17] evaluated the recent articles reporting the pathologies of cartilage and subchondral bone in combination of quality analysis and statistical analysis on animal models, which suggests that pathological changes of OA may be concurrent in cartilage and subchondral bone or priorly in subchondral bone. However, the lesser samples from the human knee joint are not able to strongly evidence the suggestion. Given that, it is more likely to separately elucidate the pathologies of cartilage and subchondral bone in the OA evolution when the clinical data is deficient. In fact, the central role of molecular dysfunction in the knee joint of OA has been endorsed by OARSI [61]. Accordingly, the invisible and specific difference of molecular crosstalk between structural joint constituents may result in the discrepant radiographs of the first pathological change. In other words, local inflammatory activities and the existence of various risk factors of OA, such as obesity and mechanical loadings, may

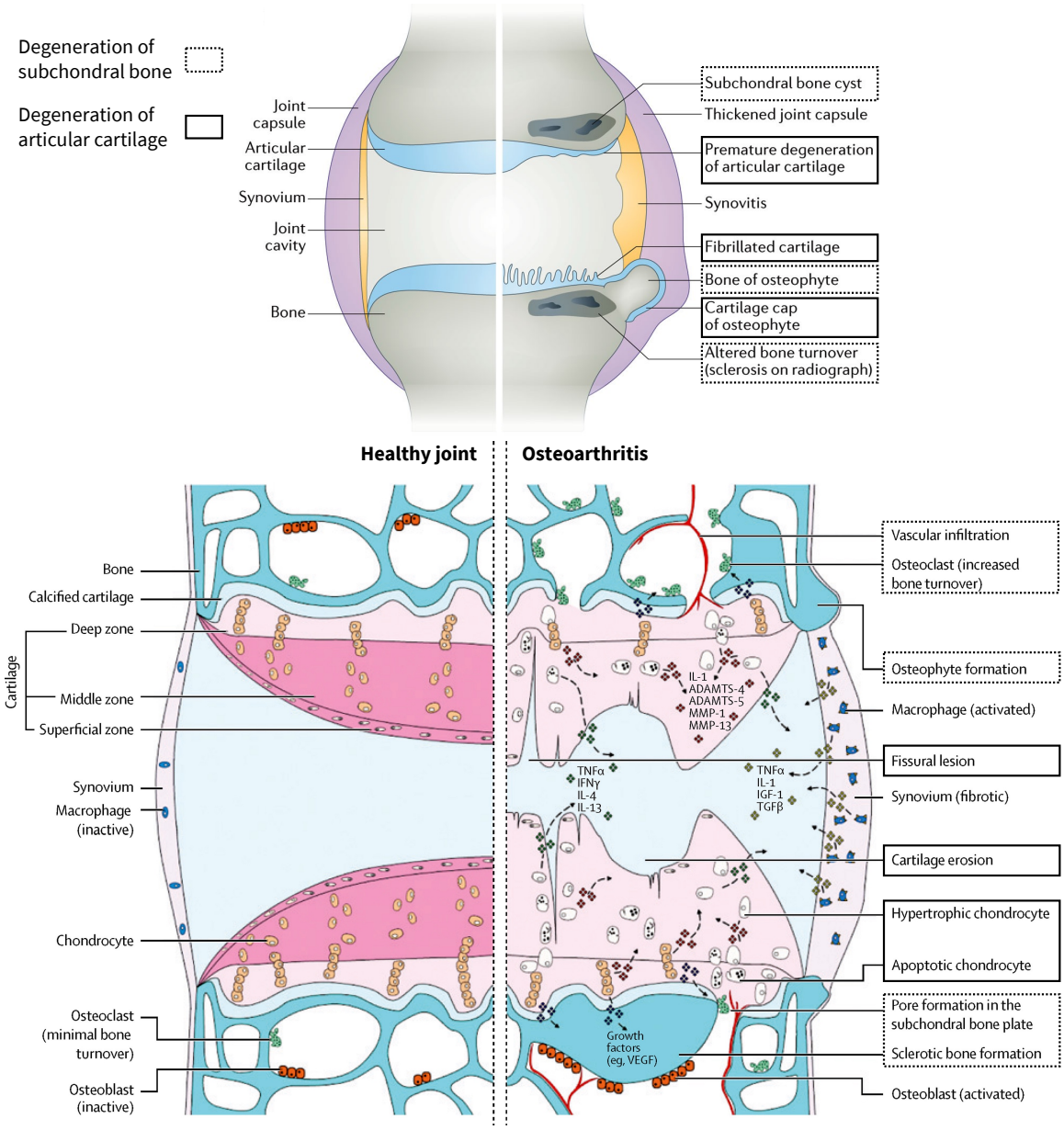

Figure 2.5: *The pathological variations of the knee joint in OA, modified from Glyn-Jones et al. [7] and Robinson et al. [16] with permissions.*

jointly initiate the progressive inflammation before the structural changes, which was identified as the stage of pre-OA by Lv et al. [62]. Therefore, the cascade of cellular and molecular interactions before the early stage of OA may be causative of the first detectable pathological change in the joint structure.

2.2.1 Degeneration of articular cartilage

Radiographically, fibrillation can be earliest detected in the degenerative articular cartilage, which is progressively deteriorated due to the disequilibrium between the synthesis and degradation of ECM. Though the exact degenerative mechanism of cartilage remains disputable, its pathophysiology admittedly encompasses histological and molecular changes. In particular, the association between the fibrillated surface of cartilage and the adhesion of chondrocytes to fibronectin has been particularly noted [63], which is nevertheless not one isolated factor involved in the degeneration of cartilage. In addition to that, the depletion of proteoglycans leads to the increase of hydraulic permeability [64] with underlying inflammation, and the hypotrophy of synovial cells results in higher water content of cartilaginous tissue at the early stage of OA [65], of which consequence is the reduction of resistance of deformation as the structural stiffness of collagen is destructed with disruptive layout of fibres. Notably, the level of fixed charge density responsible for retaining the osmotic pressure is reduced due to the loss of proteoglycans [66]. This pathological change exists in all stages of OA.

In the early stage of OA, the anabolic ability of chondrocytes is intensified in order to repair the damaged ECM [67]. The attempt of repair normally persists with chondrocyte proliferation for a long period, before which low-grade inflammation may be involved. Particularly, the expression of chondrocytes in various toll-like receptors [68] is active due to the damage-associated molecular patterns (DAMPs) [21] during the inflammation of OA. In addition, the persistent inflammatory activities prevent the damage of ECM from repair as the involvement of diverse mediators, such as cytokines, aggrecanases, collagenases and adipokines, disturbs the catabolic and anabolic processes in the cartilage. Gradually, the population of apoptotic and hypertrophic chondrocytes increases [67, 69], and the ability to repair the ECM will be ultimately lost as non-renewable chondrocytes are the only constituents capable of synthesising matrix in cartilage. As a consequence, the loss of cartilaginous tissue, such as fissural lesions, cartilage erosion and osteophyte, can be variably detected in OA progression, which is dependent on the severity of OA. Overall, the evolution of cartilage degeneration has been mapped in Figure 2.6.

2.2.2 Grading assessment of OA severity

Despite a few observations of molecular and cellular changes in the early stage of OA, the synchronous progression of inflammatory interactions and tissue deteriora-

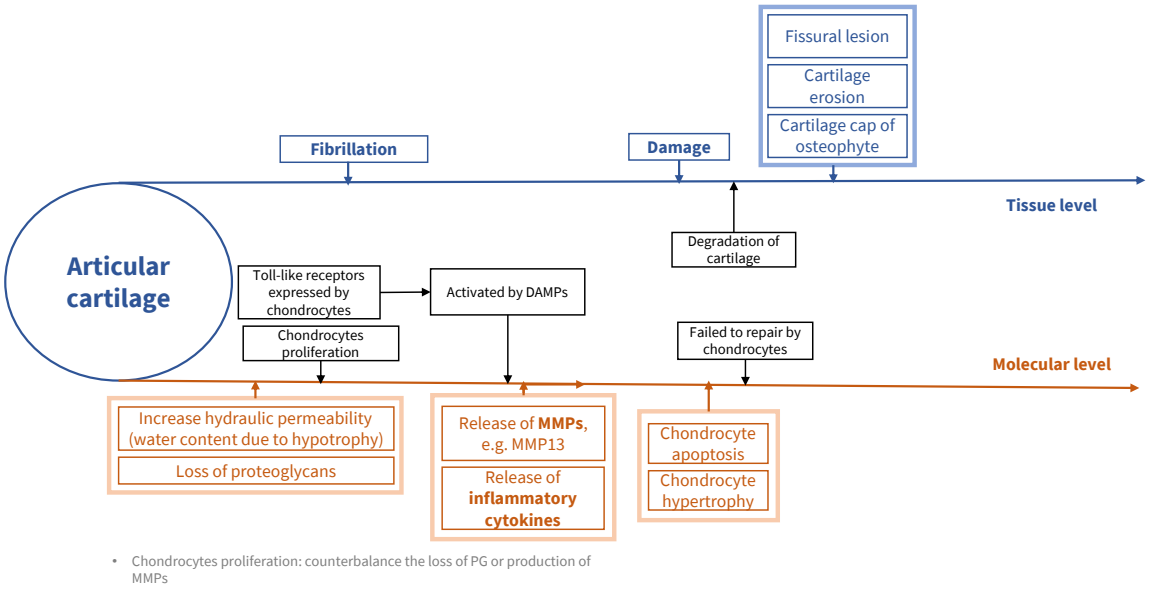

Figure 2.6: *The evolution of cartilage degenerative changes in OA.*

tions still remains vague between the early and advanced stages of OA. With respect to the latter, OARSI [70] provided a histopathological grading for the severity of OA, which was visualised with specifying articular cartilage and subchondral bone in Figure 2.7 by Palmer et al. [71]. However, the grading assessment lacks the elucidation on the early degeneration of subchondral bone. Furthermore, the unravelled implication between cartilage and bone may not be reflected in the OARSI grading system. Aho et al. [72] suggested a simplified grading system on the histopathology of subchondral bone. The significance of bone remodelling to the cartilage degradation by comparing to the OARSI grading was highlighted, though the simplified grading is still not able to clarify whether cartilage degeneration precedes the abnormalities of subchondral bone.

2.2.3 Degeneration of subchondral bone

The bone marrow lesion can be detected in subchondral bone at the earliest, and its strong association to radiography of OA progression is unequivocal. Specifically, the volume of bone marrow lesions is positively correlated to the risk of cartilage loss [73]. Aberrant loadings result in subchondral microfractures and the increase of bone remodelling so as to form bone marrow lesions that hardly recede during OA [74]. Subsequently, subchondral sclerosis is approached when the bone volume elevates but mineralisation reduces due to the high bone turnover rate. The consequence of rising bone density is mainly the higher stiffness of bone so that the

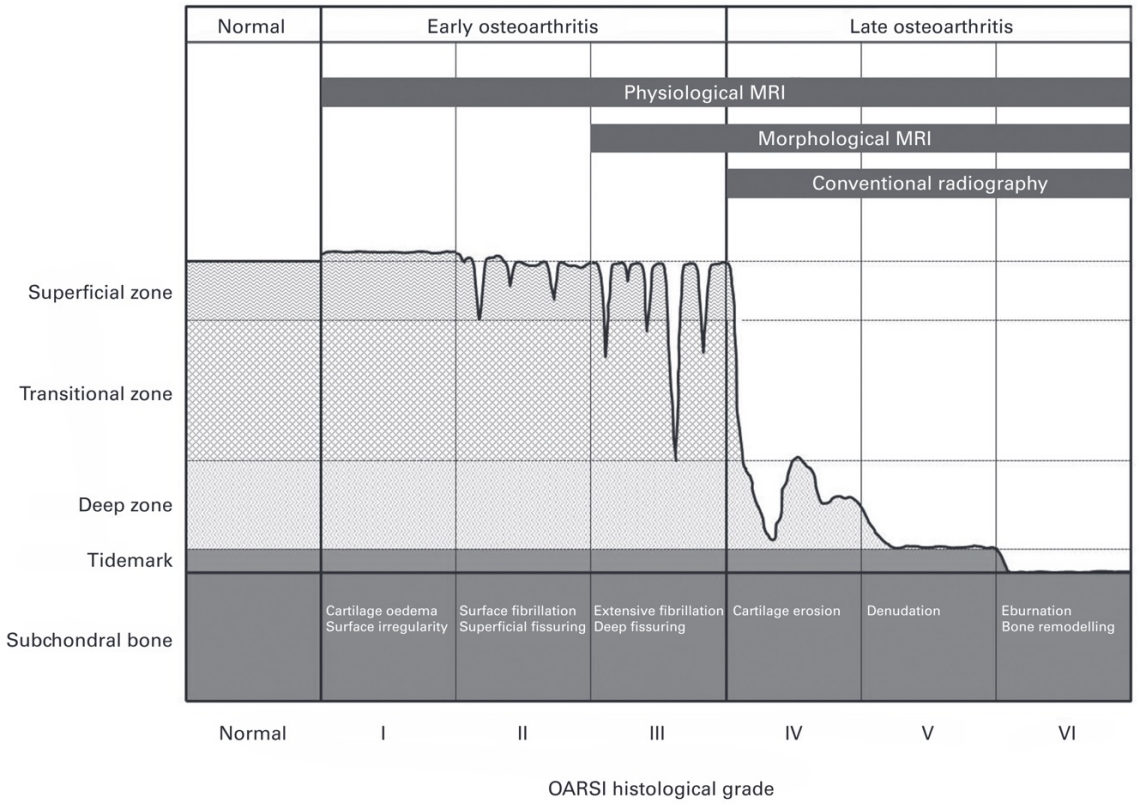

Figure 2.7: *The histology grading of cartilage in OA, reused from Palmer et al. [71] with permission.*

degradation may be prompted. Surprisingly, the structural changes of subchondral bone plate are nevertheless two-fold [75, 76]. Due to the high sensitivity to biomechanical signals [77], the bone turnover decreases at early OA stage and increases during OA progression in order to compensate for the loss of structure-bearing mechanical loadings. It should be noted that the genesis of osteoclast may be positively stimulated by activated macrophages in the innate immune response of synovitis [74], which thereby leads to thinning subchondral bone plate initially in spite of the unknown mechanism of how osteocytes migrate between bone and synovium.

Although the histological appearance of bone marrow lesions requires more evidence of high quality, it could be known that bone marrow lesions generically concentrate in the regions under maximum mechanical loadings [78] and normally reflect the increase of vascularity and cell necrosis [79]. The altered vascularity may boost the inflammatory crosstalk between bone and cartilage, which accordingly leads to the dysregulated metabolism of cartilage and bone, such as the repair of cartilage and abnormal bone remodelling. Namely, the changes of subchondral microenvironment [77] may be associated with both degeneration of cartilage

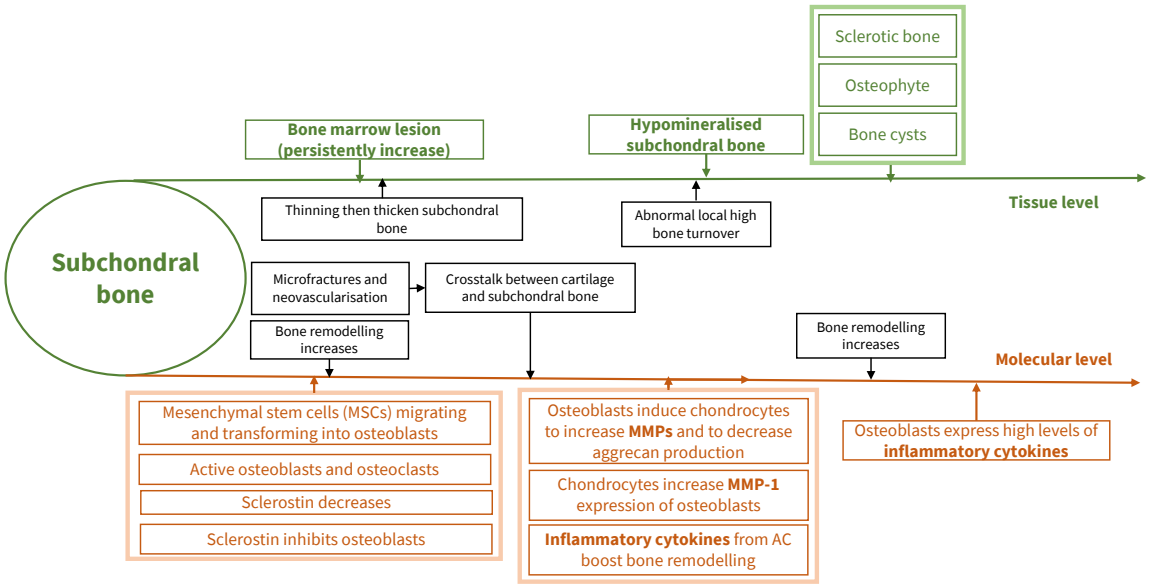

Figure 2.8: *The evolution of subchondral bone degenerative changes in OA.*

and bone, therein the homeostasis of osteoblasts, osteoclasts and chondrocytes is disrupted. Specifically, osteoblasts may signal chondrocytes to secret matrix metalloproteinases (MMPs) degrading cartilage, in turn, chondrocytes can interfere with the normal expression of osteoblasts in the late stage of OA [80]. As a dominant abnormality in the microenvironment, the microdamage of subchondral bone resulted by abnormal mechanical loadings provides cartilage and bone with more catabolic communication due to the invasion of vessel and cutting cones deriving from the subchondral bone plate [75]. It should be noted that the probability of its occurrence is significantly high in the early OA stage. Despite the emphasis on the microfracture of subchondral bone [77, 80], the difference between linear and diffuse microcracks is not clearly distinguished. In fact, the former is immediately associated with recruitment of osteoclasts induced by osteocyte apoptosis due to the repair mechanism [75]. Particularly, the osteocyte apoptosis is not induced by diffuse cracks as diffuse damage may be healed in a disparate mechanism [78]. In addition to subchondral bone sclerosis and osteophyte initiated by a high bone turnover rate, bone cysts can be also detected in advanced OA. The appearance of cysts is indeed implicated in active bone remodelling [81] whereas the cyst formation is still a mystery. Presumably, the hydraulic pressure is varied when the water permeates to the bone from cartilage through microcracks [52]. The difference of hydraulic pressure leads to the bone resorption so as to form bone cysts. However, Li et al. [75] suggest that the variation of fluid pressure may derive from

synovial fluid rather than the water from cartilage. Overall, the evolution of subchondral bone degeneration has been mapped in Figure 2.8.

2.3 The mechanism of inflammation in molecular and cellular levels

The appreciation of OA has been transformed since 1959 when its neglected inflammation level had started to be gradually revealed [82]. Historically, the overemphasis of rheumatoid arthritis (RA) inflammation is causative of the traditional cognition that OA is not an inflammatory arthritis in the histological comparison of OA and RA [83], instead OA was regarded as a disorder caused by mechanical wear and tear. Contemporarily, it is undeniable that the chronic inflammation and the innate immune response responsible for the mediation of inflammatory activities play a prominent role in the OA onset and progression, of which accumulating evidence has been examined [16, 18, 20, 83, 84]. It should be noted that OA is different from RA on the levels of inflammatory cytokines in both serum and synovial fluid [85] in spite of the fact that inflammation could be observed in OA and RA through biomarkers, which indicates that the inflammation of OA is low-grade and local to joints.

Regardless of the structural degradations, the presence of inflammation is in the synovium in the earliest stage of OA before the radiographical signs can be detected [18], namely, OA could be recognised as an inflammatory disorder before observable cartilaginous lesion. Sokolove and Lepus [83] have underlined the priority of synovitis as one of the involvements in OA, similarly, Kalaitzoglou et al. [20] suggest that synovitis and its grade may be capable of the prediction of OA development. Nonetheless, there is no evidence that synovitis is the predisposing factor of joint degeneration. Consequently, the synovial inflammation is tightly associated with the immune response to joint damage, but the inflammatory processes in cartilage and subchondral bone may be as pivotal as synovitis in OA.

The inflammation in knee OA is dominantly driven and regulated by various mediators which are produced by specialised cells from cartilage [65], bone [80, 86], synovium [18] and infrapatellar fat pad [41, 54, 55, 57]. Prominent inflammatory mediators have been interpreted along with the OA pathogenesis, as demonstrated in Figure 2.9.

In the context of various OA risk factors, including age, gender, genetics, obesity and nutrition, the injured joint tissue leads to inflammatory activities that attempt

to repair the tissue damage. However, the failed tissue repair may trigger the prolonged inflammation process so as to progressively evolve into OA. Due to the damage, DAMPs are released by cells before apoptosis to signal the activation of innate immune system. During the activation, Pattern-recognition receptors (PRRs) can recognise DAMPs to induce an inflammatory response [21], which plays a central role in the progression of the low-grade inflammation and OA. Compared to the innate immune system, the interaction between adaptive immune system and OA is unclear [16, 83]. By inducing potent inflammation during OA, complex interplays of diverse soluble mediators of inflammation exist in the knee joint, such as cytokines [87], chemokines [88], adipokines [43, 45, 89, 90], growth factors [62] and lipid mediators [62]. Despite the critical involvement of chemokines, growth factors and lipid mediators in OA inflammation, they might not be specifically emphasised in this section due to the complex cascade of chemokines and unclear evidence of how growth factors and lipid mediators respond to the inflammatory activities during OA.

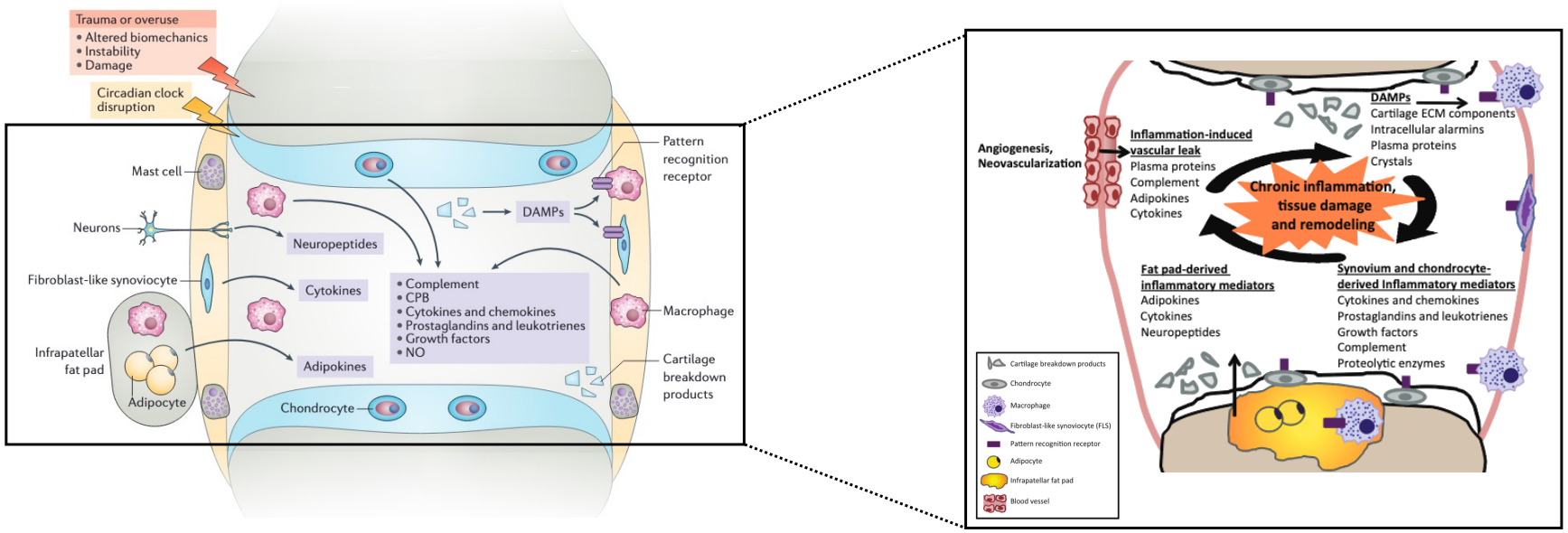

Figure 2.9: *The local inflammatory mechanism in the knee OA progression, modified from Robinson et al. [16] and Sokolove et al. [83] with permissions. Due to the trauma or overuse of the knee joint, damage occurs and induces the production of DAMPs. DAMPs instruct cells, such as macrophages and chondrocytes, to secret a variety of inflammatory mediators. Similarly, inflammation-induced vascular leak can also signal cells to increase inflammation within the knee joint. The interactive cycle of chronic inflammation, tissue damage and tissue repair induces massive proteolytic enzymes so that the joint degeneration is progressively aggravated.*

2.3.1 Inflammatory cytokines

The abnormal level of prominent inflammatory cytokines has been reviewed [83] and can be classified into two groups [87]: pro-inflammatory cytokines (IL-1β, IL-6, IL-15, IL-17, IL-18 and TNFα) and anti-inflammatory cytokines (IL-4, IL-10 and IL-13). In spite of different cytokines assorted in the same group, there are still slight differences in their sources, roles in OA and feedback to other mediators, as illustrated in Table 2.1. Specifically, IL-1β and TNFα are initially released by chondrocytes, osteoblasts, synoviocytes and mononuclear cells in the early stage of OA [87], which can further aggravate the inflammation where other pro-inflammatory cytokines are released [91]. Notably, the stimulation of MMPs production and the inhibition of differentiating chondrocytes into ECM are the predominant regulatory functions of pro-inflammatory cytokines [87]. On the contrary, anti-inflammatory cytokines contribute to interfering with the secretion of MMPs and pro-inflammatory cytokines, meanwhile, the synthesis of type-II collagen and aggrecan may be stimulated, along with enhanced protective effects on chondrocytes [87].

2.3.2 Adipokines

Inflammatory cytokines are tightly implicated in the initiation and progression of inflammation. However, adipokines (adiponectin, leptin, resistin and visfatin) are suggested to play a prominent metabolic role in the course of OA [42, 45, 89, 92–94] and even other inflammatory diseases [43, 90, 95, 96] in the context of obesity as a critical risk factor. As a molecular group produced by adipocytes, it is perspicuous that adipokines are capable of regulating the secretion of inflammatory mediators or products resulting in the degradation of cartilage and chondrocytes along with the development of OA [20]. Nevertheless, similar to cytokines, the minor variations of adipokine properties are revealed based on their types (Table 2.1). In particular, the levels of adiponectin and leptin are differently varied by the body weight due to their metabolic response of obesity [89]. The concentration of adiponectin is inversely proportional to BMI as well as abdominal obesity [97], which is contrary to leptin [42] whereas the correlation of leptin and BMI is relatively weak in statistics. Interestingly, despite the fact that the adiponectin levels in plasma are approximately 100 times higher than those in the synovial fluid of OA, the adiponectin in plasma may not be correlated with the OA progression and its levels in the synovial fluid of OA may be negatively associated with OA severity [98]. Thus, the inconsistency between plasma and synovium might result from

the crosstalk between systemic and local adipose tissues. Namely, a higher level of adiponectin in plasma is due to systemic adipokines, and local adipocytes lead to the higher concentration of leptin in the OA joint as leptin might be immediately associated with the inflammation. Compared to leptin, the role of adiponectin in OA appears disputable according to clinical observation [89], and its dual roles of activation and suppression in the inflammatory response of innate immunity have been reported [99]. Since obesity results in the elevation of leptin levels and the downregulation of adiponectin, the pro-inflammatory effects of the adipokine group on OA patients with high body weight might be dominant. With respect to molecular catabolism and anabolism, adipokines contribute to the production of MMPs in addition to upregulating the pro-inflammatory cytokines secreted by stimulated chondrocytes [100]. Correspondingly, the metabolism of proteoglycans, chondrocytes, osteoblasts and osteoclasts is dysregulated [89], which may lead to the degradation of cartilage and subchondral bone, as illustrated in Table 2.1.

2.3.3 Matrix metalloproteinases (MMPs)

As mentioned above, the production of MMPs, which predominantly participate in the degeneration of ECM [101], is stimulated by both pro-inflammatory cytokines and adipokines in OA inflammation. Distinct from cytokines and adipokines, MMPs may not be capable of the primary regulation of inflammatory mediators in OA. As a type of proteolytic enzymes, MMPs are responsible for tissue degradation in chronic OA inflammation. However, a broad review by Fingleton [102] discussed the protective role of MMPs in acute inflammation. Since the inflammatory mechanisms of OA are different from other diseases with acute inflammation, this protective role was not found in other studies [16, 18, 20, 83, 84, 88, 91, 103] on OA inflammation. In the context of OA pathogenesis, the characteristics of MMPs have been comprehensively reviewed [104], and the proteolytic role of MMP-1, MMP-3 and MMP-13 in OA progression were emphasised (Table 2.1). These MMPs have a profound impact on the cartilage degradation by interacting with proteoglycans and collagen, of which possible concomitant products might aggravate the inflammation.

Table 2.1: *Inflammatory mediators and molecules in the course of OA, summarised from [83, 87, 89, 91, 92, 97–102, 104]. Interleukin (IL); Tumour necrosis factor (TNF); Inducible nitric oxide synthase (iNOS); Prostaglandin E (PGE); Cyclooxygenase (COX); Fibroblast-like synoviocytes (FLS); Vascular endothelial growth factor (VEGF); Phospholipase A2 (PLA2).*

Pro-inflammatory cytokines	Main source	Role in OA	Positive feedback	Negative feedback
IL-1β	Chondrocytes, osteoblasts, cells of synovial membrane, mononuclear cells	Preventing chondrocytes from synthesising ECM, disturbing synthesis of type-II collagen and aggrecan, inducing the production of MMPs	MMP-1, MMP-3, MMP-13, TNFα, IL-6, iNOS, COX-2, PGE-2	Unknown
IL-6	Chondrocytes, osteoblasts, FLS, macrophages, adipocytes	Activating immune system and enhancing the inflammatory response	Unknown	Unknown
IL-15	T cells, NK cells (in synovial fluid in the early OA)	Inducing the production of MMPs	Unknown	Unknown
IL-17	Stimulated CD4+ T cells and mast cells	Preventing chondrocytes from synthesising proteoglycans, inducing the production of MMPs	MMP-1, MMP-3, MMP-13, IL-1β, IL-6, PGE-2	Unknown
IL-18	Chondrocytes, osteoblasts, FLS, macrophages	Preventing chondrocytes from synthesising proteoglycans, disturbing synthesis of type-II collagen and aggrecan, inducing the production of MMPs	MMP-1, MMP-3, MMP-13, IL-6, iNOS, COX-2, PGE-2, VEGF	Unknown

Continued on next page

TNF-α	Chondrocytes, osteoblasts, cells of synovial membrane, mononuclear cells	Preventing chondrocytes from synthesising proteoglycans, disturbing synthesis of type-II collagen and aggrecan, inducing the production of MMPs	MMP-1, MMP-3, MMP-13, IL-6, iNOS, COX-2, PGE-2	Unknown
Anti-inflammatory cytokines	Main source	Role in OA	Positive feedback	Negative feedback
IL-4	T cells (Th2)	Inhibiting the degradation of proteoglycans and production of MMPs	Unknown	IL-1β, IL-6, TNFα, iNOS, COX-2, PGE-2, PLA2
IL-10	Chondrocytes and fibroblasts	Stimulating the synthesis of type-II collagen and aggrecan, inhibiting the degradation of proteoglycans and production of MMPs, inhibiting the apoptosis of chondrocytes, inducing chondrocyte proliferation and differentiation	Unknown	MMP-1, MMP-3, MMP-13
IL-13	Fibroblasts	Stimulating the synthesis of type-II collagen and aggrecan, inhibiting the degradation of proteoglycans and production of MMPs, inhibiting the apoptosis of chondrocytes, inducing chondrocyte proliferation and differentiation	Unknown	IL-1β, TNFα, MMP-3
Adipokines	Main source	Role in OA	Positive feedback	Negative feedback
Adiponectin	Adipocytes	Regulating chondrocyte proliferation, proteoglycan synthesis, collagen synthesis, osteoblast proliferation, osteoclast differentiation and matrix mineralisation	MMP-1, MMP-3, MMP-13, IL-6	MMP-13

Continued on next page

Leptin	Chondrocytes, white adipocytes	Regulating chondrocyte proliferation, proteoglycan synthesis, collagen synthesis, osteoblast proliferation and ossification	MMP-1, MMP-3, MMP-13, IL-1β, IL-6, TNFα	FGF
Resistin	White adipocytes	Regulating osteoblast proliferation and osteoclast differentiation	MMP-3, MMP-13, IL-6, TNFα	Unknown
Visfatin	Visceral adipocytes	Regulating chondrocyte phenotype, proteoglycan synthesis, collagen synthesis, osteoblast proliferation and osteoclast differentiation	MMP-3, MMP-13, IL-1β, IL-6, TNFα	Unknown

MMPs	Main source	Role in OA	Positive feedback	Negative feedback
MMP-1	Chondrocytes, macrophages, synovial fibroblast	Breaking down interstitial collagens	Unknown	Unknown
MMP-3	Chondrocytes, macrophages, synovial fibroblast, osteoclast	Degrading the proteoglycan molecule, aggrecan, collagen fibronectin, laminin and elastin	Unknown	Unknown
MMP-13	Chondrocytes, macrophages, synovial fibroblast	Degrading the proteoglycan molecule, aggrecan and collagen	Unknown	Unknown

2.4 Mathematical modelling of inflammation in OA

Inflammation can be described as a complex homeostatic system [105], hence experiments may not be allowed to easily control or capture dynamical variables with constraints of samples, methods, tools and laboratory environments. Mathematical approaches [106–109] are capable of unravelling the dynamical mechanism of inflammation involved in complex interactions between spatial and temporal scales. In the context of emerging specific modelling methods, Kohl et al. [106] stressed that systems biology is a tool that aims to interpret the characterisation of biological entities and their interacting mechanisms underneath a regulatory system, other than a research field. The determination of mathematical framework generally depends on either biological data or biophysiological knowledge, thereby, the classification of mathematical modelling methods is commonly differentiated by the purpose and the length scales of established models with respect to specified regulatory systems. Correspondingly, there are two predominant strategies [107, 108, 110, 111]: mechanistic modelling strategy and data-driven strategy. The former is widely employed for modelling the regulatory networks including inflammation in different physiological levels [112].

Mechanistic models of inflammation generally rely on the regulatory networks derived from convinced cellular or molecular responses and mechanisms. Namely, the mechanistic modelling strategy is generally mapped out on the basis of reported biological information, hence it is also regarded as a knowledge-based approach [111] or mechanism-based method [108] responsible for mathematically modelling regulatory networks. Despite diverse definitions of the mechanistic modelling strategy in the context of disparate biological systems, the framework of mechanistic models for inflammation should include three main dependencies [113] in a broader context (Figure 2.10), which leads to a wide range of the granularity and complexity of the analysis on the inflammation system. The above classification is not rigorous in the modelling framework, namely, various approaches and models may be integrated depending on the ultimate goals [114, 115]. In general, in silico models are developed from the conceptual system of a specified physical reality, thereby, the mechanistic modelling strategy is narrowly referred to as the modelling methods employed for the development of computational models of conceptual inflammation systems in this section. The comprehensive elucidation and discussion on various mechanistic models of inflammation have been already provided by Scheff, Kamisoglu and Androulakis [113]. Due to the complexity and multi-scale characteristic of inflamma-

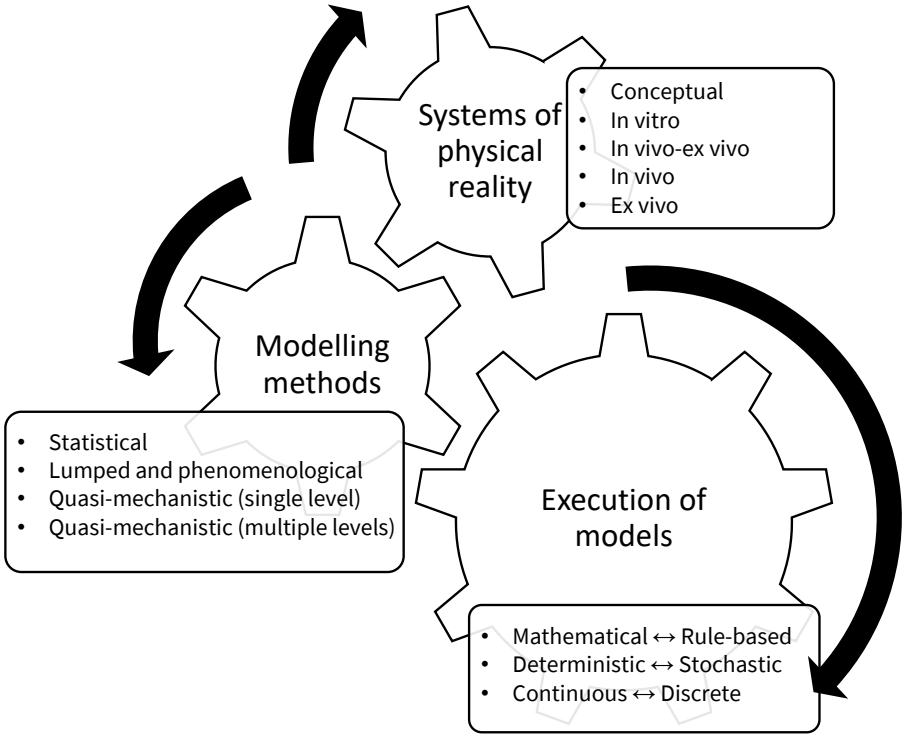

Figure 2.10: *A mechanistic modelling framework of inflammation, reproduced from Scheff, Kamisoglu and Androulakis [113] with permission.*

tion in reality, conceptual quantitative models [116–129] have been broadly used to unravel the underlying mechanism of inflammatory response implicated in actual molecules or cells in a mathematical manner. In the view of mathematical modelling of dynamics, Stalidzans et al. [110] have summarised the mainstream methods employed in mechanistic models along with different applications at multiple scales. In contrast, Eftimie et al. [130] emphasised a series of specific mathematical approaches (Figure 2.11) in a narrower context of immunology. With respect to mechanistic models of inflammation, the applications of ordinary differential equations (ODEs), partial differential equations (PDEs) and agent-based models (ABMs) have been highlighted by Vodovotz et al. [107].

2.4.1 ODE-based model

ODEs have been already widely used to analytically describe the dynamical system where variables determined by entities that encompass functional molecules and cells evolve with continuous time. On the one hand, deterministic equations are conducive to parametrising the dynamics system of OA inflammation dependent

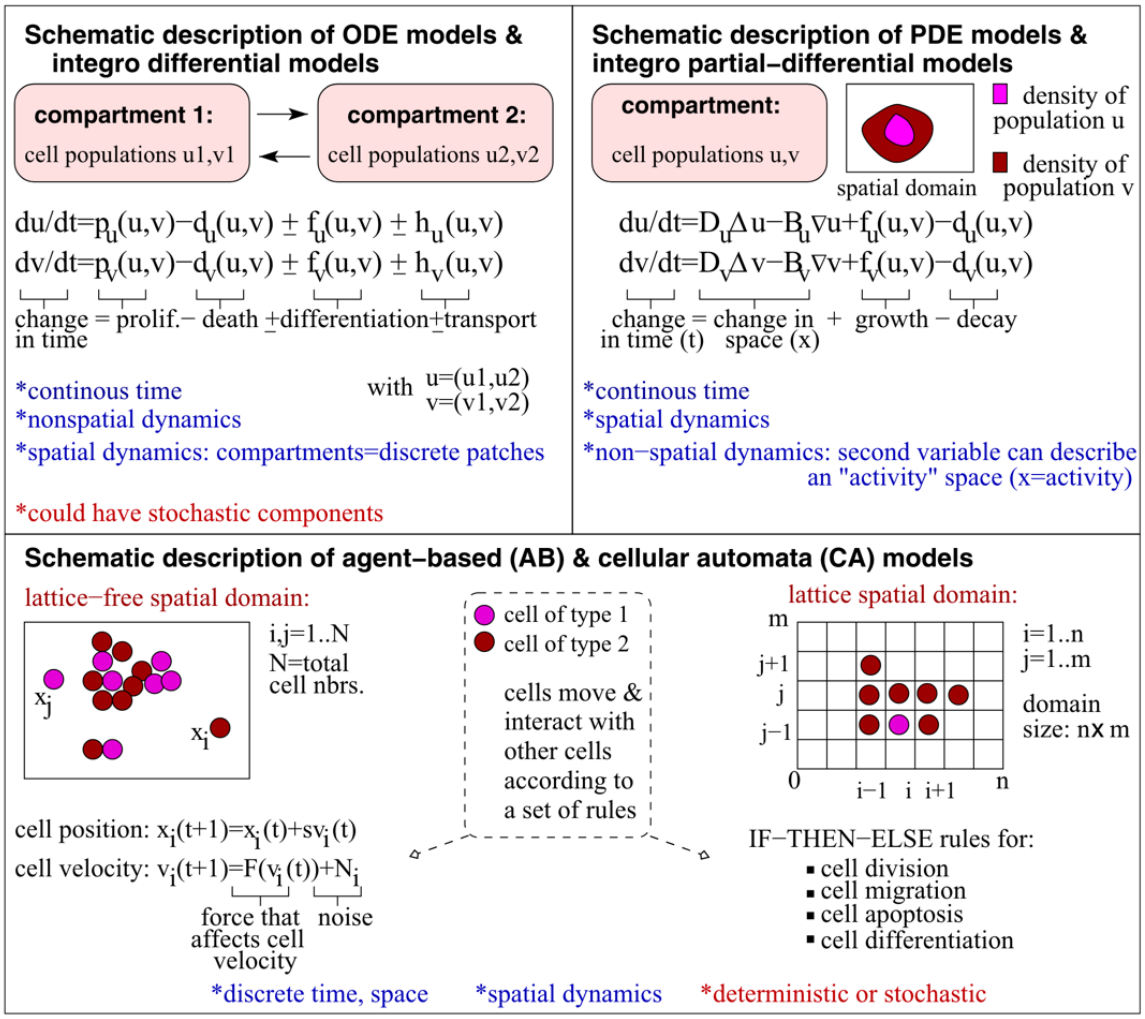

Figure 2.11: *The schematic depiction of mathematical alternatives used in mechanistic models, reused from Eftimie et al. [130] under CC BY 4.0.*

on biological knowledge or experimental data so that the steady states and stability can be captured for the investigation of system behaviours at a wide temporal scale. On the other hand, the spatial interactions are ignored between cells and molecules, hence the geometrical degeneration of the knee joint constituents can not be manifested. In the cases where the temporal evolution is solely considered, the ODE-based model is an efficacious tool in dynamic systems with complex variables in spite of the drawbacks mentioned above.

Kumar et al. [116] first presented the generic dynamics of acute inflammation by establishing ODEs that represented interactions of a pathogen group and two inflammatory mediator groups in response of the infection. The simplicity of the acute inflammation model may not be able to strictly exemplify the reality, nev-

ertheless, five main clinical manifestations (health, recurrent infection, persistent inflammatory infection, persistent non-inflammatory infection and severe immune deficiency) have been correspondingly presented while varying estimated parameters in the model. The sensitivity of parameters is in part affected by the final inflammatory response of infections caused by disparate bacteria. Similarly, Herald [117] derived a general model of chronic inflammation in the presence of pathogens that therein represented the stimulus. The initiation of inflammation is dependent on the different equilibrium states (health, inflammation, infection) altered by key parameters. Particularly, the population of macrophages has been highlighted through bifurcation analysis, and the chronic inflammation could be induced by non-aggressive bacteria or feedback of inflammatory cytokines even after the elimination of infections. The general inflammation models implicated in the role of macrophages have been reviewed by Dunster [118], the use of mathematical techniques was also suggested in order to explore the biological system behaviours at a prolonged time scale of chronic inflammation. These models demonstrate the applicability of ODEs in modelling complex inflammatory responses within a predefined temporal framework.

Contemporarily, the number of ODE-based models of dynamics specific to OA inflammation is exiguous. Baker et al. [119] proposed a four-variable ODE-based model characterising the interactions between inflammatory mediators and products of cartilage degradation, which is derived from a generic ODE-based model of RA [120] solely including pro- and anti-inflammatory cytokines. In particular, a damage factor, i.e. fibronectin fragments, was for the first time introduced as a stimulus of inflammatory response in the extended ODEs. This enables the simulation of dynamic interactions between inflammatory processes and tissue injury. Although applying consecutive doses of anti-inflammatory cytokines and MMPs inhibition was shown theoretically effective to OA treatment in the dynamical system, the mathematical model has not been validated and the estimated parameters are uncertain due to the limited clinical and experimental data. Recently, Rahman et al. [127] developed a complex modelling framework of the virtual cartilage, where ODEs of biochemical regulations were integrated with a tissue constitutive model to simulate the effects of mechanical stimulus on cartilage degradation. Despite the lack of subject-specific data on parameter estimation, this model was validated by comparing computational predictions and experimental quantifications of cartilage loss. This study reflects the appropriate assumptions of minimally essential signalling pathways and cartilage mechanics in modelling inflammation and mechan-

ical stimuli in cartilaginous environment. In addition, there are a few integrative network-based models [128, 129] formulated to a continuum dynamical system by ODEs. These network-based models contribute to understanding cellular signalling interactions and simulating the causal relationships between signalling pathways and tissue microenvironment. However, they extensively rely on prior knowledge and biological data of the OA regulatory network. Conflicts and inconsistencies in literature may introduce uncertainty in defining interactions of signalling pathways, thereby complicating the construction of the regulatory network when developing a mathematical model.

When ODE-based models specifically describing the inflammation of OA are missing, it might be ponderable to review previous works with regards to the joint degeneration during OA or inflammation models specified for other clinical phenotypes. Pollatschek and Nahir [131] modelled OA and the deterioration rates of biological factors using ODEs. Since the interactions of critical factors in different levels are complex and the larger number of considered variables leads to a more adequate explanation of the dynamic system, the reduced model might not allow the precise prediction of changes in material properties against time during OA. However, the model shows that the potential tool, mathematical modelling, could be likely used for predictive analysis of diseases. An elevated number of ODE-based models have been indeed established with respect to various diseases or general immune responses in particular for inflammation dynamics in the context of RA [120], atherosclerosis [121], traumatic brain injury [122] and lung infections and injuries [125, 126]. For instance, a simplified ODE-based model applied to investigate the inflammation mechanism of atherosclerosis has been developed by Ougrinovskaia et al. [121]. The model excludes specific cell concentration, and instead focuses on two characteristics of the lesion described by modified low density lipoproteins (LDLs) and activated macrophages. Accordingly, the interactions between lipid carriers and immune cells have been analysed during the inflammatory response, which is nevertheless limited by the spatial scale excluded in the ODE-based model. Moreover, Vaughan et al. [122] proposed a mathematical framework of neuroinflammation including specific inflammatory cytokines (IL-1, IL-12, IL-10 and IL-4), microglia (M1 and M2) and a tissue damage indicator in order to describe the acute neuroinflammation after brain injury. The calibration of the ODE-based model encompassing seven variables was carried out based on the clinical data classified into three different patient cohorts, which contributed to the investigation on the relations between acute neuroinflammation

mechanism and traumatic brain injury outcomes. Despite the calibration, the observed results might differ in altered theoretical frameworks on the purpose of prediction along with inflammatory progression or clinical interventions. The authors thereby stated that they tailored their modelling strategies in order to fit the pathophysiological consensus.

Mathematical techniques developed to reveal the mechanism of lung inflammation have been reviewed by Cantone et al. [125] whilst the potential capacity of the hybrid modelling strategy was emphasised. In contrast, Minucci et al. [126] collected representative models grouped by biological contexts instead of modelling approaches classified by identical modelling patterns. The inflammation mechanism may differ in disparate diseases so that the paradigms of reviewing mathematical frameworks or models specific to clinical problems are preeminently worthwhile. Thus far, there is nonetheless no contributed review on modelling OA inflammation due to the lack of previous research. The recent transition of consciousness that OA is a multifactorial disease may be also causative of the fact that research on the inflammation dynamics of OA emerges recently. The ODE-based models of inflammation mentioned above are summarised in Table 2.2.

Table 2.2: *ODE-based models of different inflammation systems.*

Conceptual system	Model type	Variables	Reference
Deterioration in OA	ODE (8)	Microfractures, compression modulus, tensile fracture stress, disruption of cartilage, shock absorbance of cartilage, enzyme contents, proteoglycan contents, water content	[131]
Acute inflammation	ODE (3)	Pathogen, early pro-inflammatory mediators, late pro-inflammatory mediators	[116]
General inflammation	ODE (4)	Macrophage, pro-inflammatory cytokines, anti-inflammatory cytokines, a generic pathogen	[117]
Inflammation at early stages of atherosclerosis	ODE (3)	Macrophage, modified LDLs, internalised lipid content	[121]
Inflammation in RA	ODE (2)	Pro-inflammatory cytokines, anti-inflammatory cytokines	[120]
Inflammation in OA	ODE (4)	Pro-inflammatory cytokines, anti-inflammatory cytokines, matrix metalloproteinases, fibronectin-fragments	[119]
Neuroinflammation	ODE (7)	M1-like microglia, M2-like microglia, IL-1β, IL-12, IL-10, IL-4, secondary tissue damage	[122]
Cartilage turnover	ODE (14)	Normal chondrocytes, hypertrophic chondrocytes, necrotic chondrocytes, functional and damaged type *II* collagen, proteoglycan, MMPs, ADAMTSs, TIMPs, active and latent growth factors, active and latent pro-inflammatory cytokines, suramin	[127]

2.4.2 PDE-based model

In order to introduce the spatial evolution of variables, PDEs can be deterministically extended from ODEs [132]. Due to the arising complexity in the simultaneous evolution of both space and time, the analysis of PDE-based model is a daunting task that requires tremendous computing resource. However, the complexity conduces to explore spatial dynamics of inflammation in comparison to the simplicity of ODEs. For instance, the spatial evolution of articular degradation [133–137] or the spatial spread of cells and molecules [114, 138–140] could be analytically investigated by establishing PDEs, which accordingly leads to difficulties in the parameter estimation even if experimental data is available.

Wang et al. [135] further developed a PDE-based model predicting the lesion formation of articular cartilage triggered by a blunt impact based on previous modelling works [133, 134]. This model focuses on the superficial zone of cartilage that the tension of impact loading might be mainly detrimental to. The effectiveness of simplifying massive cytokines into pro- and anti- inflammatory groups was confirmed through simulations of the model. However, the experimental data of specified inflammatory cytokines could be more feasibly collected so as to calibrate indeterminable parameters [136]. Therefore, the decision on whether sorting cytokines as groups might be dependent on the availability of biological data and the complexity of variables with respect to the model. Since plenty of mediators involve in OA inflammation and joint degeneration, functionally classified cytokine groups might be efficacious to initially represent the inflammatory activities of OA in spite of more uncertain parameters that require to be estimated [120]. In current PDE-based models [133–136], the dynamics of chondrocyte and chemical response were captured, in particular for the cartilage degeneration after an injury. Nevertheless, the model could not explore the role of mechanics and inflammation dynamics in those OA cases where an injury is not the predisposing factor.

Overall, the PDE-based models of OA in this section have been summarised in Table 2.3. At present, there is no robust model applied to clinical predictions of OA. Although the PDE-based models are able to simulate the spatial reactions of molecules and cells, the complex parameter set of PDEs requires massive computing resources and the lack of experimental data makes the validation of PDE-based models more challenging compared to ODE-based models. On the contrary to ODE-based models, there are more PDE-based models associated with OA. However, they mostly describe the progression after injuries at tissue level, and there is no model considering the biological roles of obesity. Thereby, there is potential

to use existing PDE-based models for the reference of coupling the temporal and spatial scales through understanding the parameters within those models.

Table 2.3: *PDE-based models of OA. Reactive oxygen species (ROS); Erythropoietin (EPO); Erythropoietin receptor (EPOR).*

Conceptual system	Model type	Variables	Reference
EPO/TNF-interaction in cartilage lesion	PDE (9)	ROS, DMPs, TNF-α, EPO, matrix degradation, healthy cells, catabolic cells, EPOR, apoptotic cells	[133]
Formation of articular cartilage lesion	PDE (10)	Healthy chondrocytes, catabolic chondrocytes, EPOR-active chondrocytes, necrotic chondrocytes, apoptotic chondrocytes, ROS, DAMPs, TNF-α, EPO, ECM	[134]
Inflammation in cartilage lesion formation	PDE (12)	Healthy cells, healthy cells to be catabolic, healthy cells to produce EPO, catabolic cells, EPOR-active cells, apoptotic cells, necrotic cells, ROS, DAMPs, inflammatory cytokines, EPO, ECM	[135]
IL-1 induced cartilage degeneration	PDE (10)	Chondrocytes, intact aggrecan, degraded aggrecan, stimulus aggrecan, aggrecans, IL-1, intact collagen, degraded collagen, stimulus MMPs, MMPs	[136]

2.4.3 Agent-based model

Different from differential equations, ABM is stochastic and rule-based so that components in a system can be described as agents whose heterogeneous behaviours follow the same defined rules. Whilst there are a few ABMs developed for inflammation [141], the application of ABM is rare for OA. Since simplified rules could result in complex spatial and temporal interactions between agents [125], using ABMs to study OA requires high demands of computing resource and remains challenging. Compared to PDE- and ODE-based models, ABMs could precisely explore the mechanism of cellular metabolism and interactions in spite of the more intensive computation. Above all, the application of ABMs still needs a larger amount of work to be done but there is potential for the translation between cellular dynamics and tissue variations across different scales regardless of the high requirement on computing

costs.

2.4.4 Data-driven modelling strategy in OA

As an emerging strategy to predict system outputs from given datasets, a variety of methods, such as machine learning (ML) [142] and deep learning (DL) [143], have been widely used in the data-driven models. Due to the characteristic that specific mechanism of the inferred system is excluded in data-driven models, this strategy is also named non-mechanistic strategy [110].

The quantity of data is markedly required for the model training, hence the data-driven strategy is becoming superior in the context of growing biomedical data available to be classified. However, it is still challenging to obtain informative data trained for the regulatory network from experiments [111]. In the context of knee OA, the current applications of ML and DL accordingly focus on the prediction of OA risk and the clinical diagnosis rather than molecular regulations of inflammation [144, 145].

It is undeniable that artificial intelligence (AI) techniques exhibit enormous potential on the clinical application of OA [146], however, the AI methods only identifying correlations of inputs and outputs could not explore the exact mechanism of OA progression. Thus, mechanistic models are more capable of understanding the regulations of OA at multi-scales compared to non-mechanistic modelling methods.

2.5 Finite element modelling of the knee joint in OA

Given the consensus that the degeneration of tibiofemoral joint in OA is immediately associated with biomechanics as well as inflammation, measuring mechanical responses of joint constituents is a promising approach to elucidate the tissue variations at a spatial scale. A computational method, Finite Element (FE) method, has been widely applied to examine biomechanical behaviours of various musculoskeletal systems, including the human knee joint. Joint tissues can be discretised into a number of mesh elements connected to mimic the structural characteristics of the knee joint by using FE method, which provides clinical cases with additional engineering benefits. For instance, Erdemir [147] described an open resource of joint modelling (Open Knee) and summarised its applications from the perspectives of biomechanics of the knee joint, mechanism of joint injury and clinical interventions.

A general pipeline of FE modelling of the knee joint is illustrated in Figure 2.12. To develop a subject-specific FE model of the human knee joint, morphological data

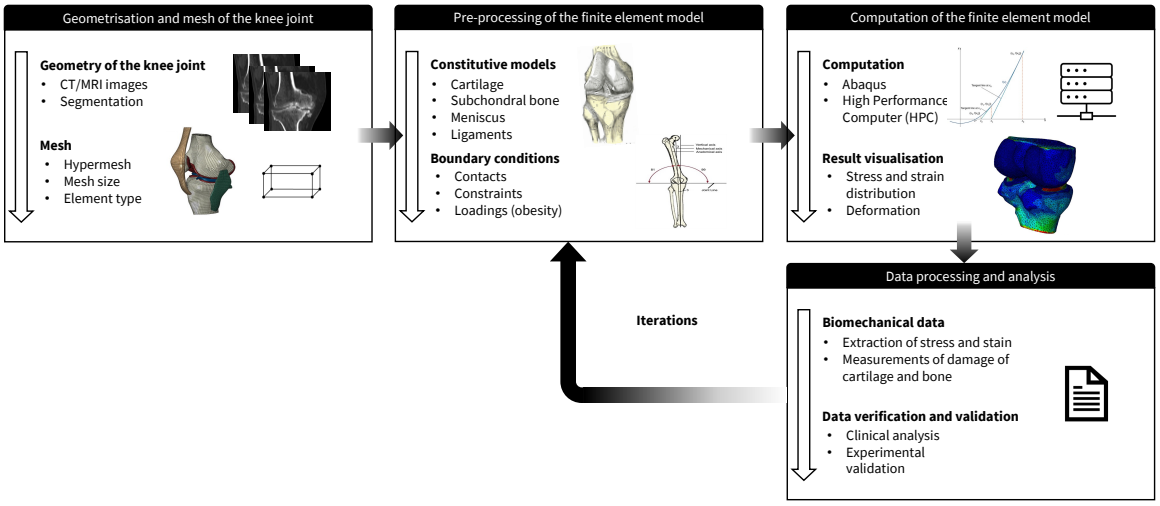

Figure 2.12: *The workflow of FE model development.*

are acquired by scanning images of computed tomography (CT) and magnetic resonance imaging (MRI) at the first step. These imaging data are used to segment different tissue structure and construct the joint geometry. In subject-specific joint models, the geometry is generally converted into a volumetric representation for the discretisation using FE method. According to the mechanical characterisation of the joint structure and the research purpose, meshing strategies can be varied and simplified regarding the volumetric element type and size. After approximating volumetric geometries to discretised mesh elements, constitutive models of different joint tissue materials are determined to describe their mechanical behaviours. To simulate the biomechanical response of the joint, loading and boundary conditions are implemented based on the discretising domain and constitutive models. Although the development of FE models of knee started from the late twentieth century [148, 149], challenges still remain regarding model validation and fidelity (geometric representation and tissue material). Model validation is an essential procedure to establish and improve the credibility of a computational model for further applications [150]. However, computational models are generally validated based on limited experimental data obtained from specifically designed scenarios. Therefore, it is critical to assess the extent to which the validated model is credible. In this regard, Cooper et al. [151] evaluated the model validation strategies of the knee for sensitivity studies, in vitro and in vivo representations. According to the research purposes, the strategies of model validation can be adjusted to provide credible predictions that are challenging to measure experimentally. In addition, it is necessary to consider the model fidelity for effective validation. A compre-

hensive review [152] has specifically summarised the FE studies on how knee joint is progressively degenerating along with OA. In this review, the authors suggested that the state-of-the-art FE modelling might be benefited by the combination with auto-segmentation technologies empowered by machine learning, thereby fast and precisely predicting the risks of OA initiation. However, the difficulties of noninvasively acquiring patient-specific tissue properties still exist and complex constitutive models also lead to computing challenges [153, 154]. Peters et al. [154] thoroughly evaluated the tissue material properties of the human tibiofemoral joint, highlighting a high variability of material properties within healthy and osteoarthritic joints. Although it is challenging to acquire detailed material data from experiments, the integration of subject-specific parameters is important to establish a realistic joint representation when determining constitutive models. In addition, appropriate modelling complexity of tissue materials can improve the efficiency of predicting the mechanical behaviours using generic values of constitutive models [155]. At present, there is no applicable FE model or pipeline in the clinical prediction of OA, hence the improvement of FE modelling methods is also needed on the iteration pipeline of updating FE models besides the segmentation in pre-processing.

2.6 Effects of obesity on the joint biomechanics in knee OA

Obesity can result in the larger mechanical loads to the knee joint at tissue level so as to increase the risk of OA, as evidenced by previous studies [156, 157]. Messier et al. [156] first investigated the association of body weight with the knee joint loads in OA (forces and moments). They found that the loads of the knee joint could be elevated by four times along with one unit increase of the body weight during walking. In turn, Aaboe et al. [157] argued that the proportion between weight loss and the reduction of joint force is more likely to be 1:2.2 instead of 1:4 by controlling the walking speed in the gait analysis. Regardless of the credit of the cohort used for their studies, the experimental validation nevertheless remains uncertain regarding motion capture and anthropometric data. Notably, the joint contact force considerably varies in different activities even though the body weights of subjects in vivo are at the same level [158], which might be due to the difference of BMI.

The systemic and chronic influence of obesity can also affect joint biomechanics in the pathogenesis of knee OA. In addition to excess joint load, obese population has a higher risk of varus malalignment and muscle dysfunction [47], which can lead

to load concentration on the medial compartment and reduce joint stability. To further study the biomechanical effects of obesity on the knee OA, computational approaches have been used. In an early computational study, Boyd et al. [159] suggested that increasing joint load could mainly cause the anterior and central stress concentration in the medial compartment. Furthermore, it has been reported that obesity is associated with a medial shift of cartilage contact locations [160] and an increase in the knee adduction moment (reaching peaks of approximately 62 Nm with increasing BMI up to 64 kg/m^2) in the lower arch group [161], implying that the high risk of OA in the medial compartment [162] may be attributed to the obesity-related biomechanical characteristics. In a comparable study of knee joint biomechanics, MacLean et al. [163] also found that obese young adults tended to reduce walking speed so that a greater knee adduction moment was exhibited due to a longer stance duration. Additionally, musculoskeletal and FE models of the knee joint were integrated to predict the biomechanics of muscles and cartilage contact in obese subjects [164, 165], indicating that obesity could lead to a significant increase in contact stresses with variations in muscle activation patterns.

Whilst the effects of obesity on the biomechanics of the knee joint are accumulatively probed, there are only a few FE studies [166–168] on how obesity is involved in OA by employing the same cartilage degeneration framework [169]. Specifically, Klets et al. [166] examined the cumulative stress of cartilage that represents the degeneration potential in a cohort where subjects are classified by the obesity level. Likewise, by calculating cumulative stress of cartilage, Liukkonen et al. [167] evaluated the impact of the weight loss resulting from bariatric surgery on the OA in particular for the degradation of cartilage. Both studies illustrate that the loss of body weight is positively correlated with the reduction of cartilage degeneration. However, the latter identifies that the correlation is not proportional and the weight loss predominantly alters the flexion displacement and rotational moments to a lower level in consideration of the subject specific gait analysis. The gait analysis could mimic the biomechanics of the knee joint during diverse daily activities from a larger scale compared to FE analysis. Thus, the subject-specificity of knee joints plays an important role in predicting cartilage degeneration. Orozco et al. [168] further emphasised that the effect of subject-specific joint geometry might be more considerable than individual gait data in the prediction of knee OA. Current research on the knee joints with OA and obesity only discusses the mechanical loading conditions. The metabolic regulation of obesity is nevertheless ignored in FE models. Therefore, it is needed for the better understanding of OA mechanism and its prediction

to either improve current degeneration algorithm by considering the biochemical effects or develop a computational model coupling joint-tissue level with molecular level.

2.7 Multi-scale modelling of the cartilage degeneration in knee OA

Since OA evolves in the entire knee joint from the molecular level to the tissue level, solely using FE models could not effectively reflect the degenerative changes of the knee OA. Mukherjee et al. [46] have widely reviewed current computational models to study the osteoarthritic changes of the joint including articular cartilage, subchondral bone, ligaments and meniscus. The multi-scale approach incorporating FE models was therein highlighted as a merit strategy to investigate OA mechanisms. In particular, cartilage degeneration is a primary hallmark of OA progression, involving complex physiological and biomechanical networks from the joint level to the cellular level [170]. Specifically, external and inertial loads are generated at the body level during physical activities. To maintain the kinematic and kinetic balance in complex motions, reaction forces and moments of the joint are dynamically regulated through active muscle contraction and internal forces resulting from passive structure restraints of the joint. As a main load-bearing structure, articular cartilage deforms across different layers to distribute the mechanical loadings at the tissue level in dynamic balance of the body. This mechanical distribution is ultimately translated to the reactions of chondrocytes that influence the turnover of cartilage properties at the molecular and cellular levels. Accordingly, multi-scale modelling method is valuable for simulating cartilage degeneration as it can provide the translation between networks at different spatial and temporal scales [171].

The current mainstream multi-scale modelling approaches in knee OA are based on the coupling of two or multiple length and time scales. Halloran et al. [172] comprehensively reviewed the modelling approaches for each tier of resolution within a multi-scale modelling framework of cartilage biomechanics (Figure 2.13). Estimated joint loading and motions from musculoskeletal systems can be integrated into joint-tissue representations to predict the biomechanical characterisations of cartilage at the tissue level according to particular physical motions [173]. As the most frequent daily activity, gait data has been implemented to study biomechanical responses of cartilage in different population, using multi-scale approaches of musculoskeletal and FE models [164, 165, 174–178]. In particular,

Mohout et al. [176] implemented a musculoskeletal-FE modelling approach to quantify the biomechanical variations of cartilage. This proof-of-concept study suggested that the strain in collagen fibril direction and maximum shear strain are potential mechanical biomarkers for identifying knee OA. Moreover, Willems et al. [177] indicated the increased risk of overloading in the medial compartment due to knee geometry and alignment in OA patients. Recently, Zhang et al. [178] developed an advanced musculoskeletal-FE pipeline to translate gait kinematics to mechanical biomarkers (strains and contact pressures) of cartilage. Mechanical outputs from the implementation of this pipeline were able to classify cohorts as OA progressors, non-progressors and healthy controls. However, simulated cartilage biomechanical behaviours are sensitive to the parameter estimation and assumptions in musculoskeletal models. Namely, inappropriate simplifications of musculoskeletal representation may lead to non-physiologic estimation of joint loading as well as tissue mechanical responses. To quantify uncertainty sources in coupling musculoskeletal and FE models, Jahangir et al. [179] recently assessed the effects of six different modelling assumptions on developing musculoskeletal-FE models. These assumptions corresponded to optimisation function, marker placement, tissue property, maximum isometric force and subject specificity of gait data. It was found that the maximum difference of simulation results could reach nearly 61% when formulating different assumptions. In addition, the significance of personalised gait data was emphasised in the translation of joint loadings and tissue mechanical responses, which is in line with a previous computational study on cartilage degeneration by Orozco et al. [168]. Due to the lack of statistical comparison, the findings could not be universally concluded and validations with a larger sample size are still required. Driven by tissue continuum mechanics of cartilage [180], chondrocyte mechanics [181] and biochemical reactions [22] could be modelled at the tissue-cell level. They reflect the regional constitutive responses in the mechanoadaptive environment of cartilage. Since the mechanism of OA is heterogeneous, the role of mechanical and biochemical factors remains unclear in cartilage degeneration. The determination of modelling strategies need to consider prior knowledge, research purpose and the complexity in the corresponding spatial and temporal domain.

To simulate cartilage degeneration, Kapitanov et al. [137] employed a multi-scale approach based on a previous mathematical model [135]. The cascade of cells, chemokines and mechanical responses were analysed in the context of post-traumatic OA (PTOA), showing an increased level of cytokines proximal to the

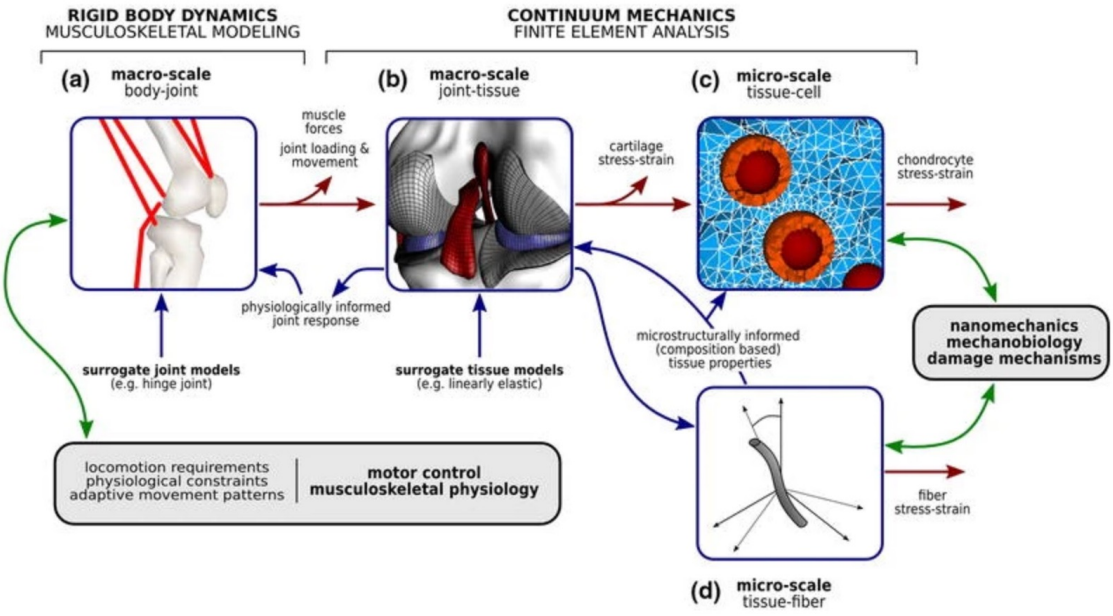

Figure 2.13: *The schematic multi-scale modelling framework of cartilage degeneration, reused from Halloran et al. [172] with permission.*

injury location. The initial density of healthy and necrotic cells was determined by the strain resulting from the implementation of a blunt impact on the cartilage. The introduction of FE results was able to couple the biochemical response with mechanical response at cellular and tissue scales, which provides a novel strategy to anticipate OA development after trauma (a blunt impact). However, the estimation of numerous parameters might be a daunting task for the complex spatial interactions, and the acceptable accuracy of the multi-scale framework necessitate continuous iterations. Similarly, a multi-scale model was proposed by Eskelinen et al. [182] to investigate the biochemical and biomechanical effects on the loss of FCD in cartilage during PTOA. It was found that the loss of FCD was significantly higher near the tissue injury with degradation. In this model, the variations of FCD were primarily measured under the biochemical responses of IL-1 [136] and the mechanical stimulus of overwhelmed shear strain [183]. Despite no explicit inclusion of cell death, parameters representing the production and decay of FCD are implicitly relevant to cell concentration as the abundance of cells decides the number of cytokine receptors and secretion of proteins. Different from the model of Kapitanov et al. [137] where FE results were only used for initial conditions of the PDE-based mechanobiological model, the approach of Eskelinen et al. [182] iteratively coupled the FE model that contributes to describing the loss of FCD around cartilaginous lesion resulting from abnormal shear strain. By

doing this, the degradation of cartilage could be simulated within both evolutionary molecular reactions and progressive biomechanical stimuli. Following on the work by Eskelinen et al. [182], Orozco et al. [184] conducted a feasibility study of the model application in cartilage degeneration after the injury and reconstruction of anterior cruciate ligament. In this study, the biomechanically and biochemically driven loss of FCD was predicted, demonstrating the capability of this multi-scale model to provide the mechanistic explanation of the mechanisms underlying FCD loss. However, model simplifications lead to a lack of subject-specificity and limited incorporation of inflammatory mediators. Extensive acquisition of subject-specific parameter values remains a major challenge in complex multi-scale models.

Therefore, minimally essential estimation of either the number of variables or parameter values is needed, which is the computational strategy applied to recent multi-scale models [127, 182, 184, 185]. In particular, Rahman et al. [185] developed a multi-scale modelling framework of cartilage degeneration by incorporating the minimal number of the critical parameters in biomechanical and biochemical regulations. The evolution of cartilage thickness and composition was predicted across different layers, and the important role of oxidative stress in cartilaginous tissue was highlighted. Different from this minimally essential multi-scale model, Segarra-Queralt et al. [129] proposed a multi-scale model based on a regulatory network where signalling pathways of chondrocytes in OA were extensively included. In this model, the role of different mechanical environments integrated with inflammation was studied by formulating a continuous dynamical system of chondrocyte mechanotransduction, showing a degrading pattern due to inflammation and injurious mechanical stimuli. Different mechanical stimuli, including cyclic dynamic compression, osmotic pressure, hydrostatic static compression, high compression and tensile strain, were represented by perturbations in the dynamical system to activate the corresponding mechanoreceptors. Despite the detailed multi-scale regulatory network, quantifying the transduction of mechanical loads is still limited between tissue and chondrocyte in the spatial and temporal domain. In fact, in addition to aforementioned multi-scale models of OA, there are several computational models [169, 186–189] coupling the damage of microstructure at the tissue-cell level with macro tissue constitutive model to simulate cartilage degeneration. In these models, mechanobiological properties of cells are not explicitly modelled to overcome the complex spatiotemporal interactions. Instead, the degenerative process of cartilage is characterised by damage functions in material constitutive model [190]. Particularly, Hosseini et al. [186] and Elahi et al. [189] indicated that damage to the

ground substance and collagen can mutually influence each other through modelling cartilage compositions. In addition, Párraga Quiroga et al. [187] studied the strain-oriented damage mechanisms of cartilage, showing a positive correlation between location-specific collagen damage and strain rate in contrast to the ground substance.

The wider biological applications of different systems approaches have been summarised by Mueller et al. [191] in the context of OA. However, the integration of prior knowledge, such as interactions of signalling pathways and mechanotransduction, is still challenging in coupling different scales. As so far, a comprehensive multi-scale model that integrates mechano-biological-chemical regulations, in particular for obesity-related mechanisms, is lacking to simulate variations of the knee joint across the joint-tissue and tissue-cell levels. Moreover, the applications of current computational models in clinical predictions and monitors of OA progression are still limited. Thus, it is important to emphasis the potential contribution of multi-scale computational models on the classifications of the heterogeneous pathways and therapeutic targets in OA onset and progression.

Chapter 3

Mathematical modelling of inflammatory process and obesity in osteoarthritis

The first mathematical model of inflammation and obesity in osteoarthritis (OA) is developed in this chapter, forming the inflammatory regulation of obesity for the integrative multi-scale approach in OA. This model includes five variables representing five inflammatory mediator groups in OA inflammation. The regulatory pathways of adipokines are for the first time introduced in a computational model of OA. This model is non-dimensionalised, contributing to the investigation on the dynamics of obesity-associated OA inflammation through parameter sensitivity and bifurcation analysis. Due to limited data on the numerical relation between adipokine production and measures of obesity, BMI is used as the representative metric for categorising obesity in the development of this model. In the subsequent chapter, where this model is parameterised in its dimensional form, the limitations of using BMI as the metric of adiposity in simulating inflammatory activities over time are further discussed. This chapter focuses on the model formulation and the analysis of system dynamics to provide a mathematical framework for simulating obesity-associated OA inflammation.

The work presented in this chapter has been published in PLoS One (2025) under CC BY 4.0, with minor adaptations for consistency and readability with the thesis format: J. Lai and D. Lacroix, "Mathematical modelling of inflammatory process and obesity in osteoarthritis", PLOS ONE, vol. 20, no. 6, p.e0323258, Jun. 2025, doi: 10.1371/journal.pone.0323258.

3.1 Introduction

As a multi-factorial disease of the entire joint, OA progressively causes the loss of joint function and pain along with tissue degeneration due to the unbalance of metabolic chronic inflammation and abnormal biomechanics. Concomitantly, disability and comorbidities occur with OA development [2], imposing significant medical burden worldwide [3, 4]. The number of patients with OA worldwide will reach more than 600 million by 2050 [5]. Obesity is a predominant risk factor aggravating the inflammation and load within the joint [103, 192, 193]. The rapidly increasing prevalence of obesity [39] will lead to severe challenges on remitting medical burden from OA. Obesity significantly rises the joint force and undermines the biomechanics of the joints [156, 157, 163, 194], whereas the awareness of the regulatory mechanism of obesity-associated OA inflammation is still limited. Regardless of that, the best strategies to manage the disease are still prevention and intervention of early OA such as controlling body weight and physical activity [7, 195, 196]. Compared to obesity commonly measured by body mass index (BMI), adiposity refers to the amount of body fat that plays a pivotal role in the inflammatory process [41]. Physical activity level (PAL) and nutritional control can reduce adiposity and increase muscle strength, resulting in weight loss for obese individuals [197]. Physiological loading is sensitive to body weight within the load-bearing joints [198]. However, conclusive evidence linking physical activity to the reduction of body weight is absent [44, 199]. This suggests that exercise might not have a direct benefit on the joint by reducing the inherent mechanical loading. Instead, physical activity might exert a more significant impact on modulating the serum level of inflammatory mediators [200, 201] in the context of OA. The variation of adiposity due to physical activity might be responsible for this impact on OA inflammation.

Low-grade inflammation is present at early stage of OA prior to structural changes [18, 20, 83], though no evidence shows that inflammation predisposes to the onset of OA as various risk factors, such as age, gender, genetics, obesity, nutrition and mechanics, might concurrently trigger OA. In general, the presence of inflammation can recruit specialised cells to repair the rupture tissue of cartilage. The lack of vascular system nevertheless results in the unbalance of inflammatory metabolism [49, 65, 202, 203], hence cartilage tissue is eventually degraded along with chronic inflammation where multiple soluble mediators interact, including pro- and anti-inflammatory cytokines (PICs and AICs) [87], matrix metalloproteinases (MMPs) [102, 104, 204] and adipokines [43, 45, 89,

90]. The potent production of PICs can be activated by the tissue breakdown including fibronectin-fragments (Fn-fs) [205]. As the PIC level increases, MMPs are secreted to catabolise the extracellular matrix (ECM) of the cartilage and AICs are released to reduce the active inflammatory activities. Furthermore, adipose tissue is dispersed across the whole body and it can systemically and locally contribute to the OA metabolism and joint biomechanics [41, 42]. Specifically, adipokines primarily derived from adipose tissue are an important class of soluble mediators associated with OA [42]. Adipokines can stimulate the production of inflammatory mediators such as PICs and MMPs [45, 89, 92–94]. The accumulation of adipose tissue leads to an excess of adipokines, which can be responsible for the metabolic effects of obesity on OA progression.

Computational approaches have demonstrated the potential to mimic the cartilage degradation and inflammatory process [114, 119, 127, 131, 133–138]. However, both mechanistic and data-driven modelling approaches are still limited by the complex molecular and cellular crosstalk. This makes it challenging to explain the precise mechanism of OA. A few attempts [128, 206, 207] are emerging to integrate knowledge-based and data-driven modelling approaches to explain the network of signal transduction of OA. The computation of signal transduction heavily relies on available concluded biological data, thereby underscoring the necessity for incorporating current knowledge of OA [22]. However, parameter complexity escalates with the increased number of signalling pathways [129]. As an alternative to study the role of cytokines in OA inflammation and to reduce the computing complexity, Baker et al. extended a two-variable RA model of cytokines [120] to a general four-variable OA model of cartilage inflammation [119]. Distinct to the autoimmune disease, rheumatoid arthritis (RA) characterised by severe synovial inflammation, OA involves low-grade inflammation due to adaptive and innate immune responses under mechanical stimuli [16]. Although inflammation is found in both diseases, the molecular inflammatory mechanisms are different. This extension provided a representative model with relatively low computational complexity to analyse molecular interplays in particular for those biological regulations lacking sufficient data support. Four characteristics of the inflammation system (homeostasis, persistent inflammation, bistable and tristable inflammation) were found and the uncertainty of estimated parameters to alter the system dynamics were analysed through bifurcations [119]. The four system behaviours represent different susceptibility of individuals to OA, which is based on the determination of parameters. Persistent inflammation is most

susceptible to OA contrary to homeostasis. However, this ordinary differential equations (ODEs)-based OA inflammation model did not consider the inhibition of MMPs [87] and the reacting feedback of adipokines. In addition, the parameter estimation was based on the assumption that the parameters differ in orders of magnitude, whilst the concentration level and half-life of different mediators exhibit considerable variability [208]. This may produce biased conclusions due to the limited measurements of molecular parameters. By contrast, Rahman et al. [127] recently proposed a mathematical framework of cartilage degradation where the mechanical stimuli, cellular and molecular behaviours are coupled and parameters are estimated based on selected experimental data. This framework was validated by simulating the evolution of cartilaginous constituent loss according to past reported experiments. Due to the low availability of cellular and molecular data, high variability still exists in the setup of parameters that determine the outputs in the above mechanistic models. Namely, the uncertainty analysis of computational deterministic model is crucial for improving the reliability by using prospective in vivo or in vitro data.

Aforementioned mathematical models [119, 127] are relatively general compared to validated models specific to cartilage lesion formation [134–138]. Nevertheless, the latter might not be able to unravel the mechanism of early OA inflammation since the source of injury (either mechanics or inflammation) that leads to the cartilage defects cannot be identified. In addition, none of them considers the regulatory mechanism of adipokines that are the critical mediators stimulating OA inflammation due to obesity. Based on the previous inflammation model of cartilage [119], a general five-variable mathematical model of adipokine-mediated inflammation was developed in this study and the aim was to evaluate the molecular regulations of cartilage inflammation under the reactions of adipokines.

Compared to the previous four-variable model [119], the feedback from adipokines and the inhibiting pathways of anti-inflammatory cytokines were appended to this five-variable model. BMI was introduced to measure adiposity. Meanwhile, physical activity and daily nutrition, regulating the amount of adiposity, were accounted to control the production rate of adipokines. Local sensitivity analysis and bifurcations of estimated non-dimensionalised parameters were conducted to verify this model and to evaluate the regulatory mechanism of inflammation dynamics by adipokines. In particular, the evolution of the inflammatory process was studied by implementing different physical activity interventions within the dimensionless model.

3.2 Methods

3.2.1 Regulatory network of inflammation

Five mediators regulating the inflammation are identified as the variables in the mathematical model. PICs and AICs, MMPs and Fn-fs, denoted respectively by P_c, A_c, M, A_d, F, interact to regulate inflammation in OA [83]. On this basis, adipokines dependent on obesity and exercise can stimulate inflammation through the concurrent upregulations of PICs and MMPs [100]. An inflammatory network of five variables (P_c, A_c, M, A_d, F) was constructed to represent stimulation, inhibition, natural production and decay of each of the variables (Figure 3.1).

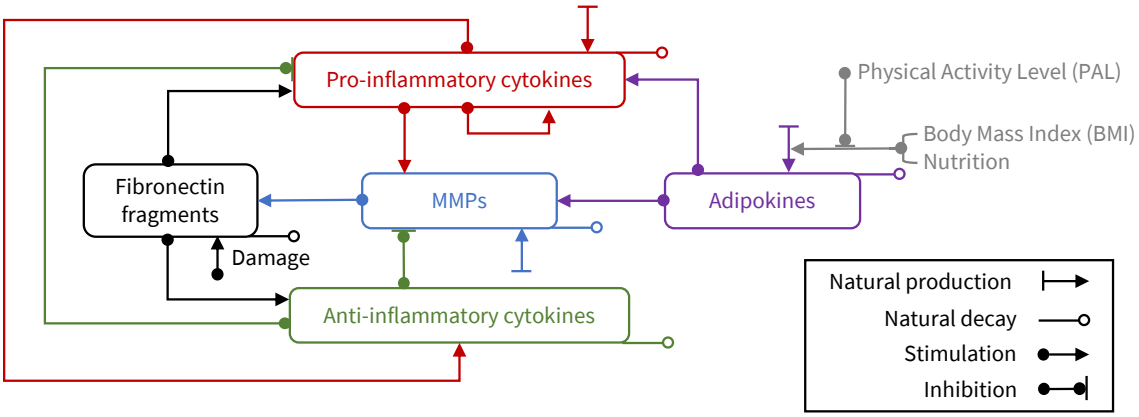

Figure 3.1: *Schematic inflammatory network of cartilage including the concentrations of PICs, AICs, MMPs, adipokines and Fn-fs. Adipokines stimulate the production of PICs and MMPs as a source mediator of which concentration is regulated by adiposity. Adiposity can be varied by the system status including PAL, BMI and nutrition. Each mediator group has a rate of natural decay and the rate of production consists of the production from background, stimuli and inhibitors. Since Fn-fs are only released due to the deconstruction of tissue, the production is determined by mechanical damage and the catabolism of MMPs. Although other damaging products exist, Fn-fs are included in the network as a group of inflammatory mediators that directly regulate cytokine production.*

3.2.2 Enzyme kinetics

Hill functions [209] were used to simulate the enzyme kinetics that is the reactive production rate of one mediator regulated by other mediators and to describe the nonlinear reduction of adipokines due to nutrition and physical activity:

$$H^{stimulus}\left(var_s\right) = MPR \times \frac{var_s^n\left(t\right)}{SC^n + var_s^n\left(t\right)} \tag{3.1}$$

$$H^{inhibitor}\left(var_i\right) = TPR \times \frac{SC^n}{SC^n + var_i^n\left(t\right)} \tag{3.2}$$

where MPR is the maximum driven production rate of the mediator regulated by the stimulatory mediator var_s, and TPR is the total production rate in the pathways inhibited by the mediator var_i. The saturation constant is SC, which is the concentration of the regulated mediator. At concentration SC, the production rates are half of MPR and TPR due to the saturated effects. The Hill coefficient n describes the cooperativity of the targeted mediator. Namely, the change of the slope for the increase or decrease of the production rate can be altered by tuning the Hill coefficient. In inflammatory regulations, each pathway normally involves multiple receptors; therefore, the value of Hill coefficient might equal or exceed 2. To reduce the complexity, it is assumed that n equals 2 in this model as the system behaviours exhibit similarity when Hill coefficients are greater than 2, which is consistent with Baker et al. [119]. The inhibition is essentially signalled by the binding between ligands and cellular receptors. Since the receptors of MMPs, PICs and AICs are distinct [87, 104], the inhibition of AICs is applicable to all production terms of each signalling pathway regardless of cell sources. In the application of Hill functions, TPR is accordingly the total production rate by summing up a natural production rate with the driven production rates, as shown in Equations (3.3) and (3.5).

3.2.3 Mathematical formulation

The production of PICs is inherently at a low level to facilitate normal ECM remodelling, leading to a term of natural production. This metabolic activity is rigorously controlled by the regulated production and the natural decay under the healthy homeostatic background. In this model, the secretion of PICs is stimulated by itself, adipokines and Fn-fs but inhibited by AICs. The production terms are additive as the activated receptors are different in those pathways [87]. Thus, the production of PICs is formulated to Equation (3.3).

$$\frac{dP_c(t)}{dt} = \left[C_0 + C_1 \cdot \frac{P_c^n(t)}{C_2^n + P_c^n(t)} + C_3 \cdot \frac{A_d^n(t)}{C_4^n + A_d^n(t)} + C_5 \cdot \frac{F^n(t)}{C_6^n + F^n(t)}\right] \cdot \frac{C_7^n}{C_7^n + A_c^n(t)} - D_1 \cdot P_c(t) \quad (3.3)$$

In turn, AICs are produced due to the increase of PICs and Fn-fs in order to counteract inflammation and maintain the homeostasis of tissue remodelling. Since the release of AICs is mainly determined by cells from the activation of immune system, there is no natural production term compared to PICs that are secreted by

immune cells as well as local cells in cartilage [87]:

$$\frac{dA_c\left(t\right)}{dt} = C_8 \cdot \frac{P_c^n\left(t\right)}{C_9^n + P_c^n\left(t\right)} + C_{10} \cdot \frac{F^n\left(t\right)}{C_{11}^n + F^n\left(t\right)} - D_2 \cdot A_c\left(t\right) \tag{3.4}$$

As the enzyme degrades the cartilage tissue, MMPs are upregulated by the signalling of PICs and adipokines with a low natural production, which could be inhibited by AICs to reduce the catabolic effects of MMPs [104]. Similar to PICs, the inhibition of AICs is applied to all production terms as shown in Equation (3.5).

$$\frac{dM\left(t\right)}{dt} = \left[C_{12} + C_{13} \cdot \frac{P_c^n\left(t\right)}{C_{14}^n + P_c^n\left(t\right)} + C_{15} \cdot \frac{A_d^n\left(t\right)}{C_{16}^n + A_d^n\left(t\right)}\right] \cdot \frac{C_{17}^n}{C_{17}^n + A_c^n\left(t\right)} - D_3 \cdot M\left(t\right) \tag{3.5}$$

Adipokines are mainly released from adipocytes, so the number and size of adipose cells presumably determine the production of adipokines. In general, an individual normally maintains a constant number of fat cells regardless of the weight loss since adolescence but the size increases due to the dramatic weight gain [210]. Proper physical activity intervention can induce the reduction of adiposity, whereas there is no strong evidence indicating that the number of adipocytes concomitantly decreases [211]. The present consensus is that physical activity is able to reduce the size of fat cells as the mass of adipose tissue [199, 211]. This leads to a background production term due to the adipocyte number, a decay term dependent on the concentration and a variable production term determined by BMI, nutrition and PAL:

$$\frac{dA_d\left(t\right)}{dt} = C_{18} + \left[C_{19} \cdot \ f\left(BMI^{meas}\right) \cdot \frac{DailyCal}{BMR \cdot PAL}\right] \cdot \frac{C_{20}^{nex}}{C_{20}^{nex} + A_d^{nex}\left(t\right)} - D_4 \cdot A_d\left(t\right) \tag{3.6}$$

where $DailyCal$ is the daily intake of calories, BMR is the value of basal metabolic rate (BMR) and PAL is the level of physical activity. The function of BMI, $f\left(BMI^{meas}\right)$, is built to assume the adipokine production due to adiposity level:

$$f\left(BMI^{meas}\right) = \frac{BMI^{meas}}{BMI^{std}} \tag{3.7}$$

where BMI^{std} is the standard value of BMI at which the inflammation system is at the normal level of body weight. Although obesity is classified by incremental ranges of BMI in Table 3.1 [39], a specific value of 25 is selected in order to measure the assumed proportional correlation [89] between the adipokine production and the measured BMI value, BMI^{meas}.

Table 3.1: *The classification of the obesity level using BMI [39].*

Level of obesity	BMI (kg/m^2)
Nutritional deficiency (ND)	< 18.5
Normal weight (NW)	$18.5 - 24.9$
Overweight (OW)	$25 - 29.9$
Obesity (O)	$\geqslant 30$
Extreme obesity (EO)	$\geqslant 40$

Table 3.2: *The category of PAL [212].*

Level of physical activity	PAL value
Sedentary (S)	$1 - 1.39$
Low active (LA)	$1.4 - 1.59$
Active (A)	$1.6 - 1.89$
Very active (VA)	$1.9 - 2.5$

Since PAL is measured by the proportion of total daily energy expenditure (TEE) to BMR [212], the nutrient term is described as the fraction of the daily intake of calories ($DailyCal$) to the total metabolic rate determined by BMR and PAL. The adipokine production decided by BMI and nutrition is altogether reduced by PAL through the Hill function. To distinguish the coefficient that modulates the effects of physical activity from other Hill coefficients that represent the order of enzyme kinetics, nex is used in Equation (3.6). The coefficient nex and saturation constant C_{20} are controlled by BMI^{meas} and PAL respectively to simulate the nonlinear effects of different exercise levels (Table 3.2) on the adiposity reduction. As nex increases, the reduction gradient of adipokine production due to PAL ascends, namely, the increase of PAL is effective for reducing the production of adipokines when adipokines are nearly or over saturated. Meanwhile, C_{20} determines the saturation of adipokines where PAL reacts on the loss of adiposity. The sensitivity of nex and C_{20} and their correlation with BMI^{meas} and PAL is analysed in a dimensionless manner (Figure 3.2).

Since the level of damage can also induce inflammation, Fn-fs, the biomarker from degraded cartilage tissue upregulates both PICs and AICs [205], is included in this model to measure the damage due to inflammation $(C_{21} \cdot M)$ and excessive

mechanical loading (C_{22}):

$$\frac{dF\left(t\right)}{dt} = C_{21} \cdot M\left(t\right) + C_{22} - D_5 \cdot F\left(t\right) \tag{3.8}$$

3.2.4 Model nondimensionalisation and parameter estimation

For the mathematical analysis, the model is non-dimensionalised by the following scaling:

$$\begin{aligned} P_c\left(t\right) &= C_2 \cdot \tilde{P_c}\left(t\right) \\ A_c\left(t\right) &= C_7 \cdot \tilde{A_c}\left(t\right) \\ M\left(t\right) &= \frac{C_6 D_2}{C_{21}} \cdot \tilde{M}\left(t\right) \\ A_d\left(t\right) &= C_4 \cdot \tilde{A_d}\left(t\right) \\ F\left(t\right) &= C_6 \cdot \tilde{F}\left(t\right) \\ t &= \frac{\tilde{t}}{D_2} \end{aligned} \tag{3.9}$$

where the concentrations of PICs, AICs, adipokines and Fn-fs are non-dimensionalised by the corresponding saturation constants, and the time is scaled by the decay rate of AICs for the convenience of model verification. The concentration of MMPs is scaled to reduce the Fn-fs production.

The formula of parameter nondimensionalisation is detailed in Appendix A, and the non-dimensionalised model is shown in Equations (3.10) to (3.14) and the parameters are estimated based on the previous model [119], as indicated in Table 3.3. Dimensional parameters are described in Appendix B. It is assumed that parameters within the same functional class are of a comparable order of magnitude.

$$\begin{aligned} \frac{d\tilde{P}_c\left(\tilde{t}\right)}{d\tilde{t}} = \Bigg[&\alpha_{BP_c} + \beta_{P_cP_c} \cdot \frac{\tilde{P_c}^n\left(\tilde{t}\right)}{1 + \tilde{P_c}^n\left(\tilde{t}\right)} + \beta_{A_dP_c} \cdot \frac{\tilde{A_d}^n\left(\tilde{t}\right)}{1 + \tilde{A_d}^n\left(\tilde{t}\right)} + \\ &\beta_{FP_c} \cdot \frac{\tilde{F}^n\left(\tilde{t}\right)}{1 + \tilde{F}^n\left(\tilde{t}\right)} \Bigg] \cdot \frac{1}{1 + \tilde{A_c}^n\left(\tilde{t}\right)} - \gamma_{P_c} \cdot \tilde{P}_c\left(\tilde{t}\right) \end{aligned} \tag{3.10}$$

$$\frac{d\tilde{A}_c\left(\tilde{t}\right)}{d\tilde{t}} = \beta_{P_cA_c} \cdot \frac{\tilde{P_c}^n\left(\tilde{t}\right)}{\theta^n_{P_cA_c} + \tilde{P_c}^n\left(\tilde{t}\right)} + \beta_{FA_c} \cdot \frac{\tilde{F}^n\left(\tilde{t}\right)}{\theta^n_{FA_c} + \tilde{F}^n\left(\tilde{t}\right)} - \tilde{A}_c\left(\tilde{t}\right) \tag{3.11}$$

$$\begin{aligned} \frac{d\tilde{M}\left(\tilde{t}\right)}{d\tilde{t}} = \Bigg[&\alpha_{BM} + \beta_{P_cM} \cdot \frac{\tilde{P_c}^n\left(\tilde{t}\right)}{\theta^n_{P_cM} + \tilde{P_c}^n\left(\tilde{t}\right)} + \\ &\beta_{A_dM} \cdot \frac{\tilde{A_d}^n\left(\tilde{t}\right)}{\theta^n_{A_dM} + \tilde{A_d}^n\left(\tilde{t}\right)} \Bigg] \cdot \frac{\theta^n_{A_cM}}{\theta^n_{A_cM} + \tilde{A_c}^n\left(\tilde{t}\right)} - \gamma_M \cdot \tilde{M}\left(\tilde{t}\right) \end{aligned} \tag{3.12}$$

Table 3.3: *The estimated dimensionless parameters of the inflammation model.*

Parameters	Description	Value	Reference
$\alpha_{BP_c}, \alpha_{BM}$	Natural production rate	0.01	[119]
$\beta_{P_cP_c}, \beta_{A_dP_c}, \beta_{FP_c}, \beta_{P_cA_c}, \beta_{FA_c}, \beta_{P_cM}, \beta_{A_dM}$	Stimulated production rate	10	[119]
$\theta_{P_cA_c}, \theta_{FA_c}, \theta_{P_cM}, \theta_{A_dM}, \theta_{A_cM}$	Saturation constant at which the capability of stimulation or inhibition is half of maximum	1	[119]
μ_{NA_d}	The background production rate of adipokines due to the number of adipocytes	0.01	Estimated
μ_{SA_d}	The background production rate of adipokines due to the size of adipocytes	0.01	Estimated
$\gamma_{P_c}, \gamma_M, \gamma_{A_d}, \gamma_F$	Clearance rate	1	[119]
$Damage$	The damage level of cartilage	0	[119]
BMI^{std}	Standard value of BMI	25	[39]
$\frac{DailyCal}{BMR}$	Nutrition factor	1	Estimated
θ_{A_d}, nex	Coefficients in the inhibition of adipokine production due to exercise	Dependent on PAL and BMI^{meas}	Estimated
n	Hill coefficient	2	[119]

$$\frac{d\tilde{A}_d\left(\tilde{t}\right)}{d\tilde{t}} = \mu_{NA_d} + \left[\mu_{SA_d} \cdot \ f\left(BMI^{meas}\right) \cdot \frac{DailyCal}{BMR \cdot PAL}\right] \cdot \frac{\theta_{A_d}^{nex}}{\theta_{A_d}^{nex} + \tilde{A}_d{}^{nex}\left(\tilde{t}\right)} - \gamma_{A_d} \cdot \tilde{A}_d\left(\tilde{t}\right) \quad (3.13)$$

$$\frac{d\tilde{F}\left(\tilde{t}\right)}{d\tilde{t}} = \tilde{M}\left(\tilde{t}\right) + Damage - \gamma_F \cdot \tilde{F}\left(\tilde{t}\right) \quad (3.14)$$

3.2.5 Sensitivity analysis

The dependence of the inflammation behaviours on the isolated non-dimensionalised parameters in this model was analysed through Local Sensitivity Analysis (LSA), which was verified by comparing with Baker et al. [119].

The LSA was implemented with the maximum ±30% perturbation of each parameter [119] for the comparison:

$$S_K^{M_r} = \frac{\delta M_r(\omega) \diagup M_r(\omega)}{\delta K \diagup K} \tag{3.15}$$

where K is the reference parameter that was perturbed and $M_r(\omega)$ is the measured response based on the system output ω. The responses include the mean steady concentration at the healthy state and inflamed limit cycles, the amplitude and period in limit cycles of inflammation [108]. Correspondingly, δK is the perturbation of the parameter K and its effect on the measured response is $\delta M_r(\omega)$. In particular, parameters were randomly perturbed $1,000$ times [119] in the range of $[-0.3, +0.3]$ that is uniformly distributed so that the relative sensitivity can be represented by the Interquartile Range (IQR) of the responses from $1,000$ perturbations. To measure the inflammatory responses without mechanical damage, $Damage$ is not perturbed and estimated as 0 at baseline.

The bifurcations of sensitive parameters were analysed to explore the dynamics of inflammation with obesity and compared to Baker et al. [119] for the verification of the five-variable model and MATLAB scripts for bifurcation analysis. In particular, the values of the parameters estimated in Table 3.3 are also the baseline for bifurcation analysis. The concentration of PICs measures the inflammation level at steady states to present the transitions of system dynamics. The steady states were accordingly given by the simultaneous equations (Appendix C) derived for calculating equilibrium solutions, in conjunction with the phase plane of the system under baseline parameters (Figure D.1). The stability of local behaviour was examined by the application of linearisation to the obtained equilibrium solutions. Due to the complex nonlinearity of this model, the Jacobian of this system and the corresponding eigenvalues were numerically computed for the linear approximation in bifurcation analysis.

In addition, the sensitivity of adiposity regulation by PAL was evaluated by measuring the variation of adipokine concentration at equilibrium when tuning nex and θ_{A_d}. The categories of obesity level (Table 3.1) and PAL (Table 3.2) are used to define the different gradients of the concentration variations (Figure 3.2). Given the sensitivity, two piecewise continuous functions, Equations (3.16) and (3.17), are provided with the boundary parameters to estimate nex and θ_{A_d} based on different combinations of BMI and PAL. It is assumed that the reduction of adipokines is approximately linear to a certain PAL range when the obesity level remains the same, leading to a linear correlation between the non-dimensionalised parameters and inputs of BMI

or PAL when they are in the same category. Figure 3.3 illustrates the concentration of adipokines at equilibrium with different values of BMI and PAL, which are governed by Equations (3.16) and (3.17).

$$nex = \begin{cases} B_{ND} - BMI^{meas} \cdot \dfrac{B_{ND} - B_{NW}}{R_{ND} - R_{ND_{min}}}, & if\ R_{ND_{min}} < BMI^{meas} < R_{ND} \\ B_{NW} - (BMI^{meas} - R_{ND}) \cdot \dfrac{B_{NW} - B_{OW}}{R_{NW} - R_{ND}}, & if\ R_{ND} \leqslant BMI^{meas} \leqslant R_{NW} \\ B_{OW} - (BMI^{meas} - R_{NW}) \cdot \dfrac{B_{OW} - B_{O}}{R_{OW} - R_{NW}}, & if\ R_{NW} < BMI^{meas} \leqslant R_{OW} \\ B_{O} - (BMI^{meas} - R_{OW}) \cdot \dfrac{B_{O} - B_{EO}}{R_{O} - R_{OW}}, & if\ R_{OW} < BMI^{meas} < R_{O} \\ \dfrac{R_O}{BMI^{meas}}, & if\ BMI^{meas} \geqslant R_{O} \end{cases} \tag{3.16}$$

$$\theta_{A_d} = \begin{cases} B_S - (PAL - R_{S_{min}}) \cdot \dfrac{B_S - B_{LA}}{R_S - R_{S_{min}}}, & if\ R_{S_{min}} \leqslant PAL \leqslant R_S \\ B_{LA} - (PAL - R_S) \cdot \dfrac{B_{LA} - B_A}{R_{LA} - R_S}, & if\ R_S < PAL \leqslant R_{LA} \\ B_A - (PAL - R_{LA}) \cdot \dfrac{B_A - B_{VA}}{R_A - R_{LA}}, & if\ R_{LA} < PAL \leqslant R_A \\ B_{VA} - (PAL - R_A) \cdot \dfrac{B_{VA}}{R_{VA} - R_A}, & if\ R_A < PAL \leqslant R_{VA} \end{cases} \tag{3.17}$$

where the boundaries of nex and θ_{A_d} are estimated according to Figure 3.2: $B_{ND} = 10$, $B_{NW} = 8$, $B_{OW} = 4$, $B_O = 2$, $B_{EO} = 1$, $B_S = 1$, $B_{LA} = 0.5$, $B_A = 0.25$, $B_{VA} = 0.1$. In addition, parameters of BMI and PAL range are determined by Tables 3.1 and 3.2: $R_{ND_{min}} = 0$, $R_{ND} = 18.5$, $R_{NW} = 24.9$, $R_{OW} = 29.9$, $R_O = 40$, $R_{S_{min}} = 1$, $R_S = 1.39$, $R_{LA} = 1.59$, $R_A = 1.89$, $R_{VA} = 2.5$.

3.2.6 Simulation of inflammatory activities

The inflammatory activities were simulated by solving the governing ODEs in MATLAB (R2022b, The Math Works, Inc., Natick, MA, USA) under the estimated parameters to evaluate the effects of obesity and PAL. The MATLAB function *ode45* was used as the solver of the explicit Runge-Kutta method with the relative tolerance of 0.001 and the absolute tolerance of 1×10^{-6} for simulations. Due to the lack of experimental data, the time scale of the model is governed by the decay rate of each variable. However, the uncertainty of decay rates remains in either the same or different mediator groups. In order to analyse the evolution of OA inflammation when the intervention of physical activity was applied, the dimensionless concentration of each mediator was measured within 100 dimensionless time units. Particularly, the

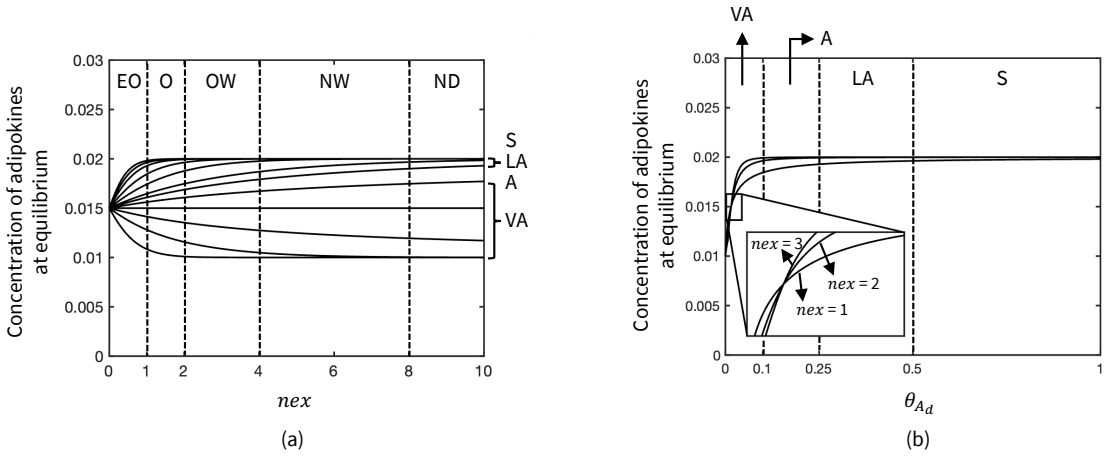

Figure 3.2: *The sensitivity of (a) nex and (b) θ_{A_d} to the adipokine concentration at equilibrium. nex is numerically correlated to obesity level so it measures the sensitivity of adipokine reduction due to different PALs at a certain level of obesity (EO: Extreme obesity; O: Obesity; OW: Overweight; NW: Normal weight; ND: Nutritional deficiency). θ_{A_d} is the dimensionless coefficient that determines the amount of adipokine reduction due to PAL (S: Sedentary; LA: Low active; A: Active; VA: Very active).*

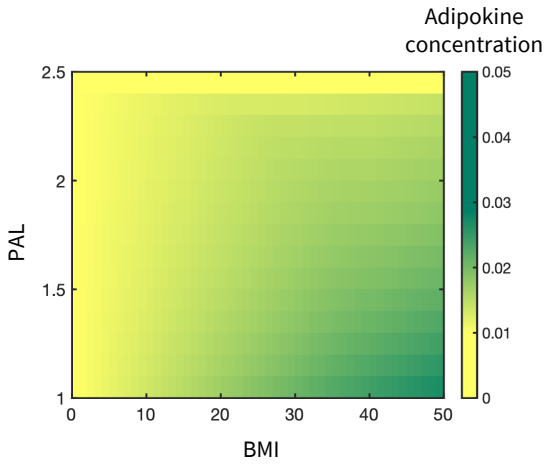

Figure 3.3: *The equilibrium adipokine concentration against PAL and BMI.*

level of cytokines reflects the inflammation process, and the concentration of Fn-fs measures the damage due to the combined effects of inflammation and mechanics.

The minimum values of mechanical damage leading to inflammation were compared over the inflammation system with different obesity levels. In addition, a sudden damage ($Damage = 0.005$) due to mechanics (injury) was applied to the model at time point 20, and PAL increases from a sedentary level ($PAL = 1$) to a low active level ($PAL = 1.5$) to simulate physical therapy. The input characteristics of this computational subject also include BMI ($BMI^{meas} = 30$) and daily nutrition

($DailyCal/BMR = 1$) to study the effects of PAL on the inflammatory process of an obese subject.

3.3 Results

3.3.1 Model verification

In order to verify the model of adipokine-mediated inflammation and analyse the variations in system behaviours due to adipokine, LSA and bifurcation diagrams of sensitive parameters were compared between Baker's model [119] and this five-variable model. The IQR of perturbed system outputs (Figure 3.4) illustrates that the parameters relevant to adipokine production and its regulation are insensitive to the inflammation state. Instead, the PIC natural production (α_{BP_c}) and clearance rates (γ_{P_c} and γ_{A_d}) of PICs and adipokines slightly affect the cytokine concentration in the healthy state. For the inflammatory oscillation, the amplitude of cytokine concentration is readily perturbed when parameters of inhibition ($\theta_{P_cA_c}$ and θ_{FA_c}) and stimulated production (β_{FP_c}, $\beta_{P_cA_c}$ and β_{FA_c}) are varied, and the relative sensitivity is similar in the inflammatory amplitude in the five-variable model and Baker's model. However, the introduction of adipokines sensitises $\beta_{P_cA_c}$, γ_M and γ_F in the response of the inflammatory period. This suggests that obesity affects the OA inflammatory process by changing the sensitivity of other parameters to the system period in limit cycle, namely, parameters of adipokines have impacts on the inflammation dynamics and they can slightly induce the release of cytokines at the healthy state.

Bifurcations of the common parameters were compared between Baker's model [119] and this five-variable model in Figures D.2 to D.5. The addition of adipokines reduces the bistability and the inflamed limit cycle of the inflammation system for a range of values of most parameters, which results in the system staying in persistent inflammation in a wider range of parameter perturbations.

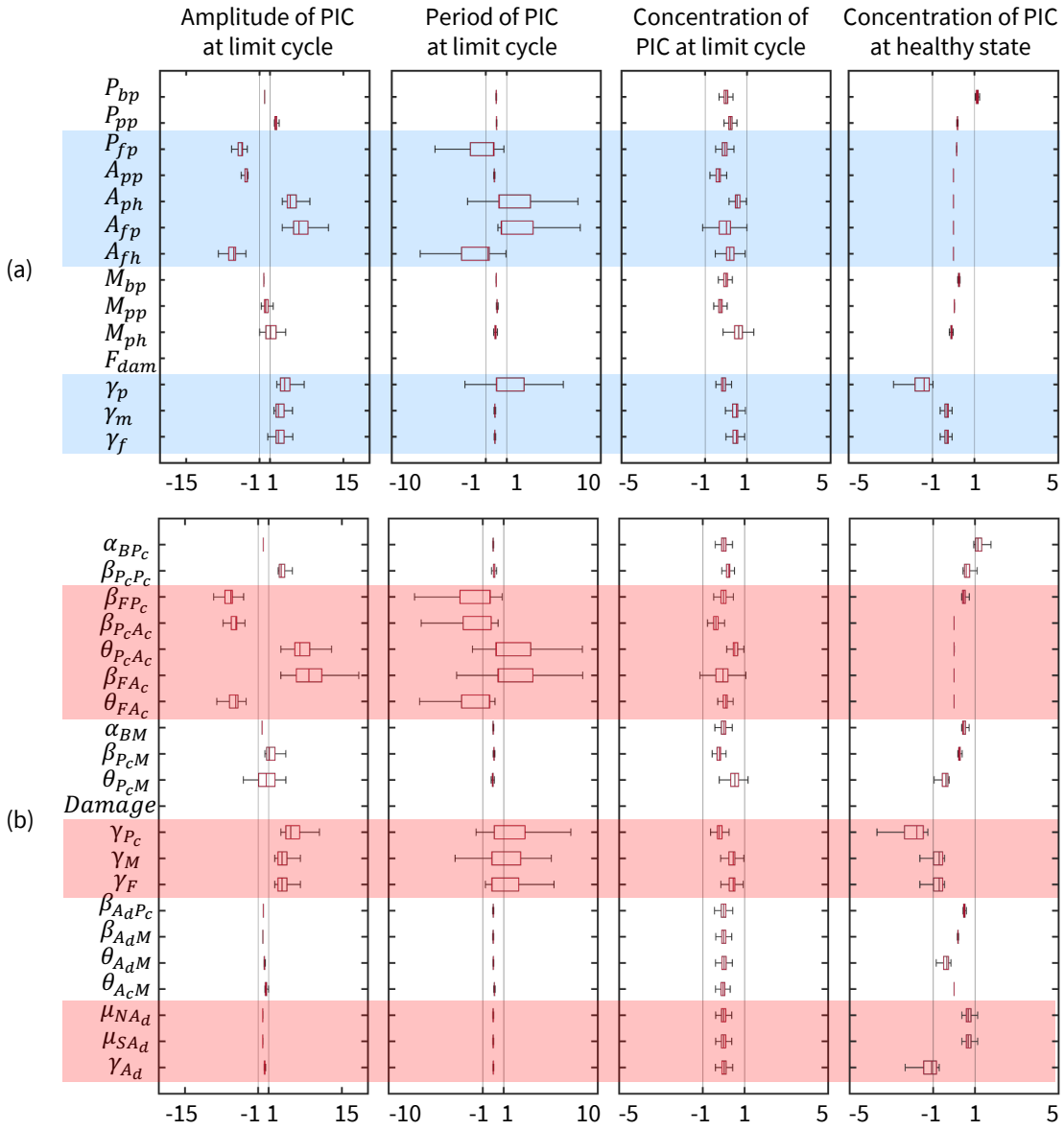

Figure 3.4: *The boxplots of the LSA for dimensionless parameters in (a) Baker's model [119] and (b) the adipokine-mediated inflammation model. The values of datasets represent the percentages of change in the measured responses from the system outputs perturbed by 1 percent change of a specified parameter at the inflamed limit cycle and the healthy state. Parameters that result in output changes over 1 percent are highlighted in blue for (a) and in red for (b).* P_{bp}*: The background production rate of PICs;* P_{pp}*: The production rate of PICs driven by PICs;* P_{fp}*: The production rate of PICs driven by Fn-fs;* A_{pp}*: The production rate of AICs driven by PICs;* A_{ph}*: The concentration of AICs at which the production rate of AICs driven by PICs is half of the maximum;* A_{fp}*: The production rate of AICs driven by Fn-fs;* A_{fh}*: The concentration of AICs at which the production rate of AICs driven by Fn-fs is half of the maximum;* M_{bp}*: The background production rate of MMPs;* M_{pp}*: The production rate of MMPs driven by PICs;* M_{ph}*: The concentration of MMPs at which the production rate of MMPs driven by PICs is half of the maximum;* F_{dam}*: Mechanical damage parameter;* γ_p*: Decay rate of PICs;* γ_m*: Decay rate of MMPs;* γ_f*: Decay rate of Fn-fs.*

3.3.2 Dynamics of the adipokine-mediated inflammation model

The types of system dynamics reflected in the bifurcation diagrams of this study are summarised in Table 3.4. Tristable behaviours with five steady states were found when varying parameters in the study by Baker et al. [119]. It is important to note that the variation of parameters might deviate from the assumptions of parameter estimation, although system tristability is potentially one of the mathematical solutions to the inflammation model. According to the intersection of nullclines in the phase plane diagram of this model (Figure D.1), five steady states also exist when artificially varying the parameters. However, in order to prevent numerical artefacts due to parameter estimation, the analysis of the system dynamics focuses on the effects of obesity when the reference parameter set is maintained at baseline. The exhaustive estimation was not implemented for the parameters irrelevant to adipokines. Representative steady states (health, oscillatory inflammation and steady inflammation) were mainly found in the state transitions resulting from the variability in parameters governing adipokine regulation.

Table 3.4: *The types of dynamics presented in bifurcations.*

Dynamics type	The number of steady state	Stability	The type of steady state
$I_{monostable}$	S_0^S	Monostable	Persistent steady inflammation
$II_{monostable}$	L_0^S	Monostable	Persistent oscillatory inflammation
$III_{bistable}$	S_0^S, S_1^U, L_0^S	Bistable	Health, oscillatory inflammation
$IV_{bistable}$	S_0^S, S_1^U, S_2^S	Bistable	Health, steady inflammation
$V_{monostable}$	S_0^S	Monostable	Health
$VI_{monostable}$	S_0^S, S_1^U, S_2^U	Monostable	Health

[1] S: Quiescent stable state; L: Limit cycle; S in superscript: Stable; U in superscript: Unstable

There are three parameters $\beta_{A_dP_c}, \beta_{A_dM}$ and θ_{A_dM}, associated with adipokine level to regulate the production of PICs and MMPs. Their bifurcations (Figures 3.5a to 3.5c) indicate that the high production rates of both PICs ($\beta_{A_dP_c}$) and MMPs (β_{A_dM} and θ_{A_dM}) driven by adipokines lead to the loss of healthy state. Unlike the inflamed

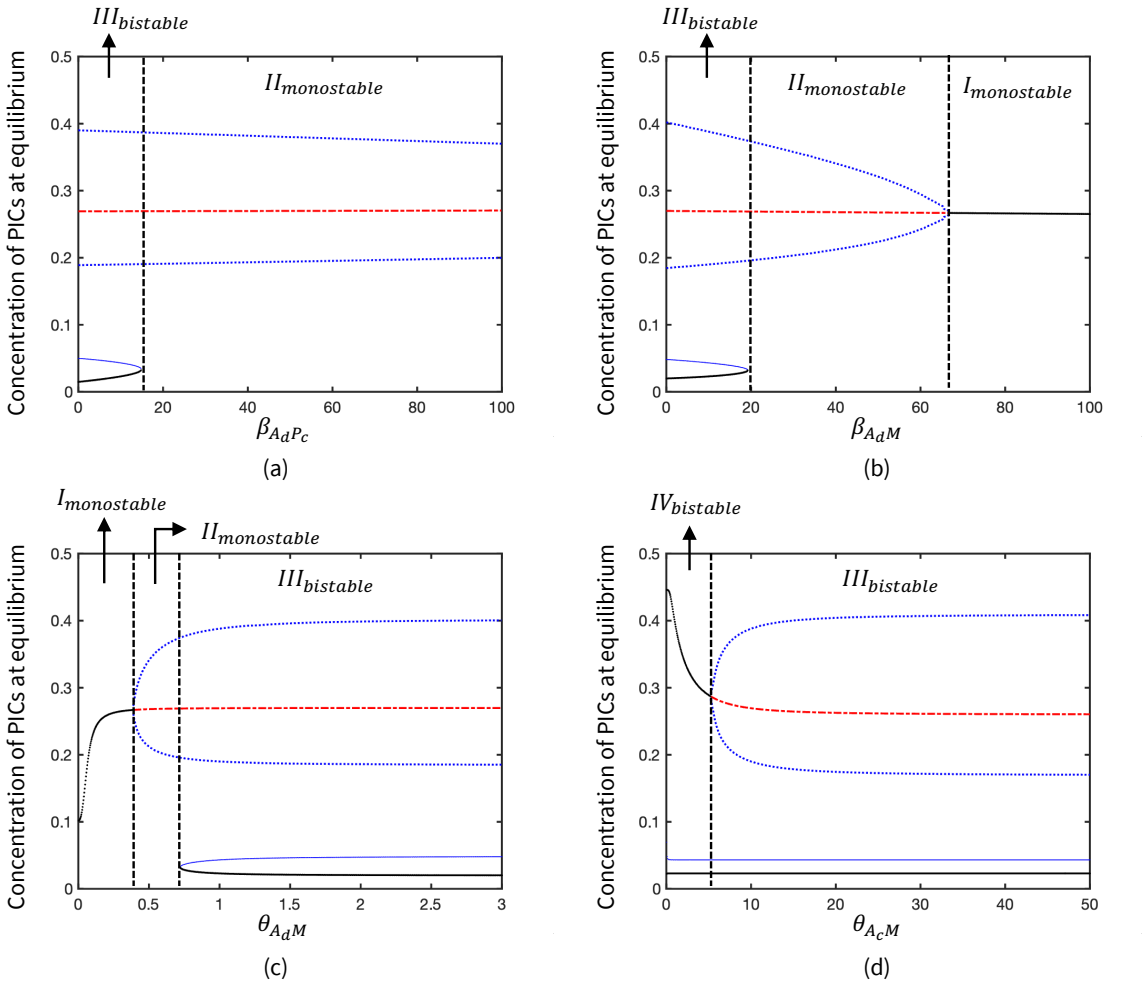

Figure 3.5: *Bifurcation diagrams of parameters in the production of PICs and MMPs: (a) Production rate of PICs driven by adipokines; (b) Production rate of MMPs driven by adipokines; (c) Saturation rate in the stimulation of MMPs by adipokines; (d) Saturation rate in the inhibition of MMPs by AICs. Solid black lines where the pro-inflammatory is at a higher level represent the inflamed states; solid black lines where the pro-inflammatory is at a lower level represent the healthy states; dash blue lines represent the unstable states; solid blue lines represent unstable states; The scatter of blue points represents the average maximum and minimum concentration in the oscillated limit cycle.*

limit cycle due to the high value of $\beta_{A_dP_c}$, the increase of β_{A_dM} and the reduction of θ_{A_dM} can result in the quiescent steady inflammation state. This suggests that the stimulation of PICs is not as sensitive as MMPs due to adipokines. Due to the nondimensionalisation of parameters, θ_{A_cM} represents the weight of two inhibition pathways, the inhibitions of PICs and MMPs by AICs. When θ_{A_cM} decreases, the weight of MMPs inhibition decreases and the system stays bistable but the inflam-

matory process tends to be stable rather than oscillatory (Figure 3.5d).

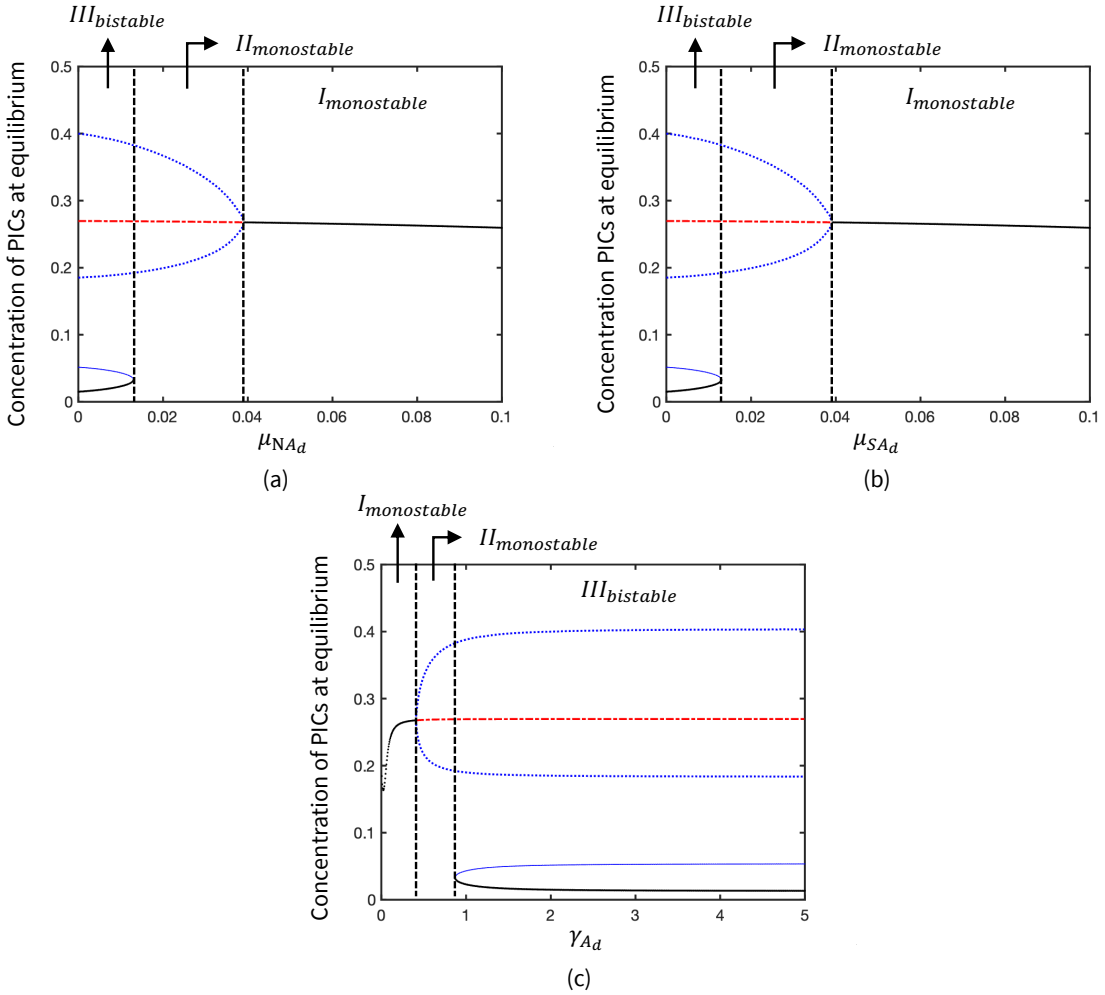

Figure 3.6: *Bifurcation diagrams of parameters in the production of adipokines: (a) Production rate of adipokines due to the number of adipocytes; (b) Production rate of adipokines due to the size of adipocytes; (c) Decay rate of adipokines.*

Figure 3.6 illustrates the variations of system dynamic behaviours due to the changes of parameters (μ_{NA_d}, μ_{SA_d} and γ_{A_d}) in adipokine production. Bifurcations of μ_{NA_d} and μ_{SA_d} (Figures 3.6a and 3.6b) are similar as the weights of adipocyte number and size represented by those two parameters of the adipokine production are initially equal in the production of adipokines. A threshold of nearly 0.02 for the adipokine production rates (μ_{NA_d} and μ_{SA_d}) indicates a transition from $III_{bistable}$ to $II_{monostable}$ (Figures 3.6a and 3.6b), resulting in persistent inflammation and the loss of quiescence healthy state. In turn, the increase of adipokine decay rate (γ_{A_d})

turns the monostable system of inflammation to bistable system so that the healthy state returns (Figure 3.6c).

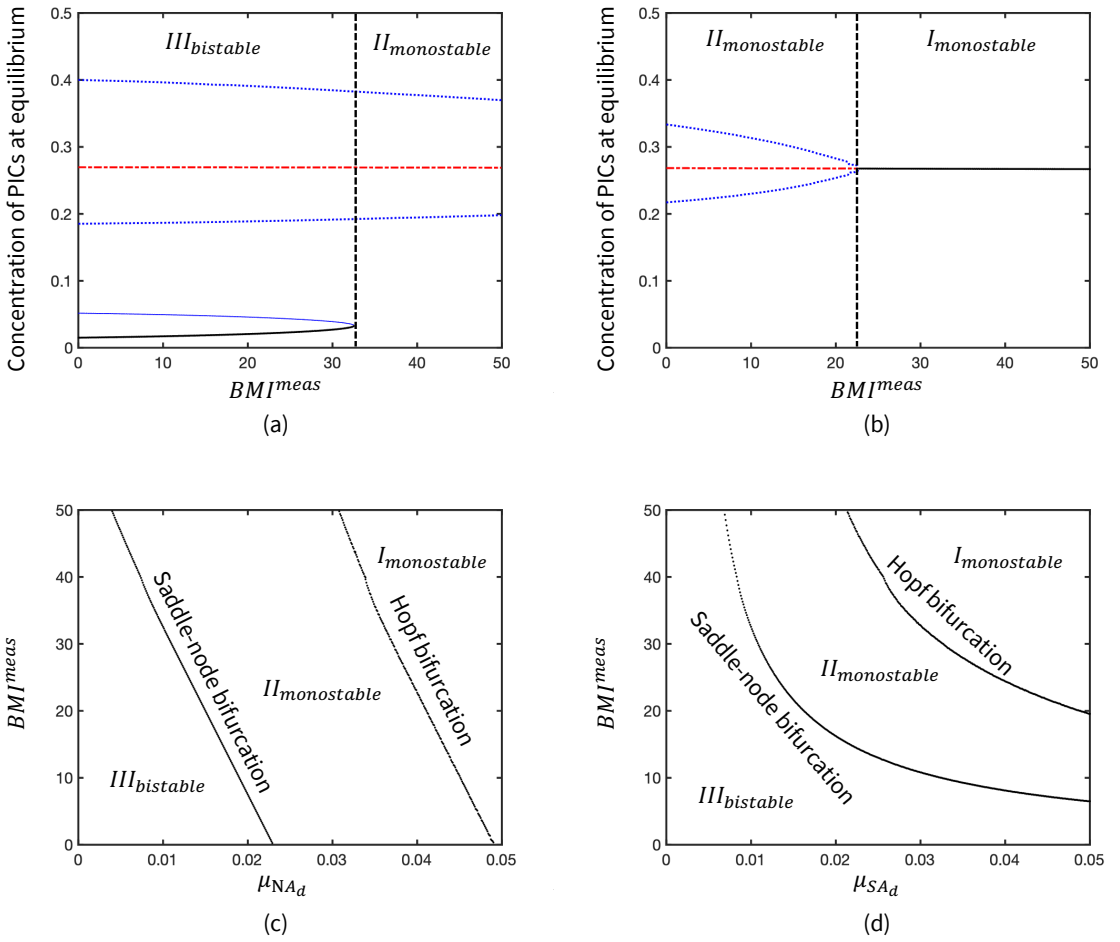

Figure 3.7: *Bifurcation diagrams of BMI^{meas} where (a) $\mu_{NA_d} = 0.01$, $\mu_{SA_d} = 0.01$; (b) $\mu_{NA_d} = 0.04$, $\mu_{SA_d} = 0.01$, and codimension-2 bifurcations of (c) μ_{NA_d} and BMI^{meas}; (d) μ_{SA_d} and BMI^{meas}.*

BMI^{meas} is an input parameter that modulates the weight of the adipokine production term associated to adipocyte size, hence its impact on the system behaviour is similar to μ_{NA_d} and μ_{SA_d}. A threshold of BMI that causes persistent inflammation is found at approximately 33 in Figure 3.7a when the parameters are at baseline, where $\mu_{NA_d} = 0.01$ and $\mu_{SA_d} = 0.01$. High BMI can reduce the bistability of the inflammation system so that it remains in a monostable inflamed limit cycle. The monostability of inflammation results in an inability of the system to return to a healthy state. In addition, the BMI threshold of bifurcation is dependent on μ_{NA_d} and μ_{SA_d}. Figure 3.7b presents the Hopf bifurcation when oscillatory inflammation

turns into persistent steady inflammation as BMI increases. In the codimension-2 bifurcations of μ_{NA_d} and μ_{SA_d}, the transitions of system behaviours are presented in the range of BMI between 0 and 50 (Figures 3.7c and 3.7d). The transitions reflect the susceptibility of OA inflammation in different cohorts.

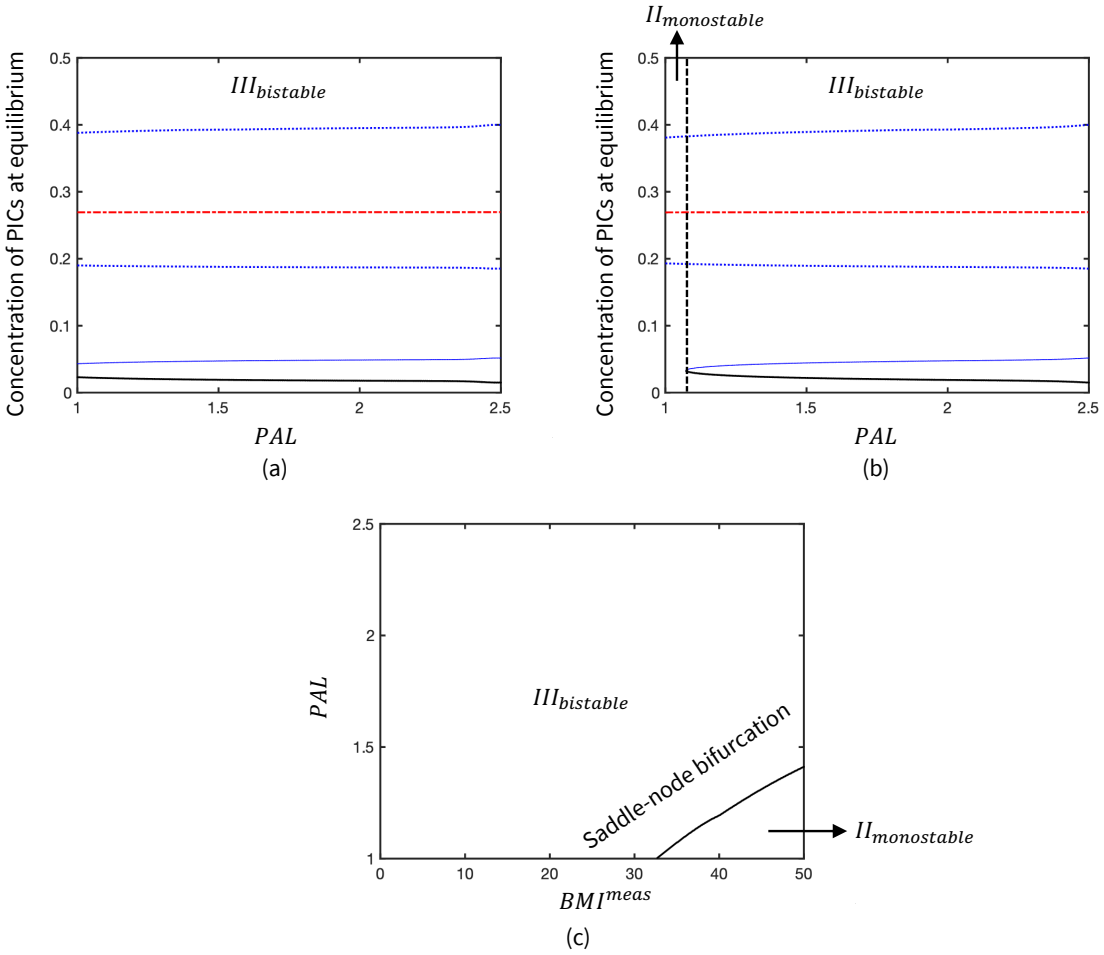

Figure 3.8: *Bifurcation diagrams of PAL when (a) $BMI^{meas} = 25$; (b) $BMI^{meas} = 35$ in the production of adipokines, and (c) Codimension-2 bifurcation of BMI^{meas} and PAL.*

However, two representative bifurcation diagrams of PAL in Figures 3.8a and 3.8b illustrate that the monostability of inflammation can be changed by increasing PAL. The effectiveness of PAL also depends on the level of BMI, so a higher PAL is required to return the bistability when BMI exceeds the threshold at 33. Figure 3.8c shows the transition between $III_{bistable}$ and $II_{monostable}$ in the parameter space via the codimension-2 bifurcation of PAL and BMI^{meas}.

In addition to BMI, mechanical damage can also lead to persistent inflammation when it exceeds a threshold, of which sensitivity is dependent on BMI as well as PAL

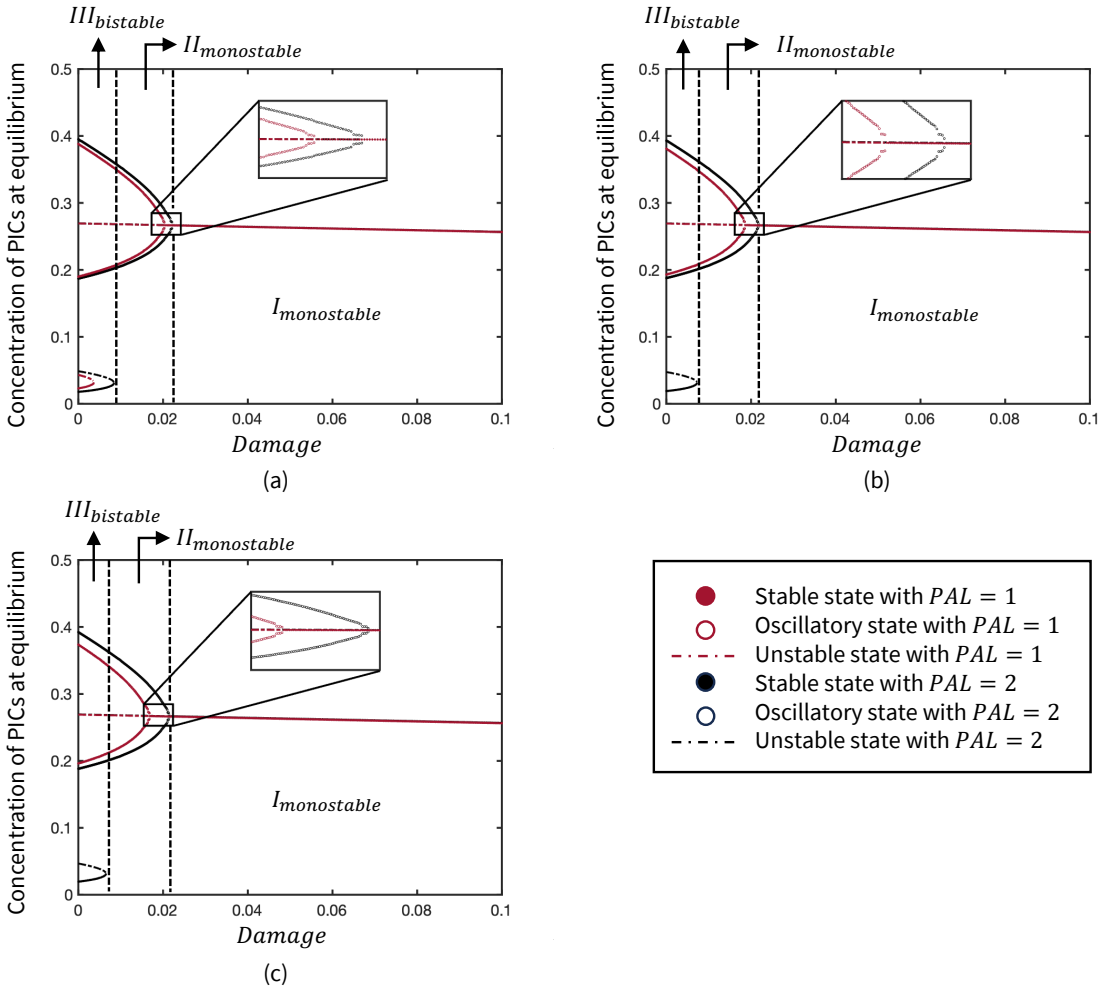

Figure 3.9: *Bifurcation diagrams of $Damage$ under different physical activity interventions when (a) $BMI^{meas} = 25$; (b) $BMI^{meas} = 35$; (c) $BMI^{meas} = 45$ in the adipokine-mediated inflammation model. The dynamics transition is presented when $PAL = 2$ as an example.*

(Figure 3.9). The system stays in the inflammation state and the damage is most sensitive to the system when BMI is 35 or 45 over the threshold, hence the oscillatory inflammation turns to persistent inflammation as damage is increased. Regardless of BMI, high PAL can reduce the sensitivity of damage leading to inflammation, and the reduction is more significant when BMI is higher. Namely, the minimum damage leading to a monostable inflammation state increases due to the higher PAL.

3.3.3 Evolution of inflammatory activities

The nonlinear inverse correlation between BMI and the minimum mechanical damage that causes chronic inflammation is illustrated in Figure 3.10. The minimum damage decreases to zero when BMI is over 33 due to the transition of system be-

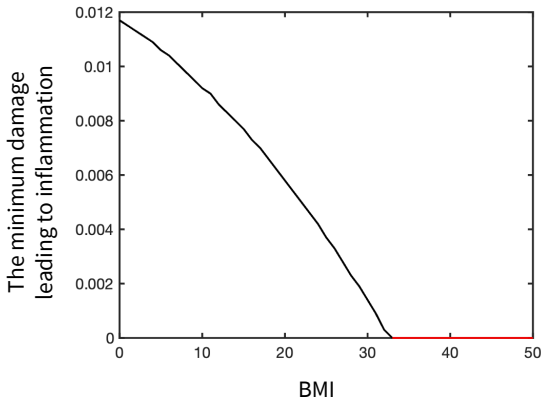

Figure 3.10: *The sensitivity of the minimum damage leading to inflammation in the evolution of inflammatory activities.*

haviour to $II_{monotable}$ from $III_{bistable}$. In addition, the risk of inflammation significantly increases in the BMI range between 20 and 30 as the minimum damage starts to sharply decrease. However, adequate physical activity interventions that are applied before the mechanical damage can reduce the inflammatory response (Figure 3.11). This exhibits the significance of the timing for physical activity intervention.

The mechanical damage occurs at time point 20 when the level of inflammatory mediators is upregulated. As the inflammatory process evolves, physical activity interventions can postpone the activation of inflammation (Figures 3.11a to 3.11c) so that the system stays in the healthy state where mediator concentrations are stable. Without damage repair, the reduction of adipokines by continuous physical activity is able to prevent the system from inflammation. In turn, Figures 3.11e to 3.11h show that the system remains in oscillatory inflammation when the intervention misses an effective window period of 7 time units after damage occurs. In the time span of inflammation, the mediator concentrations fluctuate at a high level due to the nonlinear stimulations and inhibitions among inflammatory mediators. Regardless of physical activity intervention, the steady state of inflammation cannot be transited to a healthy state without any external dose to reduce the level of inflammatory mediators. Thus, the disclosure of the window period in this model emphasises the importance of a continuous physical activity intervention maintaining a low level of adipokines.

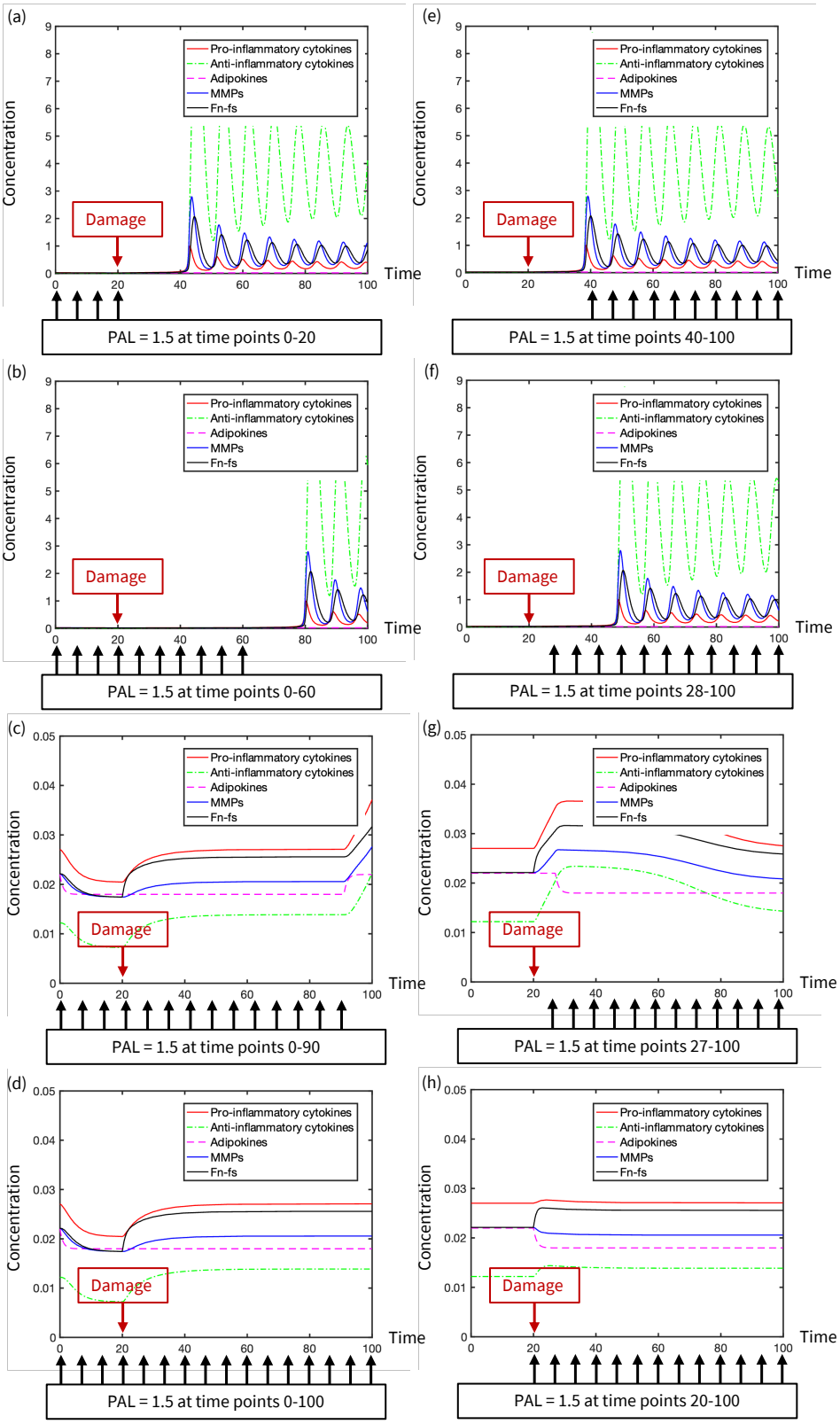

Figure 3.11: *The evolution of inflammatory activities under different strategies of physical activity intervention in the non-dimensionalised model.*

3.4 Discussion

The first general mechanistic inflammation model of OA including the effect of obesity and exercise was developed to qualitatively analyse the dynamics of the chronic inflammatory process regulated by adipokines. This model was extended from a four-variable cartilage inflammation model [119] by formulating the major inflammatory mediators and their signalling pathways regarding OA. The assumption of molecular pathways is based on Hill functions and the law of mass action. Accordingly, the inflammatory activities can be qualitatively measured by the concentration of each mediator group within this model. The introduction of obesity and physical activity provided a novel perspective on the prevention and intervention of the chronic inflammatory process at the molecular level in OA. Obesity is measured by the number and size of adipocytes associated to the production of adipokines to present the variability of individuals susceptible to obesity. Results show that ascending adipokine production can reduce the stability of healthy state in the inflammation system via a saddle-node bifurcation so the risk of OA inflammation increases. Meanwhile, the system becomes sensitive to the parameter of damage. As an intervention to reduce adiposity, an adequate increase of PAL can return a steady state of health to significantly reduce the risk of inflammation. This is approached by the same type of saddle-node bifurcation. In the evolution of inflammatory activities, physical activity intervention can prevent the system from inflammation when inducing mechanical damage.

In addition to excessive loading, obesity leads to a aberrant level of adipokines that aggravate the inflammation during OA. Despite the protective role of adiponectin inducing AICs in OA [98], a high level of adipokines is tightly associated with the production of PICs and MMPs [89, 100]. This five-variable model was verified by comparing the parameter sensitivity and bifurcations to Baker's model [119] using the same mathematical protocol. As the signalling source of stimulating PICs and MMPs, the introduction of adipokines results in additional parameters that can alter the system dynamics. Specifically, adipokines increase the sensitivity of this adipokine-mediated inflammation system to inflammatory response as it is found that the stability at a quiescent healthy state is reduced in the bifurcations of a range of parameters. However, the local and systemic impacts of obesity are not differentiated in this model. The total inflammatory response of cartilage can stem from the local stimulation of inflammatory mediator production

and systemic circulation of PICs and adipokines to the joint [41, 44, 94]. The systemic indicators (BMI, daily nutrition and PAL) were thereby used to measure the adipokine level regulating the total inflammation of cartilage other than specifying the source of adipokines, which provides a comprehensive impact of obesity on the inflammation dynamics of OA. The pathways of adipokines stimulating PICs and MMPs can both result in a monostable inflammation state. Particularly, the production of MMPs elevated by excessive stimulation or declined inhibition can lead the system to a steady state of inflammation without oscillation. This suggests that MMPs may preponderate in the aggravation of inflammatory activities, and the production of MMPs activated by adipokines contributes to steady inflammation, so the system firmly stays in the inflammatory activities that deteriorate cartilage tissue during OA progression.

Oscillatory inflamed limit cycle represents the early stage of OA where the high levels of cytokines, MMPs or Fn-fs are intermittent [119]. It has been reported that desultory pain of the joint occurs in individuals with early OA [213] in spite of the lack of a standard to ascertain the role of biomarkers in diagnosing the early OA stage [30, 32, 214]. Pathophysiologically, AICs are recruited and chondrocytes are active to repair the failure tissue at the early OA stage [67] when interactions of inflammatory mediators can disrupt the anabolic activities. Since the damage caused by the catabolism of inflammation or excessive mechanical loadings accumulates in OA progression [83], the inability to reduce inflammation and the release of damaging products lead to steady inflammation without oscillation. Nevertheless, the bifurcations of adipokine production parameters indicate that a significantly high level of adipokines can also cause steady inflammation when the parameter of mechanical damage is zero, which can be also seen in the bifurcations of other parameters that can upregulate the production of PICs and MMPs. This suggests that the tissue degraded by the overwhelming chronic inflammation prompts the OA process regardless of mechanical damage. In fact, progressive structural degeneration of the cartilage inevitably causes mechanical defects that can further intensify inflammation due to the abnormal biomechanical behaviours within the entire joint [215]. Thus, the identification of reasons for tissue rupture might contribute to diagnosing early OA. However, this identification is challenging since the reason might not be independent due to the combinations of multiple factors such as low tissue turnover, structural changes of tissue and potent inflammatory activities [25, 200].

In this model, the mechanical impact of obesity is not specified by BMI, though the parameter of damage denotes the mechanical response on the tissue due to

excessive loadings. The bifurcations of BMI and mechanical damage illustrate that a high BMI can change the sensitivity of mechanical damage to the inflammation by reducing the bistability of this system, hence the system is more susceptible to OA inflammation. Likewise, the sensitivity of minimum mechanical damage causing inflammation risk is exponentially associated with BMI. This is consistent with Berenbaum and Sellam [216] who report that the likelihood of OA onset rises by 15% with each additional unit as BMI exceeds 27. Nevertheless, the risk of OA is the concurrent outcome of the metabolic and mechanical response and the amount of injury due to high BMI is not accounted for within this model.

Body weight is one of variables in the calculation of BMI and it is reported that PAL can reduce fat mass and the correlation between PAL and body weight is weak [44, 199]. Hence the application of PAL, as an interventive status in this model, essentially reduces the production of adipokines rather than body weight to alter the system dynamics. The stability of healthy state returns when applying adequate PAL if BMI is high in the bifurcations of PAL and mechanical damage, so the risk of evolving into inflammation and inflammatory damage can be decreased. However, external mechanical damage results in a window period of reducing inflammation risk by PAL. The window period was found to be 7 time units, of which the dimension is dependent on the decay rates of mediators. Outside of the window period, the intervention of PAL can only postpone inflammatory activities before the system evolves into inflammation. Accordingly, physical activity might not be able to reduce the inflammation directly, instead the susceptibility of OA inflammation can be altered and other therapeutic treatments can be more effective to control inflammatory progress. Shumnalieva et al. [192] highlighted that the combination of physical activity and dietary intervention could improve the success rate of pharmacological therapies for the phenotypes of OA associated with obesity, though the increase of mitochondrial biogenesis that inhibits cytokine production [201] due to above interventions is not considered. In this model, physical activity intervention reduces adipokine production to inhibit cytokine production, whose role is similar to the increased mitochondrial biogenesis in the inflammatory process. Therefore, the influence of physical activity is to regulate the dynamics of the inflammation system at the molecular level.

Whereas this general model includes the regulatory pathways of adipokines in OA inflammation, the lack of biological and clinical data raises challenges on its validation. Moreover, inflammatory mediators are categorised into different functional groups so there might be no specific data for the parameter estimation. As the

consideration of model complexity and computing demands, the general classification of mediator groups is efficacious to simulate the inflammatory activities [120]. The association between inflammation and structural changes of tissue can be considered by including the spatial dimension. However, this ODE-based model can reduce computing complexity and focus on the time-dependent molecular interactions in inflammation. Molecules might derive from the cross-talk at different spatial levels, which is implicitly reflected in the outcomes of different signalling pathways in this general model. The classification of inflammatory and mechanical damage could be coupled with mechanical stimulus in the future. Due to the existence of large uncertainty and variability on the parameters [119, 127, 140], the prediction of inflammation process might differ based on different parameters, and only the adipokine and mechanical damage parameters were tuned to study the effect of obesity and exercise. In turn, the stability analysis of predominant parameters can unravel the possibilities of the inflammation dynamics involved by obesity and physical activity. The prospective work can focus on the extension of this general model and specifying mediators so that there might be relevant data to validate its application of the prediction on inflammatory activities.

3.5 Conclusion

A new mechanistic inflammation model of OA including the effect of obesity and exercise was developed to qualitatively analyse the dynamics of the chronic inflammatory process regulated by adipokines. Since tissue damage is the underlying trigger of inflammation, the production of MMPs was found to dominate the onset and development of inflammation comparing to pro-inflammatory cytokines under the regulation of adipokines. In addition, a BMI threshold of 33 was found to induce persistent inflammation. This threshold can vary depending on the individual parameter sets. The predominant role of adipokines in this model aggravates inflammatory damage but the reduction of obesity by physical activity intervention can regain the stability of healthy state. When the loss of system bistability results from mechanical damage, physical activity intervention can delay the activation of inflammation within a window period after the mechanical damage. This window period is determined by the speed of inflammation onset in general and it can provide insights on the timing of exercise therapy according to different obesity and damage levels. In the future, this model can be calibrated with specific molecular data and

used to predict the inflammatory process regulated by obesity. Moreover, the mechanical response could be coupled to the current model through the production of fibronectin fragments to study the coeffects of inflammation and mechanics on OA onset and development.

Appendix A: The formula of parameter nondimensionalisation

$$\alpha_{BP_c} = \frac{C_0}{C_2 \cdot D_2}, \beta_{P_cP_c} = \frac{C_1}{C_2 \cdot D_2}, \beta_{A_dP_c} = \frac{C_3}{C_2 \cdot D_2}, \beta_{FP_c} = \frac{C_5}{C_2 \cdot D_2}, \gamma_{P_c} = \frac{D_1}{D_2},$$
$$\beta_{P_cA_c} = \frac{C_8}{C_7 \cdot D_2}, \theta_{P_cA_c} = \frac{C_9}{C_2}, \beta_{FA_c} = \frac{C_{10}}{C_7 \cdot D_2}, \theta_{FA_c} = \frac{C_{11}}{C_6}, \alpha_{BM} = \frac{C_{12} \cdot C_{21}}{C_6 \cdot D_2^2},$$
$$\beta_{P_cM} = \frac{C_{13} \cdot C_{21}}{C_6 \cdot D_2^2}, \theta_{P_cM} = \frac{C_{14}}{C_2}, \beta_{A_dM} = \frac{C_{15} \cdot C_{21}}{C_6 \cdot D_2^2}, \theta_{A_dM} = \frac{C_{16}}{C_4}, \theta_{A_cM} = \frac{C_{17}}{C_7},$$
$$\gamma_M = \frac{D_3}{D_2}, \mu_{NA_d} = \frac{C_{18}}{C_4 \cdot D_2}, \mu_{SA_d} = \frac{C_{19}}{C_4 \cdot D_2}, \theta_{A_d} = \frac{C_{20}}{C_4}, \gamma_{A_d} = \frac{D_4}{D_2},$$
$$Damage = \frac{C_{22}}{C_6 \cdot D_2}, \gamma_F = \frac{D_5}{D_2}$$

Appendix B: The description of dimensional parameters in the adipokine-mediated inflammation model in OA

Parameters	Description
C_0	Natural production rate of PICs
C_1	Stimulated production rate of PICs by PICs
C_2	Saturation constant at which the capability of stimulating PIC production signalled by PICs is half of maximum
C_3	Stimulated production rate of PICs by adipokines
C_4	Saturation constant at which the capability of stimulating PIC production signalled by adipokines is half of maximum
C_5	Stimulated production rate of PICs by Fn-fs
C_6	Saturation constant at which the capability of stimulating PIC production signalled by Fn-fs is half of maximum
C_7	Saturation constant at which the capability of inhibiting PIC production signalled by AICs is half of maximum
C_8	Stimulated production rate of AICs by PICs
C_9	Saturation constant at which the capability of stimulating AIC production signalled by PICs is half of maximum
C_{10}	Stimulated production rate of AICs by Fn-fs
C_{11}	Saturation constant at which the capability of stimulating AIC production signalled by Fn-fs is half of maximum
C_{12}	Natural production rate of MMPs
C_{13}	Stimulated production rate of MMPs by PICs
C_{14}	Saturation constant at which the capability of stimulating MMP production signalled by PICs is half of maximum
C_{15}	Stimulated production rate of MMPs by adipokines
C_{16}	Saturation constant at which the capability of stimulating MMP production signalled by adipokines is half of maximum
C_{17}	Saturation constant at which the capability of inhibiting MMP production signalled by AICs is half of maximum
C_{18}	The background production rate of adipokines due to the number of adipocytes

Continued on next page

C_{19}	The background production rate of adipokines due to the size of adipocytes
C_{20}	Saturation constant at which the capability of reducing adiposity through physical activity is half of maximum
C_{21}	Stimulated production rate of Fn-fs by MMPs
C_{22}	Stimulated production rate of Fn-fs due to mechanical damage
D_1	Clearance rate of PICs
D_2	Clearance rate of AICs
D_3	Clearance rate of MMPs
D_4	Clearance rate of adipokines
D_5	Clearance rate of Fn-fs
nex	The coefficient that governs the nonlinearity of physical activity effects at different BMI levels
n	Hill coefficient

Appendix C: The simultaneous equations when production rates are at equilibrium for the calculation of fixed points

$$H_{A_c}^1 = \tilde{A_c}^n\left(\tilde{t}\right) = \left[\alpha_{BP_c} + \beta_{P_cP_c} \cdot \frac{\tilde{P_c}^n\left(\tilde{t}\right)}{1+\tilde{P_c}^n\left(\tilde{t}\right)} + \beta_{A_dP_c} \cdot \frac{\tilde{A_d}^n\left(\tilde{t}\right)}{1+\tilde{A_d}^n\left(\tilde{t}\right)} + \beta_{FP_c} \cdot \frac{\tilde{F}^n\left(\tilde{t}\right)}{1+\tilde{F}^n\left(\tilde{t}\right)}\right] \cdot \frac{1}{\gamma_{P_c} \cdot \tilde{P}_c\left(\tilde{t}\right)} - 1$$

$$H_{A_c}^2 = \tilde{A}_c\left(\tilde{t}\right) = \beta_{P_cA_c} \cdot \frac{\tilde{P_c}^n\left(\tilde{t}\right)}{\theta_{P_cA_c}^n + \tilde{P_c}^n\left(\tilde{t}\right)} + \beta_{FA_c} \cdot \frac{\tilde{F}^n\left(\tilde{t}\right)}{\theta_{FA_c}^n + \tilde{F}^n\left(\tilde{t}\right)}$$

where there are the equations of $\tilde{M}\left(\tilde{t}\right)$, $\tilde{A}_d\left(\tilde{t}\right)$ and $\tilde{F}\left(\tilde{t}\right)$:

$$\tilde{M}\left(\tilde{t}\right) = \left[\alpha_{BM} + \beta_{P_cM} \cdot \frac{\tilde{P_c}^n\left(\tilde{t}\right)}{\theta_{P_cM}^n + \tilde{P_c}^n\left(\tilde{t}\right)} + \beta_{A_dM} \cdot \frac{\tilde{A_d}^n\left(\tilde{t}\right)}{\theta_{A_dM}^n + \tilde{A_d}^n\left(\tilde{t}\right)}\right] \cdot \frac{\theta_{A_cM}^n}{\theta_{A_cM}^n + \tilde{A_c}^n\left(\tilde{t}\right)} \cdot \frac{1}{\gamma_M}$$

$$\tilde{A}_d\left(\tilde{t}\right) = \left\{\mu_{NA_d} + \left[\,\mu_{SA_d} \cdot\ f\left(BMI^{meas}\right) \cdot \frac{DailyCal}{BMR \cdot PAL}\,\right] \cdot \frac{\theta_{A_d}^{nex}}{\theta_{A_d}^{nex} + \tilde{A_d}^{nex}\left(\tilde{t}\right)}\right\} \cdot \frac{1}{\gamma_{A_d}}$$

$$\tilde{F}\left(\tilde{t}\right) = \frac{\tilde{M}\left(\tilde{t}\right) + Damage}{\gamma_F}$$

Appendix D: Phase plane and bifurcation diagrams of the inflammation system

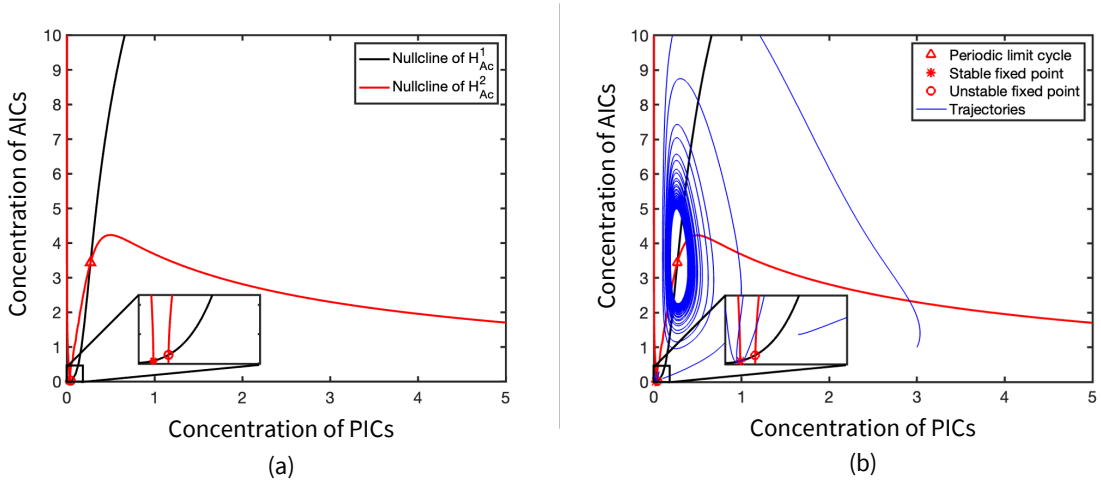

Figure D.1: *The phase plane of the inflammation system under the baseline parameters: (a) Intersections of nullclines; (b) Trajectories in the phase plane.*

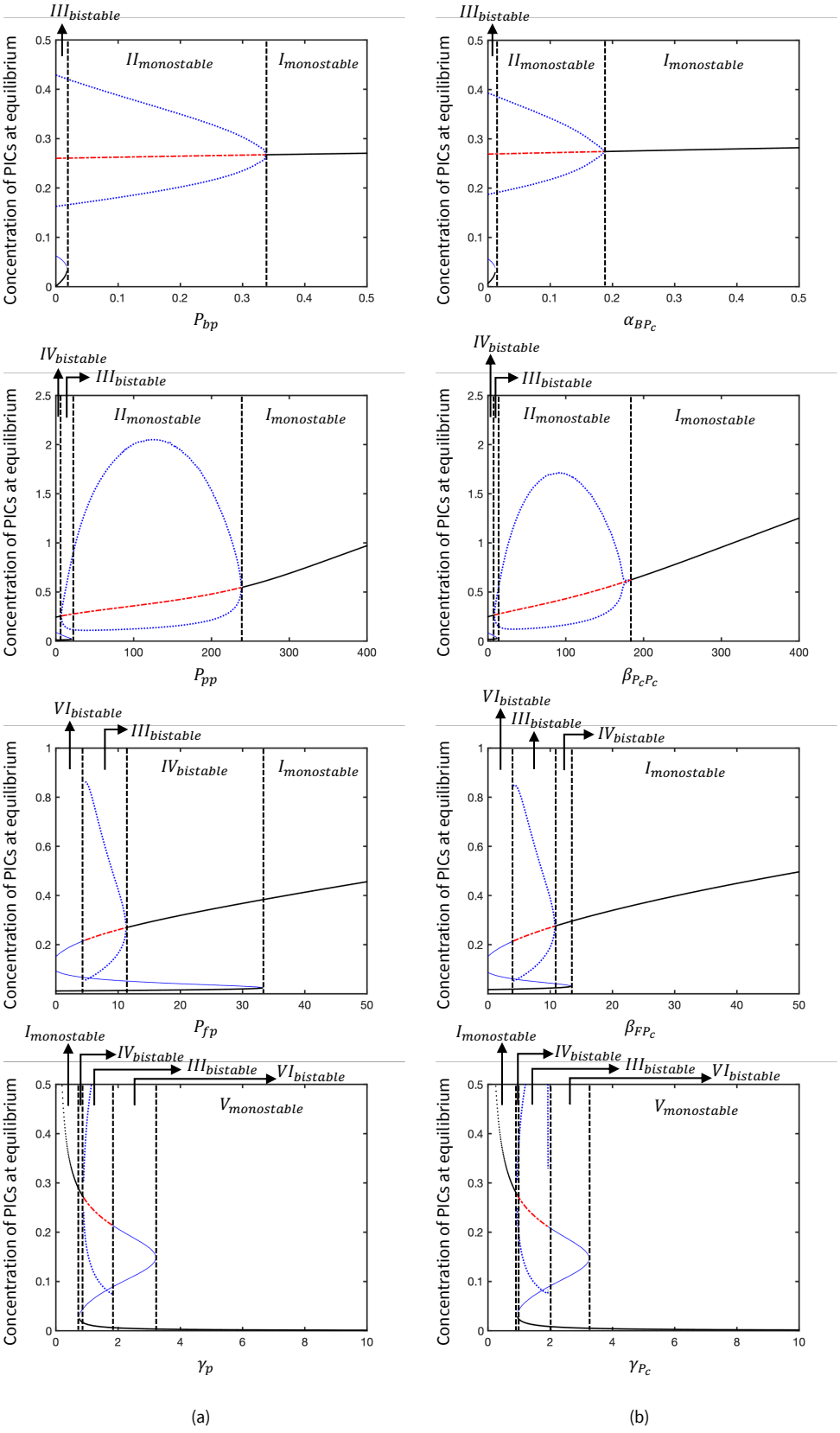

Figure D.2: *The comparison of bifurcation diagrams in the production of PICs between (a) Baker's model and (b) the adipokine-mediated inflammation model.*

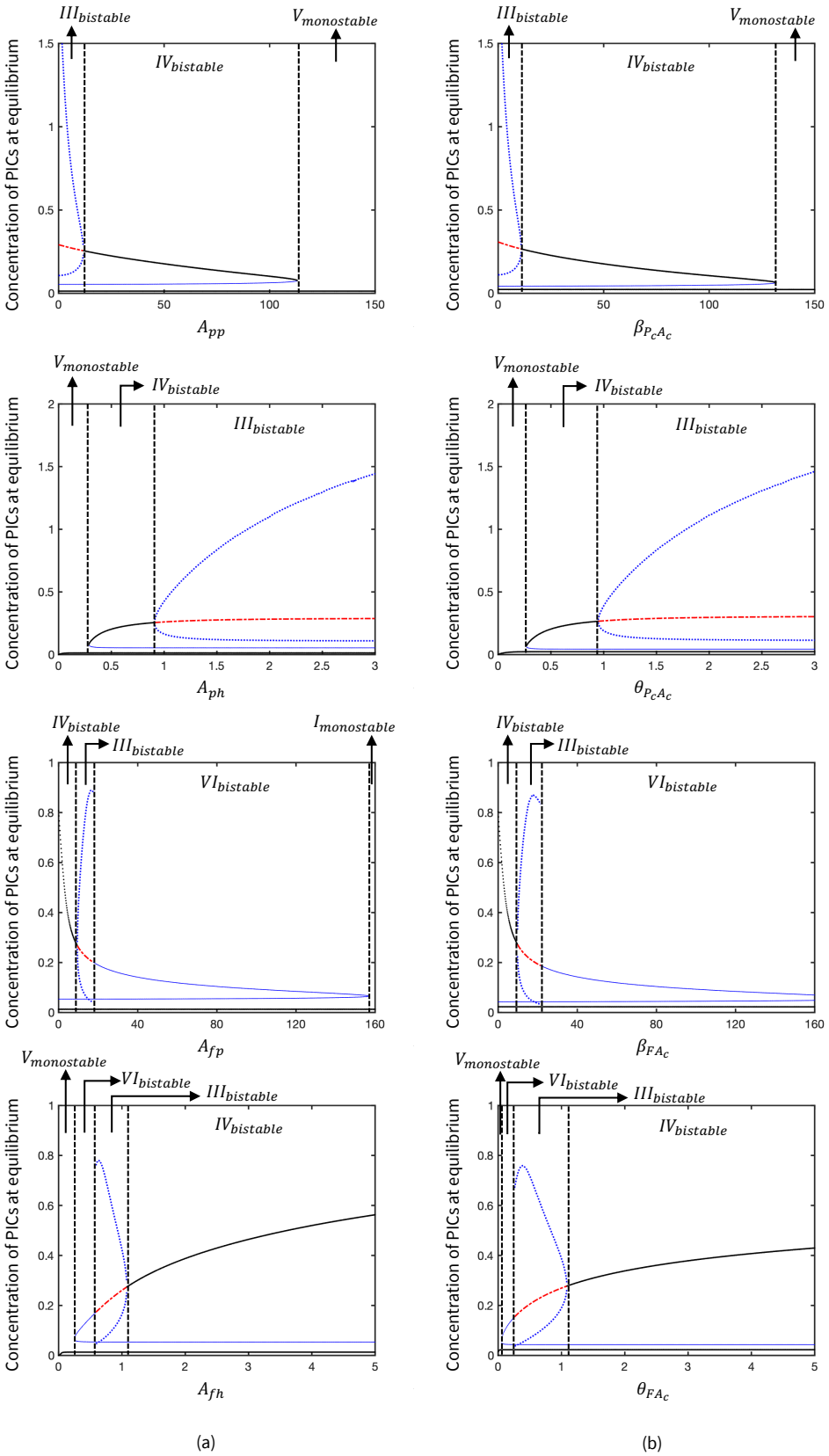

Figure D.3: *The comparison of bifurcation diagrams in the production of AICs between (a) Baker's model and (b) the adipokine-mediated inflammation model.*

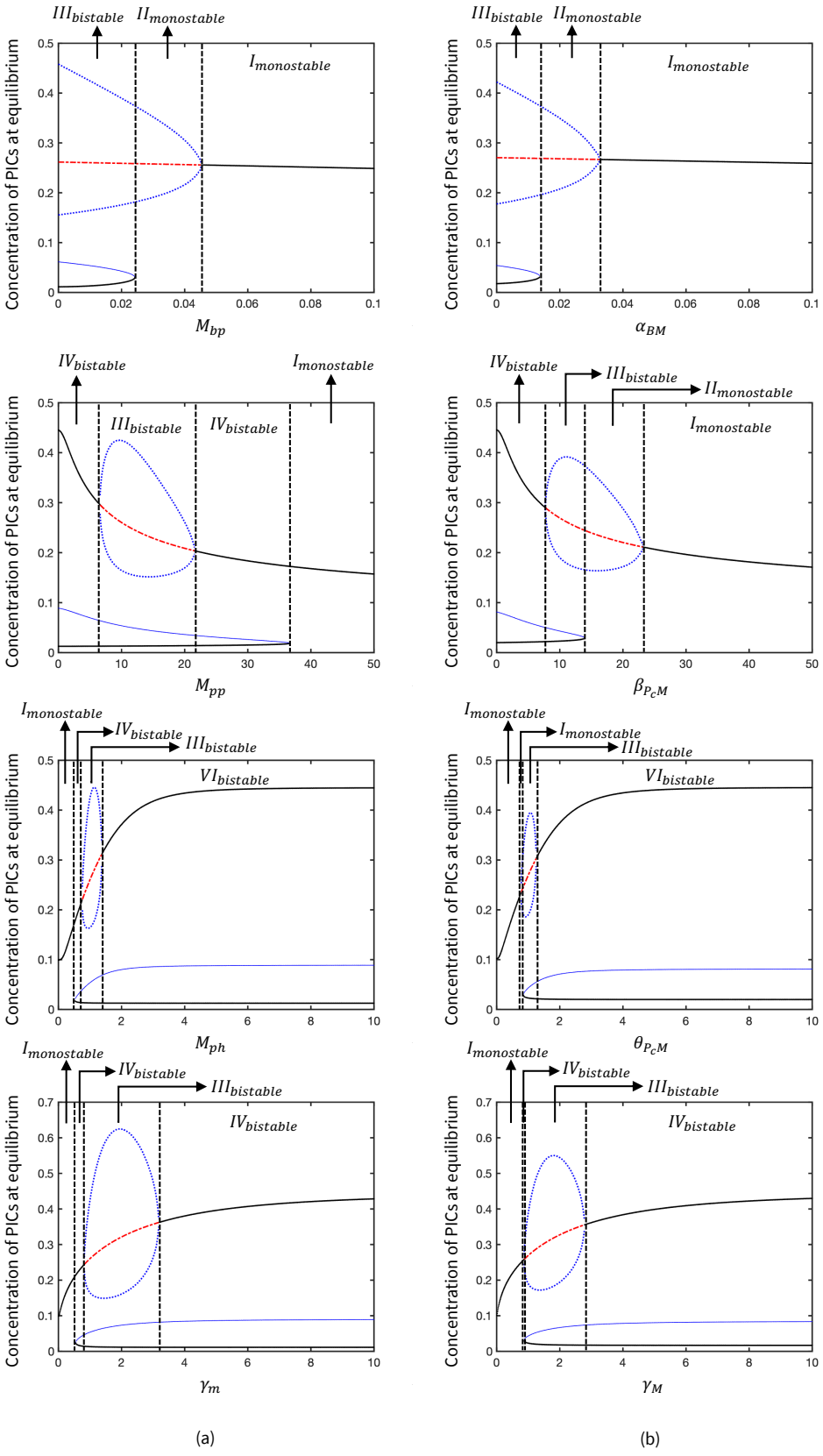

Figure D.4: *The comparison of bifurcation diagrams in the production of MMPs between (a) Baker's model and (b) the adipokine-mediated inflammation model.*

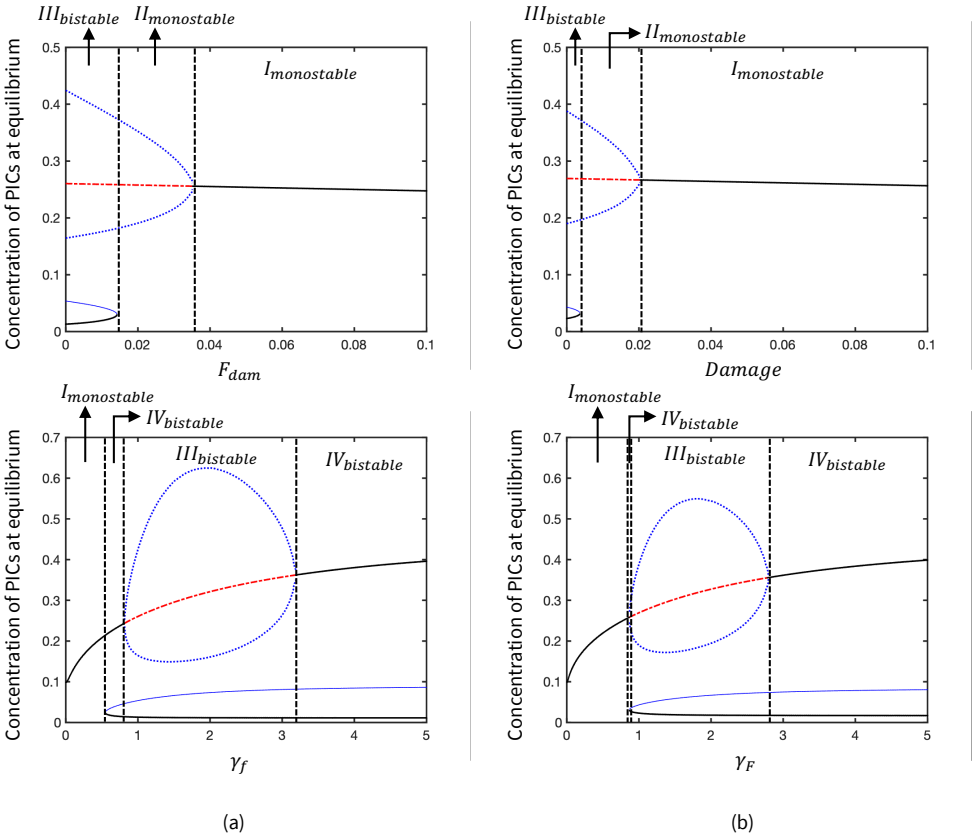

Figure D.5: *The comparison of bifurcation diagrams in the production of Fn-fs between (a) Baker's model and (b) the adipokine-mediated inflammation model.*

Chapter 4

A computational study of adiposity-associated factors in the inflammatory process of osteoarthritis

The mathematical model of adipokine-mediated inflammation developed in Chapter 3 is parameterised through literature-based estimates of parameters in this chapter. Model nondimensionalisation and the analysis of system dynamics were conducted in Chapter 3 to explore the sensitivity obesity-associated parameters. Building on this foundation, this chapter aims to understand the roles of adiposity-associated parameters, intervention strategies and mechanical damage in a physical time dimension, which necessitates model parameterisation. In particular, three physical activity intervention strategies are analysed with different levels of BMI through simulations of the inflammatory activities. This study contributes to understanding the effects of adiposity-modifying interventions and demonstrates the application of computational modelling for simulating the inflammatory activities with different intervention strategies in OA inflammation. In addition, the time scale of inflammatory responses approximated in this chapter provides a temporal interface for the integration of inflammation and mechanical loading in Chapter 5.

The work presented in this chapter has been published in Journal of Theoretical Biology, and the author accepted manuscript is available under a CC BY 4.0 license and has been adapted for consistency and readability with the thesis format: J. Lai and D. Lacroix, "A computational study of adiposity-associated factors in the inflammatory process of osteoarthritis", Journal of Theoretical Biology, vol. 625, p. 112429, May 2026, doi: 10.1016/j.jtbi.2026.112429.

4.1 Introduction

Osteoarthritis (OA) is a chronic pathological outcome within the whole synovial joint, resulting from the intricate interactions of pathogenic pathways across multiple scales [24]. These include metabolism-driven inflammation at the molecular and cellular scale and loading-induced mechanical injury at the tissue scale. As a prominent and modifiable risk factor of OA, obesity has become a global health issue at a pandemic level over the course of the last 50 years [217]. The increasing exposure to the risk of obesity is significantly contributing to the worldwide burden of OA. By 2050, the global population with OA is anticipated to reach 642 million, where there may be over 20% of OA cases associated with obesity [5]. The resulting financial burden is projected to be as high as 2.5% of gross national product (GNP) in developed countries [218]. To date, the emphasis of OA treatments is in the management of symptoms, including pain relief and improvements in joint function, through education, lifestyle modification, physical activity therapy or pharmacological prescriptions [24]. The precise mechanisms underlying OA remain unclear at present, rendering it unattainable to develop effective treatments. Modern consensus acknowledges the crucial roles of metabolic disturbance and biomechanical abnormalities in OA pathology [24]. Emerging evidence reveals that low-grade inflammation is present prior to the structural signs of OA [16, 83]. Adipose tissue has been shown to regulate the inflammatory process in the pathogenesis of OA [41, 42, 55, 57]. Body mass index (BMI) is the most common metric for the estimation of adiposity and the identification of obesity [39]. The elevation in per unit BMI correlates with a 15% increased risk of developing OA [23, 44]. At a high level of BMI, the excessive production of adipokines [45, 89, 92, 94] can stimulate OA inflammation, and the risk of tissue damage increases due to abnormal mechanical loading [215].

The cycle of the inflammatory process in OA can be activated by a variety of risk factors such as genetics, age, obesity, and injury [24]. Pattern-recognition receptors (PRRs) and damage-associated molecular patterns (DAMPs) are recognised by the innate immune system [219] when inflammatory mediators are released in response to the inflammation. The inflammatory mediator groups can be categorised by different metabolic roles. Primarily, pro- and anti-inflammatory cytokines (PICs and AICs) [87, 220] modulate the catabolic and anabolic processes reciprocally. Matrix metalloproteinases (MMPs) [104] and chemokines [88] are two key enzymes involved in the regulation of tissue composition. In the progression of OA, tissue composition degrades with the release of fibronectin fragments (Fn-fs) [205]. As a

type of damaging products within cartilage tissue, Fn-fs can stimulate inflammatory responses. In addition, adipokines serve as a critical mediator family that induces inflammation and tissue degradation by disrupting the metabolic balance within the inflammatory cycle [100].

Despite the improved understanding of OA inflammation, it is still difficult to facilitate consensus on identifying drivers of early OA due to the complex and simultaneous cascades of molecular signal transduction [32]. In the current understanding of OA, molecular signalling pathways differ not only across pathogenic tissue types, but also temporally interrelate over the progression of OA. This understanding could be responsible for the manifestation of OA as a whole-joint disease. The lack of consensus on specific OA phenotypes and endotypes is a main factor underlying challenges in developing valid treatments [34]. Empirical evidence shows that exercise contributes to OA management by influencing the heterogeneity of phenotypes and endotypes at both systemic and local levels. Specifically, exercise can ultimately modulate the levels of inflammatory mediators [197, 221–229] through the channel of mechanical transduction [22, 230] and the alteration of metabolic environments such as the reduction of adipose tissue [199, 231, 232], thereby reducing the overall risk of OA. Physical activity has accordingly become the mainstream strategy to manage OA [233–236]. Since the degeneration of joints in OA is progressive, proper physical activities play a positive role in the prevention of OA, adapting to the population with different risk levels. In addition to the aforementioned metabolism-related outcomes, physical activity can improve general health, muscle strength and joint stability, serving as primary intervention by contributing to the protection of joints from the onset of OA in susceptible populations [233]. The implementation of physical activity can also be considered as secondary prevention by aiming to slow the progressive degeneration of joints in individuals with early OA [233]. Nevertheless, there is no clear consensus yet on the specific criteria for physical activity prescriptions to maximise therapeutic benefits in OA [236].

The heterogeneity of OA pathology leads to diverse and interacting degenerative pathways across the entire joint. This makes it challenging to identify and examine the underlying mechanisms for different phenotypes and endotypes. To overcome this challenge, computational modelling approaches exhibit the advantages in exploring the pathological mechanisms of OA [46]. Aside from reducing environmental and experimental costs, computational approaches are exceptionally suited to integrate the fragmented knowledge of different pathways in OA onset and development. This knowledge-based integration allows for the classification

and analysis of distinct, simultaneously interacting pathological pathways. As a result of that, emerging mathematical models [119, 127–129, 136–138, 206, 207, 237] have been recently established to study cartilage degeneration and inflammation. However, only one mathematical model with five variables considers the metabolic effects of adipokines in the context of obesity, which was developed in our previous work [237]. This general model includes the signalling pathways of adipokines that mediate OA inflammation for the first time. While other models [127, 129, 137] incorporate mechanical loading as a stimulus, our model uniquely introduces physical activity level (PAL) as a parameter that regulates adiposity in conjunction with BMI and nutrition. This enables the possibility to computationally analyse the overall adiposity-associated effects on the inflammatory process of OA. Due to the difficulty in acquiring data, parameters were non-dimensionalised in the development of the general five-variable model [237] and the focus was the analysis of inflammation dynamics in OA. Nevertheless, the roles of physical activity and adiposity in OA inflammation remain unclear for different cohorts stratified by BMI levels. Moreover, the nondimensionalisation of this model hindered the optimisation of the strategy to reduce OA inflammation risk through physical activity within a temporal framework, due to the uncertainty in the global parametric space. Therefore, this study aimed to parameterise this dimensionless model using literature-based estimates, and to examine the effects of adiposity-associated factors (BMI and PAL) on the inflammatory activities through the pathway of altering adiposity, with identifying various temporal strategies of physical activity intervention. The representative molecular half-lives were estimated as an approximation of time granularity for the parameterisation of this five-variable model. A global sensitivity analysis was performed to identify the critical correlations between inflammatory responses and the estimated parameter space by a global mapping of system behaviours. The inflammatory processes were simulated to analyse the effects of physical activity when varying the mechanical damage level and BMI to represent different cohorts.

4.2 Methods

4.2.1 Governing equations

A minimal model of adipokine-mediated inflammation was developed in a previous study [237]. The general inflammation model includes five state variables (Figure 4.1): PICs, AICs, MMPs, adipokines and Fn-fs, as denoted respectively by P_c, A_c, M, A_d, F.

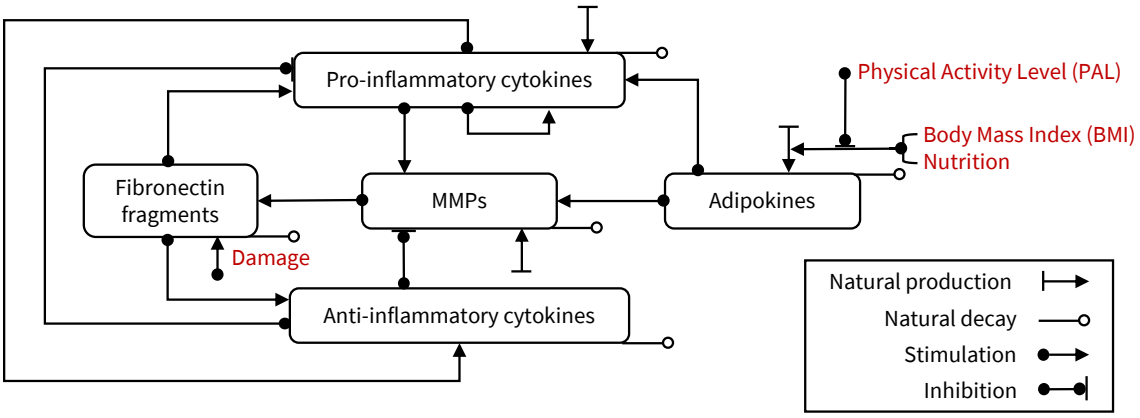

Figure 4.1: *The regulatory network of the PICs, AICs, MMPs, adipokines and Fn-fs in OA inflammation. Reproduced from Lai and Lacroix (2025) under CC BY 4.0 [237]. PICs, AICs, MMPs, adipokines and Fn-fs interact to mediate the inflammatory process of OA. Damage is an external source to stimulate the production of Fn-fs due to the tissue injury resulting from mechanics. The production of adipokines is associated with the level of adiposity. PAL, BMI and nutrition are three modifiable system attributes that measure the adiposity level to govern the adipokine production.*

The mathematical formation of this minimal model is based on several assumptions and simplifications. The dynamical effects of cells including macrophages and chondrocytes are not explicitly included, and the inflammatory process is confined to the synovial joint where a homogeneous environment is assumed. In addition, inflammatory mediators are signalled as an entire group in this minimal model, and the same mediator group exhibits similar metabolic effects on OA inflammation. Accordingly, the reaction kinetics of each mediator group is approximated by a specific molecular phenotype that dominates the group concentration or the average of different phenotypes. The kinetics of mediator reactions is formulated in Equations (4.1) to (4.6), where n is the Hill coefficient [237] of reaction kinetics. In addition to stimulation and inhibition, each production group contains a term of decay rate depending on the half-life of the representative mediator.

PICs and AICs concurrently regulate the inflammatory activities in OA and interact with other mediators. The production of PICs results from the response of the immune system as well as local chondrocytes, whereas AICs are primarily released due to the stimulation of immune cells [87]. The production source of PICs is characterised by a local natural production term supplemented by three stimulation pathways, which is modelled as Equation (4.1). Interleukin-6 (IL-6) was selected for the representation of PIC group [220] to reduce the complexity of the model, meanwhile, interleukin-4 (IL-4) represents AIC group in this model where there are two

stimulating feedback from PICs and Fn-fs. The production of AICs is modelled as Equation (4.2).

$$\frac{dP_c(t)}{dt} = \left[C_0 + C_1 \cdot \frac{P_c^n(t)}{C_2^n + P_c^n(t)} + C_3 \cdot \frac{A_d^n(t)}{C_4^n + A_d^n(t)} + C_5 \cdot \frac{F^n(t)}{C_6^n + F^n(t)}\right] \cdot \frac{C_7^n}{C_7^n + A_c^n(t)} - D_1 \cdot P_c(t) \quad (4.1)$$

$$\frac{dA_c(t)}{dt} = C_8 \cdot \frac{P_c^n(t)}{C_9^n + P_c^n(t)} + C_{10} \cdot \frac{F^n(t)}{C_{11}^n + F^n(t)} - D_2 \cdot A_c(t) \quad (4.2)$$

where C_0, C_1, C_3, C_5, C_7 are the rate parameters and C_2, C_4, C_6, C_7 are the saturation parameters in PIC production; C_8, C_{10} are the rate parameters and C_9, C_{11} are the saturation parameters in AIC production; and D_1, D_2 are the clearance parameters for PICs and AICs, respectively.

MMP-1 and MMP-13 are two main pivotal types of MMPs, and their half-lives were averaged to estimate the production of MMPs [140]. Excessive levels of PICs and adipokines can drive the release of MMPs to enhance tissue remodelling activities, leading to two stimulation terms. The inhibition sources are from AICs applied to all the pathways involved in the production of MMPs. The production of MMPs is modelled as Equation (4.3).

$$\frac{dM(t)}{dt} = \left[C_{12} + C_{13} \cdot \frac{P_c^n(t)}{C_{14}^n + P_c^n(t)} + C_{15} \cdot \frac{A_d^n(t)}{C_{16}^n + A_d^n(t)}\right] \cdot \frac{C_{17}^n}{C_{17}^n + A_c^n(t)} - D_3 \cdot M(t) \quad (4.3)$$

where C_{12}, C_{13}, C_{15} are the rate parameters and C_{14}, C_{16}, C_{17} are the saturation parameters in MMP production, and D_3 is the clearance parameter for MMPs.

Due to the lack of documented data on adipokines, leptin is selected to represent the primary behaviour of adipokine group. Leptin level is positively correlated to BMI level [92], which aligns with the assumptions of adipokine production behind this model. Specifically, the production of adipokines is determined by two main sources, the number and size of adipocytes (C_{18} and C_{19}). The variations of adiposity primarily depend on the adipocyte size that can be varied by BMI, nutrition and PAL, therein the nutritional term is defined by the proportion of daily calorie intake ($DailyCal$) to basal metabolic rate (BMR). The production of adipokines is modelled as Equation (4.4) and Equation (4.5) is the function of BMI^{meas} scaling the production rate driven by the size of adipocytes.

$$\frac{dA_d(t)}{dt} = C_{18} + \left[C_{19} \cdot \ f(BMI^{meas}) \cdot \frac{DailyCal}{BMR \cdot PAL}\right] \cdot \frac{C_{20}^{nex}}{C_{20}^{nex} + A_d^{nex}(t)} - D_4 \cdot A_d(t) \quad (4.4)$$

$$f\left(BMI^{meas}\right) = \frac{BMI^{meas}}{BMI^{std}} \tag{4.5}$$

where C_{18}, C_{19} are the rate parameters and BMI^{meas}, $DailyCal$, BMR, PAL, C_{20}, nex are the adiposity-associated parameters altering the production rate of adipokines. D_4 is the clearance parameter for adipokines. BMI^{std} is the standard BMI in measuring obesity [39]. In particular, C_{20} and nex are the parameters determined by PAL and BMI^{meas} respectively, approximating the nonlinear effects of physical activity on adipokine production at different levels of BMI [199, 231].

As the damage breakdowns, Fn-fs are released from the tissue degradation that is governed by two parameters (C_{21} and C_{22}). C_{21} is associated with the level of MMPs when C_{22} measures the level of mechanical damage. The production of Fn-fs is modelled as Equation (4.6).

$$\frac{dF\left(t\right)}{dt} = C_{21} \cdot M\left(t\right) + C_{22} - D_5 \cdot F\left(t\right) \tag{4.6}$$

where C_{21}, C_{22} are the rate parameters in the production of Fn-fs, and D_5 is the clearance parameter for Fn-fs.

4.2.2 Parameterisation

Since capturing all the chemical-biological reactions is not viable yet, the illustrative parameterisation of this model is essential to exhibit the net effects of signal transduction on the mediator production according to the molecular decay rates. The decay rates can delineate the time scale of mediator production, converted by Equation (4.7) according to the estimated half-life of each representative mediator.

$$D_{im} = \frac{\ln 2}{T^{im}_{half-life}}, (im = P_c, A_c, M, A_d, F) \tag{4.7}$$

where D_{im} is the decay rate of each mediator, and $T^{im}_{half-life}$ is the half-life of the constituent at each generation.

The estimated decay rates and the corresponding production parameters are presented in Tables 4.1 to 4.5. The half-lives of IL-6 [140] and IL-4 [208] are estimated as 4 days and 20 min respectively, leading to the decay rates of PICs and AICs (D_1 and D_2). The half-life of MMPs is approximated as 120 h by the average of MMP-1 and MMP-13 to estimate the decay rate of MMPs (D_3) [127]. The half-life of leptin is reported as 25 mins [238], from which the decay rate of adipokines (D_4) is estimated. The decay rate of Fn-fs (D_5) is estimated based on its approximate half-life of 7 days [239].

For simplicity, the natural production rates (C_0, C_{12}) are estimated as 1 percent of the corresponding decay rates so that natural production is not dominant in prompting inflammation. Additionally, the stimulated production parameters of PICs and MMPs (C_1, C_3, C_5, C_8, C_{10}, C_{13}, C_{15}) are 10 times the values of decay rates to play a primary role in regulating inflammatory processes. To maintain the balance of MMPs and Fn-fs production, the effects of MMPs are not negligible so C_{21} is set to match the magnitude of the Fn-fs decay rate. Since the variability of mediator concentration has yet to be thoroughly assessed and there exists a limited amount of data demonstrating the saturating effects of inflammatory mediators in OA, the saturation constants (C_2, C_4, C_6, C_7, C_9, C_{11}, C_{14}, C_{16}, C_{17}) are estimated to be an order of magnitude smaller than the corresponding stimulated production rate in Hill functions. This assumption helps to minimise bias from overestimating or underestimating saturation effects due to the uncertainty in mediator concentration. Accordingly, the level of mediator is illustrative to exhibit the minimally essential system behaviours of inflammation. C_{22} is an arbitrary parameter measuring the level of mechanical damage within tissue. Hill coefficient (n) is set to 2 for all the signalling feedback from multiple receptors in inflammatory regulations [119].

Table 4.1: *Descriptions of the estimated parameters in the production of PICs.*

Parameter	Description	Value	Reference
C_0	Natural production rate of PICs	0.05	Estimated
C_1	Stimulated production rate of PICs by PICs	50	Estimated
C_2	Saturation constant at which the capability of stimulating PIC production signalled by PICs is half of maximum	5	Estimated
C_3	Stimulated production rate of PICs by adipokines	50	Estimated
C_4	Saturation constant at which the capability of stimulating PIC production signalled by adipokines is half of maximum	5	Estimated
C_5	Stimulated production rate of PICs by Fn-fs	50	Estimated
C_6	Saturation constant at which the capability of stimulating PIC production signalled by Fn-fs is half of maximum	5	Estimated
C_7	Saturation constant at which the capability of inhibiting PIC production signalled by AICs is half of maximum	5	Estimated
D_1	Clearance rate of PICs	5.2	[140]
n	Hill coefficient	2	[119]

Table 4.2: *Descriptions of the estimated parameters in the production of AICs.*

Parameter	Description	Value	Reference
C_8	Stimulated production rate of AICs by PICs	1×1.5^4	Estimated
C_9	Saturation constant at which the capability of stimulating AIC production signalled by PICs is half of maximum	1×1.5^3	Estimated
C_{10}	Stimulated production rate of AICs by Fn-fs	1×1.5^4	Estimated
C_{11}	Saturation constant at which the capability of stimulating AIC production signalled by Fn-fs is half of maximum	1×1.5^3	Estimated
D_2	Clearance rate of AICs	1.5×10^3	[208]
n	Hill coefficient	2	[119]

Table 4.3: *Descriptions of the estimated parameters in the production of MMPs.*

Parameter	Description	Value	Reference
C_{12}	Natural production rate of MMPs	0.05	Estimated
C_{13}	Stimulated production rate of MMPs by PICs	50	Estimated
C_{14}	Saturation constant at which the capability of stimulating MMP production signalled by PICs is half of maximum	5	Estimated
C_{15}	Stimulated production rate of MMPs by adipokines	50	Estimated
C_{16}	Saturation constant at which the capability of stimulating MMP production signalled by adipokines is half of maximum	5	Estimated
C_{17}	Saturation constant at which the capability of inhibiting MMP production signalled by AICs is half of maximum	5	Estimated
D_3	Clearance rate of MMPs	4.2	[127]
n	Hill coefficient	2	[119]

Table 4.4: *Descriptions of the estimated parameters in the production of adipokines.*

Parameter	Description	Value	Reference
C_{18}	The background production rate of adipokines due to the number of adipocytes	500	Estimated
C_{19}	The background production rate of adipokines due to the size of adipocytes	500	Estimated
BMI^{std}	The standard BMI	25	[39]
C_{20}	Saturation constant at which the capability of reducing adiposity through physical activity is half of maximum	Dependent on PAL	Estimated
$\frac{DailyCal}{BMR}$	The nutritional term defined by the ratio of daily calorie intake to BMR	1	Estimated
nex	The coefficient that governs the nonlinearity of physical activity effects at different BMI levels	Dependent on BMI^{meas}	Estimated
D_4	Clearance rate of adipokines	1.2×10^3	[238]

Table 4.5: *Descriptions of the estimated parameters in the production of Fn-fs.*

Parameter	Description	Value	Reference
C_{21}	Stimulated production rate of Fn-fs by MMPs	3	Estimated
C_{22}	Stimulated production rate of Fn-fs due to mechanical damage	0	Estimated
D_5	Clearance rate of Fn-fs	3	[239]

The production rates driven by the number and size of adipocytes (C_{18}, C_{19}) are estimated to be 500 for the baseline in analysis. This confines the system so that the stability of steady states is sensitive to the production of adipokines governed by BMI and PAL, as presented in Figure E.1. Based on the given values of C_{18} and C_{19}, a sensitivity analysis on the coefficients (nex, C_{20}) related to BMI and PAL was performed to estimate their boundaries, as shown in Figure 4.2. Accordingly, two piecewise functions are given to determine the aforementioned coefficients, as detailed in Equations (4.8) and (4.9). The calibration of the two piecewise functions ensures that the relationship between PAL and adipokine production is aligned with the present knowledge in general [237]. In addition, the ranges of BMI and PAL are constrained according to [237], and the nutrition term ($\frac{DailyCal}{BMR}$) is assumed to be 1 for the dietary control in this study.

$$nex = \begin{cases} B_{ND} - BMI^{meas} \cdot \dfrac{B_{ND} - B_{NW}}{R_{ND} - R_{ND_{min}}}, & if\ R_{ND_{min}} < BMI^{meas} < R_{ND} \\ B_{NW} - (BMI^{meas} - R_{ND}) \cdot \dfrac{B_{NW} - B_{OW}}{R_{NW} - R_{ND}}, & if\ R_{ND} \leqslant BMI^{meas} \leqslant R_{NW} \\ B_{OW} - (BMI^{meas} - R_{NW}) \cdot \dfrac{B_{OW} - B_{O}}{R_{OW} - R_{NW}}, & if\ R_{NW} < BMI^{meas} \leqslant R_{OW} \\ B_{O} - (BMI^{meas} - R_{OW}) \cdot \dfrac{B_{O} - B_{EO}}{R_{O} - R_{OW}}, & if\ R_{OW} < BMI^{meas} < R_{O} \\ \dfrac{R_O}{BMI^{meas}}, & if\ BMI^{meas} \geqslant R_O \end{cases} \tag{4.8}$$

$$C_{20} = \begin{cases} B_S - (PAL - R_{S_{min}}) \cdot \dfrac{B_S - B_{LA}}{R_S - R_{S_{min}}}, & if\ R_{S_{min}} \leqslant PAL \leqslant R_S \\ B_{LA} - (PAL - R_S) \cdot \dfrac{B_{LA} - B_A}{R_{LA} - R_S}, & if\ R_S < PAL \leqslant R_{LA} \\ B_A - (PAL - R_{LA}) \cdot \dfrac{B_A - B_{VA}}{R_A - R_{LA}}, & if\ R_{LA} < PAL \leqslant R_A \\ B_{VA} - (PAL - R_A) \cdot \dfrac{B_{VA}}{R_{VA} - R_A}, & if\ R_A < PAL \leqslant R_{VA} \end{cases} \tag{4.9}$$

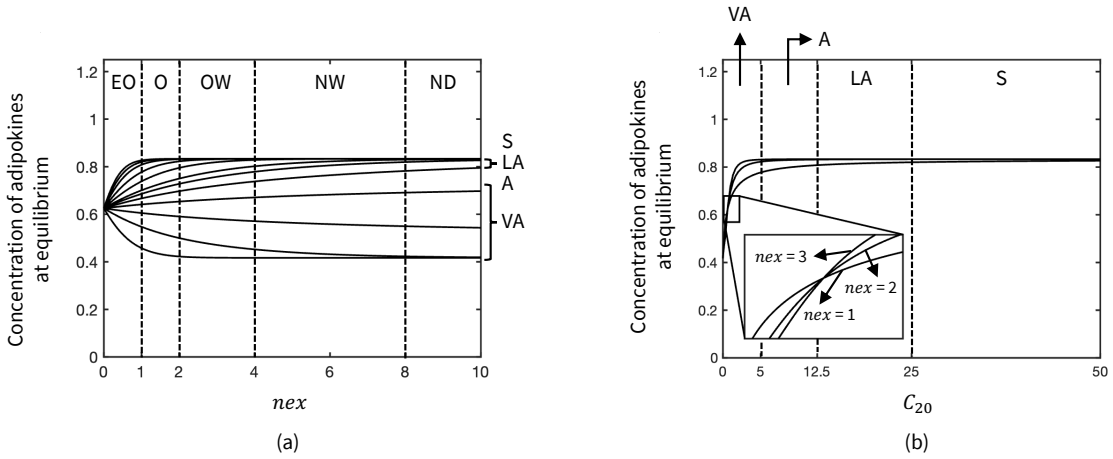

Figure 4.2: *The calibration of boundaries for the coefficients governing the decrease of adiposity: (a) nex; (b) C_{20}. The level of BMI includes extreme obesity (EO), obesity (O), overweight (OW), normal weight (NW) and nutritional deficiency (ND). The level of physical activity includes sedentary (S), low active (LA), active (A) and very active (VA). The BMI and PAL ranges are presented in Table 4.6.*

where the boundaries of nex and C_{20} are estimated to be $B_{ND} = 10$, $B_{NW} = 8$, $B_{OW} = 4$, $B_O = 2$, $B_{EO} = 1$, $B_S = 50$, $B_{LA} = 25$, $B_A = 12.5$, $B_{VA} = 5$. The range parameters of BMI level and PAL follow their categorised definitions [39, 212] in Table 4.6.

4.2.3 Sensitivity analysis of inflammation and obesity

Parameter sensitivity analysis was performed for the production of those five mediators in a global parameter space using Latin hypercube sampling/partial rank correlation coefficient (LHS/PRCC). LHS/PRCC is a global sensitivity analysis method for measuring the correlation between model inputs and outputs [240]. The inputs are the model parameters sampled by LHS, and 1,000 samples were uniformly generated, varying from 0.5 to 2 times the estimated baseline parameter values of reaction kinetics. BMI and PAL are in the range of $(0, 50]$ and $[1, 2.5]$ respectively. PRCCs and corresponding p-values were calculated for the level of each mediator at a steady state in this model, where a significance threshold of $p < 0.01$ was applied [140].

Table 4.6: *The categories and ranges of BMI and PAL.*

Level of obesity	Interval of BMI^{meas}
Nutritional deficiency (ND)	$(R_{ND_{min}}, R_{ND}) \equiv (0, 18.5)$
Normal weight (NW)	$[R_{ND}, R_{NW}] \equiv [18.5, 24.9]$
Overweight (OW)	$(R_{NW}, R_{OW}] \equiv (24.9, 29.9]$
Obesity (O)	$(R_{OW}, R_O) \equiv (29.9, 40)$
Extreme obesity (EO)	$[R_O, \infty) \equiv [40, \infty)$
Level of physical activity	**Interval of PAL**
Sedentary (S)	$[R_{S_{min}}, R_S] \equiv [1, 1.39]$
Low active (LA)	$(R_S, R_{LA}] \equiv (1.39, 1.59]$
Active (A)	$(R_{LA}, R_A] \equiv (1.59, 1.89]$
Very active (VA)	$(R_A, R_{VA}] \equiv (1.89, 2.5]$

4.2.4 Computational configurations of the inflammatory process

By implementing the baseline parameters, the system of ODEs was solved with a relative accuracy of 0.001 using *ode15s* of implicit method in MATLAB (R2024a, The Math Works, Inc., Natick, MA, USA) to simulate the inflammatory process. The threshold of mechanical damage level (C_{22}) that results in inflammation was computed for various cases, while considering the variations in BMI and PAL. To analyse the effects of physical activity intervention, the temporal variations of inflammatory mediators were simulated according to different levels of BMI (Figure 4.3). Normal weight (NO), overweight (OW), low obesity (LO) and high obesity (HO) were four representative cases in simulations. The level of PICs serves as a marker for measuring the level of inflammation. At baseline, the levels of inflammatory mediators stay in a healthy state with the PIC level at a low value of approximately 0.5. A damage level ($C_{22} = 1.2$) was applied at month 12 to induce inflammation, resulting in an increase in the PIC level over 15 in an inflamed state. Meanwhile, different physical activity intervention strategies were performed in the time domain with a mild increased level ($PAL = 1.5$) to neglect the negative effects of overloading. The interval between introducing mechanical damage and the latest allowable start of physical activity intervention that remained effective for preventing inflammation was quantified as the window period.

To explore the sensitivity of three main factors (the mechanical damage level,

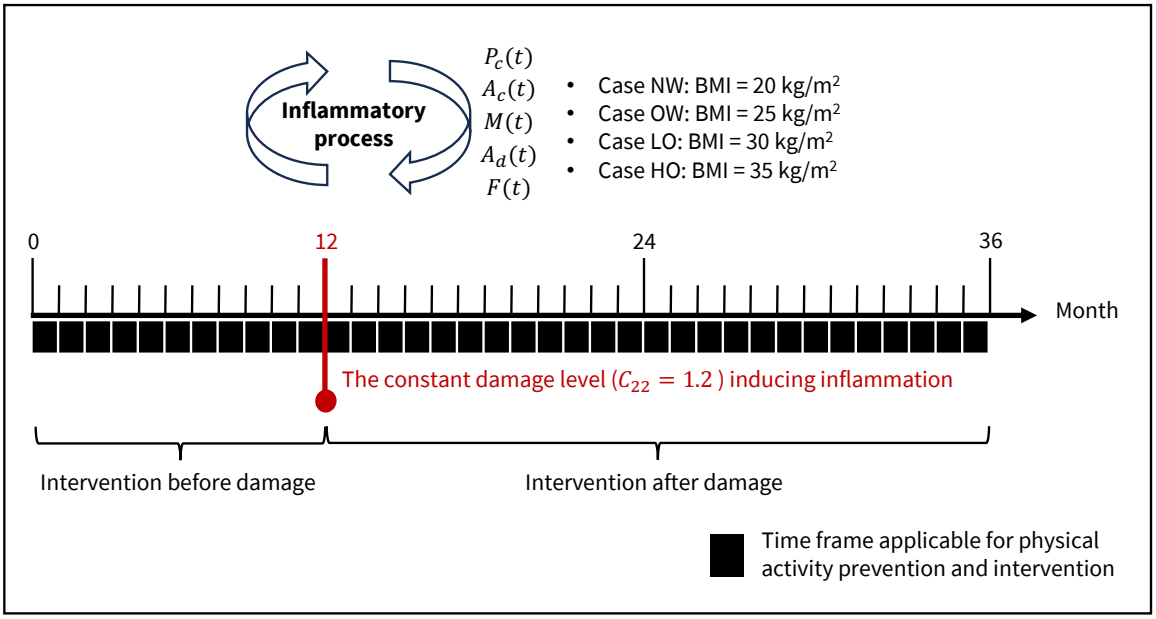

Figure 4.3: *The strategies of physical activity intervention in the inflammatory process for four representative cases (NW: Normal weight; OW: Overweight; LO: Low obesity; HO: High obesity).*

BMI, and the level of physical activity for intervention), the variations of window period were measured in the inflammatory process when varying their values respectively. As the illustrative case, mechanical damage level, BMI and PAL were controlled at 1.2, 25 and 1.5 respectively while serving as covariables.

4.3 Results

4.3.1 Parameter sensitivity

The correlations between parameters and the level of each inflammatory mediator were presented by PRCC values in Figure 4.4. The higher absolute value of PRCC that is from 0 to 1 reflects the stronger correlation between input samples and measured outputs. Within the given sample space, the production and decay rates exhibited significant correlations with the level of each corresponding mediator, excluding the natural production rates (C_0, C_{12}) in the secretion of PICs and MMPs. This suggested that the activation of the inflammatory process was primarily associated with the stimulating pathways rather than the natural releases of PICs and MMPs that maintain the metabolic balance. In addition, Figures 4.4a and 4.4b illustrate that the production of Fn-fs (C_{21}, C_{22}) was more correlated to the release of inflammatory cytokines compared with the production of MMPs (C_{12}, C_{13}, C_{14},

C_{15}, C_{16}, C_{17}). This aligns with their regulatory roles, since MMPs mainly degrade the cartilage tissue to facilitate the release of Fn-fs, the accumulation of which can provoke the immune response [16].

As a predominant risk factor of OA inflammation, the biological effects of obesity result from the regulation of adipokines in this model. The parameters governing adipokine production (C_{18}, C_{19}, BMI^{meas}, PAL, D_4) revealed a significant correlation not only in the level of adipokines (Figure 4.4d) but also in the levels of the other four inflammatory mediators (PICs, AICs, MMPs and Fn-fs). Specifically, the relationship between BMI and the inflammatory mediators included in this model was significantly positive whereas PAL negatively correlated to inflammation, as presented in Figures 4.4a to 4.4c and 4.4e.

It is notable that the parameters of AIC production (C_8, C_9, C_{10}, C_{11}) exhibited a significant correlation only in the level of AICs (Figure 4.4b). This implies that AICs, which are released by the stimulation of PICs and damaging products, might play a secondary role in counterbalancing inflammation whilst simultaneously acting as inhibitors of PICs and MMPs.

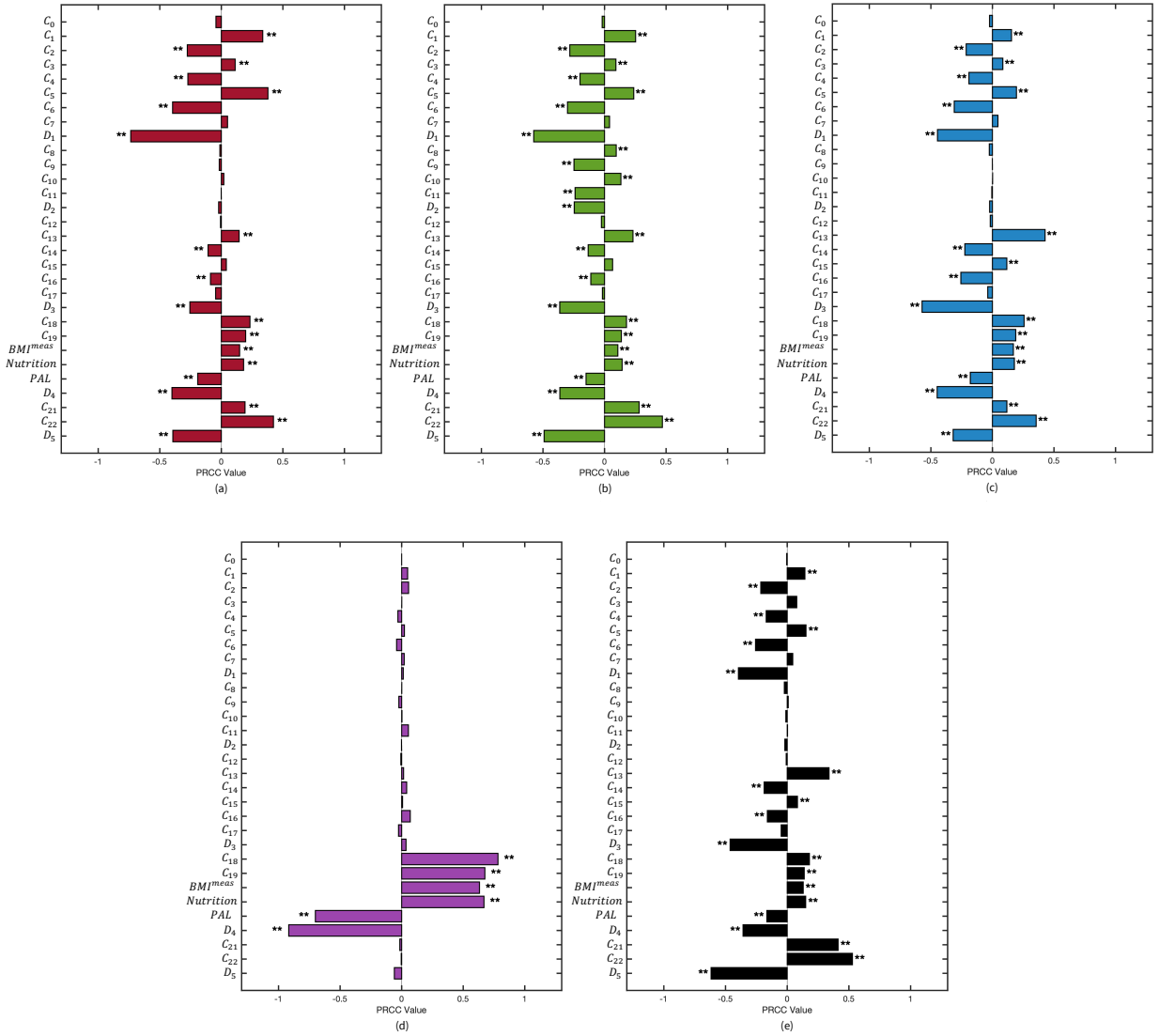

Figure 4.4: *PRCC analysis of the parameters in the inflammatory process. The correlations between parameters and (a) the level of PICs, (b) the level of AICs, (c) the level of MMPs (d) the level of adipokines, and (e) the level of Fn-fs are measured by PRCC values. The significance of correlation is denoted by (**) when p-value is less than 0.01, and PRCC varies from -1 to 1, implying negative and positive correlations between changes in parameters and mediator level.*

4.3.2 Effects of physical activity intervention

The inflammatory mediators were initially at a relatively low level within the system with the estimated baseline parameters in Tables 4.1 to 4.5. The increase of PIC level was measured to indicate inflammation in this model. Figure 4.5 illustrates the minimum degree of mechanical damage that triggers inflammation when encompassing all levels of BMI and physical activity. In Figure 4.5a, the deeper hue indicates the reduced resistance of the system to inflammation induced by mechanical damage. The elevation of PAL can enhance the resistance to inflammation by increasing the threshold for minimal mechanical damage that may initiate an inflammatory response. Compared to the cases of nutritional deficiency and extreme obesity, the increase of low PAL (sedentary and low active) was more effective when BMI level was between normal weight and obesity. Conversely, the case of extreme obesity remained at a high risk of inflammation from mechanical damage, as the sedentary physical activity failed to elevate the damage threshold.

Figure 4.5b shows a threshold of BMI leading to inflammation without mechanical damage. Namely, the minimum damage is zero when the BMI value is over the threshold. In this model, the threshold was found in the case of obesity and its value could be decided by the system parameters. In particular, it could be seen that increasing sedentary PAL led to a transition in the BMI threshold within the cases classified as obese and extremely obese in Figure 4.5a. This suggests that the enhancement of PAL may effectively increase the threshold.

The inflammatory activities of three cases (NW, OW, LO), applying different strategies of physical activity intervention under the control of mechanical damage ($C_{22} = 1.2$), are shown in Figures 4.6 to 4.8. The sign of inflammation appeared after the introduction of an instant mechanical damage in the case of NW, OW and LO (Figures 4.6a to 4.6c, 4.7a to 4.7c and 4.8a to 4.8c). This suggests that the intervention of physical activity for reducing adiposity only prior to the onset of damage was insufficient in preventing the activation of inflammatory response. However, a window period of 15 months was found for the case of NW when physical activity interventions began after damage occurred (Figures 4.6d to 4.6f), and the window period decreased to 2 months in the OW case (Figures 4.7d to 4.7f).

Within the window period, the activated inflammatory response was attenuated through a reduction in adipokine levels as a result of the continuous physical activity intervention following injury (Figures 4.6e and 4.7e). Nevertheless, the intervention strategy subsequent to injury was ineffective beyond the window period for NW and OW cases (Figures 4.6f and 4.7f). The states of NW, OW and LO stabilised

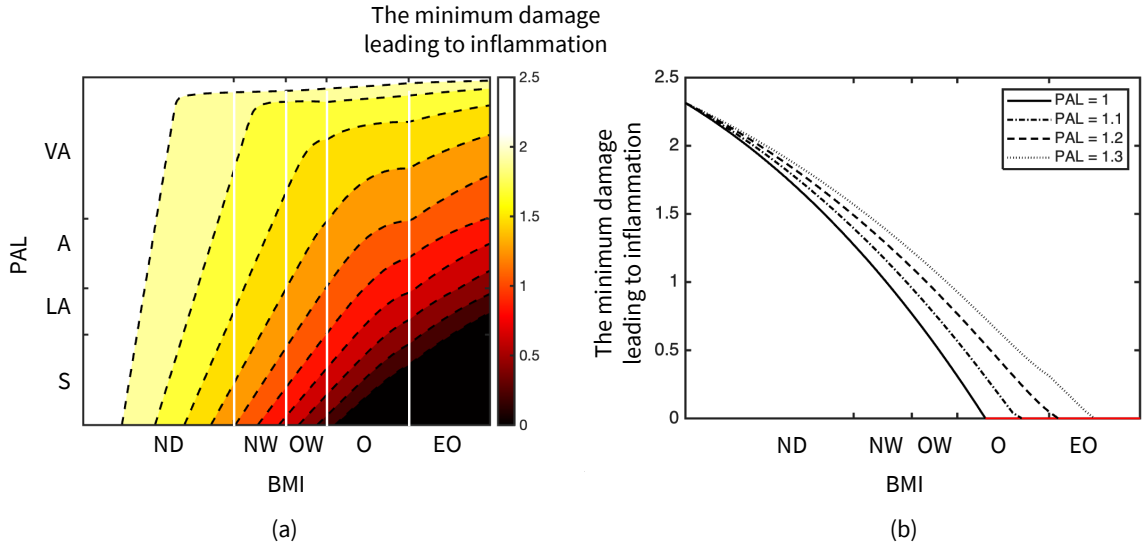

Figure 4.5: *The sensitivity of the mechanical damage threshold leading to inflammation: (a) The distribution of damage threshold (C_{22}) when PAL is from sedentary to very active and BMI is from nutritional deficiency to extreme obesity; (b) The representative relation between damage threshold and BMI at different sedentary PALs, where the red line represents the inflammation state without damage ($C_{22} = 0$).*

in the inflammatory state respectively at months 30, 20 and 16 (Figures 4.6a, 4.7a and 4.8a).This indicated that the progression of inflammatory processes was faster with a higher BMI.

Different to NW and OW cases, LO (Figure 4.8) and HO (Figure F.1) cases did not exhibit the presence of a window period and any intervention strategies of physical activity were ineffective in hindering the progression of inflammation. Inflammatory activities evolved from a heathy state alongside the mechanical damage in case LO, whilst the case of HO has already stabilised at an inflammation state at the beginning of the simulation time frame (Figure F.1). In the case with LO, the intervention of physical activity could still delay the inflammatory responses. When the mixed physical activity intervention persisted until month 18, inflammation reached a stable state at month 22 (Figure 4.8g). Extension of the intervention period postponed the time when inflammation was stable to month 32 (Figure 4.8i).

Mixed strategies of physical activity intervention appeared to be less effective if the intervention failed to persist after damage occurs, as illustrated in Figures 4.6g to 4.6i and 4.7g to 4.7i. This suggested that the duration of physical activity, during which the level of adipokines was downregulated, might play a pivotal role in the evolution of inflammatory processes, in conjunction with the aforementioned

window period. Despite being ineffective in preventing inflammation, the mixed intervention strategies that was interrupted at a later time point could still postpone the activation of inflammation. Notably, the temporal delayed effect of mixed intervention strategies in mitigating inflammation also depended on BMI level. The physical activity intervention, maintained until month 24, could effectively control the inflammatory mediators to a relatively low level at month 36, when the BMI level was normal weight (Figure 4.6h). In turn, the case of OW evolved into an inflammatory state by month 36 in response to the damage at month 12 (Figure 4.7g).

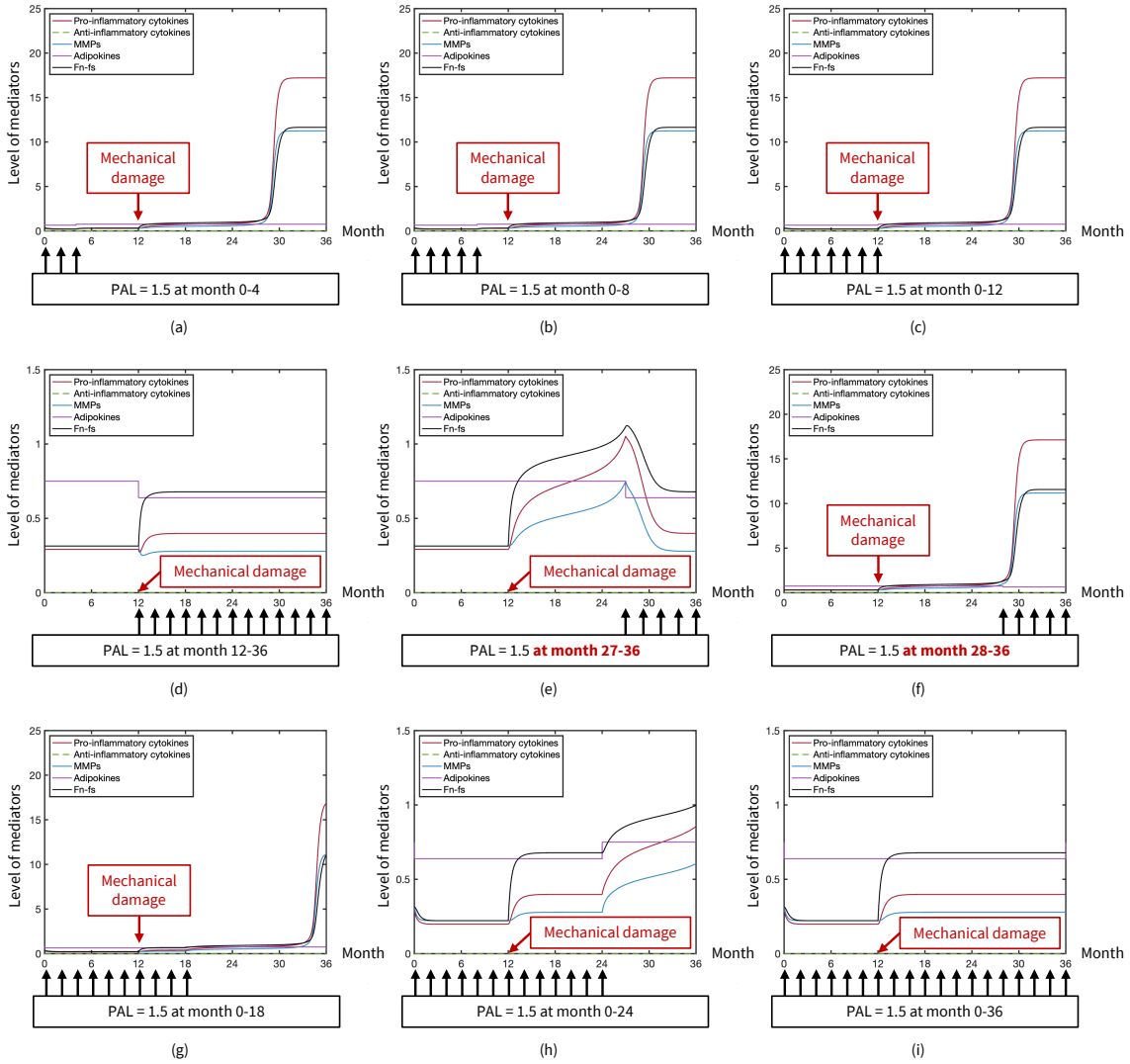

Figure 4.6: *Physical activity interventions in the inflammatory process when BMI level is normal weight: (a)– (c) Only before damage; (d) – (f) Only after damage; (g) – (i) Mixed strategy. The durations of physical activity intervention that are highlighted in red signify the transition from a healthy consequence to an inflamed result due to missing a time window after damage.*

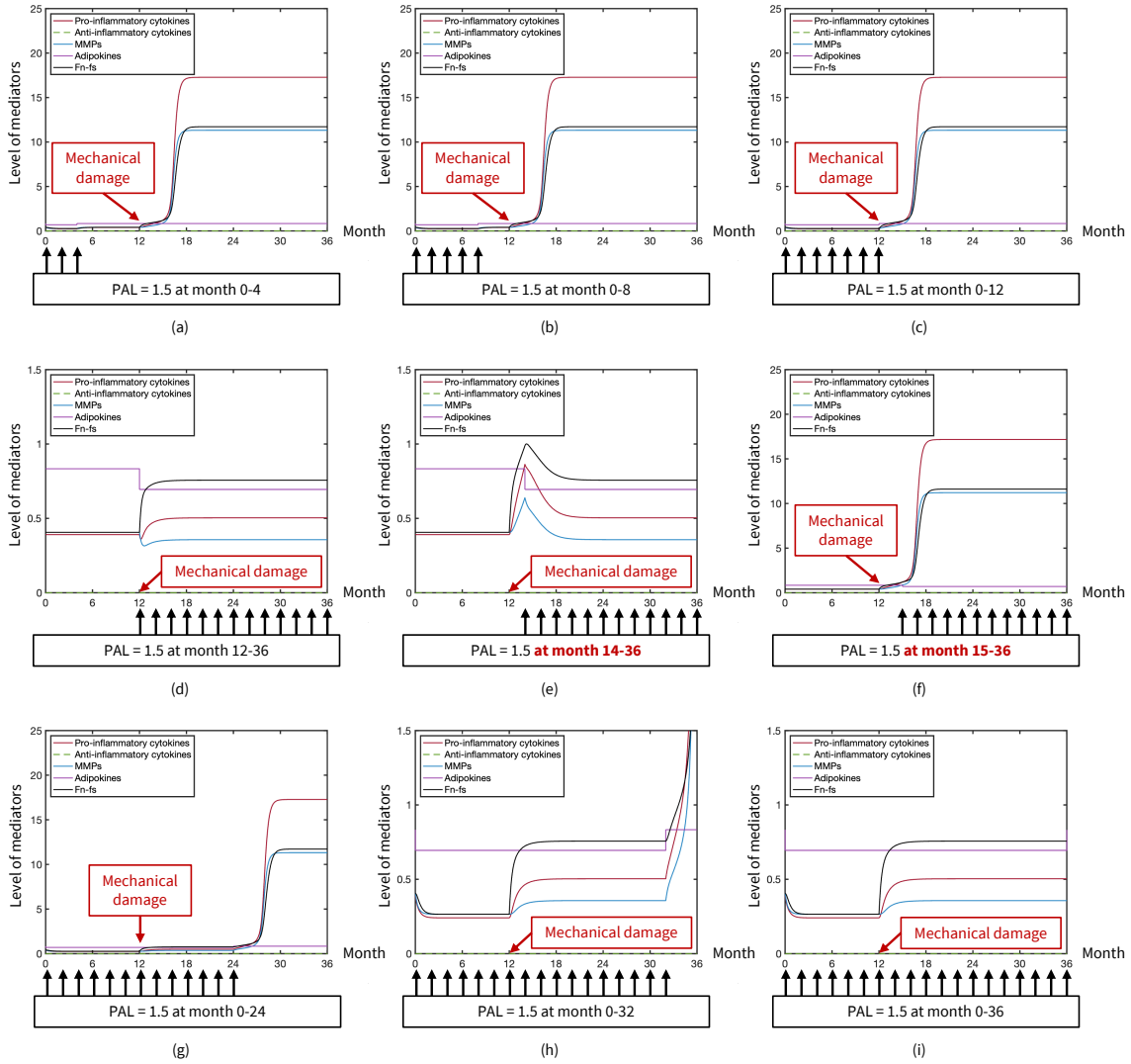

Figure 4.7: *Physical activity interventions in the inflammatory process when BMI level is overweight: (a)– (c) Only before damage; (d) – (f) Only after damage; (g) – (i) Mixed strategy. The durations of physical activity intervention that are highlighted in red signify the transition from a healthy consequence to an inflamed result due to missing a time window after damage.*

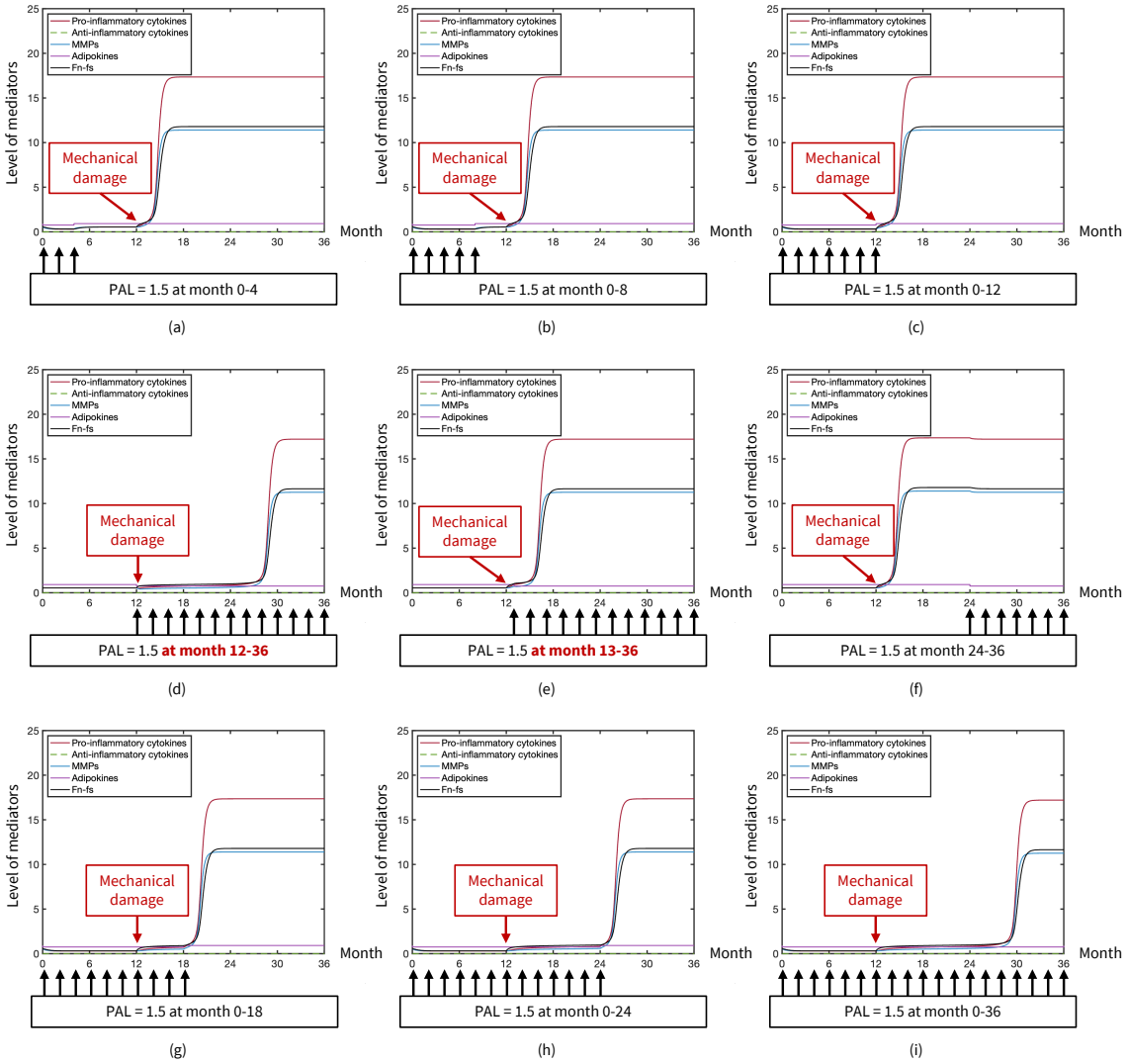

Figure 4.8: *Physical activity interventions in the inflammatory process when BMI level is low obesity: (a)– (c) Only before damage; (d) – (f) Only after damage; (g) – (i) Mixed strategy. The durations of physical activity intervention that are highlighted in red signify no transition from a healthy consequence to an inflamed result after damage.*

4.3.3 Window period of physical activity intervention

A window period, where inflammation did not reach steady state, was predicted when a physical activity intervention was simulated. Figure 4.9 presents the illustrative variations of the window period, indicating that the mechanical damage level and BMI were more responsive to the outcomes of physical activity interventions in comparison to PAL. This is supplemented by additional four representative conditions (BMI = 20 and 30 at PAL = 1.5 and 2) in Figure F.2. By incorporating the variations in damage level, BMI, and PAL, three states of the system were identified with the implementation of physical activity, as summarised in Table 4.7. The window period decreased dramatically to zero from nearly 15 months when the arbitrary value of mechanical damage increased to 1.5 or BMI level was from normal weight to obesity (Figures 4.9a and 4.9b). However, the elevation of PAL was not able to significantly extend the span of the window period (Figure 4.9c), suggesting that the window period principally depended on the levels of damage and adiposity.

Table 4.7: *The system states resulting from physical activity intervention when varying the mechanical damage level, BMI and PAL.*

System state	Description
I	The state where the system remains in a healthy state without the activation of inflammation
II	The state where the system transits to an inflamed state from a healthy state when inflammation is activated, where a window period exists for the intervention of physical activity
III	The state where the system remains in an inflamed state after the activation of inflammation, where there is no effective window period for the intervention of physical activity

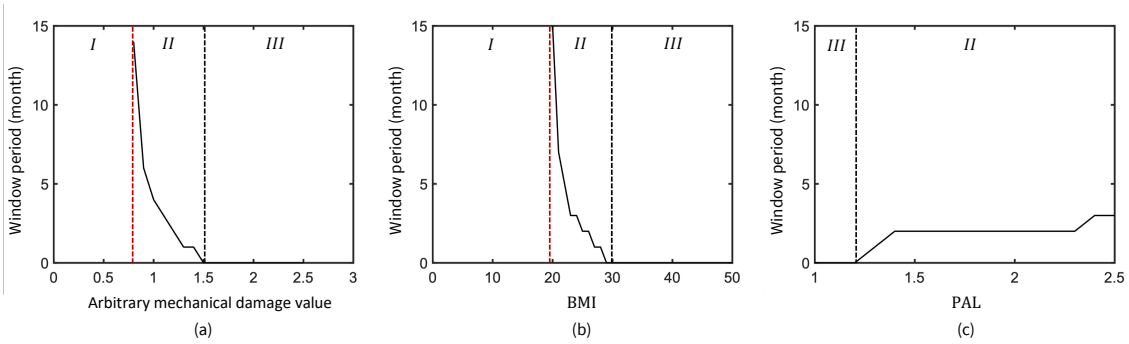

Figure 4.9: *The variations of the window period for effective physical activity interventions in the evolution of the inflammatory process: (a) Sensitivity to the mechanical damage level when BMI = 25 and PAL = 1.5; (b) Sensitivity to the level of BMI when the mechanical damage level = 1.2 and PAL = 1.5; (c) Sensitivity to PAL when the mechanical damage level = 1.2 and BMI = 25.*

4.4 Discussion

The effects of adiposity-associated factors, BMI and PAL, were first qualitatively evaluated at a temporal scale in the inflammatory process, based on an established OA inflammation model [237]. In this study, BMI and PAL concurrently govern the production of adipokines in inflammatory activities. The time scale was estimated according to the half-life of representative mediators. A global sensitivity analysis exhibited significant correlations between the parameters of adipokine production and inflammatory responses, using the LHS/PRCC method. From normal BMI level to obesity, a variety of physical activity intervention strategies were assessed during the onset and progression of inflammation in response to an instant mechanical damage. It was found that the effects of physical activity on OA inflammation differed. This depended on the intervention strategies and BMI levels. The timely and continuous physical activity interventions had the potential to diminish the individual susceptibility to inflammatory responses triggered by damage. This accordingly contributed to delaying and preventing inflammation. In addition, a window period of physical activity interventions was predicted and depended on BMI, PAL and damage level.

Obesity has been regarded as a condition of inflammation in OA due to its role in prompting the release of inflammatory mediators [100]. The regulatory effects of adipokines are critical in OA inflammation at a molecular level [41, 42, 45]. The PRCC analysis of the adipokine-mediated inflammation model showed a significant

correlation between adipokine production and inflammation. The BMI level and nutrient term positively correlated to the level of inflammatory mediators whilst the correlation between PAL and inflammatory mediators was negative. These correlations suggest the possibility of downregulating OA inflammation through reducing adiposity. In fact, weight management [241], dietary control [197, 222] and physical activity [221, 224] were reported as effective methods to alleviate inflammation levels in OA, by reducing adiposity. Despite the complexity and multifaceted nature of the regulatory mechanisms associated with adipokines and exercise [45, 230], their effects ultimately converge on the upregulation and downregulation of inflammatory mediators. This model provided minimally essential simulations to analyse the effects of BMI and PAL regulating the level of adiposity during inflammatory processes.

In this model, the level of BMI describes the baseline of inflammatory mediators, thereby the increase of BMI results in the higher susceptibility of inflammation in response to mechanical damage. A threshold of BMI was found to maintain the system in chronic inflammation, which is consistent with a previous non-dimensional study [237]. This threshold was nearly 33 in this estimated model when PAL was sedentary ($PAL = 1$), and it depended on the variations of parameters. Chronic OA inflammation could be the systemic and local consequence of excessive adipose tissue [41]. Collins et al. [42] suggested that the signalling pathways of adipokines might induce systemic inflammation and eventually activate the inflammatory responses within local joints. This regulatory effect of adipokines may also contribute to a state that is more susceptible to inflammation driven by mechanical damage, which could explain the illustrative sensitivity of the damage threshold triggering inflammation when varying BMI and PAL. Similarly, Hahn et al. [225] suggested that the threshold effect of adiposity might be the cause of the increase of OA incidence in the cohort of high-fat diet induced obesity. Despite the prevailing awareness regarding the importance of mechanical damage in inducing OA inflammation [16, 83, 192], it is not yet possible to examine how adiposity affects the susceptibility of damaged cartilaginous tissue to inflammation, due to the complex molecular interplays between joint compartments. In the present paradigm of inflammation, tissue damage signals to the innate immune system to activate a repairing metabolism through PRRs and DAMPs [219]. This metabolic balance may be disrupted by either excessive tissue damage or adiposity, leading to chronic inflammation. The variations in the BMI threshold and the minimum damage level that induce inflammation could be attributed to changes in metabolic balance driven by alterations in adiposity.

Comparing the effects of physical activity intervention across different levels of BMI (NW, OW, LO, HO), the identical moderate PAL was more effective in managing OA inflammation for cases NW and OW. Furthermore, sustained and long-term intervention strategies demonstrated the capability to inhibit inflammation. Several animal experiments [221, 222, 224, 226–228] indicated the protective role of physical activity in OA inflammation from the perspective in the outcome of early intervention. Particularly, Huesa et al. [228] examined the positive effect of exercise on reducing adipose tissue in OA pathology. However, obesity might diminish the benefits of physical activity in the OA pathology. In the study by Griffin et al. [222], obesity induced by a high-fat diet reduced both systemic and local impacts of exercise on OA. This is consistent with the dependence of intervention outcomes on BMI levels observed in this computational study. Moderate PAL might not be sufficiently effective to reduce the baseline level of inflammation through the loss of adipose tissue in obese cases. Previous studies [197, 223] have also shown the limited effect of physical activity intervention alone and suggested that the combination of dietary and exercise intervention exhibited improvements on OA pathology. Thus, a proper integration of diverse strategies, aiming for the decrease in adiposity level, might be more adaptive to manage OA inflammation for obese cases. It is notable that Runhaar et al. [229] stressed the anti-inflammatory effects of diet and exercise intervention independent of BMI. This independence might result from the minimal variations in body weight but significant changes in fat mass when BMI remained relatively constant [44, 199].

Although the adiposity-associated factors (BMI and PAL) were evaluated during OA inflammation in this computational study, there are still a number of limitations. As a standard measure of obesity, BMI is the ratio of body weight to height and lacks the accuracy to identify abdominal adiposity compared to the waist circumference [39]. This may result in a weaker correlation between BMI and inflammation level [229]. Despite the strong association between both BMI and waist circumference with OA risk [44, 242], BMI has been widely used in the present evidence of adipokine production in OA [89, 92, 100]. This limited the calibration of this model, and BMI was accordingly considered as a parameter that directly regulates the production of adipokines to alter the inflammatory process. In addition, the mechanism of early OA pathology has yet to be elaborated due to unmeasurable parameters. As the main intervention strategy of OA inflammation, the regulatory pathway of physical activity was based only on the alteration of adipokine levels. However, exercise can regulate the inflammatory process by the simultaneous actions of mechanical

transduction and endocrine effects in vivo studies [22]. The mechanical effect [22] and acute regulation [229] of physical activity were not assessed by this minimally essential model. Due to the unclear and complex interplay of molecules, this study focused on the ultimate outcomes of tuning the damage level, BMI and PAL rather than exclusively examining different signalling pathways. This model can be further extended by specifying the phenotypes of inflammatory mediators and signal transduction pathways resulting from exercise.

To date, the diagnosis of early OA still lacks a validated standard [32]. In this computational study, inflammatory processes were simulated at a continuous time frame from a steady state without mechanical damage. The structural changes at a late stage of OA were not considered. The inflammatory responses in relation to the damage reflected the fluctuation of molecular levels, exhibiting a window period for the effectiveness of physical activity intervention. This window period was tightly associated with the attributes of the inflammation, such as the mechanical damage level and BMI. Namely, the existence of a window period for exercise intervention may vary depending on more complex regulations in the inflammatory process. The duration of the window period was found to range from one month to over 15 months. This stresses the significance of stratifying the risk of OA inflammation in different susceptible groups. For the simplicity of this model, the level of adipokines negatively correlates to PAL on a short-term scale. Nevertheless, the reduction of adiposity requires a long-term implementation of exercise [232]. This could lead to a smaller window period for effective physical activity interventions. The assessment of the baseline factors contributes to the development of diagnostic criteria for early OA [243, 244]. Interestingly, acquired interventions of physical activity were effective within the window period but might not be sensitive to the span of the window period. This could be explained by the regulatory mechanism of physical activity in this model. Since the effect of physical activity depends on the level of adiposity [231], PAL is a parameter that regulates the production of adipokines in the evolution of inflammation. This is different from BMI in this model. From the view point of OA prevention strategies, minimising the risk factors of OA, such as mechanical damage and obesity, is critical to the primary prevention [233]. Regarding obese cases, proper exercise intervention can be effective in the secondary prevention strategies [234].

In the future, different biochemical entities can be specified to extend and predefine the regulatory network of this inflammation model according to available in

vitro and in vivo data [45, 91]. Due to challenges in acquiring high-quality longitudinal data, the parameter calibration of reaction kinetics is required for specified biomarkers based on their corresponding levels profiled in subject-specific samples, such as synovial fluid, serum or plasma, matching with general information including BMI, body weight, diet and physical activity. Samples can be stratified by imaging-based OA assessment to score the tissue damage [245]. The levels of specified biomarkers correspond to the primary variables in this mathematical model, which can be characterised by integrated analysis of untargeted multiomics profiles from subject-specific samples to facilitate model calibration at high resolution [40]. In addition, the temporal variations in BMI and body weight can be collected through longitudinal anthropometric measures. Lifestyle parameters (PAL and calorie consumptions) can be monitored daily by wearable trackers such as triaxial accelerometer and hear rate sensors [246]. Dietary intake can be estimated through food frequency questionnaires (FFQs) [247, 248]. Predictive mediator levels from the calibrated model can be compared with independent datasets containing above measurable data to provide more accurate estimations on the window period and the temporal effects of physical activity on the inflammatory process. This can contribute to the personalised development of physical activity strategies of managing OA.

4.5 Conclusion

This computational study provides novel insights into the interplay between adiposity-associated factors and OA inflammation, using a mechanistic adipokine-mediated inflammation model. For the first time, the critical role of managing adiposity in mitigating the risk of OA inflammation was evaluated using a computational model. It was found that a high BMI increased the baseline level of inflammation, which, in turn, diminished the efficacy of physical activity interventions. This attenuation was particularly pronounced when mechanical joint damage was present. The sensitivity of inflammatory responses to physical activity was modulated by this adiposity-driven inflammation baseline, which underscores the importance of obesity management in OA prevention. Furthermore, the window of physical activity interventions was found to range broadly from 0 to 15 months, and it was more responsive to BMI and mechanical damage than to PAL alone. While long-term physical activity can effectively prevent inflammation in response to the mechanical damage for non-obese cases, its protective benefits

are limited for those obese cases without other countermeasures such as dietary control or protection against injury. These results provide insights for designing multi-modal intervention strategies, tailored to subject-specific adiposity and joint health profiles, to better optimise the management of OA inflammation.

Appendix E: Bifurcation diagram

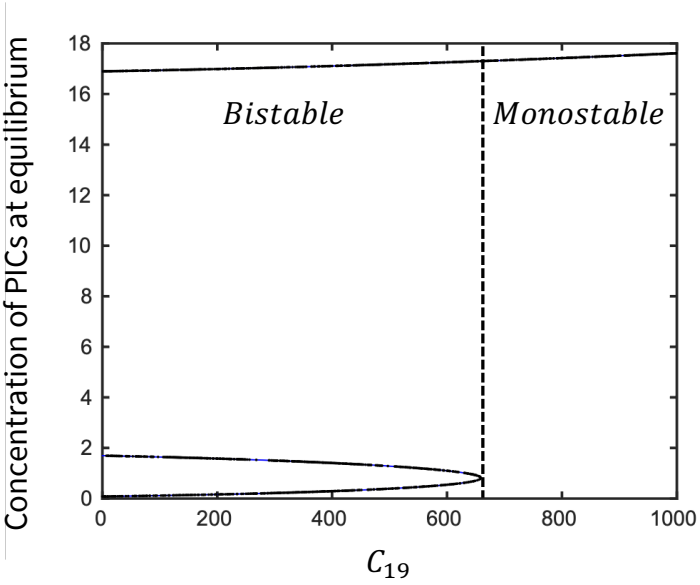

Monostable: Persistent inflammatory steady state.

Bistable: Inflammatory and healthy steady states.

Figure E.1: *The bifurcation of the adipokine production parameter (C_{19}) governed by BMI.*

Appendix F: Simulations of OA inflammation with physical activity intervention and sensitivity of window period

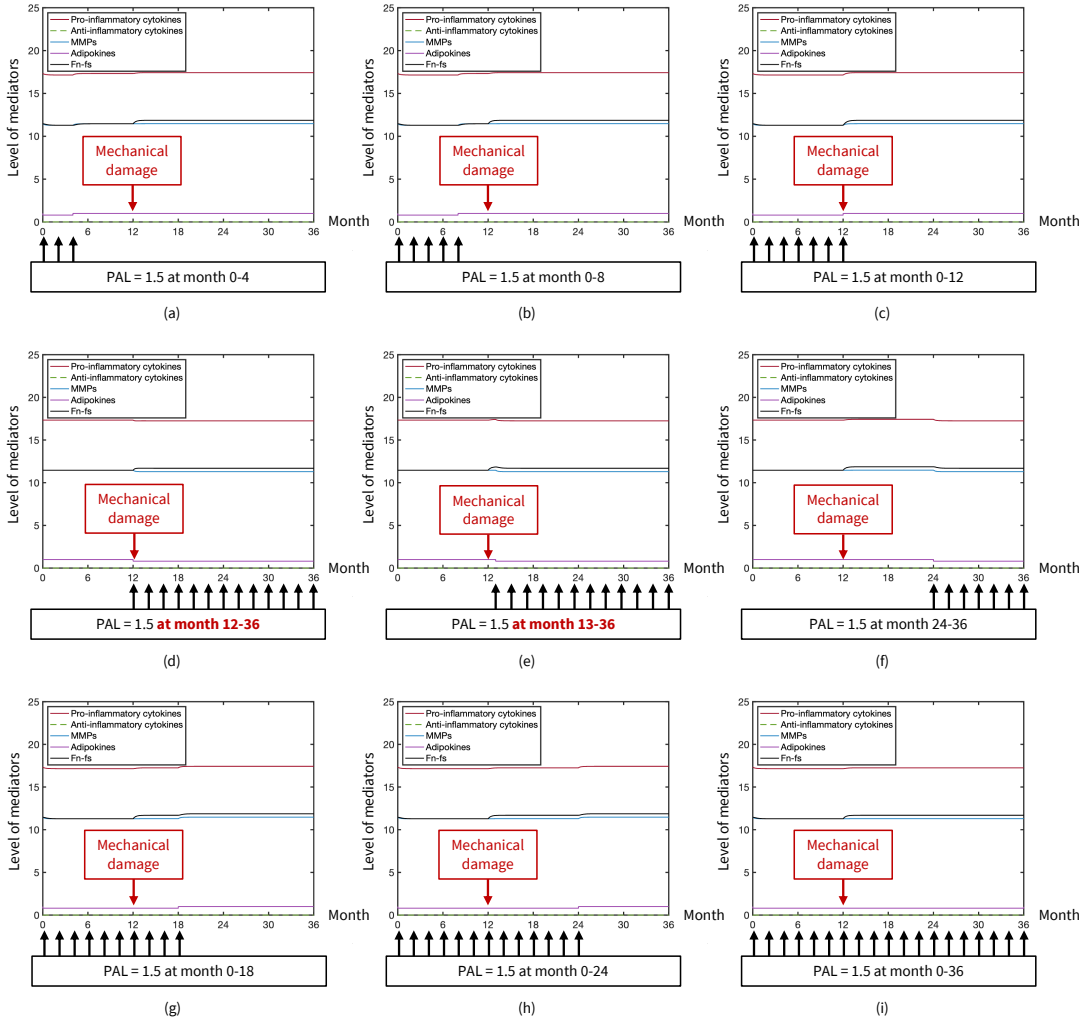

Figure F.1: *Physical activity interventions in the inflammatory process when BMI level is high obesity: (a)– (c) Only before damage; (d) – (f) Only after damage; (g) – (i) Mixed strategy. The durations of physical activity intervention that are highlighted in red signify no transition from a healthy consequence to an inflamed result after damage.*

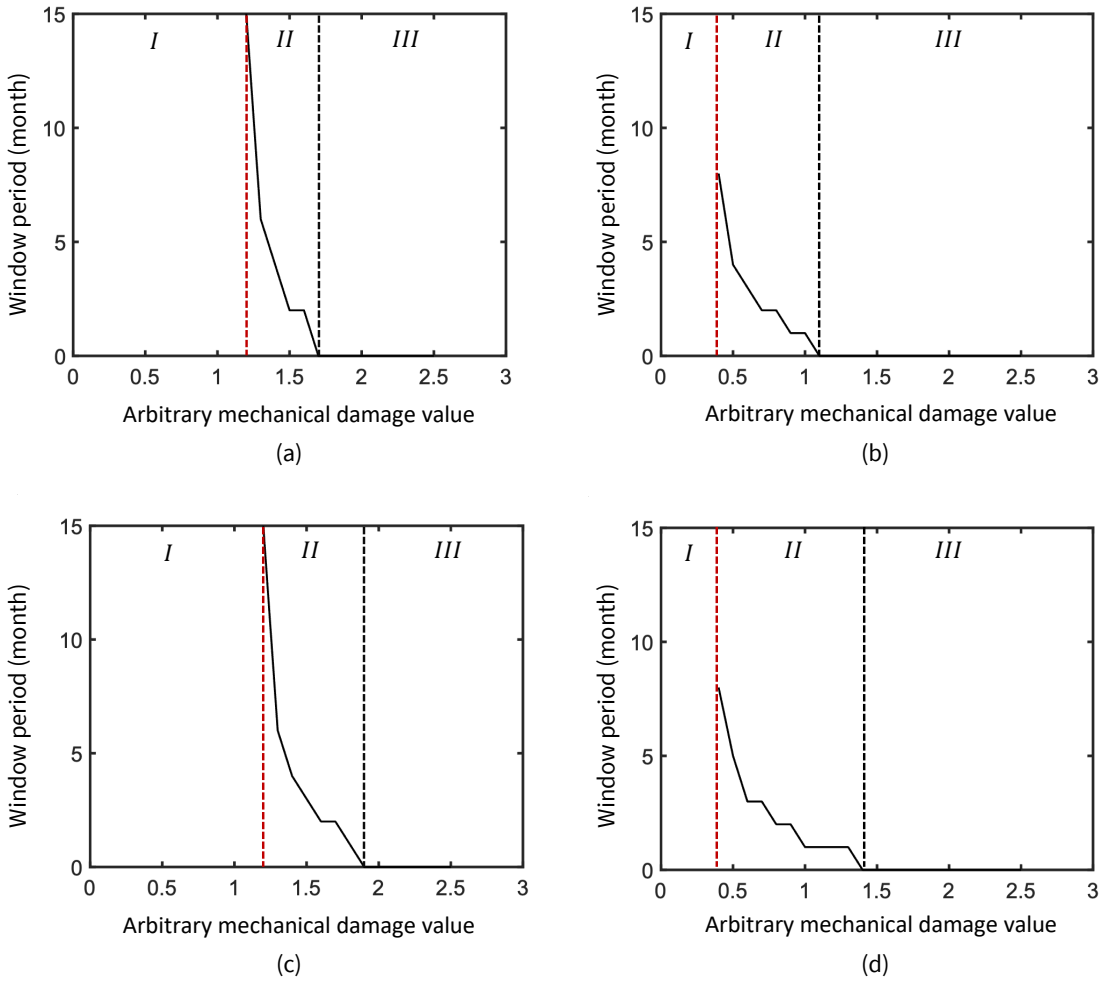

Figure F.2: *The sensitivity of the window period to the mechanical damage level when (a) BMI = 20 and PAL = 1.5, (b) BMI = 30 and PAL = 1.5, (c) BMI = 25 and PAL = 2, (d) BMI = 30 and PAL = 2.*

Chapter 5

A novel integrative multi-scale framework of inflammation and mechanical loading in knee osteoarthritis

This chapter details the development of the integrative multi-scale approach for the study of obesity-associated cartilage degeneration. The obesity-associated inflammation model was parameterised in Chapter 4, allowing the integration of mechanical damage and inflammatory activities at different time scales in this chapter. For the first time, this approach integrates obesity-related inflammation and mechanical loading, aiming to simulate the mechanobiological regulations of obesity in cartilage degeneration and to identify critical parameters in the degeneration patterns at different BMI levels. This chapter focuses on the methodology and sensitivity analysis of developing the multi-scale approach based on the inflammation model established in Chapters 3 and 4. Specifically, a knee joint FE model [249] experimentally validated based on contact area and pressure of meniscus and cartilage is used to couple the inflammation model to present this integrative approach. Parameter sensitivity analysis is conducted to demonstrate the degenerative process of cartilage within the multi-scale modelling framework. Cartilage degeneration is simulated with different BMI levels, showing the inflammatory and mechanical contributions of obesity in knee OA.

The work presented in this chapter has been published in Biomechanics and Modeling in Mechanobiology under CC BY 4.0, with minor adaptations for consistency and readability with the thesis format: Lai J and D. Lacroix, "A novel integrative multi-scale framework of inflammation and mechanical loading in knee osteoarthri-

tis", Biomechanics and Modeling in Mechanobiology, Apr. 2026, doi: 10.1007/s10237-026-02072-8.

5.1 Introduction

Osteoarthritis (OA) is a complex heterogeneous disease that causes major disability, responsible for nearly 2% of total years lived with disability globally [3]. In particular, over 80% of global burden of OA are from the knee [3]. Approximately 7.6% of the worldwide population was affected by OA in 2020, representing a 132.2% increase since 1990 [5]. Mechanisms of OA development still remain under investigation, but it is now understood that the progression of OA involves the whole joint and includes multifaceted factors such as genetics, age, gender, injury, tissue metabolism, mechanical loading and inflammation [24]. These factors interact and contribute to specific phenotypes of OA [33]. Since obesity can influence joints both locally and systemically by modulating inflammatory and biomechanical responses [41, 250], it represents a predominant risk factor in the onset and development of OA. In fact, it has been reported that a high BMI accounted for over 20% burden of OA [5]. Given the rising prevalence of obesity [217] and its substantial contribution to the burden of OA, elucidating the mechanisms of obesity-associated OA is of critical importance.

Excessive joint loading is a critical driving factor of OA due to obesity [44, 47], particularly for the knee [160–163, 251]. As the primary weight-bearing joint that supports the upper body, the compressive force in the knee is a direct reflection of changes in body weight. It has been reported that a decrease of one unit in body mass correlated with a four-unit decline in the load of the knee joint [156]. The increase of the joint load can cause a higher risk of mechanical damage in articular cartilage [187, 252–254], which is prone to the onset and development of knee OA. However, it has been challenging to define and diagnose early knee OA due to its heterogeneous pathological characteristics [31, 32]. The pathology of OA is a consecutive progress from a symptomatic stage to structural erosions [213, 220, 255, 256]. At present, two grading systems are commonly used to assess the progression of knee OA, Kellgren-Lawrence (KL) [257] and Osteoarthritis Research Society International (OARSI) atlas criteria [70, 258]. They follow the ordinal scales and are unable to well identify the early-stage where radiographic changes of the knee are unobservable. Additionally, a few scoring methods, such as Whole Organ Magnetic Resonance Imaging Score (WORMS), Knee Osteoarthritis Scoring System (KOSS)

and MRI Osteoarthritis Knee Score (MOAKS), were developed based on magnetic resonance imaging (MRI) to provide more sensitive assessments on early OA [259]. However, an established standard for phenotypic characterisation based on those methods is still lacking.

The degeneration of cartilage is a main hallmark of OA at an early stage, exhibiting compositional and metabolic disruptions [22, 83, 205, 219, 239, 260–265]. The disruptions include mechanical damage of collagen, the loss of proteoglycans or fixed charge density and activated chronic inflammation [46]. Tissue softening and the increase of permeability are the primary outcomes of those disruptions in cartilage degeneration. The early variations in the stiffness of cartilage and permeability have been reported prior to detectable structural signs [266]. In particular, obesity is a key regulator responsible for the alterations of the material properties of cartilage [250]. In addition to the aforementioned biomechanical effects, obesity can also stimulate inflammation in cartilage degeneration. Adipokines are overproduced due to the excess adipose tissue and can disturb the metabolic balance of cartilage turnover [42, 45, 100]. This multi-scale regulation of obesity is a critical factor contributing to the cartilage degeneration in knee OA. However, it remains a challenge to examine the independent effects of obesity due to the complex and interacting pathways of inflammation and biomechanical responses in cartilage degeneration [197, 267–270].

Computational approaches are well suited for integrating diverse pathways of cartilage degeneration across multi-scales. In the context of OA, the knee biomechanics, including the mechanics of articular cartilage, has been commonly explored by using the Finite Element (FE) method [155, 159, 164, 165, 174, 271–277]. Several computational algorithms have been established to study the development of cartilage degeneration [169, 186, 278]. However, those algorithms are primarily driven by mechanical damage, while biochemical factors are neglected. This limitation also appears to their derivative studies [166–168, 189, 279]. By contrast, numerical models emerge to simulate the metabolic regulations of cartilage degeneration [119, 128, 136, 138, 206, 207, 237]. Since cartilage degeneration is a process that involves the cascade of both biomechanical and inflammatory responses, there are some attempts recently to simulate the mechanobiological mechanisms of cartilage degeneration [127, 129, 137, 182] by coupling mechanical and biochemical factors. Despite difficulties in model validation, integrative computational models contribute to identifying critical pathways and their interactive effects during cartilage degeneration. As aforementioned, obesity plays a predominant role in

the multi-scale regulation of the degenerative process of cartilage. However, to date, there is no computational model that integrates the obesity-related coeffects of inflammation and mechanics on the degeneration of cartilage in knee OA. In particular, only one previously established model [237], from our prior work, has considered the inflammatory effects of obesity in OA. Previous computational research [165–168, 272] mostly focuses on the biomechanical effects of obesity and could not provide effective means to simulate the cartilage degeneration modulated by obesity-related inflammation and mechanics.

This study aimed to investigate the inflammatory and biomechanical effects of obesity on the cartilage degeneration. A novel multi-scale computational framework was developed, for the first time, integrating the interplay between obesity-associated inflammation and the biomechanics of the knee joint during cartilage degeneration. The sensitivity of the key parameters that govern the degenerative process was analysed within this framework. To evaluate the effects of obesity on cartilage degeneration, BMI levels were varied as the main attribute of the knee joint and the contributions of inflammation and mechanical damage were examined.

5.2 Materials and methods

5.2.1 Finite element modelling strategy

A validated subject-specific FE model and generic data of the human tibiofemoral joint [249] were used for the biomechanical simulation. The subject-specific data including experimental results, imaging and computational model settings were collected as part of the Institute of Medical and Biological Engineering Knee Dataset (University of Leeds). The experimental implementation was approved by East Midlands - Leicester South Research Ethics Committee (18/EM/0224). The left human cadaveric knee (LTKN8941) was donated by a male of 61-year-old (BMI = 18 kg/m^2) without meniscal extrusion.

The subject-specific FE model was modified from this validated hyperelastic model (LTKN8941) [249] in Abaqus 2021 (Dassault Systèmes, Vélizy-Villacoublay, France). The modified subject-specific knee joint model comprises of a total of 73,124 quadratic tetrahedral elements of type C3D10 for the tibia, femur and menisci, as well as 107,446 quadratic tetrahedral elements of type C3D10MP for tibiofemoral cartilages. Tibia and femur were considered as homogeneous materials with isotropic elasticity [277]. Femoral and tibial cartilages were modelled

as isotropic poroelastic materials [155] discretised on an element-wise basis according to the progression of degeneration. The medial and lateral meniscus were assigned with a transverse isotropic property with 50 MPa for the out-of-plane shear modulus and 159.6 MPa for the out-of-plane Young's modulus [273]. To simulate the restricted meniscal movement by the attachment of ligaments, each meniscal horn was respectively connected to tibial plateau by 15 linear spring elements. The sum of spring stiffness was equivalent to the meniscal modulus in the circumferential direction at each side [275], and the stiffness of each spring element was 10.64 MPa. Table 5.1 summarises the material parameters implemented in the FE model at baseline. The sensitivity of material properties is presented in Figure G.1, compared with the results from Cooper et al. [249].

Table 5.1: *The baseline parameters of tissue material in the FE model.*

Material property	Young's modulus (MPa)	Shear modulus (MPa)	Poisson's ratio	Void ratio	Permeability (10^{-3} mm^4/Ns)
Femur and tibia [277]	15,000		0.3		
Meniscus [273]	20	7.69	0.3		
	20	50	0.01		
	159.6	50	0.01		
Articular cartilage [155]	10		0.15	4	1

An axial compressive force, which can be scaled by the body weight to represent the loading at heel strike of a stance phase, was implemented to a control point kinematically coupled to the nodes on the upper surface of the femur. This loading condition was simulated within 0.1s using a transient consolidation analysis, where the fluid exchange was negligible. The surface nodes of cartilage proximal to joint cavity were permeable to ensure stable convergence [280]. To stabilise the FE model by smoothing the contacts of cartilage-cartilage (CC) and cartilage-meniscus (CM) [277, 279], varus-valgus rotation was only allowed when the other degrees of freedom (DoFs) were constrained. Hard surface-to-surface contacts were used for the discretisation method with finite sliding. The friction coefficients were set to 0.1 and 0.15 respectively for CC and CM contacts [277], using the penalty method. The sensitivity of friction coefficients is shown in Figure G.1.

5.2.2 The multi-scale algorithm of cartilage degeneration

The effect of stress accumulation has been shown to induce cartilage damage, which influences joint mechanics and may accelerate tissue wear. Within this framework, the loading condition was assumed to be repetitive over the time span, resulting in mechanical degeneration. Namely, the cumulative damage to cartilage constituents is attributed to excessive stress from a repeated loading condition within the simulated period. The levels of cartilage mechanical damage were accumulated iteratively by Equations (5.1) and (5.2) [169].

$$MDL_{\tau_i}^{ele} = \begin{cases} \dfrac{S_{\tau_i}^{ele} - S_{threshold}}{S_{threshold}}, & if S_{\tau_i}^{ele} > S_{threshold} \\ 0, & if S_{\tau_i}^{ele} \leqslant S_{threshold} \end{cases} \tag{5.1}$$

$$MDL_{total}^{ele} = \left(\sum_{i=1}^{Total\, i} MDL_{\tau_i}^{ele} \right)^{r_d} \tag{5.2}$$

where MDL is the mechanical damage level within the time interval τ at iteration i, ele is the label of each cartilage element. S is the maximum principal stress of each element and $S_{threshold}$ is the threshold of maximum principal stress leading to cartilage degradation. MDL_{total}^{ele} is the total damage level accumulated from the first iteration due to the inability of healing. In the study by Mononen et al. [169], the slope of accumulating the mechanical degeneration level could be determined by a root parameter. In this framework, r_d measures the accumulation of the total mechanical damage level that contributes to regulating inflammation by the end of each iteration. Due to the lack of evidence on determining both $S_{threshold}$ and r_d, they were set to 0.3 MPa and $\frac{2}{3}$ at the baseline according to the initial biomechanical response of this FE model.

Since inflammation evolves simultaneously with the tissue damage due to mechanics, a general ODE-based model of adipokine-mediated OA inflammation [237] was employed to simulate the cumulative damage, accounting for the combined effects of inflammation and mechanics. *ode15s* in MATLAB (R2022a, The Math Works, Inc., Natick, MA, USA) was used to solve ODEs, where the time span was 1 month for the update of material properties at each iteration. The inflammation model (Equations (5.3) to (5.7)) was parameterised according to the estimation of medi-

ator half-lives [127, 140, 208, 238, 239], detailed in Appendix H.

$$\frac{dP_c\left(\tilde{\tau}_i\right)}{d\tilde{\tau}_i} = \left[C_0 + C_1 \cdot \frac{P_c^n\left(\tilde{\tau}_i\right)}{C_2^n + P_c^n\left(\tilde{\tau}_i\right)} + C_3 \cdot \frac{A_d^n\left(\tilde{\tau}_i\right)}{C_4^n + A_d^n\left(\tilde{\tau}_i\right)} + C_5 \cdot \frac{F^n\left(\tilde{\tau}_i\right)}{C_6^n + F^n\left(\tilde{\tau}_i\right)}\right] \cdot \frac{C_7^n}{C_7^n + A_c^n\left(\tilde{\tau}_i\right)} - D_1 \cdot P_c\left(\tilde{\tau}_i\right) \quad (5.3)$$

$$\frac{dA_c\left(\tilde{\tau}_i\right)}{d\tilde{\tau}_i} = C_8 \cdot \frac{P_c^n\left(\tilde{\tau}_i\right)}{C_9^n + P_c^n\left(\tilde{\tau}_i\right)} + C_{10} \cdot \frac{F^n\left(\tilde{\tau}_i\right)}{C_{11}^n + F^n\left(\tilde{\tau}_i\right)} - D_2 \cdot A_c\left(\tilde{\tau}_i\right) \quad (5.4)$$

$$\frac{dM\left(\tilde{\tau}_i\right)}{d\tilde{\tau}_i} = \left[C_{12} + C_{13} \cdot \frac{P_c^n\left(\tilde{\tau}_i\right)}{C_{14}^n + P_c^n\left(\tilde{\tau}_i\right)} + C_{15} \cdot \frac{A_d^n\left(\tilde{\tau}_i\right)}{C_{16}^n + A_d^n\left(\tilde{\tau}_i\right)}\right] \cdot \frac{C_{17}^n}{C_{17}^n + A_c^n\left(\tilde{\tau}_i\right)} - D_3 \cdot M\left(\tilde{\tau}_i\right) \quad (5.5)$$

$$\frac{dA_d\left(\tilde{\tau}_i\right)}{d\tilde{\tau}_i} = C_{18} + \left[C_{19} \cdot \frac{BMI^{meas}}{BMI^{std}} \cdot \frac{DailyCal}{BMR \cdot PAL}\right] \cdot \frac{C_{20}^{nex}}{C_{20}^{nex} + A_d^{nex}\left(\tilde{\tau}_i\right)} - D_4 \cdot A_d\left(\tilde{\tau}_i\right) \quad (5.6)$$

$$\frac{dF\left(\tilde{\tau}_i\right)}{d\tilde{\tau}_i} = C_{21} \cdot M\left(\tilde{\tau}_i\right) + MDL_{total}^{ele} - D_5 \cdot F\left(\tilde{\tau}_i\right) \quad (5.7)$$

where $P_c\left(\tilde{\tau}_i\right)$, $A_c\left(\tilde{\tau}_i\right)$, $M\left(\tilde{\tau}_i\right)$, $A_d\left(\tilde{\tau}_i\right)$ and $F\left(\tilde{\tau}_i\right)$ are the concentrations of pro- and anti-inflammatory cytokines, matrix metalloproteinases (MMPs), adipokines and fibronectin fragments (Fn-fs) at time $\tilde{\tau}_i$. Initial conditions of the inflammatory simulation are the steady state at the first iteration and updated according to the mediator concentrations from τ_{i-1}. Thus far, the connection between the pathways of tissue degradation resulting from inflammation and biomechanics is still unclear in OA. Given the little consensus on the driven mechanism of tissue destruction, cartilage material properties were updated exclusively to local elements exhibiting mechanical damage in this framework, according to the level of inflammation at τ_i. In addition, the matrix integrity of undamaged cartilage elements was preserved to keep the consistency of the material property baseline. The aggregate modulus of cartilage decreases due to the loss of structural integrity while permeability increases due to the loss of proteoglycan during OA [154, 264, 266, 276]. It has been suggested by previous studies [186, 189] that stress- and strain-orientated constituent damage interact and contribute jointly to the degeneration progression. Thus, the mechanical damage to different cartilage constituents and the corresponding changes in the material property were assumed to be synchronised, and Equations (5.8) and (5.9) were constructed to approximate the element-wise material variations due to cartilage tissue turnover.

$$E_{\tau_{i+1}}^{ele} = E_0^{ele} \cdot \left[1 - \omega_e \cdot \left(1 - \frac{\Delta F_{\tau_i}^{ele}}{F_{max}}\right)\right] \quad (5.8)$$

$$k_{\tau_{i+1}}^{ele} = k_0^{ele} \cdot \left[1 + \omega_k \cdot \left(1 - \frac{\Delta F_{\tau_i}^{ele}}{F_{max}}\right)\right] \quad (5.9)$$

where $E^{ele}_{\tau_{i+1}}$ and $k^{ele}_{\tau_{i+1}}$ are respectively the Young's modulus of cartilage and the cartilage permeability during iteration $i+1$ after the tissue turnover from the last iteration. To ensure the stabilisation of the FE model, two boundary parameters (ω_e and ω_k) set the minimum Young's modulus and the maximum permeability respectively during tissue degradation. ω_e was set to 0.99 to prevent the convergence issue resulting from the damage concentrated to the local elements that may fail at nearly zero energy [187]. ω_k was estimated to be 3, ensuring that the maximum permeability is fourfold the baseline during the OA progression [276]. $\Delta F^{ele}_{\tau_i}$ is the difference between the current and maximum level of Fn-fs for each element, where the maximum level of Fn-fs is denoted by F_{max}. Since fibronectin contributes to the assembly of ECM and the release of Fn-fs is from the disruption of fibronectin [205], the level of ECM structural integrity at iteration i is demonstrated by a reduction factor (η^{ele}_i), the ratio of $\Delta F^{ele}_{\tau_i}$ to F_{max}. The degeneration level of each element is correspondingly calculated as $1-\eta^{ele}_i$, which reflects the adaptation of material properties in the elastic modulus and permeability according to the level of Fn-fs.

5.2.3 Integrative multi-scale computational framework

By integrating the obesity-associated inflammation and mechanics to simulate the degeneration of cartilage, a multi-scale computational framework was developed (Figure 5.1). During the overall simulation period (T), the degeneration level of cartilage tissue was iteratively computed by the multi-scale algorithm of cartilage degeneration that incorporates mechanical and inflammatory regulations. As a critical progressive event in OA, cartilage degeneration involves the pathological changes of different constituents in ECM. The loss of proteoglycan and the disruption of collagen in cartilage ECM are two primary consequences of the interplay between inflammation and mechanics in the pathogenesis of OA [265]. Since these two pathological changes occur concurrently in the progressive degeneration, it is challenging to examine the contribution of each individual constituent. Computational methods have shown potentials to individually analyse the role of a degenerative pathway in different OA etiologies [189]. However, timescales significantly vary in the metabolic mechanisms and damage of different cartilage compositions [262]. Complex time interactions may cause compatible issues in simulating the evolution of OA due to the excessive precision in computing different compositional turnovers. To overcome this when considering the multi-scale effects of obesity, the production of Fn-fs level was modelled to encapsulate the progressive degeneration [205], and

the update interval for cartilage tissue properties was estimated, ensuring the consistency in the temporal variations of material properties. Since degradation fragments and degeneration are generally on a month-basis [281], the minimum time increment at baseline (τ_i) was set to 1 month for each iteration. The sensitivity of τ_i to the progression of degeneration was shown in Appendix G.2. Within τ_i, the loading condition was assumed to be repeated by a certain number of cycles leading to mechanical damage. In addition, BMI, physical activity level (PAL) and daily nutrition are three attribute parameters of the knee joint, in relation to the loading condition and the inflammatory activities.

5.2.4 Computational analysis of cartilage degeneration

Table 5.2: *The parameters implemented in the multi-scale algorithm of cartilage degeneration*

Parameter	Description	Value	Reference
$S_{threshold}$ (MPa)	The threshold of maximum principal stress leading to mechanical damage	$\{0.1, 0.2, 0.3, 0.4, 0.5\}$	Estimated
r_d	The constant that governs the cumulative rate of mechanical damage	$\{\frac{1}{3}, \frac{2}{3}, 1, \frac{3}{2}, 2\}$	Estimated
ω_e	The boundary of the minimum Young's modulus for cartilage elements	0.99	[187]
ω_k	The boundary of the maximum permeability for cartilage elements	3	[276]
F_{max}	The boundary of the maximum level of Fn-fs	$\{25, 50, 75, 100\}$	Estimated
BMI^{meas}	The BMI value in the health profile	$\{18, 25, 36\}$	Estimated
PAL	The constant level of physical activity	1	Estimated
$\frac{DailyCal}{BMR}$	The nutritional term defined by the ratio of daily calorie intake to BMR	1	Estimated

Note: At baseline, $S_{threshold} = 0.3$ MPa, $r_d = \frac{2}{3}$, $F_{max} = 50$.

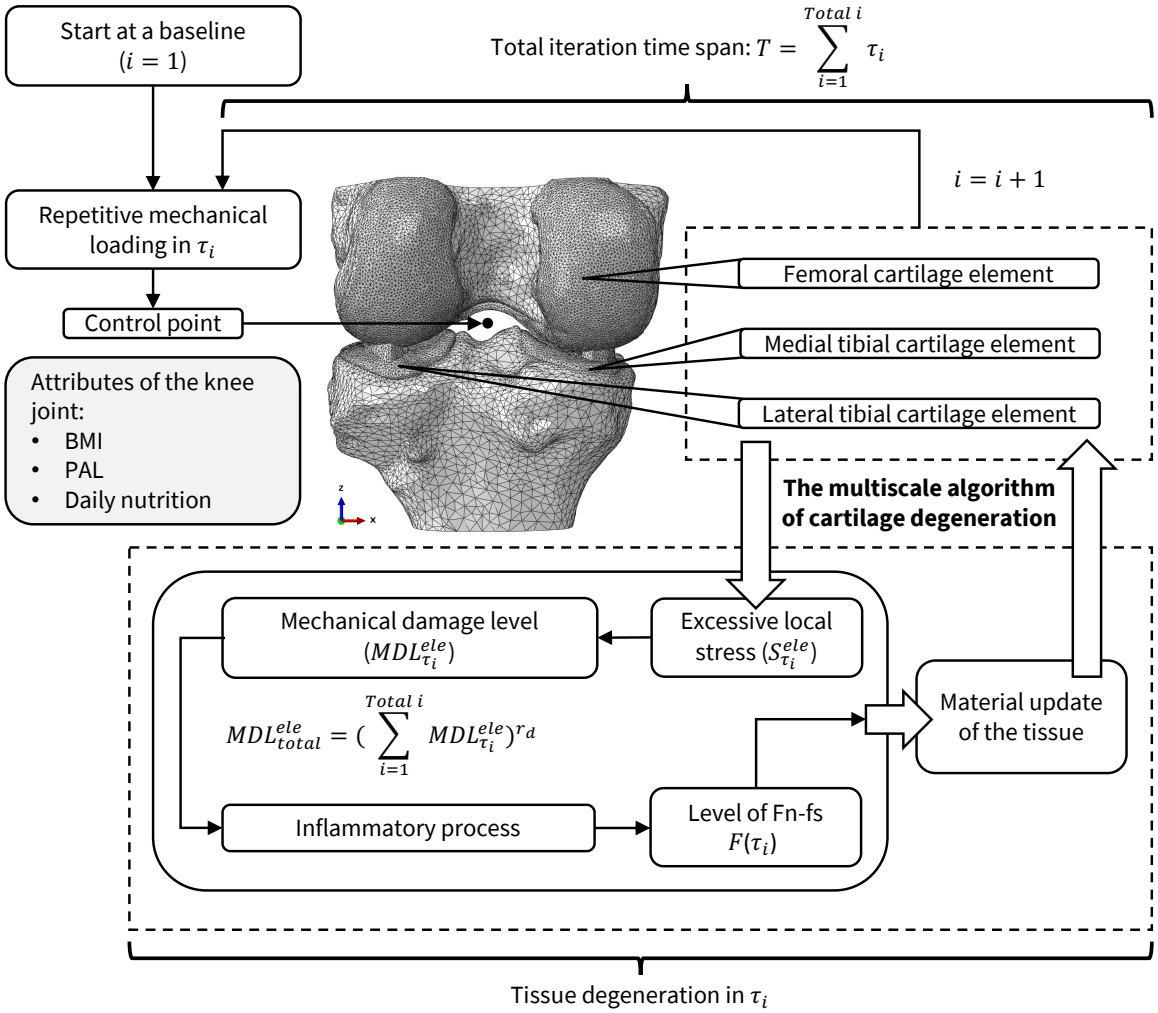

Figure 5.1: *The integrative multi-scale framework of the knee joint degeneration in mechanics and inflammation. Physical activity level (PAL) is defined by the ratio of total daily energy expenditure (TEE) to basal metabolic rate (BMR) [212], and daily nutrition is measured by the ratio of daily calorie intake to BMR. Controlling the values of the two attributes (PAL and daily nutrition) at 1 represents no physical activity and dietary interventions [237].*

The sensitivity of two parameters (r_d, F_{max}) governing the progressive degeneration of each element in this algorithm was numerically analysed due to the lack of experimental evidence. Synthetic data of maximum principal stress (ranging from 0 to 10 MPa) on individual elements of cartilage was generated for the sensitivity analysis at a single iteration. Table 5.2 presents the baseline values implemented in the computational framework and the parameters proportionally adjusted within the same order of magnitude for sensitivity analysis. Moreover, to evaluate the vari-

ability of cartilage degeneration due to obesity and the heterogeneity of degenerative mechanisms in this framework, three health profiles were generated for the subject-specific FE model when controlling PAL and the nutrition factor to be constant, as illustrated in Figure 5.2. The framework presented in Figure 5.1 was implemented in MATLAB (R2022a, The Math Works, Inc., Natick, MA, USA), coupled with Abaqus 2021 (Dassault Systèmes, Vélizy-Villacoublay, France), to govern the multiscale simulations. The variations of biomechanics and inflammatory activities were simulated for 5 years (60 iterations). The estimated value of $S_{threshold}$ was varied to evaluate the sensitivity of stress threshold for each health profile (Table 5.2). In addition, the inflammatory and mechanical effects of obesity were examined for three health profiles simulated with baseline parameters.

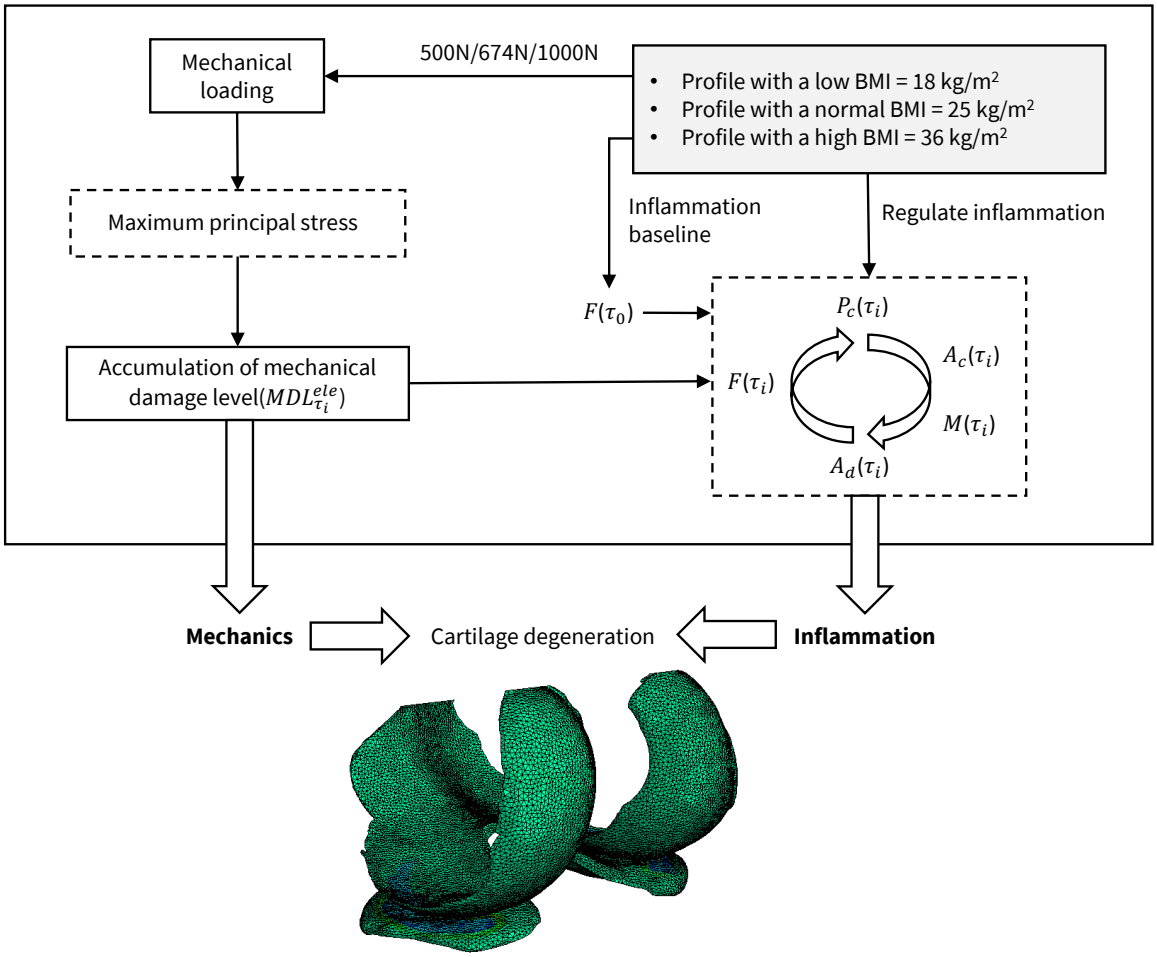

Figure 5.2: *Simulations of cartilage degeneration for three health profiles (low BMI, normal BMI and high BMI).*

5.3 Results

5.3.1 Sensitivity of mechanical damage accumulation and boundary of cartilage integrity

The sensitivity of approaches used to govern the cartilage degeneration rate and magnitude in the algorithm was analysed by a parameter variation study. The numerical relationship between two parameters (r_d, F_{max}) and the degeneration level of an individual element after one iteration was examined (Figure 5.3). The degeneration level ranges from 0 to 1, corresponding to a percentage scale from 0% (non-degeneration) to 100% (full degeneration). Three states were found during the progression of degeneration, as presented in Table 5.3. The initiation of degeneration occurred when the accumulative mechanical damage was relatively low. The increase of maximum principal stress facilitates the accumulation of mechanical damage from *I* to *III*.

Table 5.3: *States of degenerative process over the accumulation of mechanical damage.*

Degenerative process	Description
I	Initiation of degeneration
II	Transition state between initiated degeneration and chronic inflammation
III	Degeneration with chronic inflammation

It could be seen that r_d controlled the rate of degeneration (Figures 5.3a and 5.3b) and F_{max} dominated the magnitude of degeneration (Figures 5.3c and 5.3d) in this framework. The linear degenerative progression was simulated at $r_d = 1$, implying that the degeneration level was proportional to the maximum principal stress. As reaching the same degeneration level, the degeneration progressed more rapidly during the initiation of cartilage degeneration (*I*) when r_d was decreased (Figure 5.3b). At $r_d < 1$, the rate of degeneration gradually slowed in the transition between *II* and *III*, whereas an opposite trend was observed at $r_d > 1$. In addition, the increase of F_{max} only magnified the degeneration level in each state of degeneration, as illustrated in Figures 5.3c and 5.3d. This resulted in a higher degeneration level in all three states when the accumulation of mechanical damage was identical, suggesting reduced resistance to degeneration at the same stress level.

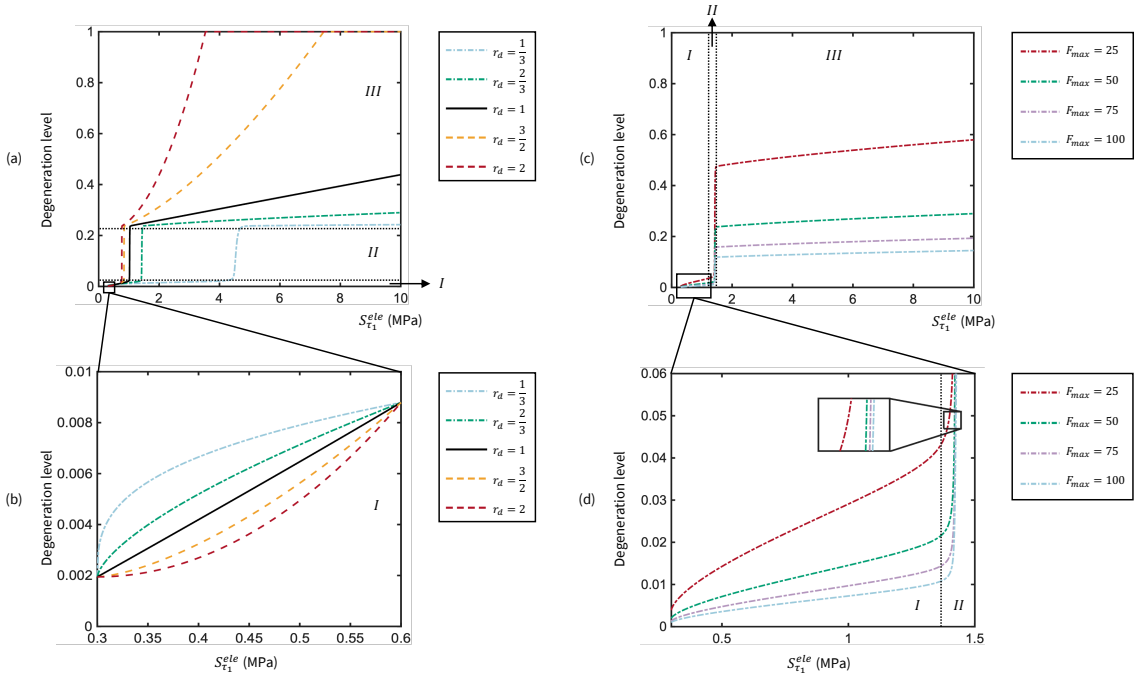

Figure 5.3: *Sensitivity of r_d and F_{max} to the degenerative process resulted from the accumulation of mechanical damage.*

5.3.2 Sensitivity of the stress threshold leading to cartilage damage and degeneration

The degenerative progression of cartilage was evaluated by calculating the volume percentage of nondegenerative elements at each iteration (Figure 5.4). For illustration, cartilage elements of which integrity surpasses 75% of the baseline were labelled as nondegenerative elements. Figure 5.4 shows that the nondegenerative elemental volume nonlinearly declined in the discrete time sequence of simulations. As the cartilage degeneration iteratively progressed, the proportion of degenerative elemental volume to the total volume of each cartilage tended to converge. This qualitative trend remained similar regardless of the difference in the parameterisation of the stress threshold ($S_{threshold}$) and the health profile (BMI^{meas}). The decrease of the stress threshold significantly accelerated the degradation process and expanded the degenerative cartilage volume. The maximum volume percentages of degenerative cartilage for a low BMI reached nearly up to 49% at $S_{threshold} = 0.1$ MPa and 7% at $S_{threshold} = 0.2$ MPa in the lateral tibial cartilage (Figure 5.4a). Likewise, the maximum degenerative volume percentages were found in the lateral tibial cartilage for a normal BMI (nearly 57% at $S_{threshold} = 0.1$ MPa and 22% at $S_{threshold} = 0.2$

MPa) and a high BMI (around 71% at $S_{threshold} = 0.1$ MPa and 39% at $S_{threshold} = 0.2$ MPa), as presented in Figure 5.4b and Figure 5.4c respectively. In comparison of three health profiles, the profile with a higher BMI was more sensitive to the stress threshold. The maximum degenerative volume percentage of lateral tibial cartilage increased to around 20% at $S_{threshold} = 0.3$ MPa and 9% at $S_{threshold} = 0.4$ MPa with a high BMI (Figure 5.4c) when only up to 6% degenerative volume of cartilage was found at $S_{threshold} = 0.3$ MPa in the profile with a normal BMI (Figure 5.4b). Additionally, the sensitivity of the stress threshold appeared to differ for femoral and medial tibial cartilages. This might result from the dissimilar biomechanical responses and intact tissue volumes, which are unlikely to change the overall sensitivity pattern.

Figure 5.5 presents the Interquartile Range (IQR) of the degeneration level for degenerated cartilage elements across different health profiles at the end of iterations. It was observed that the median degeneration level of femoral cartilage with a high BMI decreased to 22.9% (IQR 22.8%-25.1% at $S_{threshold} = 0.5$ MPa from 32.6% (IQR 26.7%-38.5%) at $S_{threshold} = 0.1$ MPa (Figure 5.5a), indicating that the increase of stress threshold significantly reduces the degeneration. This is likewise to the lateral and medial tibial cartilages for profiles with both a low and normal BMI (Figures 5.5b and 5.5c). Compared to a high BMI, the health profile with a lower BMI showed a reduced median level of degeneration in both femoral and tibial cartilages regardless of changes in stress threshold. At $S_{threshold} = 0.1$ MPa, the median degeneration level of the femoral cartilage was 30.2% (IQR 25.7%-35.1%) for a normal BMI, decreasing to 27.6% (IQR 24.6%-31.6%) in the knee joint with a low BMI (Figure 5.5a). It is noteworthy that different locations of cartilage also exhibited variability in the sensitivity of the stress threshold. As the stress threshold was raised from 0.3 MPa to 0.5 MPa, the median degeneration declined from 24.1% (IQR 23.2%-26.1%) to 1.8% (IQR 1.1%-23.1%) in the lateral tibial cartilage with a normal BMI (Figure 5.5b). Similarly, the median degeneration was 23.3% (IQR 23.1%-25.4%) at $S_{threshold} = 0.3$ MPa and 23.1% (IQR 23.1%-23.2%) at $S_{threshold} = 0.5$ MPa in the medial tibial cartilage with a normal BMI (Figure 5.5c). Interestingly, the degeneration level of medial cartilage was higher when the threshold was over 0.4 MPa, compared to the lateral cartilage with a low and normal BMI. This is contradictory to the degeneration of tibial cartilages for a high BMI. The significant differences in cartilage compartment were also manifested in the degenerative volume at the identical stress threshold across all three health profiles, suggesting the heterogeneity of cartilage degeneration.

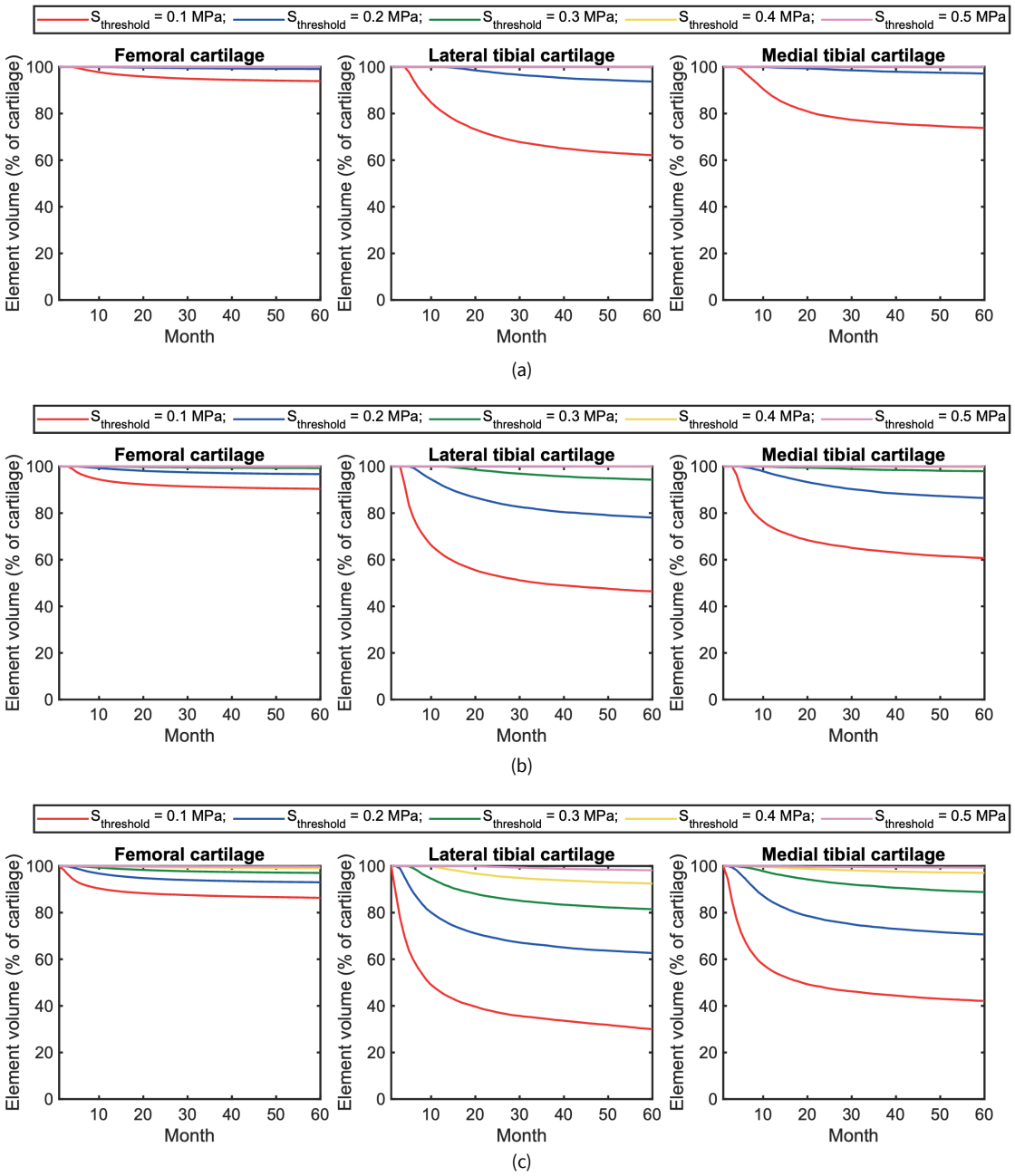

Figure 5.4: *Temporal variations in the percentage of nondegenerative cartilage volume when* $S_{threshold} = \{0.1, 0.2, 0.3, 0.4, 0.5\}$ *for different BMI levels: (a) low BMI, (b) normal BMI, and (c) high BMI.*

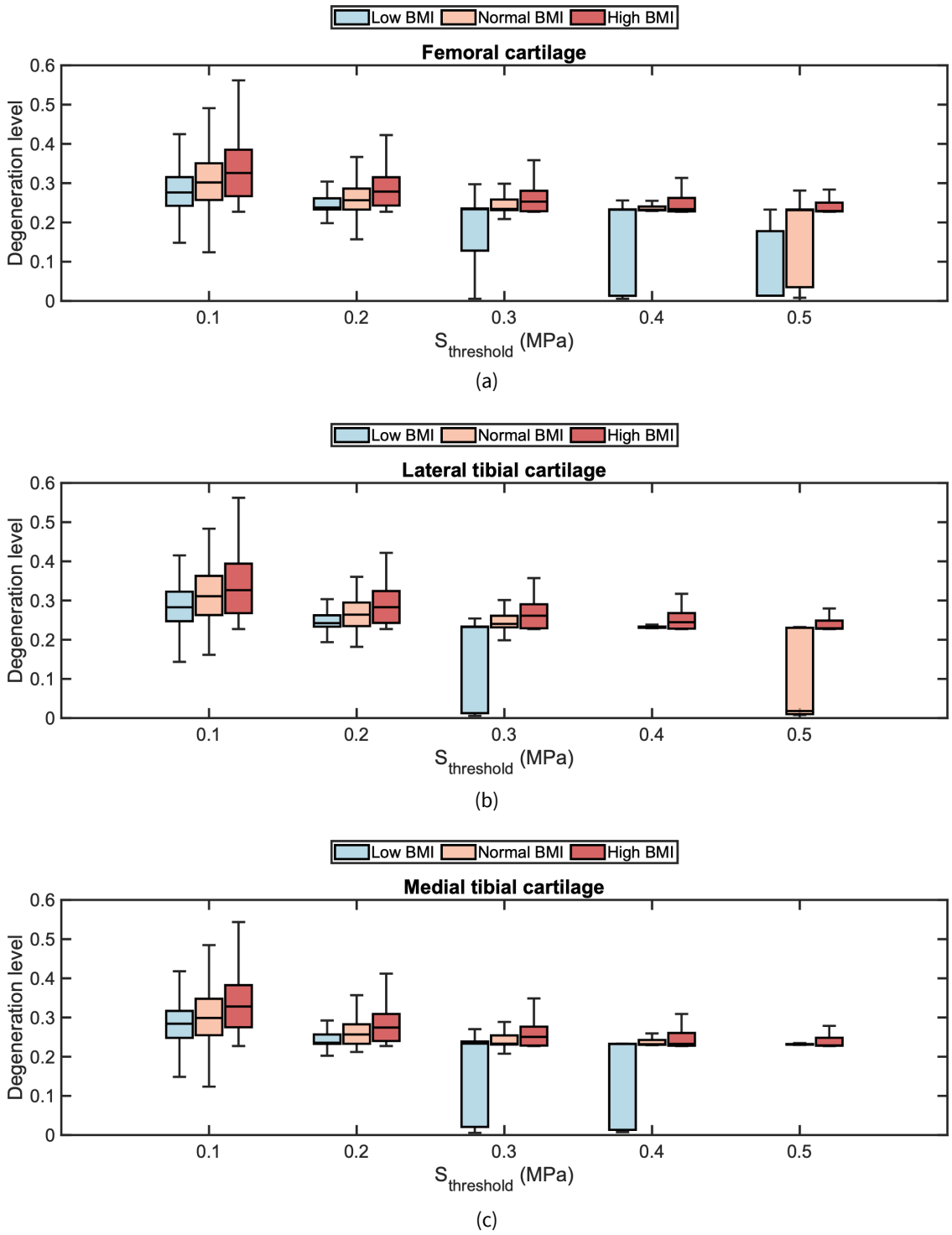

Figure 5.5: *The overall degeneration level of the degenerated elements in (a) femoral cartilage, (b) lateral tibial cartilage and (c) medial tibial cartilage when* $S_{threshold} = \{0.1, 0.2, 0.3, 0.4, 0.5\}$ *for different BMI levels. In the box chart, the median, interquartile range, and whiskers that extend to the minimum and maximum degeneration levels are indicated.*

5.3.3 Effects of obesity-associated inflammation and mechanics during cartilage degeneration

After five-year simulations of cartilage degeneration, both the cumulative mechanical damage level and the total degeneration level were elevated for the femoral and tibial cartilages with a normal and high BMI in comparison to a low BMI (Figures 5.6 to 5.8). The distributions of mechanical damage and total degeneration differed between femoral and tibial cartilages across the medial and lateral compartments. This variability was more pronounced in the profile with a high BMI, since the increase of BMI resulted in a larger degenerative area of cartilage. Due to the function of menisci, mechanical damage and degeneration appeared along the medial and lateral contact margins of the femoral cartilage (Figures 5.6c and 5.6f). However, the degenerative region was concentrated laterally on the lateral tibial cartilage (Figure 5.7f), and a larger area in degeneration was found compared to the medial tibial cartilage (Figure 5.8f), where the degenerative elements were mainly located on the medial side. This was also found in the distribution of mechanical damage (Figures 5.7c and 5.8c), with the medial tibial cartilage showing a less damaged area than the lateral tibial cartilage. It is noteworthy that the distributions of mechanical damage and total degeneration were not matched for the femoral (Figures 5.6c and 5.6f), lateral tibial (Figures 5.7c and 5.7f) and medial tibial cartilage (Figures 5.8c and 5.8f) due to inflammation.

To visualise the contribution of mechanical damage for each cartilage element, the ratio of damage level and total degeneration level was calculated as a metric, representing the damage level that introduces 1% degeneration. Figures 5.6g, 5.7g and 5.8g show the IQR and kernel density estimate (KDE) of the data on degenerative elements with different proportional contributions of mechanics and inflammation. The median value of the mechanical damage level leading to 1% degeneration and the number of degenerative elements were increased with a higher BMI due to the difference in the progression of cartilage degeneration. Accordingly, the median values might not be directly comparable across different health profiles. Instead, the vertically oriented KDE curves illustrated that a wider section occurred at the lower values of this metric from a low BMI to a high BMI. This suggests that the increase in BMI leads to more pronounced inflammatory effects on cartilage degeneration. In addition, the KDE curves displayed an uneven pattern with two peaks of the curve width for three levels of BMI. Particularly, the KDE curves extended upwards, showing the distribution of cartilage elements with larger mechanical contributions to degeneration. At a low BMI, the width of the KDE curve increased form-

ing a first peak, followed by a long decline. A second peak appeared towards the end where the metric reached its highest value near 0.8. Differently, the second peak was found in the middle of the KDE curves for a normal and high BMI. These non-uniform patterns indicate that the contributions of mechanical damage and inflammation are distributed differently across cartilage elements, which may result from the varying states in the degenerative process.

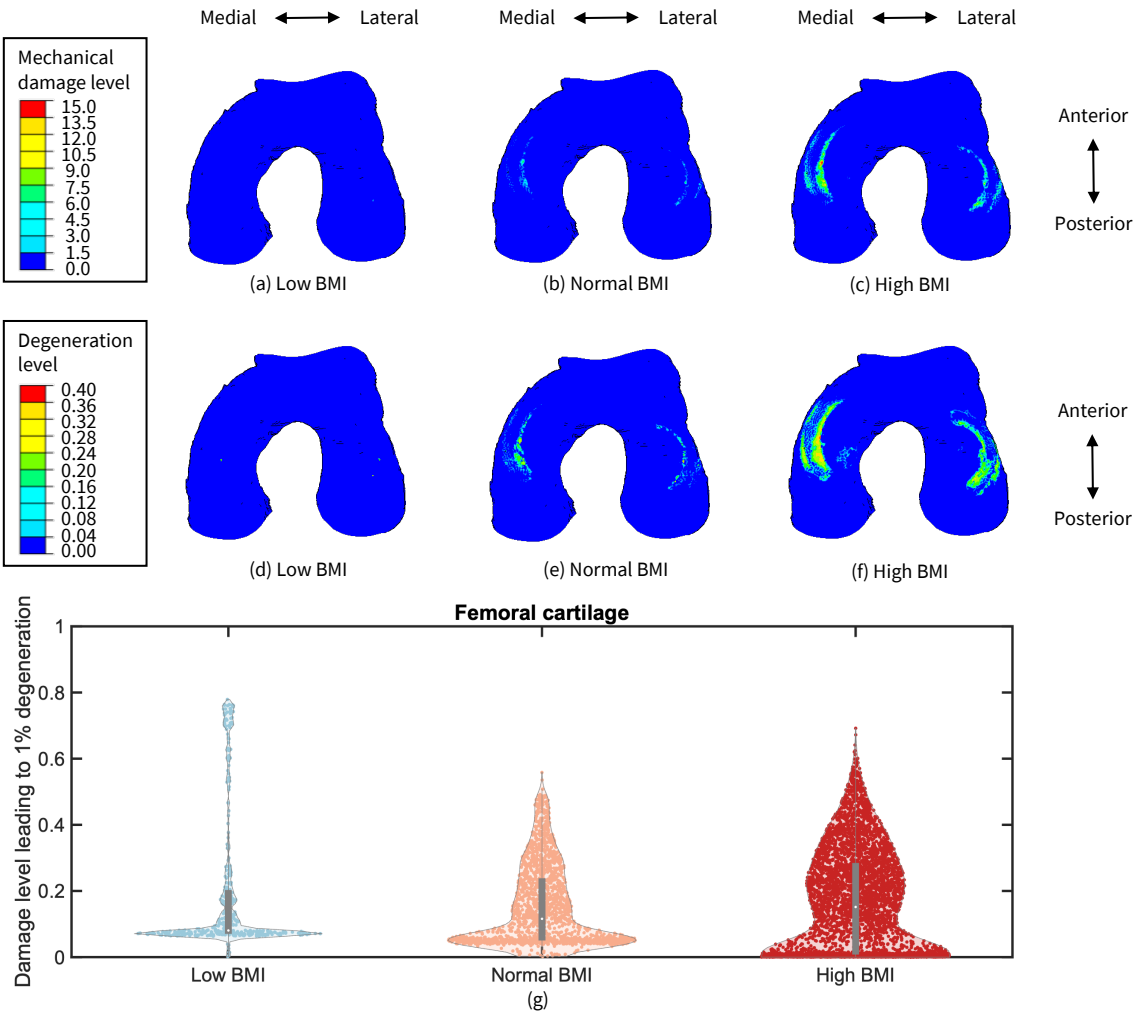

Figure 5.6: *Distribution of mechanical damage level and total degeneration level on the femoral cartilage for a low BMI (a) & (d), a normal BMI (b) & (e), and a high BMI (c) & (f). The damage level leading to 1% degeneration (g) illustrates the relative mechanical and inflammatory contributions to cartilage degeneration. The mechanical damage tends to contribute more with a lower value of this metric compared to inflammation. The width of the KDE curves indicate the density of element distribution. Wider regions correspond to a larger number of cartilage elements, whereas narrower regions represent sparse distributions.*

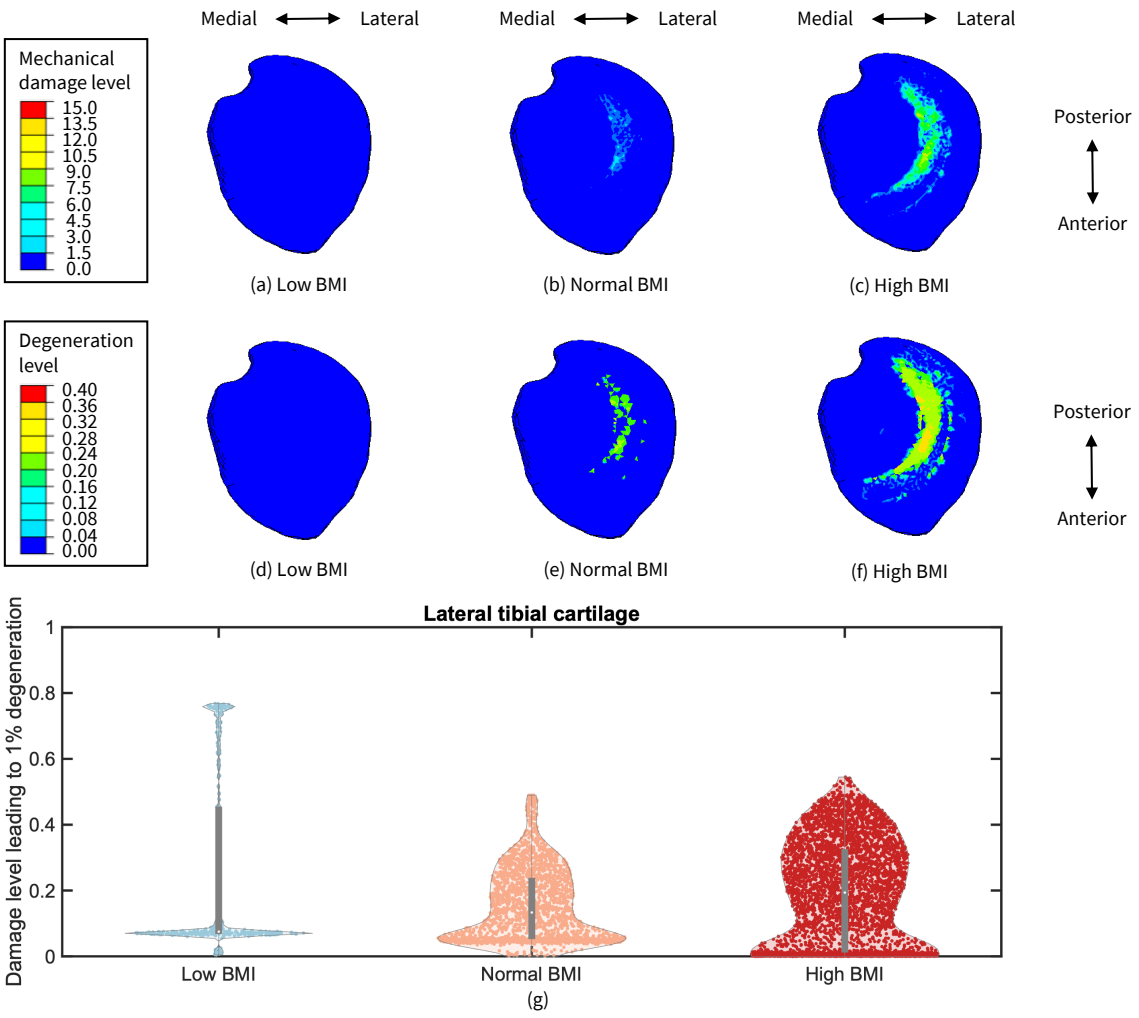

Figure 5.7: *Distribution of mechanical damage level and total degeneration level on the lateral tibial cartilage for a low BMI (a) & (d), a normal BMI (b) & (e), and a high BMI (c) & (f). The damage level leading to 1% degeneration (g) illustrates the relative mechanical and inflammatory contributions to cartilage degeneration. The mechanical damage tends to contribute more with a lower value of this metric compared to inflammation. The width of the KDE curves indicate the density of element distribution. Wider regions correspond to a larger number of cartilage elements, whereas narrower regions represent sparse distributions.*

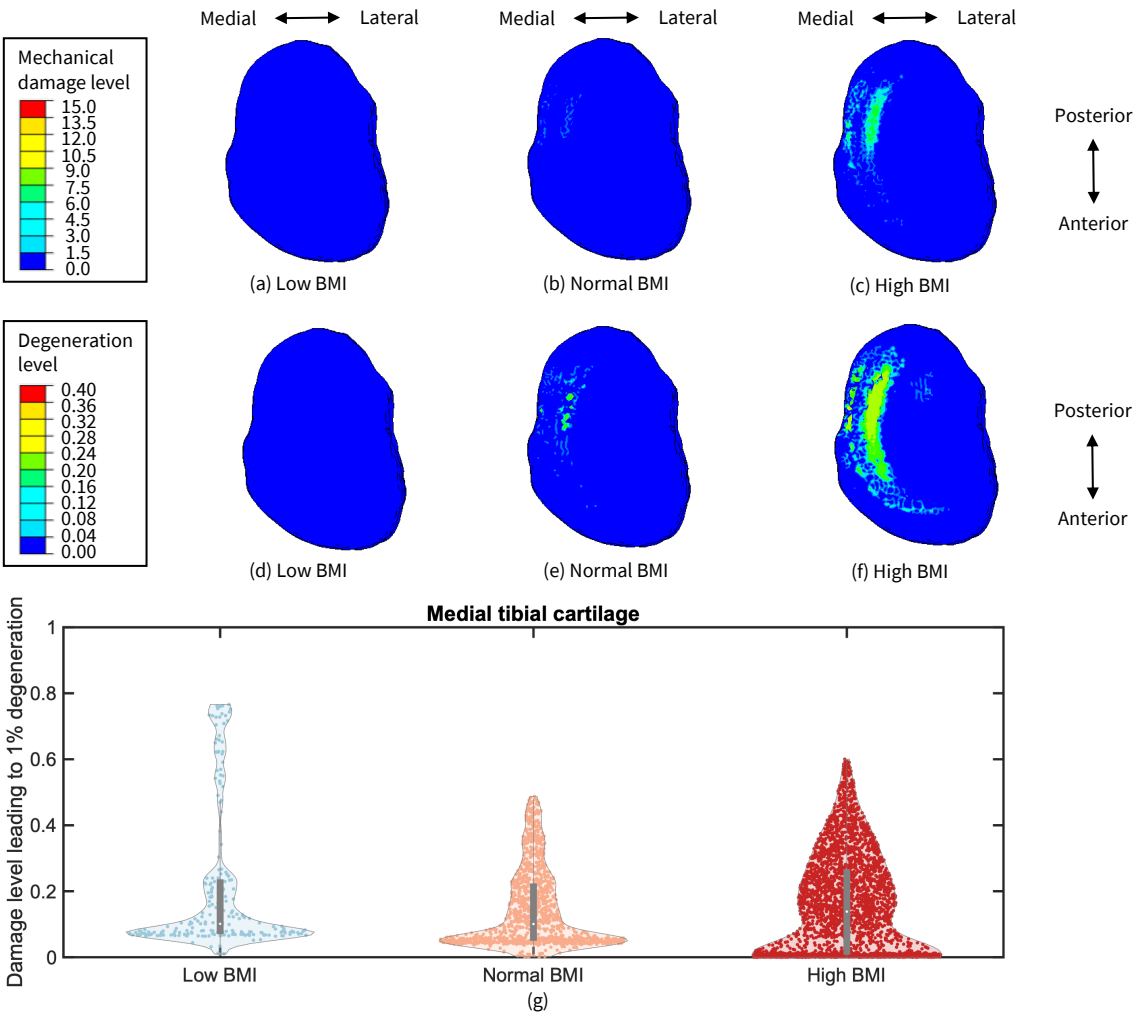

Figure 5.8: *Distribution of mechanical damage level and total degeneration level on the medial tibial cartilage for a low BMI (a) & (d), a normal BMI (b) & (e), and a high BMI (c) & (f). The damage level leading to 1% degeneration (g) illustrates the relative mechanical and inflammatory contributions to cartilage degeneration. The mechanical damage tends to contribute more with a lower value of this metric compared to inflammation. The width of the KDE curves indicate the density of element distribution. Wider regions correspond to a larger number of cartilage elements, whereas narrower regions represent sparse distributions.*

5.4 Discussion

A novel multi-scale framework was developed, integrating for the first time the obesity-associated inflammation and mechanics in the context of knee OA. The complex interplay between inflammatory activities and biomechanical behaviours affected by obesity was simulated by coupling the adipokine-mediated inflammation [237] with knee joint biomechanics at both spatial and temporal scales. This framework focused on the cartilage degeneration initiated by accumulative mechanical damage at different levels of inflammation, providing an advanced tool to assess the risk of OA according to the subject-specific joint profiles. In the degeneration algorithm, the heterogeneity of tissue turnover was approached through element-wise simulations of the poroelastic cartilage. The sensitivity of two governing parameters (r_d, F_{max}) was studied. Adjusting r_d and F_{max} could modulate the rate and magnitude of degeneration during progression, respectively. Moreover, the cartilage degeneration was simulated within 5 years (60 iterations) for the subject-specific knee joint (LTKN8964). The degeneration was found to be sensitive to the stress threshold as well as the level of BMI, with higher levels of BMI potentially accelerating the time-varying process. The distribution of mechanical damage and total degeneration was location-specific in cartilages, and obesity considerably elevated their levels. In particular, excess adiposity raised the baseline level of inflammation in cartilaginous environment. Consequently, inflammation became the dominant factor of cartilage degeneration as BMI increased.

Cartilage degeneration is a nonlinear progression during OA due to complex inflammatory and biomechanical regulations [22, 260, 265]. At an early stage, the degeneration is not observable from radiographic assessments, and prodromal symptoms are the critical sign of knee OA [32, 255]. Knee pain is an established symptom [31, 213] whereas it could be the outcome of other symptoms such as inflammatory activities [220] and tissue damage [256]. As degeneration progresses, the balance of anabolic and catabolic activities is disrupted within cartilage. This leads to chronic inflammation and accumulative mechanical damage accompanied by intermittent pain, ultimately resulting in structural changes. The algorithm of cartilage degeneration in this framework was able to capture three primary hallmarks (*I*, *II*, *III*) for localised degenerative elements when considering the interactions of inflammation and mechanical damage. The repetitive loading over the threshold leads to damage accumulation in articular cartilage [253, 267]. This accumulation gradually alters the metabolism of cartilage to initiate degeneration, which corresponds to *I*. The

damage level accumulates to degrade tissue, and PRRs and DAMPs are activated in the innate immune response [219], resulting in the transition of anabolism towards catabolism (*II*). Progressively, chronic inflammation evolves in the degenerative process [83], corresponding to *III*. Nevertheless, there is yet little evidence on the quantitative relationship between the level of accumulative damage and those three states. Degeneration results from the dysregulation of cartilage metabolism that is affected by local and systemic inflammation [41, 42] and crosstalks between surrounding tissues [55, 282], while individual differences also provide a large variability due to effects of genetics, age, gender and lifestyles [267]. Thus, it is significantly challenging to fully validate the algorithm of cartilage degeneration in this framework. Despite that, two parameters (r_d, F_{max}) of the algorithm were able to govern the rate and level of cartilage degeneration, which can minimally represent the outcomes of unmeasurable local and systemic confounding effects rather than extensively simulating them. The degeneration of cartilage has been described through variations in tissue constituents in previous computational models [127, 169, 182, 183, 186–189, 278]. In particular, the biomechanical characterisations of tissue material are functions of compositional changes, such as collagen destruction, proteoglycan depletion or the loss of fixed charge density. Loading rate and magnitude [187, 252] are tightly associated with the degradation of different constituents, and its cyclic exposure [253, 254] determines the fatigue life of cartilage material. Thus, results are not able to be quantitatively compared due to the difference in time dependencies and loading conditions. However, tuning r_d could mimic the variations of the degeneration rate that was found in the study by Mononen et al. [169], which demonstrates an excellent adaptivity of this multi-scale framework. Additionally, the decrease of F_{max} significantly reduced the cartilage degeneration level at the same stress magnitude. As a product of ECM degradation, the level of Fn-fs is an indication of cartilage degeneration [205, 239]. The boundary of Fn-fs level could be adapted to individuals with different susceptibilities to cartilage degeneration [267, 268]. In future work, incorporating additional patient-specific data could enable the estimation and interaction analysis of these parameters to characterise different patient groups based on longitudinal assessments of cartilage degeneration. This may contribute to subject-specific simulations of cartilage degeneration, thereby improving patient stratification and investigating personalised treatment strategies.

The stress threshold that determines damage accumulation was found markedly sensitive to the degenerative process. The cartilage degeneration was

accelerated and exacerbated with a lower threshold but tended to slow over time. This is consistent with previous models [166, 169], though the values of threshold are not comparable. In addition to time dependencies and loading conditions, cartilage conditioning [267], modulated by individual differences, may also underlie the specificity of the threshold. In particular, Vincent and Wann [268] suggested that the threshold may be decreased if cartilage loses its mechanoprotective mechanisms where transforming growth factor-β-activated kinase 1 (TAK1) [261] may play a critical role as an important upstream inflammatory regulator in response to mechanical damage. The activation of TAK1 still remains unclear and may not involve soluble mediators [263]. Therefore, the damage threshold may vary widely across individuals. Different modelling strategies of tissue damage can also contribute to the uncertainty of the threshold, highlighting the importance of analysing its sensitivity. In this framework, the sensitivity of the threshold is the result of the synergistic interaction of the increased inflammation baseline [42] and mechanical loading [47]. The results showed that the degeneration was more sensitive to the threshold at a higher level of BMI, while obesity increased the level and volume of degenerative elements. This relationship between obesity and cartilage degeneration is in line with the results from previous computational models [159, 164–168, 272] whereas they have focused on the obesity-mediated biomechanics in knee OA. From a biomechanical perspective, obesity can increase the adduction moment of the knee joint [161] and may result in the medial concentration of cartilage contact [160]. In fact, Stoddart et al. [162] reported a higher risk of OA in the medial compartment of the tibiofemoral joint. However, this study showed that the degeneration of all three profiles appeared to be more severe in the lateral tibial cartilage compared to the medial tibial cartilage. It should be noted that the validated FE model in this framework was created from the healthy knee joint of a male with BMI = 18 kg/m^2. The increased risk to the medial compartment might result from the malalignment or muscle weakness caused by a long-term effect of obesity [47]. In addition, subject-specific gait pattern [163, 165, 174] and joint geometry [159, 168, 277] are tightly associated with the mechanical responses of the knee in OA. In this computational model, the gait kinetics and kinematics of the knee joint were simplified to one loading condition for the study of the interacting effects of obesity-associated mechanical damage and inflammation. Consequently, the effect of the external adduction moment [174] was not included, and compartmental load distribution only resulted from the interactions among joint geometry, contact conformity, and material behaviour. This may explain the

higher level of degeneration on the lateral side in this study. In fact, it has been reported that obese individuals may tend to walk at a lower speed so that the knee adduction moment increases [163]. However, the major influence of the external adduction moment generally appears across most of the stance phase apart from the heel strike and the first 5% of the gait cycle [174]. This study thereby provides conservative estimates of cartilage degeneration under one loading condition resulting from obesity rather than other precise predictions. Integrating kinetic and kinematic data of the joint can improve the framework to capture the compartmental degeneration distribution for clinical predictions in the future.

As the first computational framework considering both inflammatory and mechanical effects of obesity, it simulated the progression of mechanical damage and degeneration triggered by the local maximum principal stress of cartilage over a threshold. It was revealed that obesity significantly exacerbated cartilage degeneration which was location-specific according to the mechanical damage. This location specificity is consistent with the computational predictions in the study by Klets et al. [166] regarding the location of cartilage degeneration due to the effects of body weight. However, the distribution of cartilage degeneration was not congruent with the mechanical damage, a discrepancy that became more pronounced as the BMI level increased. This could be explained by the difference in the contributions of inflammation and mechanical damage due to obesity. The results showed that a higher level of BMI increased the degenerative cartilage volume dominated by inflammation. The previous dynamics analysis [237] of obesity-associated inflammation has suggested that obesity can significantly increase the susceptibility of OA inflammation. Moreover, the pivotal role of obesity in OA inflammation has been widely reported [41, 42, 45], which is in line with the aforementioned effects of obesity in this study. As degeneration progressed, it was predicted that the accumulation of mechanical damage led to different patterns of degeneration and the contribution of mechanical damage varied across cartilage elements. This suggests that the orientation of local cartilage degeneration may shift with BMI levels between the damage-driven progression and the inflammation-dominated process at an early stage of the obesity-associated OA. However, the relative contributions of mechanical damage against inflammation likely depend on a complex dynamic interplay of individual factors that are not yet fully understood. In addition, the relationship between obesity and numerical variations of cartilage constituents remains unestablished in cartilage degeneration. Accordingly, this framework postulated the synchronised degradation of different compositions [186, 189], which was implicitly

approached by the production of Fn-fs. Despite that, the results showed that the average level of cartilage degeneration was positively correlated with BMI, which aligns with the cartilage property alterations due to obesity reported by Collins et al. [250].

Since BMI level, cartilage metabolisms and loading conditions of the knee joint all vary simultaneously and dynamically according to physical activities and diet [197, 250, 251], it is challenging to assess the dynamic evolution of specific obesity effects in OA. Thus, the development of this framework necessitates appropriate simplifications with a set of underlying assumptions. Due to the lack of longitudinal subject-specific data, the validity of this framework was evaluated by qualitatively comparing the degenerative process and the outcomes of obesity with previous findings. The subject-specificity could be improved by including more detailed data such as levels of specific biomarkers, gait patterns and body weight to examine the cartilage degeneration influenced by obesity. In addition, the obesity-mediated inflammatory process was simulated by an ODE-based model of five general mediator groups. Specifying the regulatory network could contribute to a more precise assessment on the mechanism of cartilage degeneration due to obesity [237]. Similarly, implementing the depth-dependent fibril-reinforced biphasic constitutive model of cartilage [188, 271] can also increase the precision by providing more accurate biomechanical behaviours during simulations. Nevertheless, a more granular simulation requires a much more precise patient-specificity of the cartilage material properties. The constitutive model of isotropic poroelasticity could not simulate directional biomechanical responses of cartilage and might underestimate the tensile stress on the contact surface [155]. However, the primary purpose of this study was to investigate the interactions of obesity-associated mechanical damage and inflammation, thereby the degeneration in this study was a conservative estimate. This framework includes a relatively minimal number of parameters and variables to integrate the effects of obesity on the cartilage degeneration. Aside from the calibration of parameters, the estimation of initial conditions for the knee joint is also limited. Specifically, the initial bone properties were not adjusted according to the changes in BMI. BMI and mechanical properties of subchondral bone were found correlated but still remain disputed [269, 270]. However, an FE study by Orava et al. [274] indicated that subchondral bone variations had no significant effect on the mechanics of articular cartilage in early OA. Given that, the observed effects of obesity on cartilage degeneration remain valid within the scope of the present study. In the future, this framework could be extended to simulate and predict the risk of

cartilage degeneration due to obesity, by including more granular subject-specific data and specifying additional regulatory pathways of OA.

5.5 Conclusion

A novel integrative multi-scale modelling framework was developed to evaluate the inflammatory and biomechanical effects of obesity on cartilage degeneration in knee OA. This is the first computational framework incorporating the degenerative pathway of obesity-associated inflammation. Results suggested that the inflammatory process modulated by BMI could differentiate the progression of cartilage degeneration. Increasing BMI resulted in a higher level of inflammation and stress in cartilage. This altered the threshold of cartilage to mechanical damage and its degenerative process. In the obese profile, a larger degenerative volume of cartilage was found with inflammation contributing more to the cartilage degeneration than mechanical damage. These computational results provide a transparent pathway of cartilage degeneration modulated by obesity. With future calibration, this framework could facilitate the identification of endotypes underlying obesity-related OA.

Appendix G: Sensitivity analysis of material properties and time increment for the knee joint (LTKN8941)

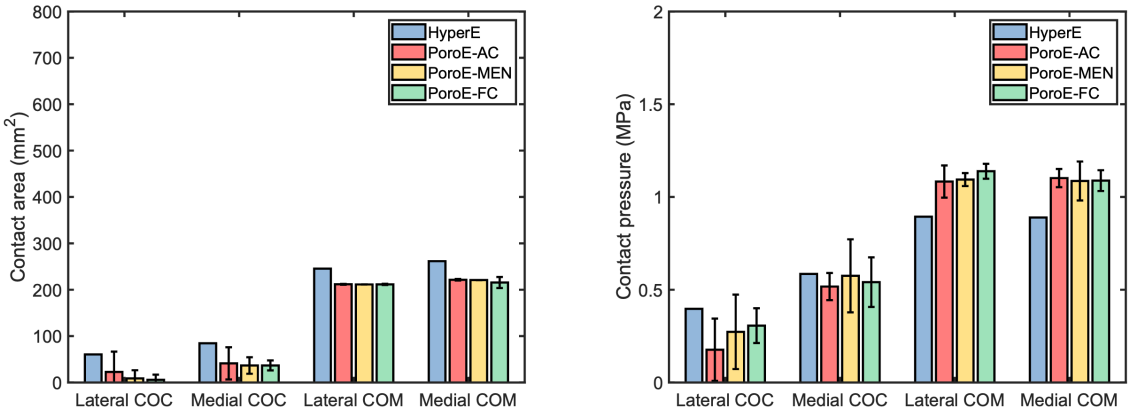

Model cohort	Articular cartilage	Meniscus	Contact friction coefficient
PoroE-AC	[25%, 175%] of baseline properties	Baseline	Baseline
PoroE-MEN	Baseline	[25%, 175%] of baseline properties	Baseline
PoroE-FC	Baseline	Baseline	[25%, 175%] of baseline properties
HyperE	Neo-hookean: C_{10} = 1.0274 D_1 = 0.08	$E_1 = E_2$ = 6 MPa; E_3 = 21 MPa; $\nu_{in\text{-}plane}$ = 0.3; $\nu_{out\text{-}plane}$ = 0.2; $G_{out\text{-}plane}$ = 8.08 MPa	$F_{CART\text{-}CART}$ = 0.1 $F_{CART\text{-}MEN}$ = 0.15

Figure G.1: *The sensitivity analysis of the material properties for the knee joint (LTKN8941).*

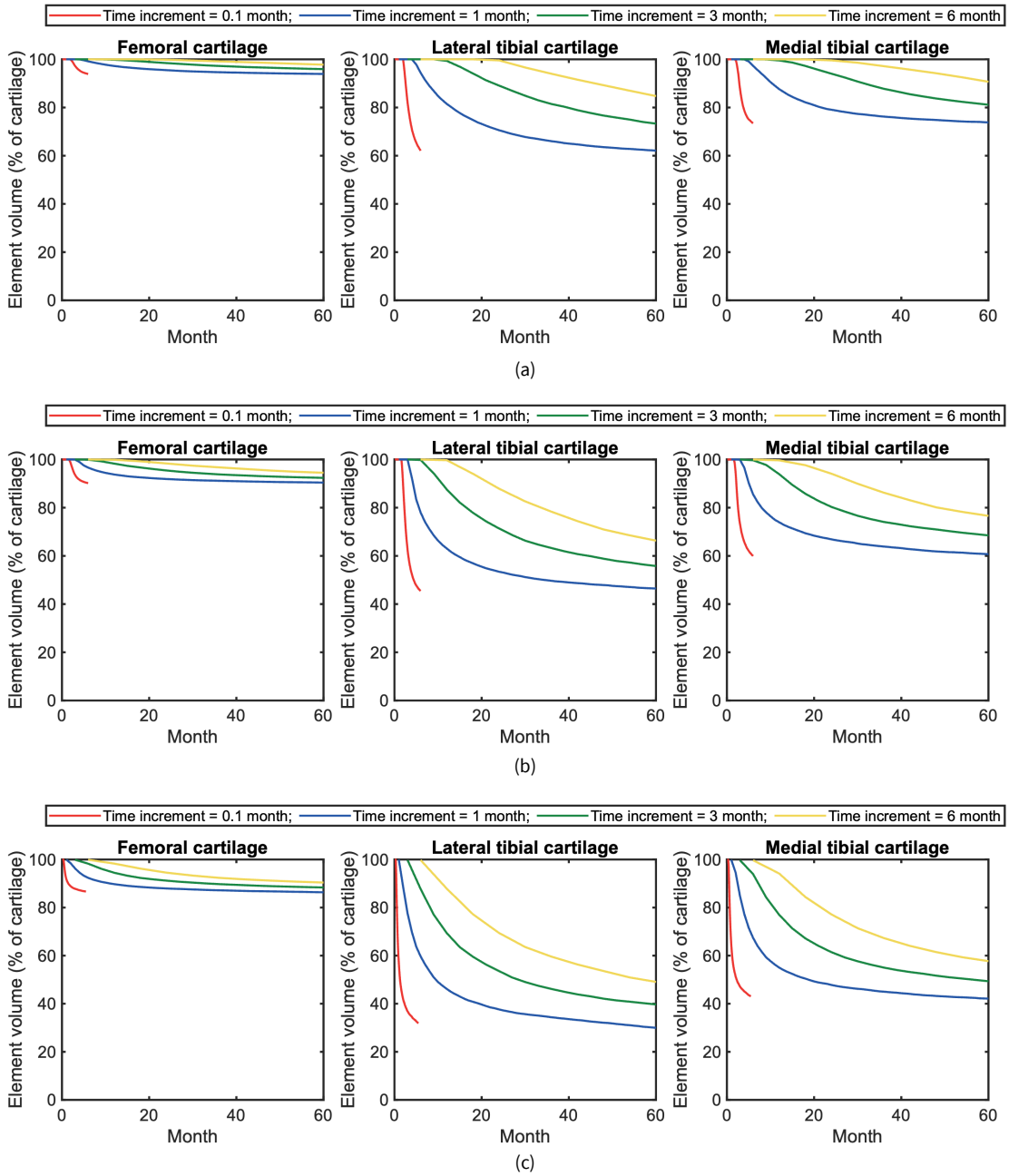

Figure G.2: *The sensitivity analysis of the minimum time increment for different BMI levels: (a) low BMI, (b) normal BMI, and (c) high BMI. The simulation was not converged when the minimum time increment was 0.1 month due to a relatively fast degeneration.*

Appendix H: The parameterisation of the obesity-associated inflammation model

Parameter	Description	Value
C_0	Natural production rate of PICs	0.05
C_1	Stimulated production rate of PICs by PICs	50
C_2	Saturation constant at which the capability of stimulating PIC production signalled by PICs is half of maximum	5
C_3	Stimulated production rate of PICs by adipokines	50
C_4	Saturation constant at which the capability of stimulating PIC production signalled by adipokines is half of maximum	5
C_5	Stimulated production rate of PICs by Fn-fs	50
C_6	Saturation constant at which the capability of stimulating PIC production signalled by Fn-fs is half of maximum	5
C_7	Saturation constant at which the capability of inhibiting PIC production signalled by AICs is half of maximum	5
C_8	Stimulated production rate of AICs by PICs	1×1.5^4
C_9	Saturation constant at which the capability of stimulating AIC production signalled by PICs is half of maximum	1×1.5^3
C_{10}	Stimulated production rate of AICs by Fn-fs	1×1.5^4
C_{11}	Saturation constant at which the capability of stimulating AIC production signalled by Fn-fs is half of maximum	1×1.5^3
C_{12}	Natural production rate of MMPs	0.05
C_{13}	Stimulated production rate of MMPs by PICs	50
C_{14}	Saturation constant at which the capability of stimulating MMP production signalled by PICs is half of maximum	5
C_{15}	Stimulated production rate of MMPs by adipokines	50

Continued on next page

C_{16}	Saturation constant at which the capability of stimulating MMP production signalled by adipokines is half of maximum	5
C_{17}	Saturation constant at which the capability of inhibiting MMP production signalled by AICs is half of maximum	5
C_{18}	The background production rate of adipokines due to the number of adipocytes	500
C_{19}	The background production rate of adipokines due to the size of adipocytes	500
BMI^{std}	The standard BMI	25
C_{20}	Saturation constant at which the capability of reducing adiposity through physical activity is half of maximum	Depending on PAL
C_{21}	Stimulated production rate of Fn-fs by MMPs	3
D_1	Clearance rate of PICs	5.2
D_2	Clearance rate of AICs	1.5×10^3
D_3	Clearance rate of MMPs	4.2
D_4	Clearance rate of adipokines	1.2×10^3
D_5	Clearance rate of Fn-fs	3
nex	The coefficient that governs the nonlinearity of physical activity effects at different BMI levels	Depending on BMI^{meas}
n	Hill coefficient	2

Chapter 6

Subject-specific multi-scale modelling of obesity-driven cartilage degeneration in knee osteoarthritis

In Chapter 5, the multi-scale modelling framework was developed based on a validated joint model, and the sensitivity of critical parameters in this framework was systematically studied. By implementing this established framework, the present chapter investigates the subject-specific variations of joint behaviour in cartilage degeneration. In particular, three subject-specific knee joint models are introduced, where both joint geometry and body mass index (BMI) are treated as individualised inputs. Consistent with Chapter 5, the coupling regulation and underlying assumptions between inflammatory processes and biomechanical responses are preserved. In contrast to Chapter 5, which focused on parameter sensitivity and effects of obesity on the processes of cartilage degeneration using a representative joint model, the emphasis of this chapter is the subject-specific variability in cartilage degeneration influenced by joint geometry and BMI. Under the regulations of obesity-associated inflammation and mechanical loading, the subject-specific biomechanical responses and cartilage degeneration patterns are quantified through simulations, and the effects of obesity are evaluated by varying the level of BMI across the three subjects. Through this approach, this chapter underscores the importance of subject-specific knee joint characteristics, particularly geometric features, in simulating obesity-associated cartilage degeneration within the multi-scale modelling framework.

6.1 Introduction

Osteoarthritis (OA) has become a major global health problem and this disease leads to a significant global burden, affecting over 600 million individuals [5]. Particularly, around 80% of OA cases involve the knee joint as it is the main weight-bearing joint frequently loaded during daily activities [3]. The degeneration of articular cartilage is a predominant pathological change in knee OA. Articular cartilage is a mechanoadaptive hyaline cartilage responsible for maintaining joint stability, frictionless motion, and the homeostasis of mechanical loads within the joint [49, 268]. However, effective treatments remain limited as the mechanisms of cartilage degeneration are still not fully understood. Since injury to one component of the joint can compromise other tissues, the pathology of OA involves the entire joint [24] and it is challenging to identify different phenotypes and endotypes at an early stage [32]. The understanding of OA phenotypes and endotypes can facilitate the development of therapeutic targets and approaches according to stratification of diverse cohorts [33].

Obesity is a pivotal risk factor that can be modified in knee OA [23, 44, 193, 234, 242, 251]. High body weight leads to mechanical overloading within the joint [156, 157, 161]. Moreover, the role of adipose tissue in regulating OA inflammation was reported [41, 42]. Excessive release of adipokines is associated with the degeneration of cartilage and the stimulation of OA inflammation [45]. Under the long-term mechanobiological regulation of obesity, the knee joint may become more susceptible to OA. Collins et al. [250] reported the association between obesity and the decrease of cartilage thickness and proteoglycan level, indicating the higher risk of OA in obese subjects prior to the observable structural changes. In addition, sarcopenia [283], chronic inflammation [44] and joint malalignment [47] jointly contribute to the characteristic of obesity-related OA. Nevertheless, it remains unclear to classify the sources of tissue degeneration in OA due to the synergistic interplay between biomechanical and biochemical regulation.

The degeneration of cartilage involves multiple pathomechanisms that correspond to different phenotypes and endotypes of OA [33]. Obesity-driven cartilage degeneration primarily is associated with mechanical overloading and metabolic disruptions along with inflammation. Mukherjee et al. [46] reviewed the recent computational models classified by degeneration pathways at single level and multi-scale. There have been computational models simulating various degeneration pathways, such as biomechanically oriented degeneration of cartilage

extracellular matrix (ECM) [169, 186–189, 278], biologically oriented variations in cartilage metabolism [128, 136, 237], and the injury-driven mechanobiological regulations in cartilage degeneration [182, 284]. Despite a few attempts [127, 185] to integrate the mechano-chemical-biological regulations of cartilage turnover, obesity-related pathways were not included. In previous studies of obesity-driven cartilage degeneration [159, 161, 166–168], obesity was modelled as a source of overloading contributing to the disruption of joint biomechanical responses and cartilage homeostasis. Liukkonen et al. [167] pointed out that the biomechanical effect of obesity was dependent on subject specificity of the joint. Furthermore, Orozco et al. [168] found that the joint geometry might be the most important subject specificity of the joint in the prediction of cartilage degeneration. However, this conclusion is limited as only the biomechanical pathway of cartilage degeneration was considered. So far, there is little computational model evaluating the subject-specific cartilage degeneration driven by the mechanobiological effect of obesity.

Obesity-driven cartilage degeneration may be highly subject-specific due to the variability of individuals in mechanobiological regulations. Thus, this study aimed to examine the obesity-driven degeneration pathway of cartilage across three subject-specific knee joints. A novel multi-scale modelling framework, developed in a previous work, was implemented. This framework integrates the biomechanical and inflammatory effects of obesity in cartilage degeneration. By comparing the variations in biomechanical responses and cartilage degeneration across subjects, the subject-specific effects of obesity were investigated for the improvement in understanding obesity-related OA pathomechanisms.

6.2 Materials and methods

6.2.1 Subject-specific tibiofemoral joints

Three validated subject-specific FE models of the human knee joint with location-specific articular cartilage were used from the dataset developed by Cooper et al. [249], see Figure 6.1. The validated FE models were created from imaging data of two left and one right human cadaveric tibiofemoral knee specimens. Computational modelling and experimental protocols were detailed in the open access dataset [249]. Two left specimens (LTKN8941 and LTKN1468) were respectively donated by a 61-year-old male with BMI = 18 kg/m^2 (Figure 6.1a) and an 81-year-old male

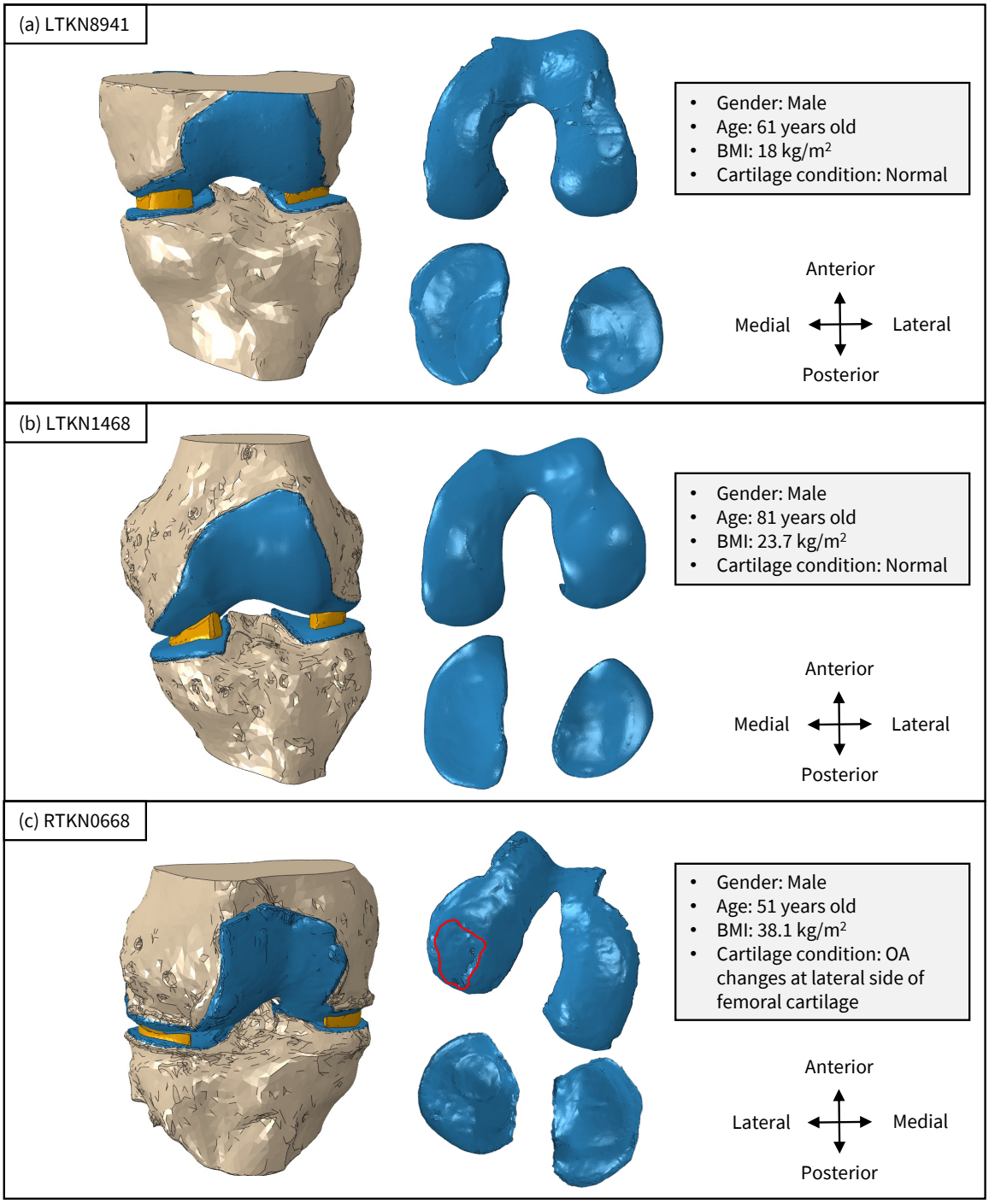

Figure 6.1: *Subject-specific profiles of the knee joints, summarised based on the dataset developed by Cooper et al. under CC BY 4.0 [249].*

with BMI = 23.7 kg/m^2 (Figure 6.1b). The right male specimen (RTKN0668) was obtained from a 51-year-old donor with BMI = 38.1 kg/m^2 (Figure 6.1c). In particular, osteoarthritic changes of articular cartilage were identified in the right knee spec-

imen (RTKN0668).

6.2.2 Modification of finite element models

Table 6.1 presents the initial tissue material properties of the three FE models. For simplification, femur and tibia were represented by a linear elastic property in simulating the degeneration of cartilage. Similarly, the menisci were modelled as anisotropic, with a modulus of 159.6 MPa in the circumferential direction and 20 MPa in both the radial and axial directions [273]. Articular cartilages were modified to the biphasic property of element-wise linear poroelasticity for the integration of the FE models and the multi-scale framework. Due to the lack of data in terms of the joint baseline conditions, the initial material properties were identical for the three subjects. The sensitivity of material parameters was studied for all three joints by comparing the results of this study with the original dataset [249], as shown in Figures G.1, I.1 & I.2.

Table 6.1: *Material properties of the subject-specific FE models.*

Material parameter	Tibia and femur [277]	Tibiofemoral cartilage [155]	Meniscus [273]
E_b (MPa)	15,000		
ν_b	0.3		
E_0 (MPa)		10	
ν_0		0.15	
k_0 (10^{-3} mm^4/Ns)		1	
v_0		4	
E_p (MPa)			20
E_{op} (MPa)			159.6
ν_p			0.3
ν_{op}			0.01
G_{op} (MPa)			50

E_b: Young's modulus of bones (femur and tibia); ν_b: Poisson's ratio of bones (femur and tibia); E_0: Initial Young's modulus of cartilage; ν_0: Initial Poisson's ratio of cartilage; k_0: Initial permeability of cartilage; v_0: Initial void ratio of cartilage; E_p: In-plane Young's modulus of meniscus; E_{op}: Out-of-plane Young's modulus of meniscus; ν_p: In-plane Poisson's ratio of meniscus; ν_{op}: Out-of-plane Poisson's ratio of meniscus; G_{op}: Out-of-plane shear modulus of meniscus

The mechanical loading applied to the knee joint was normalised to BMI. The

numerical stabilisation has been a challenge in the heterogeneous variations of cartilage property when implementing dynamic loadings. To reduce convergence issue due to numerical singularity, a pure compressive force at heal strike was applied to a kinematic coupling reference node axially connected to the top surface of femur. The force magnitude was scaled from 500N to 1058N, corresponding to BMIs ranging from 18 kg/m^2 to 38.1 kg/m^2 across the three subject-specific joints. In addition, only varus-valgus rotation was free for the femur and the bottom of tibia was fully fixed [277, 279]. Initial contacts were built at the first transient analysis step by applying a small displacement to femur. The contacts of cartilage-on-cartilage (CoC) and cartilage-on-meniscus (CoM) were defined as hard surface-to-surface with finite sliding.

6.2.3 Computational algorithm of cartilage degeneration

The modified subject-specific FE models of the knee joints (LTKN8941, LTKN1468, RTKN0668) were implemented in the multi-scale framework that was developed in Chapter 5, see Figure 6.2. The FE models were modified and simulated in Abaqus 2021 (Dassault Systèmes, Vélizy-Villacoublay, France). Cartilage degeneration was simulated for five years using the algorithm that integrates the accumulative mechanical damage and obesity-related inflammation (Figure 6.2b). In this algorithm, the time step size of each iteration (τ_i) was 1 month and 60 iterations were simulated. Mechanical damage ($MDL^{ele}_{\tau_i}$) was calculated for cartilaginous elements according to the distribution of maximum principal stress at each iteration (i). This assumes that the excessive stress leads to damage under a repetitive mechanical loading within one month. The accumulation of mechanical damage (MDL^{ele}_{total}), governed by an exponential parameter (r_d), was coupled to a set of ODEs that simulated the adipokine-mediated inflammatory activities ($\Theta^{ele}_{\tau_i}$). Parameters and the time step size of the inflammation model were estimated according to the decay rate of mediators [127, 140, 208, 238, 239]. To solve ODEs, *ode15s* was used with a relative accuracy of 0.001 in MATLAB (R2022a, The Math Works, Inc., Natick, MA, USA). In the inflammatory process, the level of fibronectin fragments (Fn-fs) was used to measure the overall degeneration level resulting from the regulation of inflammation and mechanical damage. As a function of Fn-fs level, cartilage material properties ($E^{ele}_{\tau_{i+1}}$, $K^{ele}_{\tau_{i+1}}$) were iteratively updated to represent the variations of mechanical characterisation in degeneration (Figure 6.2c). The level of degeneration was normalised between 0 and 1, representing non-degeneration and full degeneration respectively. Table 6.2 presents the estimated and subject-specific parameters

in this algorithm. Due to the lack of information on the joint profile, estimated parameters were consistent for the three subjects to evaluate the effects of obesity on the cartilage degeneration of the subject-specific knee joints.

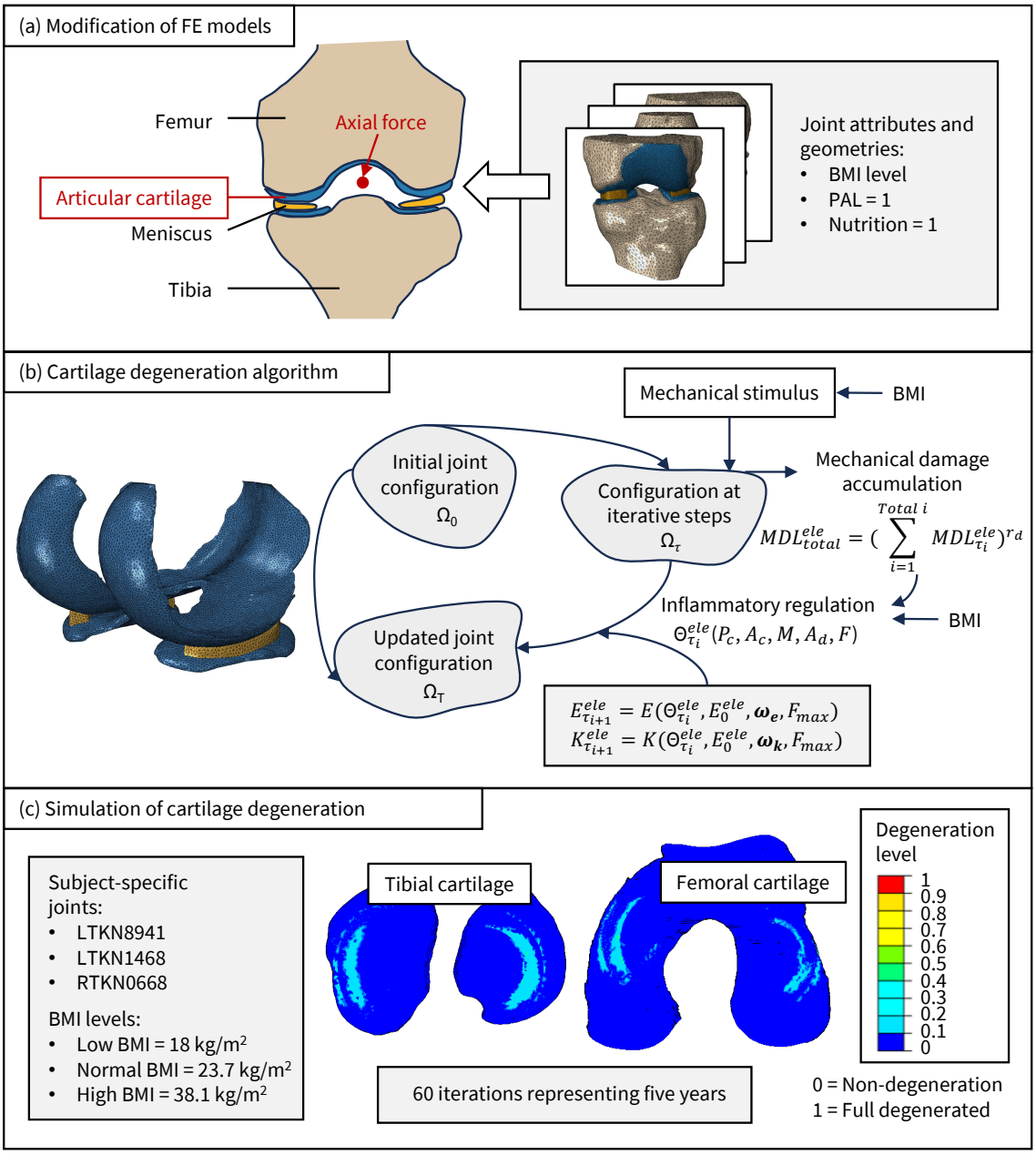

Figure 6.2: *The multi-scale modelling workflow of cartilage degeneration.*

Table 6.2: *Parameters implemented to the multi-scale modelling framework of cartilage degeneration.*

Parameter	Description	Value	Reference
$S_{threshold}$ (MPa)	Stress threshold	0.3	Estimated
r_d	The constant that governs the mechanical damage accumulation	$\frac{2}{3}$	Estimated
ω_e	The boundary condition of Young's modulus for cartilage elements	0.99	[187]
ω_k	The boundary condition of permeability for cartilage elements	3	[276]
F_{max}	The boundary condition of Fn-fs level	50	Estimated
$BMI^{meas}_{subjects}$ (kg/m^2)	The BMI values of the subject-specific joints (LTKN8941, LTKN1468, RTKN0668)	$\{18, 23.7, 38.1\}$	[249]
PAL	The constant of physical activity level	1	Estimated
$\frac{DailyCal}{BMR}$	The nutritional constant defined by the ratio of daily calorie intake to BMR	1	Estimated

6.2.4 Quantification of variations in cartilage degeneration

The maximum principal stress and strain, as well as the minimum principal stress, were quantified at the element level for each subject-specific cartilage by frequency plots, both at the first and last iterations. This allows a direct comparison of biomechanical patterns in degeneration. Additionally, peak values were extracted separately for tensile and compressive regions to identify the influence of the heterogeneous variations in cartilage modulus and permeability [154, 266] after a chronic degenerative process. To assess the effects of obesity, differences in the frequency distribution plot of stress were quantified across three levels of BMI. The weighted root-mean-square error (WRMSE) was calculated for pairwise comparisons of nor-

mal BMI and high BMI subjects against the low BMI baseline.

$$\text{WRMSE}_{BMI^{meas}_{\text{low}-j}} = \sqrt{\frac{\sum_{a=1}^{N} w_a \left(x_a^{(\text{low})} - x_a^{(j)}\right)^2}{\sum_{a=1}^{N} w_a}} \tag{6.1}$$

where $x_a^{(\text{low})}$ is the cartilage volume fraction within bin a for stress at a low BMI, and j denotes the results from the other two BMI levels ($x_a^{(\text{normal})}$, $x_a^{(\text{high})}$). Volume fraction represents the proportion of cartilage volume whose element-wise stress values are distributed within a specified bin. Each bin corresponds to a predefined range of stress and the total number of bins in the frequency plot is N. w_a is the weight of bin a, and the relation between w_a and the level of stress follows a monotonic increase. This weighted method can ensure that larger mechanical loads are given proportionally greater weight in the WRMSE calculation. Furthermore, the Interquartile Range (IQR) of cartilage degeneration level and the distribution on the contact surface were visualised for the three subject-specific joints with varying BMIs.

6.3 Results

6.3.1 Mechanical responses of three subjects in degeneration

Figures 6.3 to 6.5 presents the variations in mechanical responses of the three subject-specific joints after five-year simulations of cartilage degeneration. In the comparisons, the degeneration of each joint was simulated with the subject-specific BMI level. Due to the increase in the mechanical loading resulting from a higher BMI, the highest peak stress and strain were observed in RTKN0668. In addition, the highest peak stresses and strain were observed in the femoral cartilage of the three subjects, independent on BMI levels. By comparing with the femoral and lateral tibial cartilage, the peak maximum principal stress and strain of the medial tibial cartilage was significantly smaller for both LTKN1468 and RTKN0668 (Figure 6.3i). Despite the higher level of BMI in LTKN1468, lower peak values of maximum principal stress and strain were found compared with LTKN8941 (Figures 6.3i and 6.5i), and the peak minimum principal stress was close (Figure 6.4i). This subject-specific pattern was shown at both the first and last iterations. In comparison between initial and degenerative results, cartilage degeneration was associated with a decrease in peak maximum principal stress

and an increase in both peak minimum principal stress and maximum principal strain. This trend was consistent across the three subjects.

Figures 6.3d, 6.3e, 6.5d and 6.5e showed that the maximum principal stress and strain of LTKN1468 and RTKN0668 were mainly distributed at larger values within the lateral tibial cartilage. Differently, the concentration of minimum principal stress in the upper range was observed in the medial tibial cartilage of LTKN8941 and RTKN0668 at both the first and last iterations (Figures 6.4g and 6.4h). In the lateral tibial cartilage, the cartilage volume fractions were similar between LTKN8941 and RTKN0668 in the range of minimum principal stress from 0.3 MPa to 0.6 MPa whereas a larger volume fraction concentrated to this range appeared in LTKN1468 (Figures 6.4d and 6.4e). Compared with the first iteration, cartilage degeneration led to significant variations in the frequency distribution of volume fraction for the maximum principal stress and strain in the lateral tibial cartilage for the subjects with a normal (LTKN1468) and high BMI (RTKN0668). In turn, variations were modest in the cartilages of LTKN8941 and in the medial tibial cartilage of LTKN1468 and RTKN0668, suggesting a less sensitivity of these regions to degeneration driven by the increase in BMI.

6.3.2 Comparison of obesity-dependent mechanical distributions in subject-specific joints

The variations of WRMSE values ($\text{WRMSE}_{BMI^{meas}_{\text{low-normal}}}$, $\text{WRMSE}_{BMI^{meas}_{\text{low-high}}}$) indicated that the biomechanical responses were dependent on the level of BMI during cartilage degeneration, as presented in Tables 6.3 and 6.4. Specifically, the increase in BMI led to a higher WRMSE reflecting greater alterations in the distributions of maximum and minimum principal stress. It should be noted that the absolute magnitude of WRMSE was relatively lower in the femoral cartilage. Since WRMSE was calculated based on the global distribution, local variations might be attenuated in the range of higher stress where the volume fraction was small. However, the comparison of WRMSE aimed to examine the biomechanical differences resulting from obesity rather than assessing the absolute magnitude. Local variations could be seen by the peak values in Figures J.1 - J.6, showing that a higher BMI significantly increased the peak maximum and minimum principal stress in the three subjects.

In comparison of the tibial cartilage in the three subjects, both LTKN8941 and LTKN1468 demonstrated the higher sensitivity to the changes in maximum principal stress distribution when varying BMI levels, corresponding to greater WRMSEs in Table 6.3. Moreover, the joint of LTKN1468 exhibited the highest WRMSE values

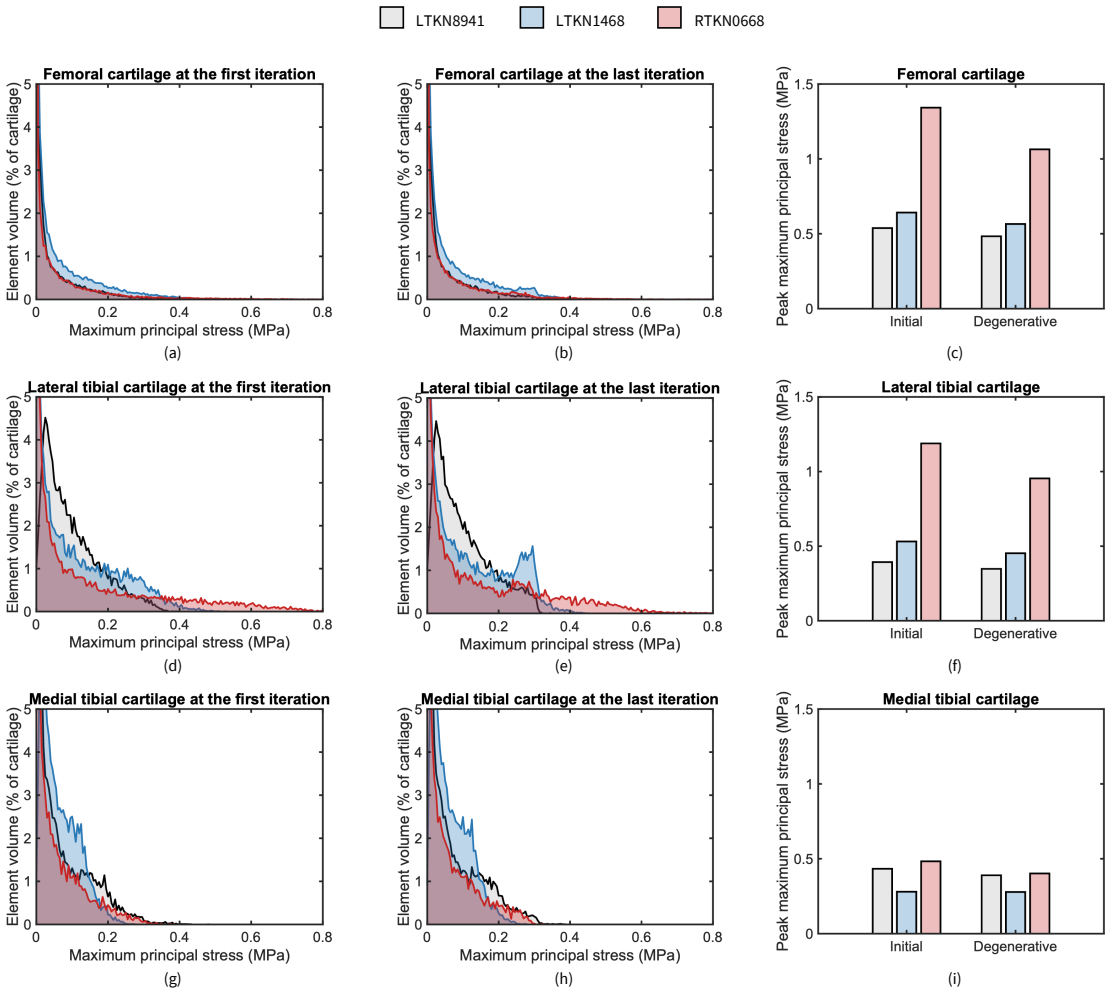

Figure 6.3: *Comparison of variations in maximum principal stress for subject-specific joints during cartilage degeneration. The frequency distributions of maximum principal stress are plotted for (a) - (b) femoral cartilage, (d) - (e) lateral tibial cartilage, (g) - (h) medial tibial cartilage. The corresponding peak values are highlighted in (c), (f) and (i) respectively.*

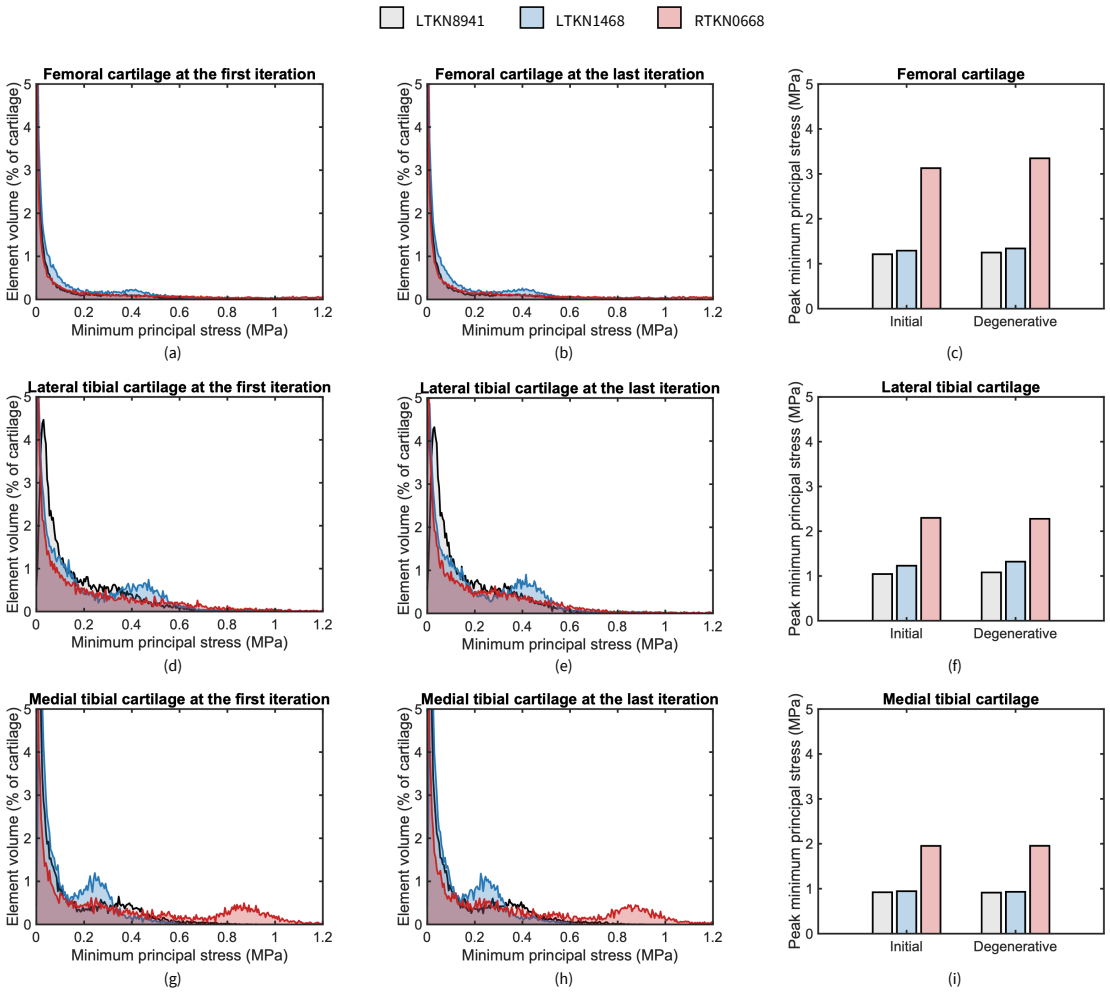

Figure 6.4: *Comparison of variations in minimum principal stress for subject-specific joints during cartilage degeneration. The frequency distributions of minimum principal stress are plotted for (a) - (b) femoral cartilage, (d) - (e) lateral tibial cartilage, (g) - (h) medial tibial cartilage. The corresponding peak values are highlighted in (c), (f) and (i) respectively.*

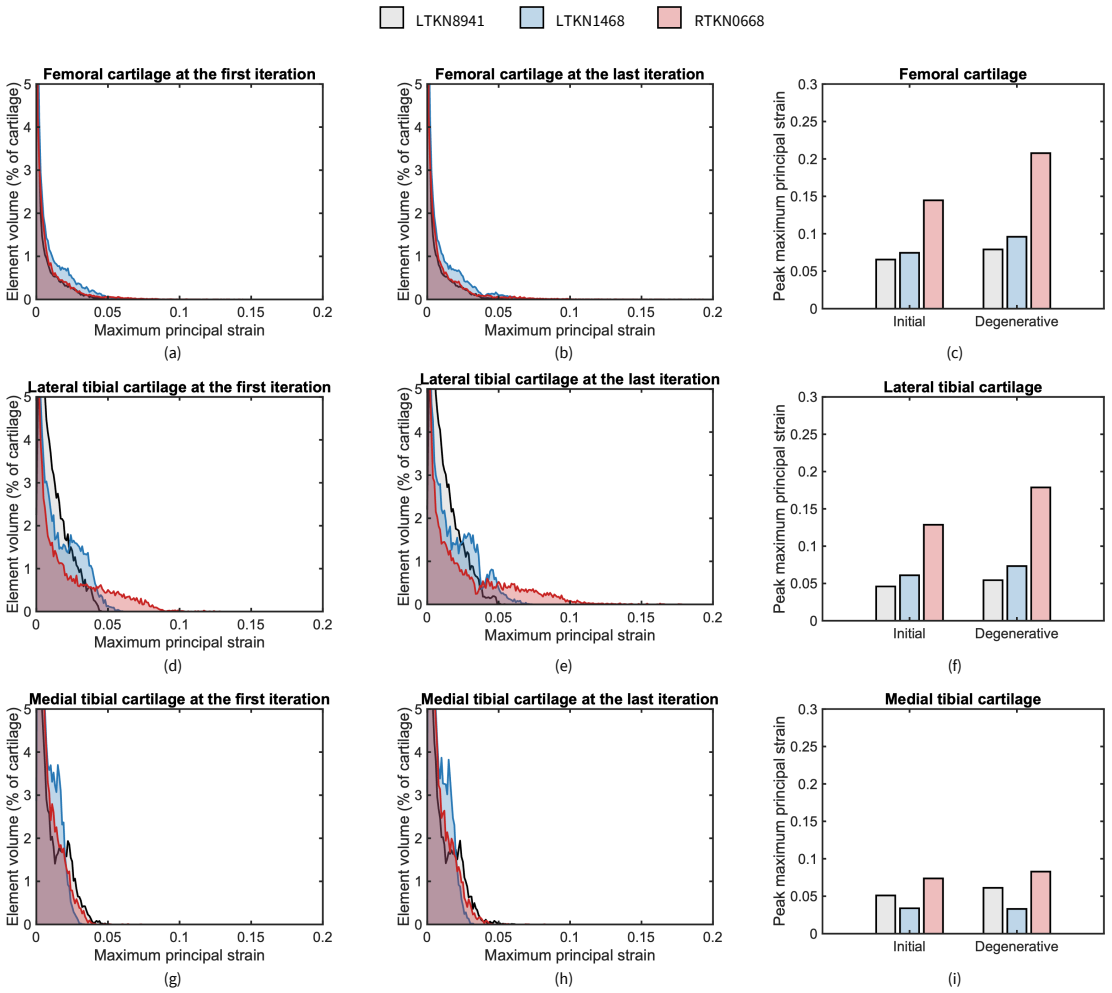

Figure 6.5: *Comparison of variations in maximum principal strain for subject-specific joints during cartilage degeneration. The frequency distributions of maximum principal strain are plotted for (a) - (b) femoral cartilage, (d) - (e) lateral tibial cartilage, (g) - (h) medial tibial cartilage. The corresponding peak values are highlighted in (c), (f) and (i) respectively.*

Table 6.3: *WRMSE quantification of differences between the frequency distributions of maximum principal stress.*

Articular cartilage	$\text{WRMSE}_{BMI^{meas}_{\text{low}-\text{normal}}}$			$\text{WRMSE}_{BMI^{meas}_{\text{low}-\text{high}}}$		
	LTKN8941	LTKN1468	RTKN0668	LTKN8941	LTKN1468	RTKN0668
Femoral cartilage	0.032	0.048	0.024	0.077	0.109	0.054
Lateral tibial cartilage	0.202	0.25	0.083	0.406	0.356	0.165
Medial tibial cartilage	0.164	0.208	0.086	0.378	0.413	0.192

Table 6.4: *WRMSE quantification of differences between the frequency distributions of minimum principal stress.*

Articular cartilage	$\text{WRMSE}_{BMI^{meas}_{\text{low}-\text{normal}}}$			$\text{WRMSE}_{BMI^{meas}_{\text{low}-\text{high}}}$		
	LTKN8941	LTKN1468	RTKN0668	LTKN8941	LTKN1468	RTKN0668
Femoral cartilage	0.016	0.032	0.021	0.034	0.058	0.031
Lateral tibial cartilage	0.09	0.119	0.043	0.191	0.209	0.097
Medial tibial cartilage	0.078	0.107	0.075	0.165	0.205	0.121

of minimum principal stress in Table 6.4. This suggests that the minimum principal stress distribution of LTKN1468 is more sensitive to obesity than LTKN8941 and RTKN0668 in cartilage degeneration, which could also be found in the frequency plots (Figures J.2 - I.2).

6.3.3 Effects of obesity on the cartilage degeneration of three subject-specific knee joints

Figures 6.6 to 6.8 present the IQRs and distributions of degeneration levels in the femoral, lateral tibial and medial tibial cartilage of the three different subjects with varying BMI after five-year simulations, illustrating that obesity increased the overall degeneration level and expanded the degenerated cartilage area. In

the femoral cartilage of LTKN8941, the median degeneration level increased to 25.6% (IQR 22.9%-28.4%) at a high BMI from 23.4% (IQR 12.8%-23.5%) at a low BMI (Figure 6.6a). This trend was consistent in different cartilage compartments of LTKN8941 and likewise appeared in the femoral and lateral tibial cartilage of LTKN1468. Nevertheless, the degeneration in the medial tibial cartilage of LTKN1468 was different in response to the reduction in BMI. The median degeneration level was 22.9% (IQR 22.8%-24.1%) at a high BMI whilst there was no degenerated element at both the low and normal BMI level (Figure 6.8a). Although RTKN0668 exhibited a similar sensitivity of tibial cartilage degeneration to variations in BMI levels, the effect of reducing BMI on the degeneration was different in the femoral cartilage. At a low BMI, the degeneration level of the femoral cartilage was concentrated to 24.5%(IQR 23.3%-28%) in RTKN0668 in contrast to the more dispersed data in both LTKN8941 (IQR 12.8%-23.5%) and LTKN1468 (IQR 1.6%-23.5%). This suggests that reducing BMI might have a limited effect on mitigating degeneration in the femoral cartilage of RTKN0668.

Figures 6.6d, 6.7d and 6.8d showed the largest area with over 20% degeneration at a high BMI compared with the distributions at a low and normal BMI. However, the degeneration distributions resulting from a high BMI differed in the three subject-specific joints. The distribution of cartilage degeneration was more uniform on both lateral and medial sides in the femoral cartilage of LTKN8941. In turn, degeneration was concentrated to the lateral side of the femoral cartilage in the both joints of LTKN1468 and RTKN0668. In RTKN0668, whose femoral cartilage on the lateral side was osteoarthritic before simulations, little degeneration was estimated on the medial side, whereas the healthy joint of LTKN1468 still exhibited small medial regions of degeneration. This subject-specific difference was also observed in the tibial cartilage.

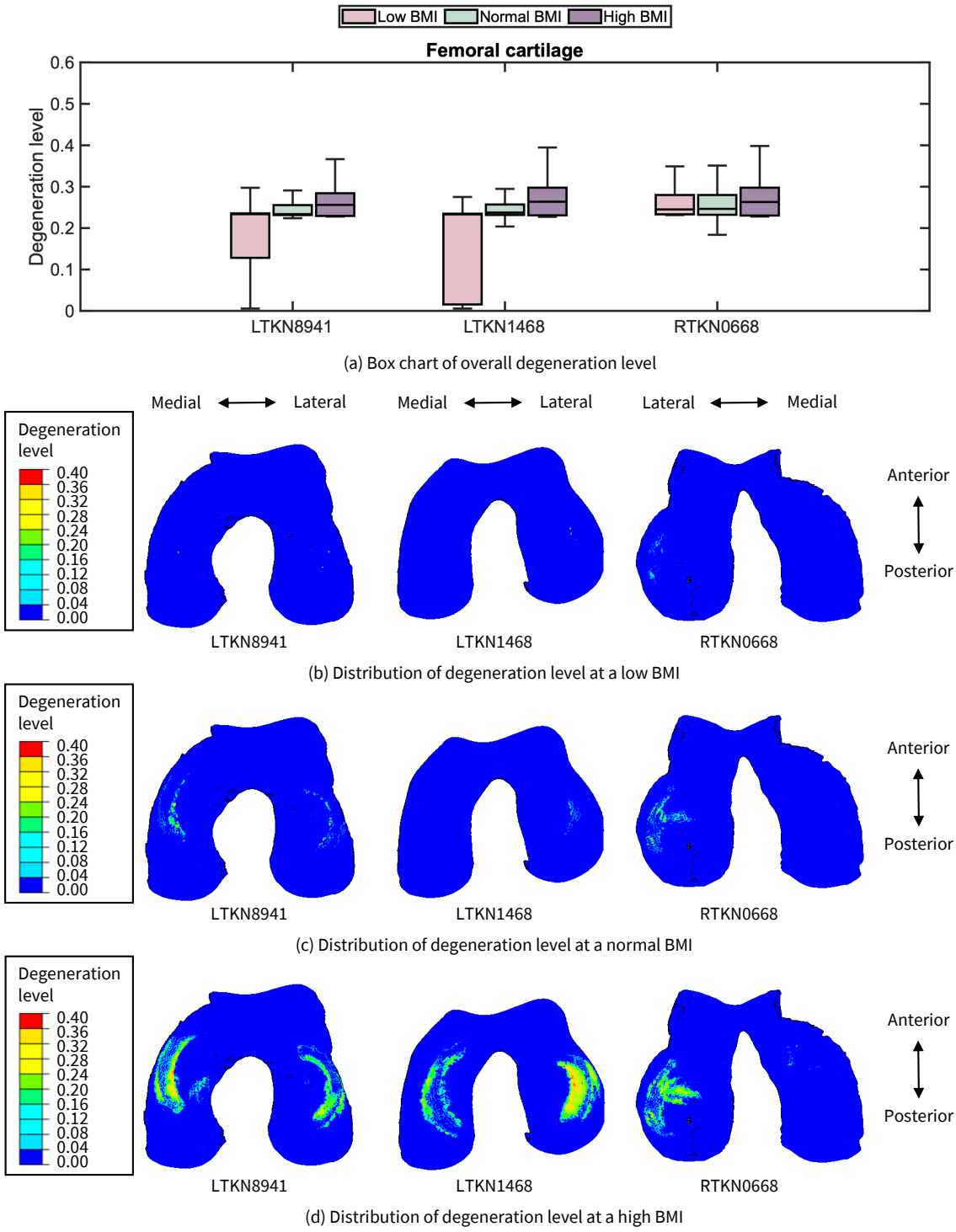

Figure 6.6: *Degeneration of the femoral cartilage in the three subject-specific joints with different BMI levels: (a) Box chart of overall degeneration level, (b) Distribution of degeneration level at a low BMI, (c) Distribution of degeneration level at a normal BMI, (d) Distribution of degeneration level at a high BMI. The median and interquartile range are displayed with whiskers that represent the minimum and maximum degeneration levels.*

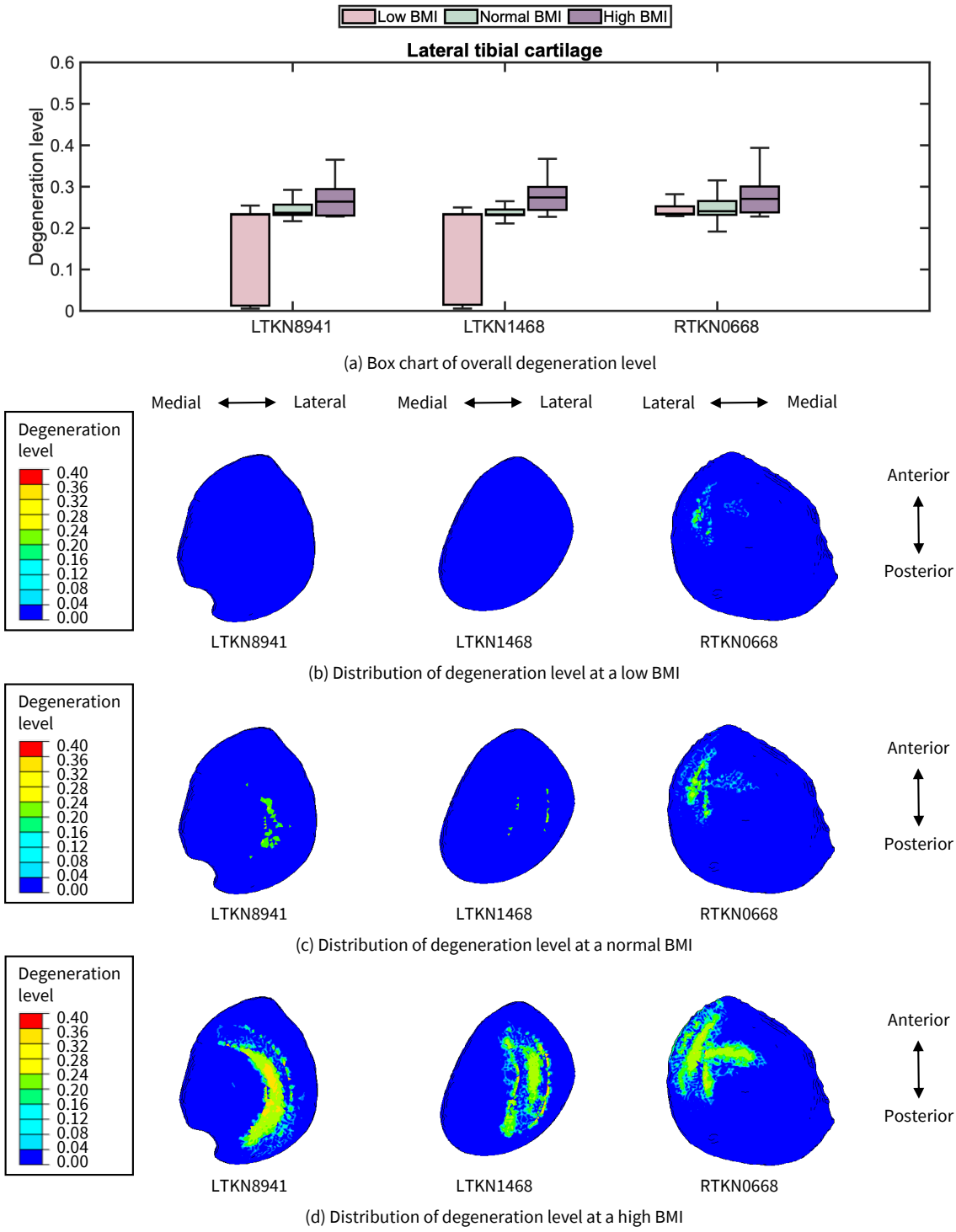

Figure 6.7: *Degeneration of the lateral tibial cartilage in the three subject-specific joints with different BMI levels: (a) Box chart of overall degeneration level, (b) Distribution of degeneration level at a low BMI, (c) Distribution of degeneration level at a normal BMI, (d) Distribution of degeneration level at a high BMI. The median and interquartile range are displayed with whiskers that represent the minimum and maximum degeneration levels.*

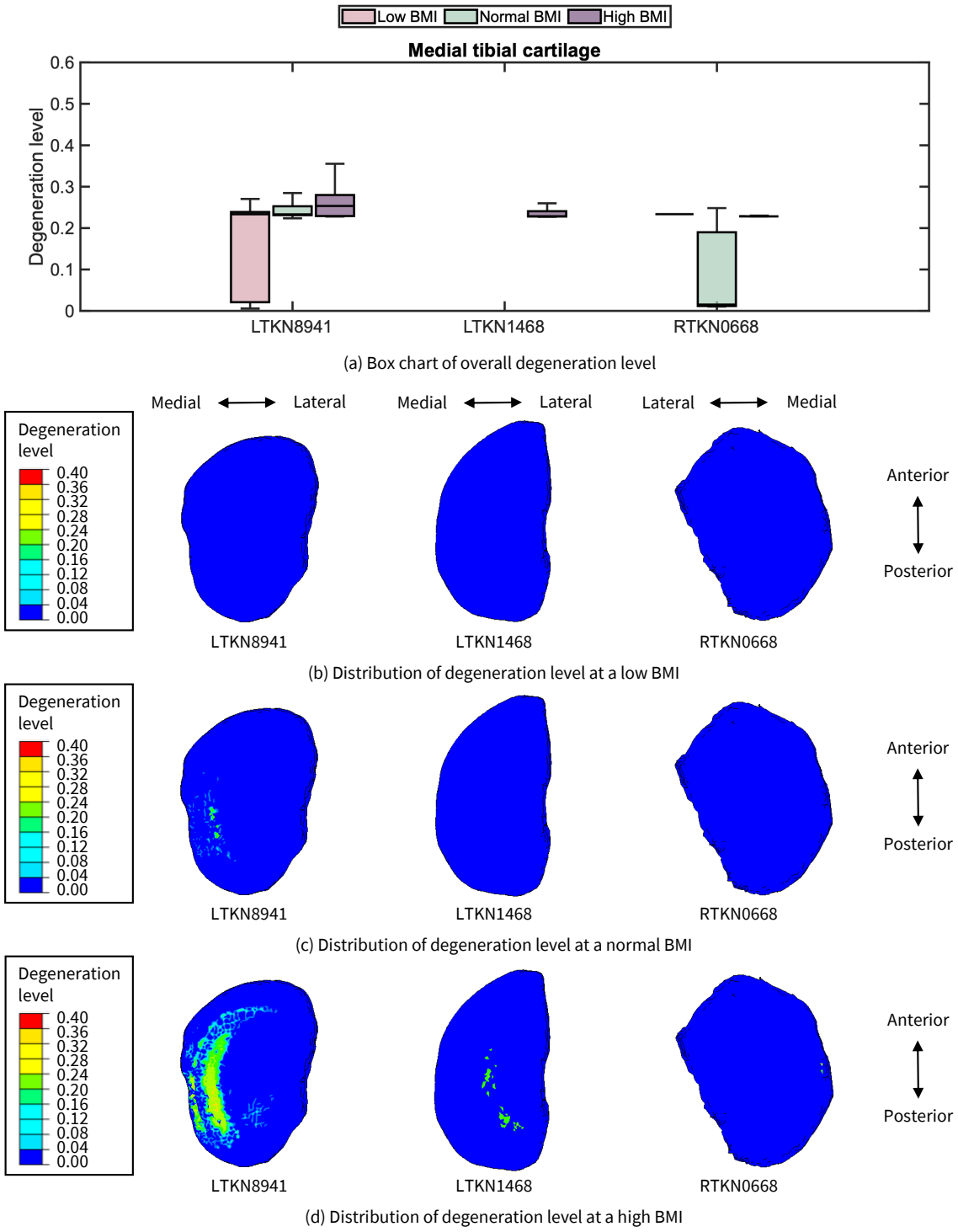

Figure 6.8: *Degeneration of the medial tibial cartilage in the three subject-specific joints with different BMI levels: (a) Box chart of overall degeneration level, (b) Distribution of degeneration level at a low BMI, (c) Distribution of degeneration level at a normal BMI, (d) Distribution of degeneration level at a high BMI. The median and interquartile range are displayed with whiskers that represent the minimum and maximum degeneration levels.*

6.4 Discussion

This research investigated the endotype of obesity-driven cartilage degeneration across three subject-specific knee joints, using a novel integrative multi-scale modelling approach that couples mechanical loading and inflammation. Cartilage degeneration was simulated when varying BMI levels, highlighting a critical role of joint subject specificity in the obesity-associated endotype of OA. A higher BMI could lead to a larger peak compressive stress and tensile stress and strain, which contributed to a higher risk of cartilage degeneration. By comparing the effects of obesity in different subjects, it was found that cartilage degeneration was localised and sensitive to the variations in BMI. In particular, a healthy left knee joint (LTKN8941) showed a relatively uniform degeneration of cartilage on both lateral and medial side, whereas the degeneration was concentrated to the lateral cartilage in the other healthy left knee joint (LTKN1468) and the right osteoarthritic knee joint (RTKN0668). In addition, the IQR of cartilage degeneration levels differed across the three joints, suggesting the subject-specific degeneration levels and distribution in the obesity-associated endotype of OA. This proof-of-concept study provides a computational solution that can enable subject-specific prediction of obesity-related cartilage degeneration and evaluation of obesity-targeted interventions.

As a result of the location-specific degeneration of tissue property, it was observed that the peak maximum principal stress decreased and the corresponding distribution became non-uniform, which in turn led to the larger maximum principal strain. In addition, the changes in the compressive stress were modest in both distribution and the increase of peak value. These biomechanical variations correspond to the degeneration level and reflect the reduction in the resistance of cartilage to tension and compression, which is in line with the reported alterations in the cartilage mechanical characterisations [266]. Compositional changes of cartilage, such as the destruction of the collagen network [285] and loss of proteoglycans [286], progressively disturb the cartilage homeostasis by altering the mechanical environment and inducing inflammation. This overall trend in the degenerative process was similar in different subjects. Although cartilage constituents were not explicitly modelled in this framework, the variation in the integrity of cartilage was simulated based on the inflammatory regulation driven by the accumulative mechanical damage. Hosseini et al. [186] and Elahi et al. [189] implied that degradation in each constituent could be mutually responsive due to mechanical interactions.

Accordingly, overall outcomes of the degradation in different cartilage constituents were reflected by the changes in the poroelasticity of each discrete tissue element. Due to the limited data of the specific relationships between obesity and changes in cartilage constituents during inflammation, this simplification allows the study to focus on the subject-specific cartilage degeneration driven by obesity-related mechanical overloading and inflammation.

When comparing the three subjects, the osteoarthritic joint (RTKN0668) showed the highest peak stress and strain due to a high BMI, indicating a higher risk of cartilage degeneration due to overloading. This aligns with previous biomechanical studies on the effect of body weight during cartilage degeneration [166–168]. However, the peak stress on medial tibial cartilage was smaller in LTKN1468 at a normal BMI compared with LTKN8941 at a low BMI. This indicates that the mechanical effect of obesity may not be linear and it is dependent on subject specificities of the joint, such as cartilage geometry [277] and joint alignment [47]. Similarly, Orozco et al. [168] highlighted a more important role of joint subject-specific geometry in predicting cartilage degeneration compared to individualised gait pattern. Furthermore, it was found that the sensitivity of obesity-related biomechanical variations differed in the three subject-specific joints. The cartilage of LTKN1468 demonstrated the highest sensitivity of minimum principal stress distribution to BMI, and the sensitivity of maximum principal stress was similarly higher in both LTKN8941 and LTKN1468 compared with RTKN0668. This illustrates the heterogeneity of cartilage degeneration pathways in response to mechanical overloading among individual subjects. The heterogeneity may be the long-term morphological outcome of the cartilage mechanoadaptation [268, 287]. However, it is challenging to include the evolutionary changes in the cartilage morphology due to the complex dynamic interplay of mechanical and inflammatory factors [185]. At present, subject specificities of the knee joint are generally the input information for simulating OA [46]. The effectiveness of different degeneration algorithms relies on the granularity of subject-specific information and the associated degeneration pathways interact with one another [182, 189]. Thus, this study emphasises that the subject-specific biomechanical responses resulting from obesity may be responsible for the difference in the susceptibility to various degeneration pathways.

The degeneration level and distribution at different BMI levels were also associated with joint subject specificities. Under the regulations of mechanical loading and inflammation, the degeneration was mainly concentrated to the lateral side

of the cartilage in both LTKN1468 and RTKN0668. Although it was reported that a higher risk of OA was found in the medial side of the joint [162], Klets et al. [166] demonstrated an exceptional case where obesity significantly increased the degenerative volume of the lateral tibial cartilage in a 4-year follow-up prediction. Due to the limited data, this conflict could be explained by joint subject specificities and the difference in degeneration pathways. When considering the mechanobiological effects of obesity, the results of this study showed that obesity primarily augmented cartilage degeneration on both sides for LTKN8941 and on the lateral side for LTKN1468 and RTKN0668. This increased cartilage degeneration resulting from obesity is consistent with prior findings by Klets et al. [166]. Specifically, the degeneration level and distribution of the tibial cartilage were associated with the femoral cartilage in the three subjects, which is also in line with a previous prospective study [288]. It should be noted that the decrease in BMI reduced the degeneration area significantly in all the three subjects, however, this reduction was limited in the degeneration level for RTKN0668. Due to observable structural changes in the lateral tibial cartilage, the biomechanical responses of RTKN0668 were different to the healthy joints. This resulted in a relatively higher stress concentrated to a small cartilage region so that the mechanical damage increased to prompt the obesity-associated inflammation. Therefore, the joint of RTKN0668 is more susceptible to a higher level of cartilage degeneration in spite of the decrease in BMI, compared with the healthy joints.

Similar to previous computational analyses [166–168], this study further emphasises the important role of joint subject-specific geometry in simulating cartilage degeneration by incorporating the obesity-associated regulations of both mechanical damage and inflammation. Nevertheless, the subject specificity mainly refers to the joint anatomical characteristics due to the limited data [249] in this research. Initial conditions of material property and inflammation baseline were generic across subjects. Subject-specific calibration could contribute to more accurate predictions in cartilage degeneration. Since the purpose of this study was to evaluate the obesity-associated degeneration pathway of cartilage in subject-specific joints, this simplification on the initial conditions could ensure comparability. Namely, the impact of varying BMI was examined when including the anatomical initial conditions across subject-specific joints. The anatomical initial conditions reflect the long-term outcome of complex mechanobiological interactions [250, 251] within each subject. In addition, the inclusion of subject-specific gait data could improve the

prediction in the location-specific cartilage damage, since gait pattern varies biomechanical responses in different individuals [163, 174]. Combining subject-specific mechanochemical data, this framework can be tuned to predict and quantify the effect of obesity on cartilage degeneration in the future. The statistical analysis of a larger cohort will be needed to validate the obesity-related degeneration pathway and to optimise the intervention of reducing BMI for the subject-specific treatment of OA.

6.5 Conclusion

This computational study evaluated the subject-specific cartilage degeneration patterns dependent on BMI levels. For the first time, the multi-scale modelling framework, which integrates obesity-associated mechanical overloading and inflammation, was implemented for simulating cartilage degeneration across three subject-specific knee joints. All the three subjects showed a similar reduction in the tissue resistance to tension and compression. Whilst the femoral cartilage experienced the highest peak tensile and compressive stresses, the stress distribution of the tibial cartilage was more sensitive to variations in BMI. Compared with the more uniform cartilage degeneration in LTKN8941 at a high level of BMI, degeneration was concentrated mostly to the medial side of cartilage in both LTKN1468 and RTKN0668. Although managing obesity could significantly reduce the degeneration area, the degeneration level remained high in the OA joint as BMI decreased. This indicates the irreversible characteristic of degeneration in OA stage, with obesity further contributing to higher degeneration levels. These findings suggest the effect of BMI reduction is individualised during the degeneration of cartilage driven by both mechanical damage and inflammation, highlighting the significance of joint subject specificity in obesity-related OA endotypes. With further subject-specific data, this framework has the potential to identify therapeutic targets for obesity-associated cartilage degeneration and enable optimisation of tailored interventions.

Appendix I: Sensitivity analysis of material properties for the knee joints (LTKN1468 and RTKN0668)

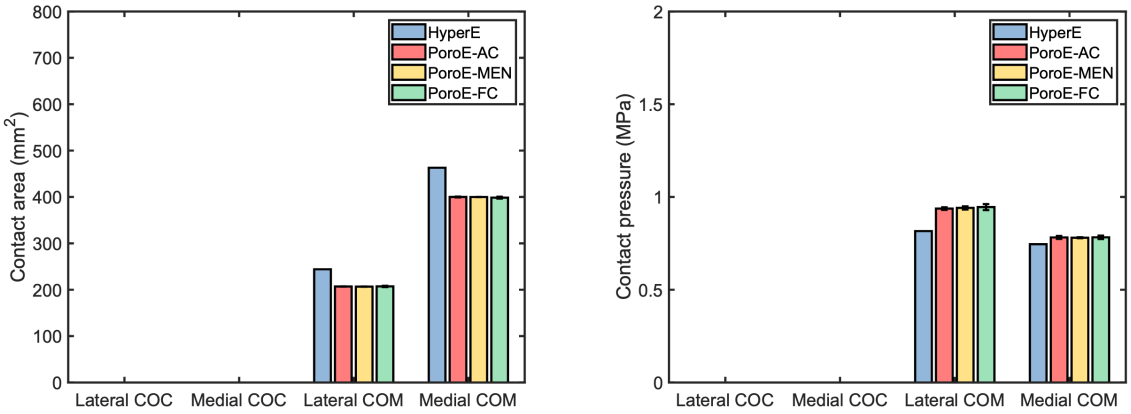

Model cohort	Articular cartilage	Meniscus	Contact friction coefficient
PoroE-AC	[25%, 175%] of baseline properties	Baseline	Baseline
PoroE-MEN	Baseline	[25%, 175%] of baseline properties	Baseline
PoroE-FC	Baseline	Baseline	[25%, 175%] of baseline properties
HyperE	Neo-hookean: C_{10} = 1.0274 D_1 = 0.08	$E_1 = E_2$ = 6 MPa; E_3 = 21 MPa; $\nu_{in\text{-}plane}$ = 0.3; $\nu_{out\text{-}plane}$ = 0.2; $G_{out\text{-}plane}$ = 8.08 MPa	$F_{CART\text{-}CART}$ = 0.1 $F_{CART\text{-}MEN}$ = 0.15

Figure I.1: *The sensitivity analysis of the material properties for the knee joint (LTKN1468).*

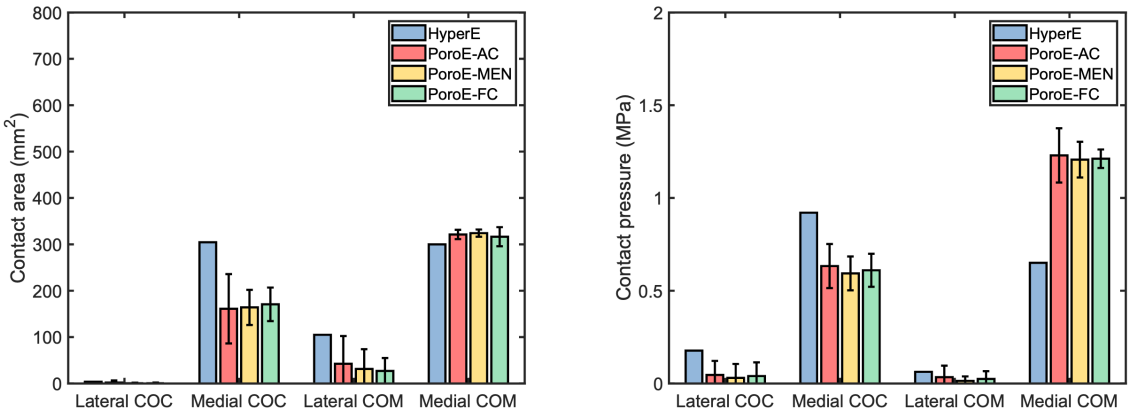

Model cohort	Articular cartilage	Meniscus	Contact friction coefficient
PoroE-AC	[25%, 175%] of baseline properties	Baseline	Baseline
PoroE-MEN	Baseline	[25%, 175%] of baseline properties	Baseline
PoroE-FC	Baseline	Baseline	[25%, 175%] of baseline properties
HyperE	Neo-hookean: C_{10} = 1.0274 D_1 = 0.08	$E_1 = E_2$ = 6 MPa; E_3 = 21 MPa; $\nu_{in\text{-}plane}$ = 0.3; $\nu_{out\text{-}plane}$ = 0.2; $G_{out\text{-}plane}$ = 8.08 MPa	$F_{CART\text{-}CART}$ = 0.1 $F_{CART\text{-}MEN}$ = 0.15

Figure I.2: *The sensitivity analysis of the material properties for the knee joint (RTKN0668).*

Appendix J: Simulations of biomechanical responses in cartilage degeneration

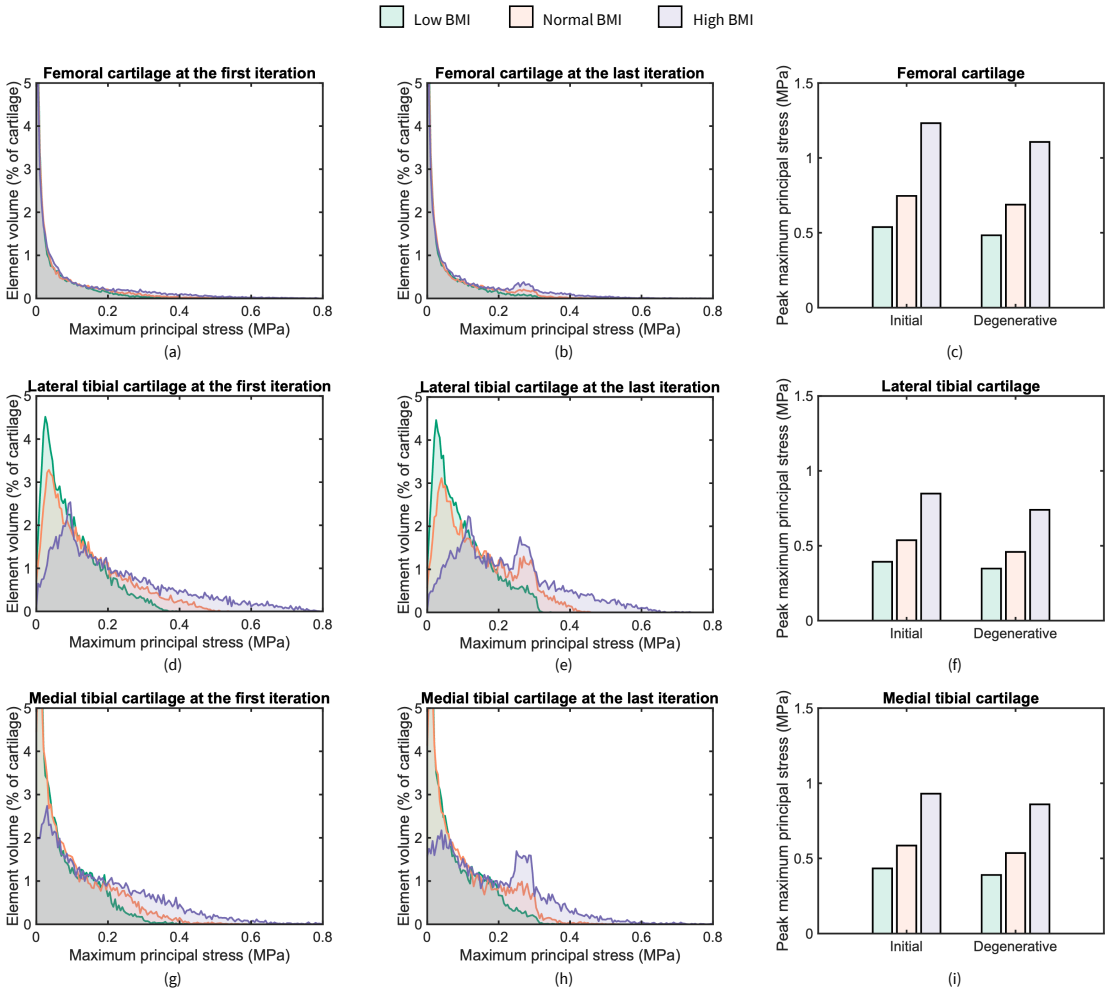

Figure J.1: *Comparison of variations in maximum principal stress for LTKN8941 across different BMI levels during cartilage degeneration. The frequency distributions of maximum principal strain are plotted for (a) - (b) femoral cartilage, (d) - (e) lateral tibial cartilage, (g) - (h) medial tibial cartilage. The corresponding peak values are highlighted in (c), (f) and (i) respectively.*

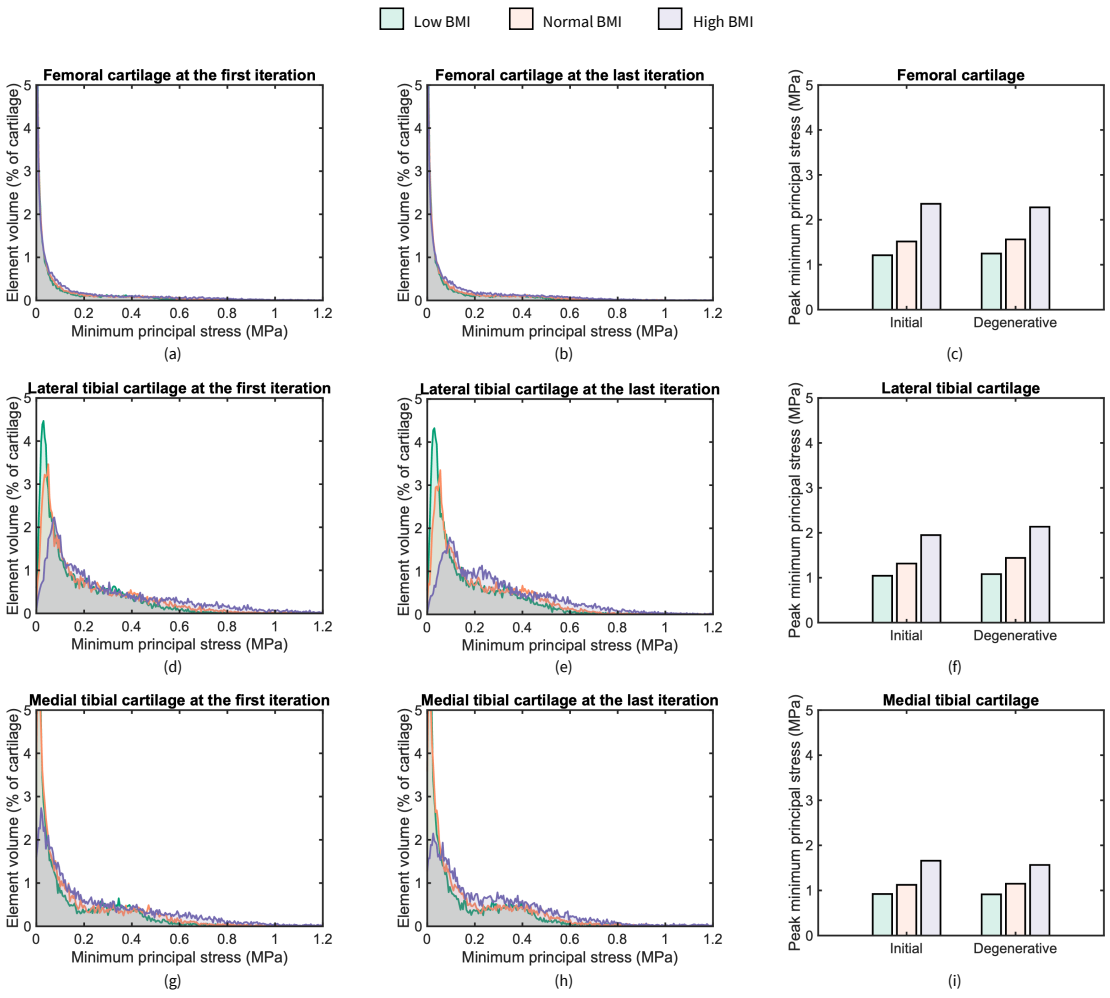

Figure J.2: *Comparison of variations in minimum principal stress for LTKN8941 across different BMI levels during cartilage degeneration. The frequency distributions of maximum principal strain are plotted for (a) - (b) femoral cartilage, (d) - (e) lateral tibial cartilage, (g) - (h) medial tibial cartilage. The corresponding peak values are highlighted in (c), (f) and (i) respectively.*

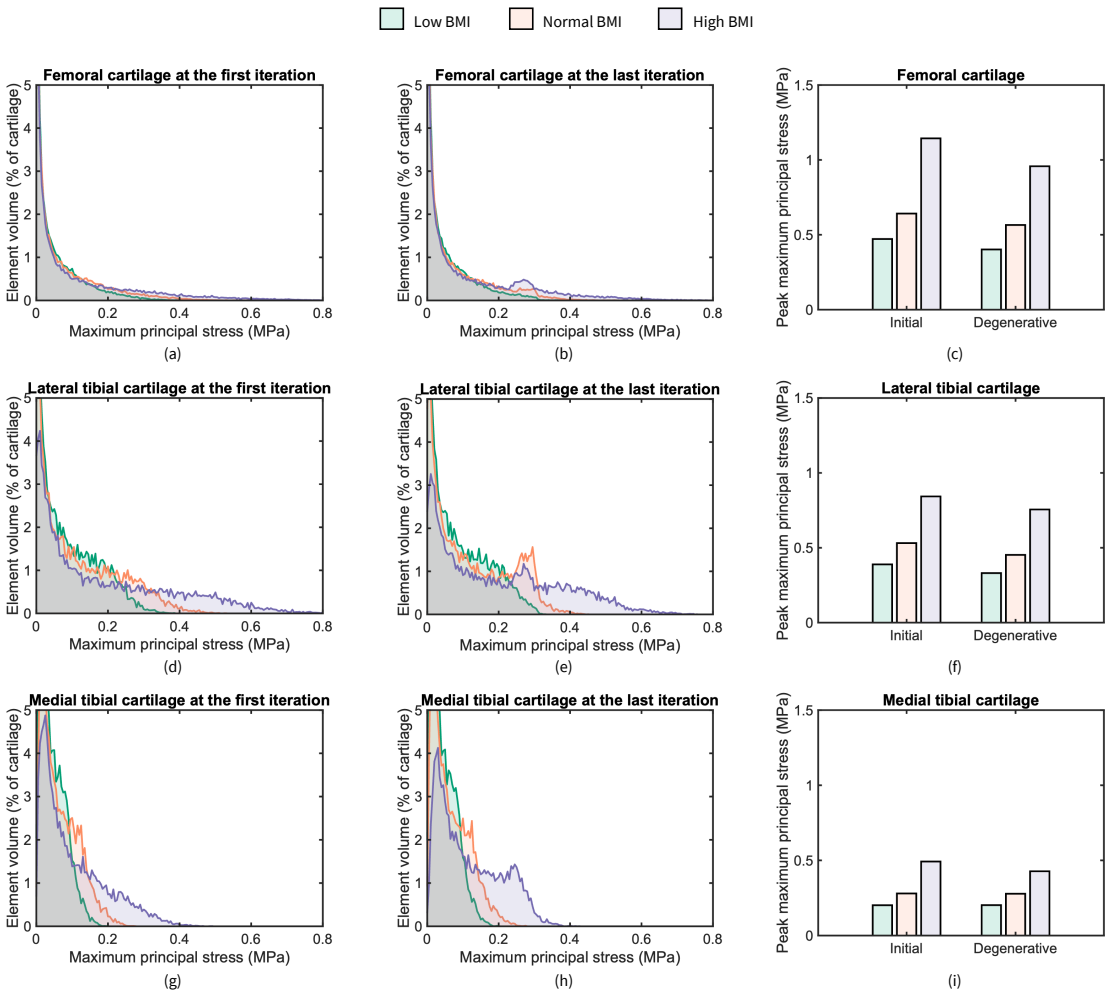

Figure J.3: *Comparison of variations in maximum principal stress for LTKN1468 across different BMI levels during cartilage degeneration. The frequency distributions of maximum principal strain are plotted for (a) - (b) femoral cartilage, (d) - (e) lateral tibial cartilage, (g) - (h) medial tibial cartilage. The corresponding peak values are highlighted in (c), (f) and (i) respectively.*

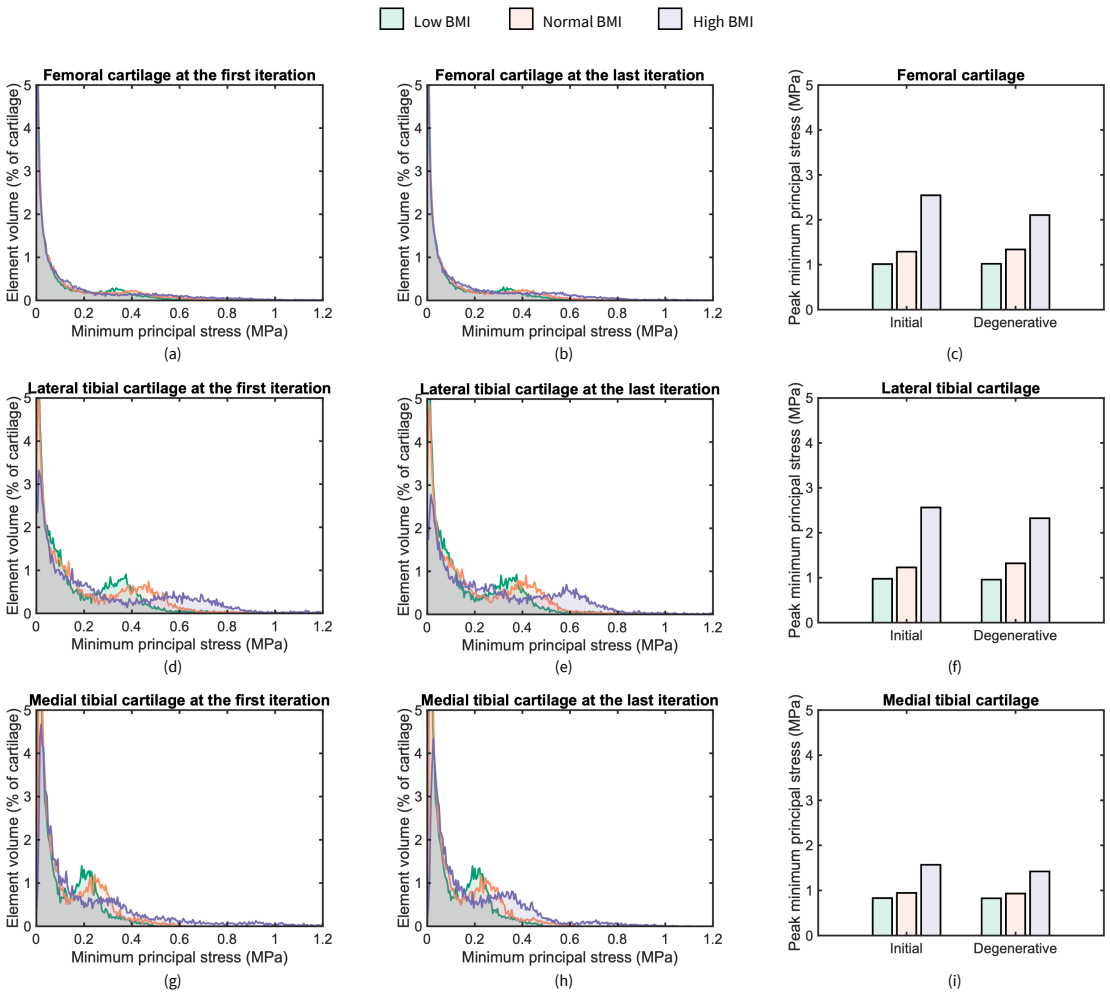

Figure J.4: *Comparison of variations in minimum principal stress for LTKN1468 across different BMI levels during cartilage degeneration. The frequency distributions of maximum principal strain are plotted for (a) - (b) femoral cartilage, (d) - (e) lateral tibial cartilage, (g) - (h) medial tibial cartilage. The corresponding peak values are highlighted in (c), (f) and (i) respectively.*

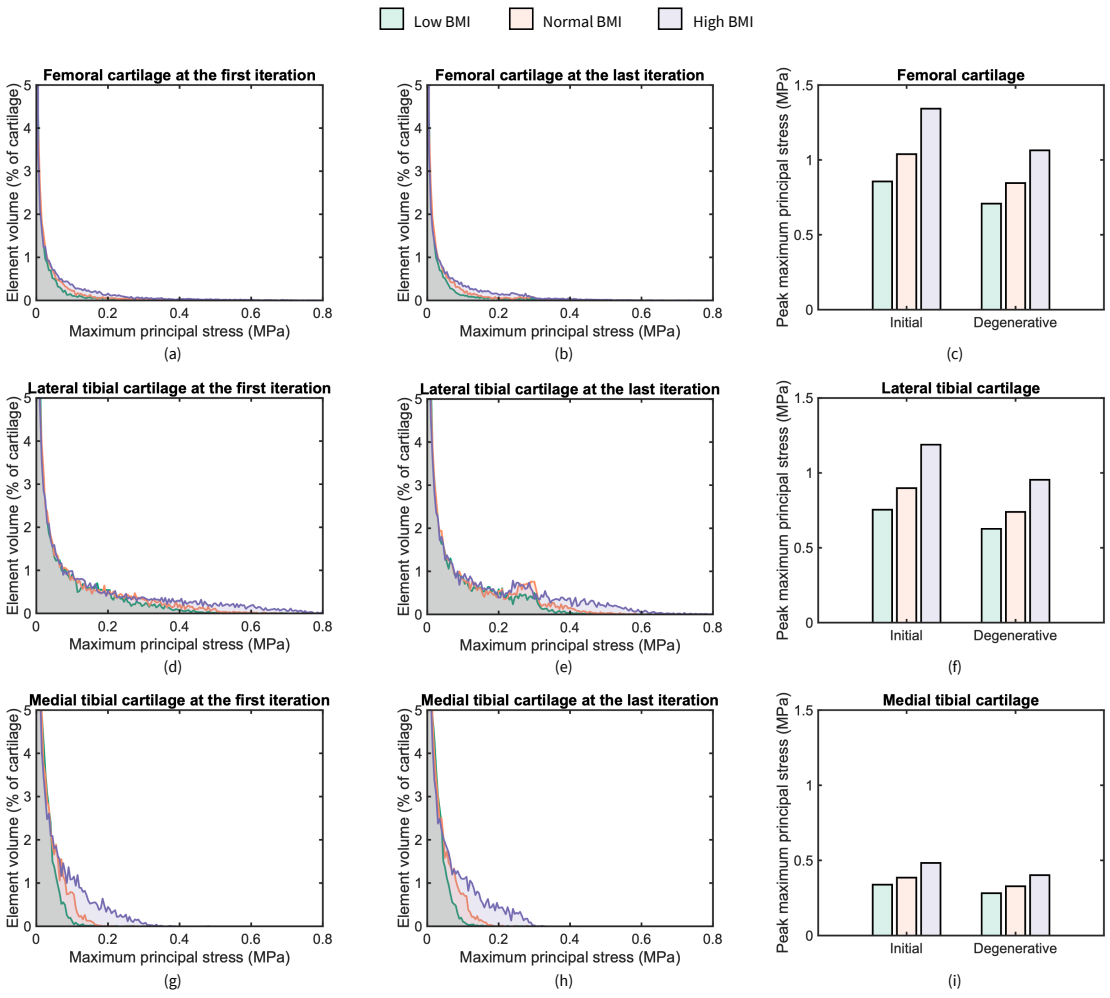

Figure J.5: *Comparison of variations in maximum principal stress for RTKN0668 across different BMI levels during cartilage degeneration. The frequency distributions of maximum principal strain are plotted for (a) - (b) femoral cartilage, (d) - (e) lateral tibial cartilage, (g) - (h) medial tibial cartilage. The corresponding peak values are highlighted in (c), (f) and (i) respectively.*

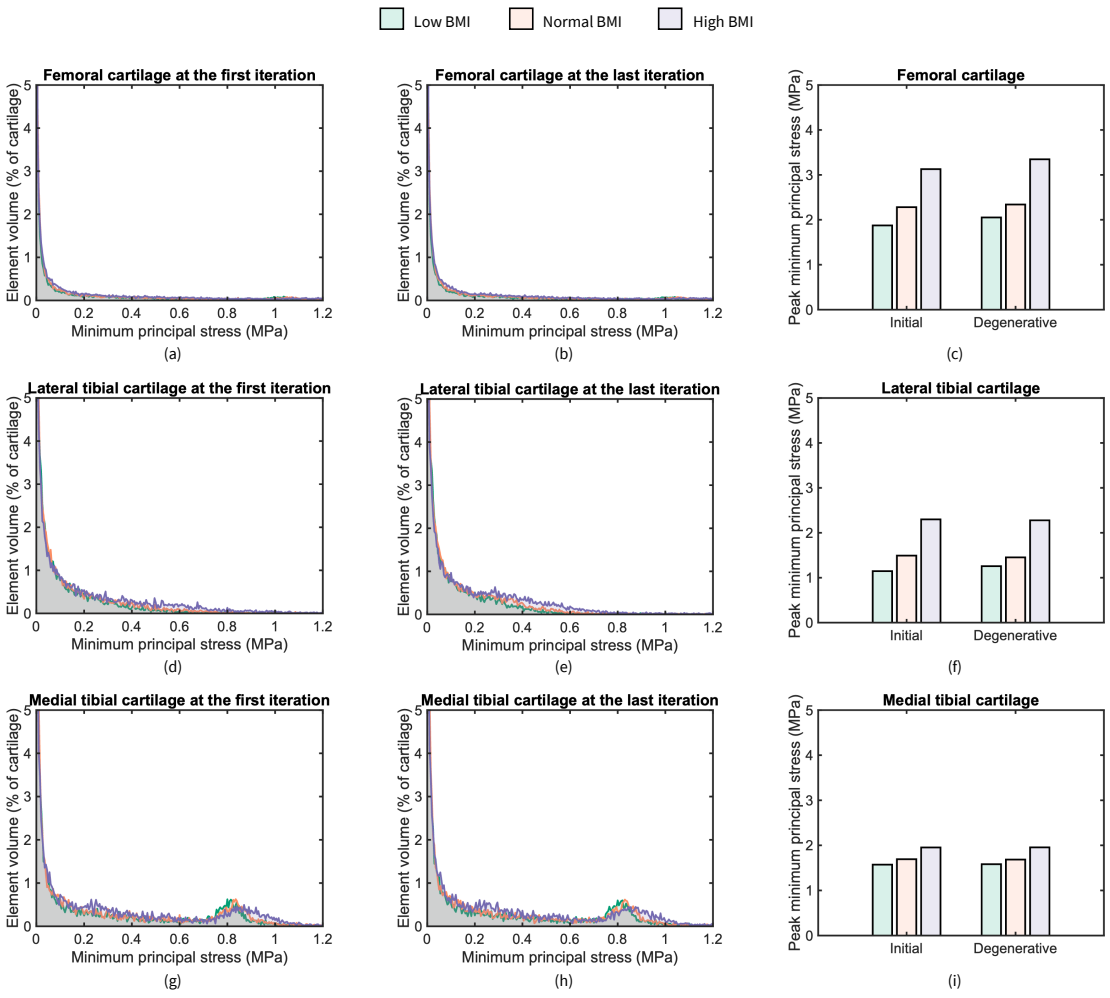

Figure J.6: *Comparison of variations in minimum principal stress for RTKN0668 across different BMI levels during cartilage degeneration. The frequency distributions of maximum principal strain are plotted for (a) - (b) femoral cartilage, (d) - (e) lateral tibial cartilage, (g) - (h) medial tibial cartilage. The corresponding peak values are highlighted in (c), (f) and (i) respectively.*

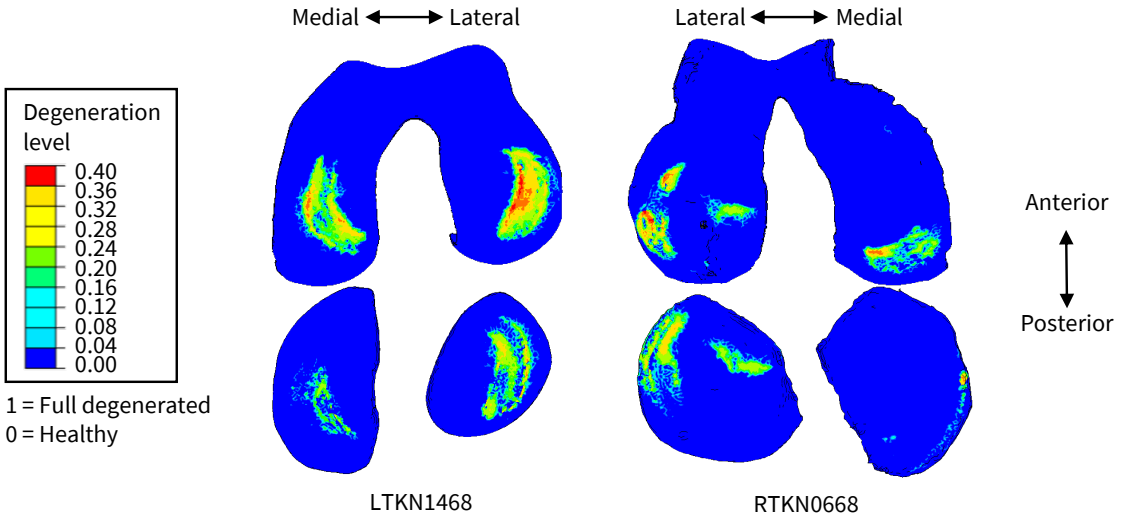

Figure J.7: *Cartilage degeneration level and distribution in LTKN1468 and RTKN0668 after five-year simulations when a flexion of 10° was applied with an axial force of 1058N.*

Chapter 7

Discussion and conclusions

This chapter summarises the primary contributions of this thesis on developing a novel multi-scale computational approach that integrates obesity-associated inflammation and mechanics in osteoarthritis (OA). The development of this multi-scale approach is based on the present consensus and assumptions on the association between obesity and OA, aiming to advance the study of the endotypes in obesity-related OA and provide a mechanistic basis for understanding subject-specific cartilage degeneration in OA. The broader significance of the research in this thesis is discussed alongside the primary contributions. Limitations and future work are evaluated in relation to the research scope of this thesis. Main outcomes from Chapter 3 to Chapter 6 are crystallised into the conclusion of this thesis.

7.1 General discussion

The current understanding of OA increasingly frames it as a systemic disease with inflammatory, metabolic and mechanical regulations across the entire body. Thus, identifying and understanding specific endotypes are urgent to develop effective and precise therapeutic solutions according to the stratification of OA phenotypes. Limited by the spatial and temporal complexity of OA progression, it is challenging to quantify the isolated pathomechanism of different endotypes in OA. Particularly, individuals may follow multiple pathomechanistic pathways resulting in the same symptoms or structural manifestations of OA, and it is extremely difficult to identify these involving pathways at an early stage. This thesis focuses on the obesity-associated endotypes of OA, and it provides novel insights and computational tools to advance the understanding of obesity-associated OA, accelerate treatment development, and facilitate the establishment of virtual human twins for OA prediction and intervention.

The development of a multi-scale computational approach that integrates obesity-related inflammation and mechanical loading is the main goal of this thesis. The model developed in Chapter 3 is the first inflammation model of OA that describes the regulations of adipokines. In this mathematical model, body mass index (BMI), physical activity level (PAL) and nutrition were for the first time introduced as three main adiposity factors in the OA inflammatory regulation network. These adiposity factors were simplified to three parameters for the representation of adipokine level. Since there are no conclusive findings to interpret the precise relations of BMI, PAL, nutrition and adipokine level, this mathematical model focused on the qualitative relationship between adiposity factors and the production of adipokines rather than extensive time-dependent interactions. Namely, the three adiposity factors (BMI, PAL and nutrition) were introduced to govern the production of adipokines, reflecting the level of adiposity. Although the existing conflicts on the roles of adiponectin and leptin [89, 99] limited the investigation on their specific impacts, the emphasis of this model was on the pro-inflammatory effects of adipokines as a mediator group. In this model, each inflammatory mediator was simplified as a representative group and adipokines were modelled as the inflammatory stimulus due to excessive adipose tissue. It should be noted that increased fat deposition is a typical feature of obesity [39]. Since adipose tissue is present across the entire human body and contributes to human physiological activities [41], it is difficult to measure the complex interactions of systemic and local adipose tissue in OA pathology. Collins et al. [42] suggested that abnormal amount of adipose tissue might activate signalling pathways of adipokines to stimulate chronic inflammation systemically and affect the regulation of OA inflammation in the local joint. In addition, the biological roles of infrapatellar fat pad (IFP) in OA development, a type of local adipose tissue in the joint, have been recently demonstrated [55]. However, the exact mechanisms still remain unclear. The model in Chapter 3 is extensible to explore the multi-scale effects of obesity on OA inflammation, which can in turn aid the experimental design for unravelling obesity-associated regulating mechanisms in OA onset and development.

Due to the limited availability of data and understanding of systemic signalling pathways, it is infeasible to fully validate the mathematical model of adipokine-mediated OA inflammation, and the model was non-dimensionalised to explore the inflammation dynamics as the primary aim of Chapter 3. The development of this model was based on established knowledge from previous studies. With appropriate parameterisation, this model could be used to optimise adiposity-related

therapies or intervention strategies across the time domain. Accordingly, based on the findings on the inflammation dynamics in Chapter 3, the mathematical model was parameterised according to the decay life of each mediator group in Chapter 4 to investigate the sensitivity of adiposity factors in a dimensional parameter space. Through time-dependent simulations, Chapter 4 demonstrates the effectiveness of different physical activity intervention strategies in OA inflammation. This computational study provides simplified solutions on obesity-associated OA inflammation by modulating BMI and PAL according to the level of mechanical damage. The sensitivity of adiposity factors analysed in Chapter 4 emphasises the urgent need for the optimisation of exercise therapy by identifying obesity-driven and injury-induced OA inflammation. In fact, the present guidelines of physical activity therapies are not unified and the multi-scale effect of different activity types, intensities and frequencies remains unclear [236]. In the computational modelling of OA, the form of physical activity is commonly the mechanical loading translated to the joint-tissue level from measurable gait data. The complex multi-scale regulations of exercise, including the long-term regulation to adiposity [230] and acute reaction [229], are not incorporated. For instance, obesity-induced insulin resistance and disruptions in lipid metabolism may contribute to activating cartilage inflammation and the increase in the risk of OA through specialised biochemical responses [289]. As the first computational model of obesity-associated inflammation in OA, the complex exercise-induced mechanobiological interactions were simplified in this thesis. The regulations of the inflammatory responses were modelled through minimally essential parameters in the scope of studying the obesity-related inflammation. The mechanistic model developed and parameterised in Chapters 3 and 4 can bridge the multi-scale effects of obesity, providing a foundation for further development of computational approaches to simulate the onset and progression of obesity-associated OA.

The heterogeneity of OA pathomechanisms and the slow disease progression poses challenges for its diagnosis, prognosis, and treatment. Computational approaches can advance the investigation on different endotypes of OA by modelling mechanobiological regulations and measurable tissue constituents when longitudinal data is lacking. Mainstream modelling approaches are discussed in Chapter 2, where multi-scale modelling approaches are highlighted for simulating the heterogenous pathology of OA. Based on the works presented in Chapter 3 and Chapter 4, a novel multi-scale modelling framework that integrates obesity-associated inflammation and mechanical loading in OA was proposed in Chapter 5. This is the

first multi-scale modelling framework revealing the obesity-driven mechanism of cartilage degeneration in OA. The multi-scale effects of obesity were translated to inflammatory and biomechanical responses, showing the critical role of obesity in regulating the degenerative process prior to structural changes of cartilage in knee OA. Despite challenges in the full validation of this framework, a good validity was shown in Chapter 5 by comparing with previous computational models. Thus, this integrative computational approach provides novel insights on identifying the endotypes of obesity-associated OA. In order to characterise the underlying mechanisms of systemic and local mechanobiological communication, emerging computational models [127, 129, 182, 185] attempt to quantify the relative contributions of different cartilage degenerative pathway in OA. Integrating identified critical pathways of cartilage degeneration in a computational framework can accelerate the effective translation between preclinical results and clinical outcomes. Chapter 5 is thereby an important cornerstone of destructing obesity-driven cartilage degeneration, and the computational framework can be extended to explore the interactive responses of distinct endotypes across multiple scales.

Since a computational model is constructed based on a variety of parameters with physiological meanings, parameter estimation and calibration determine the simulation accuracy. General population data could be used to uncover mechanisms underlying different OA phenotypes within the framework presented in Chapter 5. However, subject specificities are important for translating computational insights into individualised treatments and predictions of OA. For instance, a large variability is shown in joint geometry [276] and tissue properties [154, 250, 266] in cartilage degeneration, which could constrain the performance of computational models in predicting OA. Within the research scope of obesity-associated OA, this thesis also highlights the critical parameters in simulating OA inflammation and cartilage degeneration through parameter sensitivity analysis. In addition, Chapter 6 stresses the significant difference in cartilage degeneration of subject-specific joints. The anatomical characteristics of the knee joint play a critical role in simulating cartilage degeneration and the effect of obesity. The works presented in Chapter 6 constitute the first subject-specific study of cartilage degeneration driven by both obesity-related inflammation and mechanical loading, which further highlights the significance of incorporating subject-specific information when predicting cartilage degeneration.

Overall, this thesis represents a fundamental component of the broader effort to understand the highly complex and interconnected pathological mechanisms of

OA, with a particular focus on the computational modelling of obesity-associated pathways in cartilage degeneration. The development of mechanistic computational models can reflect complex interactions of tissue biomechanics and inflammatory activities. The models established in this thesis demonstrate potential for OA endotype investigation, OA risk assessment, treatment optimisation, and cartilage degeneration prediction in the context of obesity. This mechanistic integrative computational approach is an important step towards the construction of personalised joint digital twins. A personalised joint digital twin requires quantifiable and measurable parameters that can represent its physiological activities. At present, the understanding of OA pathomechanisms remains unclear as it is a systemic disease. This thesis can also contribute to identifying critical parameters that should be targeted in experimental measurements, ultimately augmenting the parameter database for the joint digital twin. Although data-driven approaches have shown promise in identifying candidate targets and enabling early risk prediction of OA, their reliance on statistical associations limits their capacity to explain causal mechanistic interactions. Given that, this thesis offers a mechanistically modelling foundation upon which data-driven methods may be integrated to support patient stratification, early risk assessment, treatment personalisation and the development of robust digital twins of joints for the prediction of OA.

7.2 Limitations and future work

While the multi-scale computational modelling framework of cartilage degeneration offers novel insights in the context of obesity, a few limitations should be acknowledged. As the first computational approach developed in Chapter 5, which integrates obesity-associated inflammatory regulations formulated and parameterised in Chapters 3 and 4, signalling pathways were simplified to the interactions of five representative subsets of critical inflammatory mediators: Pro- and anti-inflammatory cytokines (PICs and AICs), matrix metalloproteinases (MMPs), adipokines, and fibronectin fragments (Fn-fs). This simplification described in Chapters 3 and 4 provides a reduced-order representation of the complex biochemical networks according to the general roles of mediators. However, different mediators in the same group may not have identical signalling pathways and half-lives in the obesity-associated inflammation and cartilage degeneration [127, 140]. In addition, the interactive systemic and local effects of obesity, gender differences and ageing were not classified due to the limited available data. The biological

fidelity is accordingly limited in the both inflammation model and multi-scale framework, and the computational models in this thesis capture dominant trends of inflammation and cartilage degeneration resulting from obesity rather than the full spectrum of molecular interactions and underlying tissue structural changes. Future work can extend the framework to incorporate additional pathways or specific cellular responses in microenvironment of cartilage, enabling mechanistic exploration of the interplay between distinct OA endotypes. In particular, defining the source of adipose tissue and corresponding signalling pathways can contribute to the integration of systemic and local metabolic and biomechanical regulatory mechanisms. For instance, the level of adiposity in Chapters 3 and 4 is indicated by BMI, which could be parameterised using different measures of adiposity to simulate systemic or local contributions due to adipokines in OA inflammation. However, this requires reliable data mapping between adipokine levels and adiposity measures.

The aforementioned simplification of inflammatory mediators also limits the parameterisation of the models at time scale. Despite variability in the same mediator group, the time scale was determined based on estimated species decay rates in the inflammation model, as presented in Chapter 4. Moreover, the coupling of inflammation and mechanical damage was implemented using an estimated interval of one month for tissue property evolution in Chapter 5, which approximates the slower tissue turnover relative to inflammatory signalling. While this simplification enables computational tractability in simulating cartilage degeneration, it remains an approximation, as interactions among the degradation of different tissue compositions [186, 189] at intermediate time scales may not be fully captured. The differences in the degeneration pathways of tissue constituents may constitute critical therapeutic targets for OA intervention. Accordingly, the improvement in the approach of scale separation, achieved by introducing different compositional degradation mechanisms or spatial resolutions of inflammatory responses, is needed to provide simulations with higher resolution of tissue degeneration pathways while preserving assumptions in the computational models in future work.

In the study of obesity-associated inflammatory and mechanical effects during OA presented in both Chapters 5 and 6, full gait cycles and multiple loading conditions were not simulated due to the expensive computational cost. Each simulation of cartilage degeneration in 5 years requires over 3 days of computation using 8 cores. Additionally, the strong nonlinearity of joint models and cartilage degeneration can lead to convergence difficulties and numerical instability in long-term sim-

ulations for more complex loading scenarios. Thus, the mechanical stimuli and tissue loss resulting from different physical activities were not thoroughly simulated in this thesis. Instead, as a supplementary material, Figure J.7 shows the distribution of cartilage degeneration levels in the two subject-specific knee joints (LTKN1468 and RTKN0668) when the loading condition is the first peak load of a stance phase. Due to the model instability and the lack of individualised gait data, the axial force was not scaled for a comprehensive analysis and only two joints were simulated. However, it was found that the changes in the loading condition could alter the degeneration distribution in Figure J.7 compared with the results in Chapter 6. In the computational framework, the incorporation of the effect of loading frequency into the degeneration pathways is limited, and the applicability of this framework is constrained for development as a real-time joint digital twin. Therefore, future work should integrate the full gait data and analyse the accumulative effects of cartilage degeneration resulting from different loading conditions. Additionally, the connections of loading patterns and PALs can be established in future improvements, potentially incorporating element-depletion modelling strategies to represent tissue failure due to instant overloading. To address the limitation of computational expense, data-driven surrogate models can be trained for rapid evaluation of biomechanical responses when preserving mechanistic interpretability in the future.

It should be noted that the development of the integrative multi-scale approach in Chapter 5 is based on single anatomical location, the tibiofemoral joint. This leads to a limitation in the translation between musculoskeletal kinetics and kinematics from physical activities and tissue mechanobiological responses. Adouni et al. [165] indicated obesity-altered muscle activations and joint passive reactions significantly varied the joint load during gait. Furthermore, Esrafilian et al. [173] stressed the importance of subject-specific muscle activation patterns in other motion modes. The application of musculoskeletal models is beyond the research scope of this thesis, however, the integration of adjacent musculoskeletal segments is a potential future direction for the optimisation of muscle rehabilitation and exercise therapies in the population susceptible to obesity-associated OA.

Another important limitation is the absence of a presentation of pain and bone adaption in the current computational models. As a result of various systemic factors in OA progression, the correlation between observable structural changes and pain is poor [256]. However, it should be noted that pain is a symptomatic sign of inflammation [290]. In OA pathology, vascularisation of cartilage and tissue neuroplasticity enhances the communication along vascular canals traversing the cartilage-

bone interface [282]. Synovitis and lesions associated with subchondral bone have been reported to correlate strongly with pain intensity [291]. Given that, modelling mechanobiological regulations of bone and pain signalling pathways in inflammation may facilitate the elucidation of mechanisms underlying the crosstalk between articular cartilage and subchondral bone. The absence of modelling pain mechanisms in Chapter 3 limits model parameterisation using pain-related metrics in OA inflammation. In the multi-scale approach presented in Chapter 5, pain signalling pathways and bone degradation are also not included, thereby symptomatic signs are not assessed along with the predictions in tissue structural damage. This limits the investigation of OA pathomechanisms related to cartilage-bone unit and the clinical translation of the computational predictions. Thus, integrating pain-associated biomarkers and bone adaption can be a critical future direction to improve understanding of the association between pain mechanisms and tissue degeneration affected by multifaceted factors in OA, particularly for the roles of subchondral bone and cartilage degradation in OA progression.

The scarcity of quantitative and longitudinal data leads to challenges in the validation of the current computational approach, whereas model validity was demonstrated through comparison with previously published computational models in Chapter 5. It should be noted that this is the first mechanistic computational approach integrating obesity-related mechanobiological effects. Individualised data of model parameters are lacking in the research scope of this thesis. In addition, the full validation of a multi-scale model requires multi-modal data including imaging, mechanobiological and clinical measurements with corresponding interpretations of data interconnections. Suitable extended datasets will be able to support a robust calibration and validation of this computational approach at both individual and population levels. Furthermore, longitudinal track records on lifestyle factors such as nutrition status and physical activity will enhance the interpretability of the model predictions across different individuals in the future work.

7.3 Conclusion

This thesis presents a novel multi-scale computational approach that integrates obesity-associated inflammation and mechanics in OA. In Chapter 3, it was found that the increase in BMI could reduce the system bistability by developing the first mathematical model of adipokine-mediated OA inflammation. In addition, the physical activity intervention that aimed to reduce adiposity could recover the stability

of the healthy state, and a window period of the intervention was found when inflammation was activated by tissue injury. The sensitivity of this window period was analysed in Chapter 4, showing a range from 0 to 15 months that could be modulated by both mechanical damage and adiposity level. Three intervention strategies to inhibit or delay chronic inflammatory responses were simulated for different levels of BMI, suggesting the adiposity-modified intervention should be optimised by assessing the individual level of adiposity and mechanical damage. A novel multi-scale modelling approach of cartilage degeneration was developed to incorporate inflammation and mechanical loading of obesity in Chapter 5, where a parameter sensitivity study showed that a higher BMI could accelerate cartilage degeneration and increase the sensitivity of time-varying degenerative volume to the stress threshold. In simulations of cartilage degeneration spanning five years, it was found that the relative significance of mechanical and inflammatory factors might not remain constant during the course of cartilage degeneration, accompanied by obesity-driven alterations in inflammatory activities. Thereafter, the subject-specific variations in biomechanical responses during cartilage degeneration were simulated and compared for three subjects in Chapter 6. A consistent trend of reduced tissue resistance to tensile and compressive loading in degeneration was shown for the three subjects, and obesity could increase the cartilage degeneration area and level. However, the degeneration was more uniform in the joint of LTKN8941. Differently, the lateral side of cartilage was more susceptible to the degeneration driven by obesity in the joints of LTKN1468 and RTKN0668. Particularly, the osteoarthritic joint (RTKN0668) showed little effect of reducing BMI on altering the cartilage degeneration level. In summary, these findings contribute to the understanding of obesity-related phenotypes and endotypes of OA, revealing the potential therapeutic solutions associated with obesity. As the first mechanobiological modelling framework of obesity-associated OA, it provides insights into pinpointing the critical variables needed for acquiring individualised data. Additionally, the computational models established in this thesis demonstrate the adaptivity and extensibility for mechanistic study of OA, identification of therapeutic targets, and predictions in cartilage degeneration. Future valid datasets could improve the validation of these models to support both specific research purposes and the development of joint digital twins in OA prediction.

References

[1] A. Mobasheri et al., "Osteoarthritis research society international (oarsi): Past, present and future," *Osteoarthritis and Cartilage Open*, vol. 3, no. 2, p. 100 146, Jun. 2021, ISSN: 26659131. DOI: 10.1016/j.ocarto.2021.100146

[2] L. King, "Osteoarthritis and comorbidity: Time for action," *Osteoarthritis and Cartilage*, vol. 31, no. 4, pp. 423–424, Apr. 2023, ISSN: 10634584. DOI: 10.1016/j.joca.2023.01.007

[3] S. L. James et al., "Global, regional, and national incidence, prevalence, and years lived with disability for 354 diseases and injuries for 195 countries and territories, 1990–2017: A systematic analysis for the global burden of disease study 2017," *The Lancet*, vol. 392, no. 10159, pp. 1789–1858, Nov. 2018, ISSN: 01406736. DOI: 10.1016/S0140-6736(18)32279-7

[4] A. Cui, H. Li, D. Wang, J. Zhong, Y. Chen, and H. Lu, "Global, regional prevalence, incidence and risk factors of knee osteoarthritis in population-based studies," *EClinicalMedicine*, vol. 29–30, p. 100 587, Dec. 2020, ISSN: 25895370. DOI: 10.1016/j.eclinm.2020.100587

[5] J. D. Steinmetz et al., "Global, regional, and national burden of osteoarthritis, 1990–2020 and projections to 2050: A systematic analysis for the global burden of disease study 2021," *The Lancet Rheumatology*, vol. 5, no. 9, e508–e522, Sep. 2023, ISSN: 26659913. DOI: 10.1016/S2665-9913(23)00163-7

[6] S. Swain et al., "Trends in incidence and prevalence of osteoarthritis in the united kingdom: Findings from the clinical practice research datalink (cprd)," *Osteoarthritis and Cartilage*, vol. 28, no. 6, pp. 792–801, Jun. 2020, ISSN: 10634584. DOI: 10.1016/j.joca.2020.03.004

[7] S. Glyn-Jones et al., "Osteoarthritis," *The Lancet*, vol. 386, no. 9991, pp. 376–387, Jul. 2015, ISSN: 01406736. DOI: 10.1016/S0140-6736(14)60802-3

[8] G. Dobson et al., "Defining the osteoarthritis patient: Back to the future," *Osteoarthritis and Cartilage*, vol. 26, no. 8, pp. 1003–1007, Aug. 2018, ISSN: 10634584. DOI: 10.1016/j.joca.2018.04.018

[9] G. H. Lo et al., "Is there an association between a history of running and symptomatic knee osteoarthritis? a cross-sectional study from the osteoarthritis initiative," *Arthritis Care & Research*, vol. 69, no. 2, pp. 183–191, 2017, ISSN: 2151-4658. DOI: 10.1002/acr.22939

[10] G. H. Lo et al., "Running does not increase symptoms or structural progression in people with knee osteoarthritis: Data from the osteoarthritis initiative," *Clinical Rheumatology*, vol. 37, no. 9, pp. 2497–2504, Sep. 1, 2018, ISSN: 1434-9949. DOI: 10.1007/s10067-018-4121-3

[11] L. Stefan Lohmander, P. J. Neame, and J. D. Sandy, "The structure of aggrecan fragments in human synovial fluid. evidence that aggrecanase mediates cartilage degradation in inflammatory joint disease, joint injury, and osteoarthritis," *Arthritis & Rheumatism*, vol. 36, no. 9, pp. 1214–1222, 1993, ISSN: 1529-0131. DOI: 10.1002/art.1780360906

[12] J.-P. Pelletier, J. Martel-Pelletier, and S. B. Abramson, "Osteoarthritis, an inflammatory disease: Potential implication for the selection of new therapeutic targets," *Arthritis & Rheumatism*, vol. 44, no. 6, pp. 1237–1247, 2001, ISSN: 1529-0131. DOI: 10.1002/1529-0131(200106)44:6<1237::AID-ART214>3.0.CO;2-F

[13] F. Iannone and G. Lapadula, "The pathophysiology of osteoarthritis," *Aging Clinical and Experimental Research*, vol. 15, no. 5, pp. 364–372, Oct. 2003, ISSN: 1594-0667. DOI: 10.1007/BF03327357 PMID: 14703002.

[14] A. R. Poole, "Osteoarthritis as a whole joint disease," *HSS Journal*, vol. 8, no. 1, pp. 4–6, Feb. 2012, ISSN: 1556-3316, 1556-3324. DOI: 10.1007/s11420-011-9248-6

[15] P. M. Moon and F. Beier, "Novel insights into osteoarthritis joint pathology from studies in mice," *Current Rheumatology Reports*, vol. 17, no. 8, p. 50, Aug. 2015, ISSN: 1523-3774, 1534-6307. DOI: 10.1007/s11926-015-0524-1

[16] W. H. Robinson et al., "Low-grade inflammation as a key mediator of the pathogenesis of osteoarthritis," *Nature Reviews Rheumatology*, vol. 12, no. 10, pp. 580–592, Oct. 2016, ISSN: 1759-4790, 1759-4804. DOI: 10.1038/nrrheum.2016.136

[17] M. E. Casper-Taylor, A. J. Barr, S. Williams, R. K. Wilcox, and P. G. Conaghan, "Initiating factors for the onset of oa: A systematic review of animal bone and cartilage pathology in oa," *Journal of Orthopaedic Research*, vol. 38, no. 8, pp. 1810–1818, Aug. 2020, ISSN: 0736-0266, 1554-527X. DOI: 10.1002/jor.24605

[18] E. Sanchez-Lopez, R. Coras, A. Torres, N. E. Lane, and M. Guma, "Synovial inflammation in osteoarthritis progression," *Nature Reviews Rheumatology*, vol. 18, no. 5, pp. 258–275, May 2022, ISSN: 1759-4790, 1759-4804. DOI: 10.1038/s41584-022-00749-9

[19] J. Thoenen, J. W. MacKay, H. J. C. Sandford, G. E. Gold, and F. Kogan, "Imaging of synovial inflammation in osteoarthritis, from the ajr special series on inflammation," *American Journal of Roentgenology*, vol. 218, no. 3, pp. 405–417, Mar. 2022, ISSN: 0361-803X. DOI: 10.2214/AJR.21.26170

[20] E. Kalaitzoglou, T. M. Griffin, and M. B. Humphrey, "Innate immune responses and osteoarthritis," *Current Rheumatology Reports*, vol. 19, no. 8, p. 45, Aug. 2017, ISSN: 1523-3774, 1534-6307. DOI: 10.1007/s11926-017-0672-6

[21] J. S. Roh and D. H. Sohn, "Damage-associated molecular patterns in inflammatory diseases," *Immune Network*, vol. 18, no. 4, e27, 2018, ISSN: 1598-2629, 2092-6685. DOI: 10.4110/in.2018.18.e27

[22] M. Segarra-Queralt, K. Crump, A. Pascuet-Fontanet, B. Gantenbein, and J. Noailly, "The interplay between biochemical mediators and mechanotransduction in chondrocytes: Unravelling the differential responses in primary knee osteoarthritis," *Physics of Life Reviews*, vol. 48, pp. 205–221, Mar. 2024, ISSN: 15710645. DOI: 10.1016/j.plrev.2024.02.003

[23] C. Reyes, K. M. Leyland, G. Peat, C. Cooper, N. K. Arden, and D. Prieto-Alhambra, "Association between overweight and obesity and risk of clinically diagnosed knee, hip, and hand osteoarthritis: A population-based cohort study," *Arthritis & Rheumatology*, vol. 68, no. 8, pp. 1869–1875, Aug. 2016, ISSN: 2326-5191, 2326-5205. DOI: 10.1002/art.39707

[24] S. Tang et al., "Osteoarthritis," *Nature Reviews Disease Primers*, vol. 11, no. 1, pp. 1–22, Feb. 13, 2025, ISSN: 2056-676X. DOI: 10.1038/s41572-025-00594-6

[25] W. E. Van Spil, O. Kubassova, M. Boesen, A.-C. Bay-Jensen, and A. Mobasheri, "Osteoarthritis phenotypes and novel therapeutic targets," *Biochemical Pharmacology*, vol. 165, pp. 41–48, Jul. 2019, ISSN: 00062952. DOI: 10.1016/j.bcp.2019.02.037

[26] S. Jang, K. Lee, and J. H. Ju, "Recent updates of diagnosis, pathophysiology, and treatment on osteoarthritis of the knee," *International Journal of Molecular Sciences*, vol. 22, no. 5, p. 2619, Mar. 5, 2021, ISSN: 1422-0067. DOI: 10.3390/ijms22052619

[27] D. P. Collins, K. N. Elsouri, and M. Demory Beckler, "Osteoarthritis: Can we do better?" *Cureus*, Nov. 14, 2022, ISSN: 2168-8184. DOI: 10.7759/cureus.31505

[28] S. Kennedy, J. R. Tambiah, and N. E. Lane, "Osteoarthritis today: Lost in translation?" *Best Practice & Research Clinical Rheumatology*, p. 101 810, Jan. 2023, ISSN: 15216942. DOI: 10.1016/j.berh.2022.101810

[29] L. A. Salman, G. Ahmed, S. G. Dakin, B. Kendrick, and A. Price, "Osteoarthritis: A narrative review of molecular approaches to disease management," *Arthritis Research & Therapy*, vol. 25, no. 1, p. 27, Feb. 18, 2023, ISSN: 1478-6362. DOI: 10.1186/s13075-023-03006-w

[30] G. Iolascon et al., "Early osteoarthritis: How to define, diagnose, and manage. a systematic review," *European Geriatric Medicine*, vol. 8, no. 5–6, pp. 383–396, Nov. 2017, ISSN: 18787649. DOI: 10.1016/j.eurger.2017.07.008

[31] C. A. Emery et al., "Establishing outcome measures in early knee osteoarthritis," *Nature Reviews Rheumatology*, vol. 15, no. 7, pp. 438–448, Jul. 2019, ISSN: 1759-4790, 1759-4804. DOI: 10.1038/s41584-019-0237-3

[32] A. Mahmoudian, L. S. Lohmander, A. Mobasheri, M. Englund, and F. P. Luyten, "Early-stage symptomatic osteoarthritis of the knee — time for action," *Nature Reviews Rheumatology*, vol. 17, no. 10, pp. 621–632, Oct. 2021, ISSN: 1759-4790, 1759-4804. DOI: 10.1038/s41584-021-00673-4

[33] A. Dell'Isola, R. Allan, S. L. Smith, S. S. P. Marreiros, and M. Steultjens, "Identification of clinical phenotypes in knee osteoarthritis: A systematic review of the literature," *BMC Musculoskeletal Disorders*, vol. 17, no. 1, p. 425, Oct. 12, 2016, ISSN: 1471-2474. DOI: 10.1186/s12891-016-1286-2

[34] D. J. Hunter and L. A. Deveza, "Deconstructing the "types" of osteoarthritis," *Osteoarthritis Imaging*, vol. 5, no. 1, p. 100 257, Mar. 1, 2025, ISSN: 2772-6541. DOI: 10.1016/j.ostima.2024.100257

[35] C. Franceschi, P. Garagnani, P. Parini, C. Giuliani, and A. Santoro, "Inflammaging: A new immune–metabolic viewpoint for age-related diseases," *Nature Reviews Endocrinology*, vol. 14, no. 10, pp. 576–590, Oct. 2018, ISSN: 1759-5029, 1759-5037. DOI: 10.1038/s41574-018-0059-4

[36] F. Motta, E. Barone, A. Sica, and C. Selmi, "Inflammaging and osteoarthritis," *Clinical Reviews in Allergy & Immunology*, Jun. 18, 2022, ISSN: 1559-0267. DOI: 10.1007/s12016-022-08941-1

[37] A. J. Gibbs et al., "Recommendations for the management of hip and knee osteoarthritis: A systematic review of clinical practice guidelines," *Osteoarthritis and Cartilage*, vol. 31, no. 10, pp. 1280–1292, Oct. 1, 2023, ISSN: 1063-4584. DOI: 10.1016/j.joca.2023.05.015

[38] G. A. Bray, "Obesity: A 100 year perspective," *International Journal of Obesity*, vol. 49, no. 2, pp. 159–167, Feb. 2025, ISSN: 1476-5497. DOI: 10.1038/s41366-024-01530-6

[39] P. González-Muniesa et al., "Obesity," *Nature Reviews Disease Primers*, vol. 3, no. 1, p. 17 034, Jun. 15, 2017, ISSN: 2056-676X. DOI: 10.1038/nrdp.2017.34

[40] K. H. Collins, I. K. Haugen, T. Neogi, and F. Guilak, "Osteoarthritis as a systemic disease," *Nature Reviews Rheumatology*, pp. 1–13, Dec. 3, 2025, ISSN: 1759-4804. DOI: 10.1038/s41584-025-01332-8

[41] J. Chang, Z. Liao, M. Lu, T. Meng, W. Han, and C. Ding, "Systemic and local adipose tissue in knee osteoarthritis," *Osteoarthritis and Cartilage*, vol. 26, no. 7, pp. 864–871, Jul. 2018, ISSN: 10634584. DOI: 10.1016/j.joca.2018.03.004

[42] K. H. Collins et al., "Adipose tissue is a critical regulator of osteoarthritis," *Proceedings of the National Academy of Sciences*, vol. 118, no. 1, e2021096118, Jan. 5, 2021, ISSN: 0027-8424, 1091-6490. DOI: 10.1073/pnas.2021096118

[43] X. Unamuno, J. Gómez-Ambrosi, A. Rodríguez, S. Becerril, G. Frühbeck, and V. Catalán, "Adipokine dysregulation and adipose tissue inflammation in human obesity," *European Journal of Clinical Investigation*, vol. 48, no. 9, e12997, Sep. 2018, ISSN: 00142972. DOI: 10.1111/eci.12997

[44] M. Duclos, "Osteoarthritis, obesity and type 2 diabetes: The weight of waist circumference," *Annals of Physical and Rehabilitation Medicine*, vol. 59, no. 3, pp. 157–160, Jun. 2016, ISSN: 18770657. DOI: 10.1016/j.rehab.2016.04.002

[45] C. Zhang, Y. Lin, C. H. Yan, and W. Zhang, "Adipokine signaling pathways in osteoarthritis," *Frontiers in Bioengineering and Biotechnology*, vol. 10, p. 865 370, Apr. 19, 2022, ISSN: 2296-4185. DOI: 10.3389/fbioe.2022.865370

[46] S. Mukherjee, M. Nazemi, I. Jonkers, and L. Geris, "Use of computational modeling to study joint degeneration: A review," *Frontiers in Bioengineering and Biotechnology*, vol. 8, p. 93, Feb. 28, 2020, ISSN: 2296-4185. DOI: 10.3389/fbioe.2020.00093

[47] L. Chen et al., "Pathogenesis and clinical management of obesity-related knee osteoarthritis: Impact of mechanical loading," *Journal of Orthopaedic Translation*, vol. 24, pp. 66–75, Sep. 1, 2020, ISSN: 2214-031X. DOI: 10.1016/j.jot.2020.05.001

[48] J. G. Betts et al., *Anatomy and Physiology*, 2e. Houston, Texas: OpenStax ; Rice University, 2022, ISBN: 978-1-938168-13-0.

[49] A. J. Sophia Fox, A. Bedi, and S. A. Rodeo, "The basic science of articular cartilage: Structure, composition, and function," *Sports Health: A Multidisciplinary Approach*, vol. 1, no. 6, pp. 461–468, Nov. 2009, ISSN: 1941-7381, 1941-0921. DOI: 10.1177/1941738109350438

[50] C. R. Henak, A. E. Anderson, and J. A. Weiss, "Subject-specific analysis of joint contact mechanics: Application to the study of osteoarthritis and surgical planning," *Journal of Biomechanical Engineering*, vol. 135, no. 2, p. 021 003, Feb. 1, 2013, ISSN: 0148-0731, 1528-8951. DOI: 10.1115/1.4023386

[51] S. Oliveira, B. B. Hinckel, F. S. Silva, Ó. Carvalho, and A. Leal, "A guide to articular cartilage functioning: A comprehensive review, current challenges and mechanobiological solutions," *Progress in Biomedical Engineering*, vol. 7, no. 3, p. 032 009, Jul. 2025, ISSN: 2516-1091. DOI: 10.1088/2516-1091/ade83a

[52] H. Madry, C. N. van Dijk, and M. Mueller-Gerbl, "The basic science of the subchondral bone," *Knee Surgery, Sports Traumatology, Arthroscopy*, vol. 18, no. 4, pp. 419–433, Apr. 2010, ISSN: 0942-2056, 1433-7347. DOI: 10.1007/s00167-010-1054-z

[53] K. Yamada, R. Healey, D. Amiel, M. Lotz, and R. Coutts, "Subchondral bone of the human knee joint in aging and osteoarthritis," *Osteoarthritis and Cartilage*, vol. 10, no. 5, pp. 360–369, May 2002, ISSN: 10634584. DOI: 10.1053/joca.2002.0525

[54] A. Ioan-Facsinay and M. Kloppenburg, "An emerging player in knee osteoarthritis: The infrapatellar fat pad," *Arthritis Research & Therapy*, vol. 15, no. 6, p. 225, 2013, ISSN: 1478-6354. DOI: 10.1186/ar4422

[55] N. Zeng, Z.-P. Yan, X.-Y. Chen, and G.-X. Ni, "Infrapatellar fat pad and knee osteoarthritis," *Aging and disease*, vol. 11, no. 5, p. 1317, 2020, ISSN: 2152-5250. DOI: 10.14336/AD.2019.1116

[56] W. Han et al., "Infrapatellar fat pad in the knee: Is local fat good or bad for knee osteoarthritis?" *Arthritis Research & Therapy*, vol. 16, no. 4, R145, 2014, ISSN: 1478-6354. DOI: 10.1186/ar4607

[57] S. Zhou et al., "Source and hub of inflammation: The infrapatellar fat pad and its interactions with articular tissues during knee osteoarthritis," *Journal of Orthopaedic Research*, vol. 40, no. 7, pp. 1492–1504, Jul. 2022, ISSN: 0736-0266, 1554-527X. DOI: 10.1002/jor.25347

[58] E. S. Mameri et al., "Review of meniscus anatomy and biomechanics," *Current Reviews in Musculoskeletal Medicine*, vol. 15, no. 5, pp. 323–335, Aug. 10, 2022, ISSN: 1935-9748. DOI: 10.1007/s12178-022-09768-1

[59] N. Ozeki, H. Koga, and I. Sekiya, "Degenerative meniscus in knee osteoarthritis: From pathology to treatment," *Life*, vol. 12, no. 4, p. 603, Apr. 18, 2022, ISSN: 2075-1729. DOI: 10.3390/life12040603

[60] B. C. Fleming, M. J. Hulstyn, H. L. Oksendahl, and P. D. Fadale, "Ligament injury, reconstruction and osteoarthritis:" *Current Opinion in Orthopaedics*, vol. 16, no. 5, pp. 354–362, Oct. 2005, ISSN: 1041-9918. DOI: 10.1097/01.bco.0000176423.07865.d2

[61] V. B. Kraus, D. E. Hargrove, D. J. Hunter, J. B. Renner, and J. M. Jordan, "Establishment of reference intervals for osteoarthritis-related soluble biomarkers: The fnih/oarsi oa biomarkers consortium," *Annals of the Rheumatic Diseases*, vol. 76, no. 1, pp. 179–185, Jan. 2017, ISSN: 0003-4967, 1468-2060. DOI: 10.1136/annrheumdis-2016-209253

[62] Z. Lv et al., "Molecular classification of knee osteoarthritis," *Frontiers in Cell and Developmental Biology*, vol. 9, p. 725 568, Aug. 27, 2021, ISSN: 2296-634X. DOI: 10.3389/fcell.2021.725568

[63] M. Piperno et al., "Osteoarthritic cartilage fibrillation is associated with a decrease in chrondrocyte adhesion to fibronectin," *Osteoarthritis and Cartilage*, vol. 6, no. 6, pp. 393–399, Nov. 1, 1998, ISSN: 1063-4584. DOI: 10.1053/joca.1998.0138

[64] J. A. Buckwalter, H. J. Mankin, and A. J. Grodzinsky, "Articular cartilage and osteoarthritis.," *Instructional course lectures*, vol. 54, pp. 465–480, 2005, ISSN: 0065-6895. PMID: 15952258.

[65] H. Lorenz and W. Richter, "Osteoarthritis: Cellular and molecular changes in degenerating cartilage," *Progress in Histochemistry and Cytochemistry*, vol. 40, no. 3, pp. 135–163, Jul. 3, 2006, ISSN: 00796336. DOI: 10.1016/j.proghi.2006.02.003

[66] X. L. Lu and V. C. Mow, "Biomechanics of articular cartilage and determination of material properties," *Medicine & Science in Sports & Exercise*, vol. 40, no. 2, pp. 193–199, Feb. 2008, ISSN: 0195-9131. DOI: 10.1249/mss.0b013e31815cb1fc

[67] L. J. Sandell and T. Aigner, "Articular cartilage and changes in arthritis: Cell biology of osteoarthritis," *Arthritis Research & Therapy*, vol. 3, no. 2, p. 107, Jan. 22, 2001, ISSN: 1478-6362. DOI: 10.1186/ar148

[68] H. A. Kim et al., "The catabolic pathway mediated by toll-like receptors in human osteoarthritic chondrocytes," *Arthritis & Rheumatism*, vol. 54, no. 7, pp. 2152–2163, Jul. 2006, ISSN: 0004-3591, 1529-0131. DOI: 10.1002/art.21951

[69] L. Zheng, Z. Zhang, P. Sheng, and A. Mobasheri, "The role of metabolism in chondrocyte dysfunction and the progression of osteoarthritis," *Ageing Research Reviews*, vol. 66, p. 101 249, Mar. 2021, ISSN: 15681637. DOI: 10.1016/j.arr.2020.101249

[70] K. Pritzker et al., "Osteoarthritis cartilage histopathology: Grading and staging," *Osteoarthritis and Cartilage*, vol. 14, no. 1, pp. 13–29, Jan. 2006, ISSN: 10634584. DOI: 10.1016/j.joca.2005.07.014

[71] A. J. R. Palmer et al., "Non-invasive imaging of cartilage in early osteoarthritis," *The Bone & Joint Journal*, vol. 95-B, no. 6, pp. 738–746, Jun. 2013, ISSN: 2049-4394, 2049-4408. DOI: 10.1302/0301-620X.95B6.31414

[72] O.-M. Aho, M. Finnilä, J. Thevenot, S. Saarakkala, and P. Lehenkari, "Subchondral bone histology and grading in osteoarthritis," *PLOS ONE*, vol. 12, no. 3, L. Malaval, Ed., e0173726, Mar. 20, 2017, ISSN: 1932-6203. DOI: 10.1371/journal.pone.0173726

[73] F. W. Roemer et al., "Change in mri-detected subchondral bone marrow lesions is associated with cartilage loss: The most study. a longitudinal multicentre study of knee osteoarthritis," *Annals of the Rheumatic Diseases*, vol. 68, no. 9, pp. 1461–1465, Sep. 2009, ISSN: 0003-4967, 1468-2060. DOI: 10.1136/ard.2008.096834

[74] T. Hügle and J. Geurts, "What drives osteoarthritis?—synovial *versus* subchondral bone pathology," *Rheumatology*, kew389, Dec. 21, 2016, ISSN: 1462-0324, 1462-0332. DOI: 10.1093/rheumatology/kew389

[75] G. Li et al., "Subchondral bone in osteoarthritis: Insight into risk factors and microstructural changes," *Arthritis Research & Therapy*, vol. 15, no. 6, p. 223, 2013, ISSN: 1478-6354. DOI: 10.1186/ar4405

[76] B. Li, D. Marshall, M. Roe, and R. M. Aspden, "The electron microscope appearance of the subchondral bone plate in the human femoral head in osteoarthritis and osteoporosis," *Journal of Anatomy*, vol. 195, no. 1, pp. 101–110, Jul. 1999, ISSN: 0021-8782, 1469-7580. DOI: 10.1046/j.1469-7580.1999.19510101.x

[77] Y. Hu, X. Chen, S. Wang, Y. Jing, and J. Su, "Subchondral bone microenvironment in osteoarthritis and pain," *Bone Research*, vol. 9, no. 1, p. 20, Dec. 2021, ISSN: 2095-6231. DOI: 10.1038/s41413-021-00147-z

[78] D. Muratovic, D. M. Findlay, F. M. Cicuttini, A. E. Wluka, Y.-R. Lee, and J. S. Kuliwaba, "Bone matrix microdamage and vascular changes characterize bone marrow lesions in the subchondral bone of knee osteoarthritis," *Bone*, vol. 108, pp. 193–201, Mar. 2018, ISSN: 87563282. DOI: 10.1016/j.bone.2018.01.012

[79] G. S. Man and G. Mologhianu, "Osteoarthritis pathogenesis - a complex process that involves the entire joint," *Journal of Medicine and Life*, vol. 7, no. 1, pp. 37–41, Mar. 15, 2014, ISSN: 1844-122X. PMID: 24653755.

[80] S. Donell, "Subchondral bone remodelling in osteoarthritis," *EFORT Open Reviews*, vol. 4, no. 6, pp. 221–229, Jun. 2019, ISSN: 2396-7544, 2058-5241. DOI: 10.1302/2058-5241.4.180102

[81] H. Dürr, H. Martin, C. Pellengahr, M. Schlemmer, M. Maier, and V. Jansson, "The cause of subchondral bone cysts in osteoarthrosis-a finite element analysis," *Acta Orthopaedica Scandinavica*, vol. 75, no. 5, pp. 554–558, Jan. 2004, ISSN: 0001-6470. DOI: 10.1080/00016470410001411

[82] E. G. Nettelbladt and L. K. M. Sundblad, "Protein patterns in synovial fluid and serum in rheumatoid arthritis and osteoarthritis," *Arthritis & Rheumatism*, vol. 2, no. 2, pp. 144–151, Apr. 1959, ISSN: 00043591, 15290131. DOI: 10.1002/1529-0131(195904)2:2<144::AID-ART1780020206>3.0.CO;2-G

[83] J. Sokolove and C. M. Lepus, "Role of inflammation in the pathogenesis of osteoarthritis: Latest findings and interpretations," *Therapeutic Advances in Musculoskeletal Disease*, vol. 5, no. 2, pp. 77–94, Apr. 2013, ISSN: 1759-720X, 1759-7218. DOI: 10.1177/1759720X12467868

[84] J. Shen, Y. Abu-Amer, R. J. O'Keefe, and A. McAlinden, "Inflammation and epigenetic regulation in osteoarthritis," *Connective Tissue Research*, vol. 58, no. 1, pp. 49–63, Jan. 2, 2017, ISSN: 0300-8207, 1607-8438. DOI: 10.1080/03008207.2016.1208655

[85] D. Sohn et al., "Plasma proteins present in osteoarthritic synovial fluid can stimulate cytokine production via toll-like receptor 4," *Arthritis Research & Therapy*, vol. 14, no. 1, R7, 2012, ISSN: 1478-6354. DOI: 10.1186/ar3555

[86] D. B. Burr and M. A. Gallant, "Bone remodelling in osteoarthritis," *Nature Reviews Rheumatology*, vol. 8, no. 11, pp. 665–673, Nov. 2012, ISSN: 1759-4790, 1759-4804. DOI: 10.1038/nrrheum.2012.130

[87] P. Wojdasiewicz, Ł. A. Poniatowski, and D. Szukiewicz, "The role of inflammatory and anti-inflammatory cytokines in the pathogenesis of osteoarthritis," *Mediators of Inflammation*, vol. 2014, pp. 1–19, 2014, ISSN: 0962-9351, 1466-1861. DOI: 10.1155/2014/561459

[88] C. R. Scanzello, "Chemokines and inflammation in osteoarthritis: Insights from patients and animal models: Chemokines in osteoarthritis," *Journal of Orthopaedic Research*, vol. 35, no. 4, pp. 735–739, Apr. 2017, ISSN: 07360266. DOI: 10.1002/jor.23471

[89] T. Poonpet, "Adipokines: Biomarkers for osteoarthritis?" *World Journal of Orthopedics*, vol. 5, no. 3, p. 319, 2014, ISSN: 2218-5836. DOI: 10.5312/wjo.v5.i3.319

[90] V. Francisco et al., "Adipokines and inflammation: Is it a question of weight?: Obesity and inflammatory diseases," *British Journal of Pharmacology*, vol. 175, no. 10, pp. 1569–1579, May 2018, ISSN: 00071188. DOI: 10.1111/bph.14181

[91] Y. Y. Chow and K.-Y. Chin, "The role of inflammation in the pathogenesis of osteoarthritis," *Mediators of Inflammation*, vol. 2020, pp. 1–19, Mar. 3, 2020, ISSN: 0962-9351, 1466-1861. DOI: 10.1155/2020/8293921

[92] H. Dumond et al., "Evidence for a key role of leptin in osteoarthritis," *Arthritis & Rheumatism*, vol. 48, no. 11, pp. 3118–3129, 2003, ISSN: 1529-0131. DOI: 10.1002/art.11303

[93] M.-L. Hülser et al., "Systemic versus local adipokine expression differs in a combined obesity and osteoarthritis mouse model," *Scientific Reports*, vol. 11, no. 1, p. 17 001, Dec. 2021, ISSN: 2045-2322. DOI: 10.1038/s41598-021-96545-8

[94] F. Kroon et al., "The role of leptin and adiponectin as mediators in the relationship between adiposity and hand and knee osteoarthritis," *Osteoarthritis and Cartilage*, vol. 27, no. 12, pp. 1761–1767, Dec. 2019, ISSN: 10634584. DOI: 10.1016/j.joca.2019.08.003

[95] E. B. Taylor, "The complex role of adipokines in obesity, inflammation, and autoimmunity," *Clinical Science*, vol. 135, no. 6, pp. 731–752, Mar. 26, 2021, ISSN: 0143-5221, 1470-8736. DOI: 10.1042/CS20200895

[96] Y. Deng and P. E. Scherer, "Adipokines as novel biomarkers and regulators of the metabolic syndrome: Adipokines as novel biomarkers and regulators of the metabolic syndrome," *Annals of the New York Academy of Sciences*, vol. 1212, no. 1, E1–E19, Nov. 2010, ISSN: 00778923. DOI: 10.1111/j.1749-6632.2010.05875.x

[97] M. Cnop et al., "Relationship of adiponectin to body fat distribution, insulin sensitivity and plasma lipoproteins: Evidence for independent roles of age and sex," *Diabetologia*, vol. 46, no. 4, pp. 459–469, Apr. 2003, ISSN: 0012-186X, 1432-0428. DOI: 10.1007/s00125-003-1074-z

[98] T.-H. Chen, L. Chen, M.-S. Hsieh, C.-P. Chang, D.-T. Chou, and S.-H. Tsai, "Evidence for a protective role for adiponectin in osteoarthritis," *Biochimica et Biophysica Acta (BBA) - Molecular Basis of Disease*, vol. 1762, no. 8, pp. 711–718, Aug. 2006, ISSN: 09254439. DOI: 10.1016/j.bbadis.2006.06.008

[99] Y. Luo and M. Liu, "Adiponectin: A versatile player of innate immunity," *Journal of Molecular Cell Biology*, vol. 8, no. 2, pp. 120–128, Apr. 2016, ISSN: 1674-2788, 1759-4685. DOI: 10.1093/jmcb/mjw012

[100] T. Wang and C. He, "Pro-inflammatory cytokines: The link between obesity and osteoarthritis," *Cytokine & Growth Factor Reviews*, vol. 44, pp. 38–50, Dec. 2018, ISSN: 13596101. DOI: 10.1016/j.cytogfr.2018.10.002

[101] A. Mukherjee and B. Das, "The role of inflammatory mediators and matrix metalloproteinases (mmps) in the progression of osteoarthritis," *Biomaterials and Biosystems*, vol. 13, p. 100 090, Mar. 1, 2024, ISSN: 2666-5344. DOI: 10.1016/j.bbiosy.2024.100090

[102] B. Fingleton, "Matrix metalloproteinases as regulators of inflammatory processes," *Biochimica et Biophysica Acta (BBA) - Molecular Cell Research*, vol. 1864, no. 11, pp. 2036–2042, Nov. 2017, ISSN: 01674889. DOI: 10.1016/j.bbamcr.2017.05.010

[103] H. Urban and C. B. Little, "The role of fat and inflammation in the pathogenesis and management of osteoarthritis," *Rheumatology*, vol. 57, pp. iv10–iv21, suppl_4 May 1, 2018, ISSN: 1462-0324, 1462-0332. DOI: 10.1093/rheumatology/kex399

[104] E.-S. E. Mehana, A. F. Khafaga, and S. S. El-Blehi, "The role of matrix metalloproteinases in osteoarthritis pathogenesis: An updated review," *Life Sciences*, vol. 234, p. 116 786, Oct. 2019, ISSN: 00243205. DOI: 10.1016/j.lfs.2019.116786

[105] R. Medzhitov, "Origin and physiological roles of inflammation," *Nature*, vol. 454, no. 7203, pp. 428–435, Jul. 24, 2008, ISSN: 0028-0836, 1476-4687. DOI: 10.1038/nature07201

[106] P. Kohl, E. J. Crampin, T. A. Quinn, and D. Noble, "Systems biology: An approach," *Clinical Pharmacology & Therapeutics*, vol. 88, no. 1, pp. 25–33, Jul. 2010, ISSN: 0009-9236, 1532-6535. DOI: 10.1038/clpt.2010.92

[107] Y. Vodovotz, G. Constantine, J. Rubin, M. Csete, E. O. Voit, and G. An, "Mechanistic simulations of inflammation: Current state and future prospects," *Mathematical Biosciences*, vol. 217, no. 1, pp. 1–10, Jan. 2009, ISSN: 00255564. DOI: 10.1016/j.mbs.2008.07.013

[108] N. A. van Riel, "Dynamic modelling and analysis of biochemical networks: Mechanism-based models and model-based experiments," *Briefings in Bioinformatics*, vol. 7, no. 4, pp. 364–374, Sep. 26, 2006, ISSN: 1467-5463, 1477-4054. DOI: 10.1093/bib/bbl040

[109] J. Dunster and I. Dransfield, "Mathematical approaches to studying inflammation," in *Encyclopedia of Cell Biology*, Elsevier, 2016, pp. 95–101, ISBN: 978-0-12-394796-3. DOI: 10.1016/B978-0-12-394447-4.40015-5

[110] E. Stalidzans et al., "Mechanistic modeling and multiscale applications for precision medicine: Theory and practice," *Network and Systems Medicine*, vol. 3, no. 1, pp. 36–56, May 1, 2020, ISSN: 2690-5949. DOI: 10.1089/nsm.2020.0002

[111] R. Lesage, J. Kerkhofs, and L. Geris, "Computational modeling and reverse engineering to reveal dominant regulatory interactions controlling osteochondral differentiation: Potential for regenerative medicine," *Frontiers in Bioengineering and Biotechnology*, vol. 6, p. 165, Nov. 13, 2018, ISSN: 2296-4185. DOI: 10.3389/fbioe.2018.00165

[112] P. Hunter and P. Nielsen, "A strategy for integrative computational physiology," *Physiology*, vol. 20, no. 5, pp. 316–325, Oct. 2005, ISSN: 1548-9213, 1548-9221. DOI: 10.1152/physiol.00022.2005

[113] J. D. Scheff, K. Kamisoglu, and I. P. Androulakis, "Mechanistic modeling of inflammation," in *Systems Pharmacology and Pharmacodynamics*, D. E. Mager and H. H. Kimko, Eds., vol. 23, Cham: Springer International Publishing, 2016, pp. 325–352, ISBN: 978-3-319-44532-8. DOI: 10.1007/978-3-319-44534-2_15

[114] M.-C. Weber et al., "Macroscale mesenchymal condensation to study cytokine-driven cellular and matrix-related changes during cartilage degradation," *Biofabrication*, vol. 12, no. 4, p. 045 016, Aug. 10, 2020, ISSN: 1758-5090. DOI: 10.1088/1758-5090/aba08f

[115] H. J. Samvelyan, D. Hughes, C. Stevens, and K. A. Staines, "Models of osteoarthritis: Relevance and new insights," *Calcified Tissue International*, vol. 109, no. 3, pp. 243–256, Sep. 2021, ISSN: 0171-967X, 1432-0827. DOI: 10.1007/s00223-020-00670-x

[116] R. Kumar, G. Clermont, Y. Vodovotz, and C. C. Chow, "The dynamics of acute inflammation," *Journal of Theoretical Biology*, vol. 230, no. 2, pp. 145–155, Sep. 2004, ISSN: 00225193. DOI: 10.1016/j.jtbi.2004.04.044

[117] M. C. Herald, "General model of inflammation," *Bulletin of Mathematical Biology*, vol. 72, no. 4, pp. 765–779, May 2010, ISSN: 0092-8240, 1522-9602. DOI: 10.1007/s11538-009-9468-9

[118] J. L. Dunster, "The macrophage and its role in inflammation and tissue repair: Mathematical and systems biology approaches," *WIREs Systems Biology and Medicine*, vol. 8, no. 1, pp. 87–99, Jan. 2016, ISSN: 1939-5094, 1939-005X. DOI: 10.1002/wsbm.1320

[119] M. Baker, B. S. Brook, and M. R. Owen, "Mathematical modelling of cytokines, mmps and fibronectin fragments in osteoarthritic cartilage," *Journal of Mathematical Biology*, vol. 75, no. 4, pp. 985–1024, Oct. 2017, ISSN: 0303-6812, 1432-1416. DOI: 10.1007/s00285-017-1104-y

[120] M. Baker, S. Denman-Johnson, B. S. Brook, I. Gaywood, and M. R. Owen, "Mathematical modelling of cytokine-mediated inflammation in rheumatoid arthritis," *Mathematical Medicine and Biology*, vol. 30, no. 4, pp. 311–337, Dec. 1, 2013, ISSN: 1477-8599, 1477-8602. DOI: 10.1093/imammb/dqs026

[121] A. Ougrinovskaia, R. S. Thompson, and M. R. Myerscough, "An ode model of early stages of atherosclerosis: Mechanisms of the inflammatory response," *Bulletin of Mathematical Biology*, vol. 72, no. 6, pp. 1534–1561, Aug. 2010, ISSN: 0092-8240, 1522-9602. DOI: 10.1007/s11538-010-9509-4

[122] L. E. Vaughan, P. R. Ranganathan, R. G. Kumar, A. K. Wagner, and J. E. Rubin, "A mathematical model of neuroinflammation in severe clinical traumatic brain injury," *Journal of Neuroinflammation*, vol. 15, no. 1, p. 345, Dec. 2018, ISSN: 1742-2094. DOI: 10.1186/s12974-018-1384-1

[123] F. J. Solis and D. Azofeifa, "Mathematical modeling of the immune system response to pathogens," *Mathematical Methods in the Applied Sciences*, vol. 43, no. 14, pp. 8273–8289, Sep. 30, 2020, ISSN: 0170-4214, 1099-1476. DOI: 10.1002/mma.6532

[124] A. Bayani, J. L. Dunster, J. J. Crofts, and M. R. Nelson, "Mechanisms and points of control in the spread of inflammation: A mathematical investigation," *Bulletin of Mathematical Biology*, vol. 82, no. 4, p. 45, Apr. 2020, ISSN: 0092-8240, 1522-9602. DOI: 10.1007/s11538-020-00709-y

[125] M. Cantone, G. Santos, P. Wentker, X. Lai, and J. Vera, "Multiplicity of mathematical modeling strategies to search for molecular and cellular insights into bacteria lung infection," *Frontiers in Physiology*, vol. 8, p. 645, Aug. 30, 2017, ISSN: 1664-042X. DOI: 10.3389/fphys.2017.00645

[126] S. B. Minucci, R. L. Heise, and A. M. Reynolds, "Review of mathematical modeling of the inflammatory response in lung infections and injuries," *Frontiers in Applied Mathematics and Statistics*, vol. 6, p. 36, Aug. 26, 2020, ISSN: 2297-4687. DOI: 10.3389/fams.2020.00036

[127] M. M. Rahman, P. N. Watton, C. P. Neu, and D. M. Pierce, "A chemo-mechano-biological modeling framework for cartilage evolving in health, disease, injury, and treatment," *Computer Methods and Programs in Biomedicine*, vol. 231, p. 107 419, Apr. 2023, ISSN: 01692607. DOI: 10.1016/j.cmpb.2023.107419

[128] M. Segarra-Queralt et al., "Regulatory network-based model to simulate the biochemical regulation of chondrocytes in healthy and osteoarthritic environments," *Scientific Reports*, vol. 12, no. 1, p. 3856, Mar. 9, 2022, ISSN: 2045-2322. DOI: 10.1038/s41598-022-07776-2

[129] M. Segarra-Queralt, G. Piella, and J. Noailly, "Network-based modelling of mechano-inflammatory chondrocyte regulation in early osteoarthritis," *Frontiers in Bioengineering and Biotechnology*, vol. 11, p. 1 006 066, Feb. 3, 2023, ISSN: 2296-4185. DOI: 10.3389/fbioe.2023.1006066

[130] R. Eftimie, J. J. Gillard, and D. A. Cantrell, "Mathematical models for immunology: Current state of the art and future research directions," *Bulletin of Mathematical Biology*, vol. 78, no. 10, pp. 2091–2134, Oct. 2016, ISSN: 0092-8240, 1522-9602. DOI: 10.1007/s11538-016-0214-9

[131] M. Pollatschek and A. Nahir, "A mathematical model of osteoarthosis," *Journal of Theoretical Biology*, vol. 143, no. 4, pp. 497–505, Apr. 1990, ISSN: 00225193. DOI: 10.1016/S0022-5193(05)80026-8

[132] S. Daun, J. Rubin, Y. Vodovotz, and G. Clermont, "Equation-based models of dynamic biological systems," *Journal of Critical Care*, vol. 23, no. 4, pp. 585–594, Dec. 2008, ISSN: 08839441. DOI: 10.1016/j.jcrc.2008.02.003

[133] J. M. Graham, B. P. Ayati, L. Ding, P. S. Ramakrishnan, and J. A. Martin, "Reaction-diffusion-delay model for epo/tnf-α interaction in articular cartilage lesion abatement," *Biology Direct*, vol. 7, no. 1, p. 9, Feb. 21, 2012, ISSN: 1745-6150. DOI: 10.1186/1745-6150-7-9

[134] X. Wang, B. P. Ayati, M. J. Brouillette, J. M. Graham, P. S. Ramakrishnan, and J. A. Martin, "Modeling and simulation of the effects of cyclic loading on articular cartilage lesion formation: Effects of cyclic loading on articular cartilage lesion formation," *International Journal for Numerical Methods in Biomedical Engineering*, vol. 30, no. 10, pp. 927–941, Oct. 2014, ISSN: 20407939. DOI: 10.1002/cnm.2636

[135] X. Wang, M. J. Brouillette, B. P. Ayati, and J. A. Martin, "A validated model of the pro- and anti-inflammatory cytokine balancing act in articular cartilage lesion formation," *Frontiers in Bioengineering and Biotechnology*, vol. 3, Mar. 10, 2015, ISSN: 2296-4185. DOI: 10.3389/fbioe.2015.00025

[136] S. Kar, D. W. Smith, B. S. Gardiner, Y. Li, Y. Wang, and A. J. Grodzinsky, "Modeling il-1 induced degradation of articular cartilage," *Archives of Biochemistry and Biophysics*, vol. 594, pp. 37–53, Mar. 2016, ISSN: 00039861. DOI: 10.1016/j.abb.2016.02.008

[137] G. I. Kapitanov, X. Wang, B. P. Ayati, M. J. Brouillette, and J. A. Martin, "Linking cellular and mechanical processes in articular cartilage lesion formation: A mathematical model," *Frontiers in Bioengineering and Biotechnology*, vol. 4, Oct. 31, 2016, ISSN: 2296-4185. DOI: 10.3389/fbioe.2016.00080

[138] K. Campbell, S. Naire, and J. H. Kuiper, "A mathematical model of cartilage regeneration after chondrocyte and stem cell implantation – i: The effects of growth factors," *Journal of Tissue Engineering*, vol. 10, p. 204 173 141 982 779, Jan. 2019, ISSN: 2041-7314, 2041-7314. DOI: 10.1177/2041731419827791

[139] C. Catt et al., "Mathematical modelling of tissue formation in chondrocyte filter cultures," *European Cells and Materials*, vol. 22, pp. 377–392, Dec. 17, 2011. DOI: 10.22203/eCM.v022a28

[140] N. Moise and A. Friedman, "Rheumatoid arthritis - a mathematical model," *Journal of Theoretical Biology*, vol. 461, pp. 17–33, Jan. 2019, ISSN: 00225193. DOI: 10.1016/j.jtbi.2018.10.039

[141] Y. Vodovotz and G. An, "Agent-based models of inflammation in translational systems biology: A decade later," *WIREs Systems Biology and Medicine*, vol. 11, no. 6, Nov. 2019, ISSN: 1939-5094, 1939-005X. DOI: 10.1002/wsbm.1460

[142] I. H. Sarker, "Machine learning: Algorithms, real-world applications and research directions," *SN Computer Science*, vol. 2, no. 3, p. 160, May 2021, ISSN: 2662-995X, 2661-8907. DOI: 10.1007/s42979-021-00592-x

[143] J. Schmidhuber, "Deep learning in neural networks: An overview," *Neural Networks*, vol. 61, pp. 85–117, Jan. 2015, ISSN: 08936080. DOI: 10.1016/j.neunet.2014.09.003

[144] C. Kokkotis, S. Moustakidis, E. Papageorgiou, G. Giakas, and D. Tsaopoulos, "Machine learning in knee osteoarthritis: A review," *Osteoarthritis and Cartilage Open*, vol. 2, no. 3, p. 100 069, Sep. 2020, ISSN: 26659131. DOI: 10.1016/j.ocarto.2020.100069

[145] P. S. Q. Yeoh et al., "Emergence of deep learning in knee osteoarthritis diagnosis," *Computational Intelligence and Neuroscience*, vol. 2021, B. Y. Ding, Ed., pp. 1–20, Nov. 10, 2021, ISSN: 1687-5273, 1687-5265. DOI: 10.1155/2021/4931437

[146] M. Binvignat et al., "Use of machine learning in osteoarthritis research: A systematic literature review," *RMD Open*, vol. 8, no. 1, e001998, Mar. 2022, ISSN: 2056-5933. DOI: 10.1136/rmdopen-2021-001998

[147] A. Erdemir, "Open knee: Open source modeling and simulation in knee biomechanics," *The Journal of Knee Surgery*, vol. 29, pp. 107–116, Oct. 7, 2015, ISSN: 1538-8506. DOI: 10.1055/s-0035-1564600

[148] J. Wismans, F. Veldpaus, J. Janssen, A. Huson, and P. Struben, "A three-dimensional mathematical model of the knee-joint," *Journal of Biomechanics*, vol. 13, no. 8, pp. 677–685, Jan. 1980, ISSN: 00219290. DOI: 10.1016/0021-9290(80)90354-1

[149] M. Bendjaballah, A. Shirazi-Adl, and D. Zukor, "Biomechanics of the human knee joint in compression: Reconstruction, mesh generation and finite element analysis," *The Knee*, vol. 2, no. 2, pp. 69–79, Jun. 1995, ISSN: 09680160. DOI: 10.1016/0968-0160(95)00018-K

[150] A. E. Anderson, B. J. Ellis, and J. A. Weiss, "Verification, validation and sensitivity studies in computational biomechanics," *Computer Methods in Biomechanics and Biomedical Engineering*, vol. 10, no. 3, pp. 171–184, Jun. 2007, ISSN: 1025-5842, 1476-8259. DOI: 10.1080/10255840601160484

[151] R. J. Cooper, R. K. Wilcox, and A. C. Jones, "Finite element models of the tibiofemoral joint: A review of validation approaches and modelling challenges," *Medical Engineering & Physics*, vol. 74, pp. 1–12, Dec. 2019, ISSN: 13504533. DOI: 10.1016/j.medengphy.2019.08.002

[152] A. Paz, G. A. Orozco, R. K. Korhonen, J. J. García, and M. E. Mononen, "Expediting finite element analyses for subject-specific studies of knee osteoarthritis: A literature review," *Applied Sciences*, vol. 11, no. 23, p. 11 440, Dec. 2, 2021, ISSN: 2076-3417. DOI: 10.3390/app112311440

[153] M. Freutel, H. Schmidt, L. Dürselen, A. Ignatius, and F. Galbusera, "Finite element modeling of soft tissues: Material models, tissue interaction and challenges," *Clinical Biomechanics*, vol. 29, no. 4, pp. 363–372, Apr. 2014, ISSN: 02680033. DOI: 10.1016/j.clinbiomech.2014.01.006

[154] A. E. Peters, R. Akhtar, E. J. Comerford, and K. T. Bates, "Tissue material properties and computational modelling of the human tibiofemoral joint: A critical review," *PeerJ*, vol. 6, e4298, Jan. 25, 2018, ISSN: 2167-8359. DOI: 10.7717/peerj.4298

[155] O. Klets, M. E. Mononen, P. Tanska, M. T. Nieminen, R. K. Korhonen, and S. Saarakkala, "Comparison of different material models of articular cartilage in 3d computational modeling of the knee: Data from the osteoarthritis initiative (oai)," *Journal of Biomechanics*, vol. 49, no. 16, pp. 3891–3900, Dec. 8, 2016, ISSN: 0021-9290. DOI: 10.1016/j.jbiomech.2016.10.025

[156] S. P. Messier, D. J. Gutekunst, C. Davis, and P. DeVita, "Weight loss reduces knee-joint loads in overweight and obese older adults with knee osteoarthritis," *Arthritis & Rheumatism*, vol. 52, no. 7, pp. 2026–2032, Jul. 2005, ISSN: 0004-3591, 1529-0131. DOI: 10.1002/art.21139

[157] J. Aaboe, H. Bliddal, S. Messier, T. Alkjær, and M. Henriksen, "Effects of an intensive weight loss program on knee joint loading in obese adults with knee osteoarthritis," *Osteoarthritis and Cartilage*, vol. 19, no. 7, pp. 822–828, Jul. 2011, ISSN: 10634584. DOI: 10.1016/j.joca.2011.03.006

[158] I. Kutzner et al., "Loading of the knee joint during activities of daily living measured in vivo in five subjects," *Journal of Biomechanics*, vol. 43, no. 11, pp. 2164–2173, Aug. 2010, ISSN: 00219290. DOI: 10.1016/j.jbiomech.2010.03.046

[159] J. L. Boyd, A. B. Zavatsky, and H. S. Gill, "Does increasing applied load lead to contact changes indicative of knee osteoarthritis? a subject-specific fea study," *International Journal for Numerical Methods in Biomedical Engineering*, vol. 32, no. 4, e02740, Apr. 2016, ISSN: 20407939. DOI: 10.1002/cnm.2740

[160] J.-S. Li, T.-Y. Tsai, M. M. Clancy, C. L. Lewis, D. T. Felson, and G. Li, "Cartilage contact characteristics of the knee during gait in individuals with obesity," *Journal of Orthopaedic Research*, vol. 40, no. 11, pp. 2480–2487, 2022, ISSN: 1554-527X. DOI: 10.1002/jor.25288

[161] D. Kim, C. L. Lewis, and S. V. Gill, "Effects of obesity and foot arch height on gait mechanics: A cross-sectional study," *PLOS ONE*, vol. 16, no. 11, e0260398, Jan. 29, 2021, ISSN: 1932-6203. DOI: 10.1371/journal.pone.0260398

[162] J. C. Stoddart, O. Dandridge, A. Garner, J. Cobb, and R. J. van Arkel, "The compartmental distribution of knee osteoarthritis – a systematic review and meta-analysis," *Osteoarthritis and Cartilage*, vol. 29, no. 4, pp. 445–455, Apr. 1, 2021, ISSN: 1063-4584. DOI: 10.1016/j.joca.2020.10.011

[163] K. F. MacLean, J. P. Callaghan, and M. R. Maly, "Effect of obesity on knee joint biomechanics during gait in young adults," *Cogent Medicine*, vol. 3, no. 1, Z. Jin, Ed., p. 1173778, Dec. 31, 2016, ISSN: 2331-205X. DOI: 10.1080/2331205X.2016.1173778

[164] F. Al Khatib, A. Gouissem, R. Mbarki, and M. Adouni, "Biomechanical characteristics of the knee joint during gait in obese versus normal subjects," *International Journal of Environmental Research and Public Health*, vol. 19, no. 2, p. 989, Jan. 16, 2022, ISSN: 1660-4601. DOI: 10.3390/ijerph19020989

[165] M. Adouni, H. Aydelik, T. R. Faisal, and R. Hajji, "The effect of body weight on the knee joint biomechanics based on subject-specific finite element-musculoskeletal approach," *Scientific Reports*, vol. 14, no. 1, p. 13777, Jun. 14, 2024, ISSN: 2045-2322. DOI: 10.1038/s41598-024-63745-x

[166] O. Klets et al., "Estimation of the effect of body weight on the development of osteoarthritis based on cumulative stresses in cartilage: Data from the osteoarthritis initiative," *Annals of Biomedical Engineering*, vol. 46, no. 2, pp. 334–344, Feb. 2018, ISSN: 0090-6964, 1573-9686. DOI: 10.1007/s10439-017-1974-6

[167] M. K. Liukkonen et al., "Evaluation of the effect of bariatric surgery-induced weight loss on knee gait and cartilage degeneration," *Journal of Biomechanical Engineering*, vol. 140, no. 4, p. 041008, Apr. 1, 2018, ISSN: 0148-0731, 1528-8951. DOI: 10.1115/1.4038330

[168] G. A. Orozco et al., "Effect of patient specificity on predicting knee cartilage degeneration in obese adults: Musculoskeletal finite-element modeling of data from the carot trial," *Journal of Orthopaedic Research*, vol. 42, no. 11, pp. 2437–2449, 2024, ISSN: 1554-527X. DOI: 10.1002/jor.25912

[169] M. E. Mononen, P. Tanska, H. Isaksson, and R. K. Korhonen, "A novel method to simulate the progression of collagen degeneration of cartilage in the knee: Data from the osteoarthritis initiative," *Scientific Reports*, vol. 6, no. 1, p. 21415, Feb. 24, 2016, ISSN: 2045-2322. DOI: 10.1038/srep21415

[170] A. Erdemir, C. Bennetts, S. Davis, A. Reddy, and S. Sibole, "Multiscale cartilage biomechanics: Technical challenges in realizing a high-throughput modelling and simulation workflow," *Interface Focus*, vol. 5, no. 2, p. 20140081, Apr. 6, 2015, ISSN: 2042-8898, 2042-8901. DOI: 10.1098/rsfs.2014.0081

[171] J. Walpole, J. A. Papin, and S. M. Peirce, "Multiscale computational models of complex biological systems," *Annual Review of Biomedical Engineering*, vol. 15, no. 1, pp. 137–154, Jul. 11, 2013, ISSN: 1523-9829, 1545-4274. DOI: 10.1146/annurev-bioeng-071811-150104

[172] J. P. Halloran et al., "Multiscale mechanics of articular cartilage: Potentials and challenges of coupling musculoskeletal, joint, and microscale computational models," *Annals of Biomedical Engineering*, vol. 40, no. 11, pp. 2456–2474, Nov. 2012, ISSN: 0090-6964, 1573-9686. DOI: 10.1007/s10439-012-0598-0

[173] A. Esrafilian et al., "An emg-assisted muscle-force driven finite element analysis pipeline to investigate joint- and tissue-level mechanical responses in functional activities: Towards a rapid assessment toolbox," *IEEE Transactions on Biomedical Engineering*, vol. 69, no. 9, pp. 2860–2871, Sep. 2022, ISSN: 1558-2531. DOI: 10.1109/TBME.2022.3156018

[174] M. Adouni, A. Shirazi-Adl, and R. Shirazi, "Computational biodynamics of human knee joint in gait: From muscle forces to cartilage stresses," *Journal of Biomechanics*, vol. 45, no. 12, pp. 2149–2156, Aug. 9, 2012, ISSN: 0021-9290. DOI: 10.1016/j.jbiomech.2012.05.040

[175] L. Shu, K. Yamamoto, R. Yoshizaki, J. Yao, T. Sato, and N. Sugita, "Multiscale finite element musculoskeletal model for intact knee dynamics," *Computers in Biology and Medicine*, vol. 141, p. 105 023, Feb. 2022, ISSN: 00104825. DOI: 10.1016/j.compbiomed.2021.105023

[176] I. Mohout et al., "Signatures of disease progression in knee osteoarthritis: Insights from an integrated multi-scale modeling approach, a proof of concept," *Frontiers in Bioengineering and Biotechnology*, vol. 11, p. 1 214 693, Jul. 27, 2023, ISSN: 2296-4185. DOI: 10.3389/fbioe.2023.1214693

[177] M. Willems et al., "Population-based in silico modeling of anatomical shape variation of the knee and its impact on joint loading in knee osteoarthritis," *Journal of Orthopaedic Research*, vol. 42, no. 11, pp. 2473–2484, 2024, ISSN: 1554-527X. DOI: 10.1002/jor.25934

[178] Y. Zhang et al., "Cartilage mechanical responses during gait as in silico biomarkers for medial knee oa progression," *Scientific Reports*, vol. 15, no. 1, p. 35 303, Oct. 9, 2025, ISSN: 2045-2322. DOI: 10.1038/s41598-025-19371-2

[179] S. Jahangir et al., "Effect of uncertainties in musculoskeletal modeling inputs on sensitivity of knee joint finite element simulations," *Medical Engineering & Physics*, vol. 138, p. 104 313, Apr. 1, 2025, ISSN: 1350-4533. DOI: 10.1016/j.medengphy.2025.104313

[180] W. Wilson, C. Van Donkelaar, R. Van Rietbergen, and R. Huiskes, "The role of computational models in the search for the mechanical behavior and damage mechanisms of articular cartilage," *Medical Engineering & Physics*, vol. 27, no. 10, pp. 810–826, Dec. 2005, ISSN: 13504533. DOI: 10.1016/j.medengphy.2005.03.004

[181] C. Chen, D. T. Tambe, L. Deng, and L. Yang, "Biomechanical properties and mechanobiology of the articular chondrocyte," *American Journal of Physiology-Cell Physiology*, vol. 305, no. 12, pp. C1202–C1208, Dec. 15, 2013, ISSN: 0363-6143, 1522-1563. DOI: 10.1152/ajpcell.00242.2013

[182] A. S. A. Eskelinen et al., "Mechanobiological model for simulation of injured cartilage degradation via pro-inflammatory cytokines and mechanical stimulus," *PLOS Computational Biology*, vol. 16, no. 6, A. Marsden, Ed., e1007998, Jun. 25, 2020, ISSN: 1553-7358. DOI: 10.1371/journal.pcbi.1007998

[183] G. A. Orozco, P. Tanska, C. Florea, A. J. Grodzinsky, and R. K. Korhonen, "A novel mechanobiological model can predict how physiologically relevant dynamic loading causes proteoglycan loss in mechanically injured articular cartilage," *Scientific Reports*, vol. 8, no. 1, p. 15 599, Oct. 22, 2018, ISSN: 2045-2322. DOI: 10.1038/s41598-018-33759-3

[184] G. A. Orozco et al., "Shear strain and inflammation-induced fixed charge density loss in the knee joint cartilage following acl injury and reconstruction: A computational study," *Journal of Orthopaedic Research*, vol. 40, no. 7, pp. 1505–1522, Jul. 2022, ISSN: 0736-0266, 1554-527X. DOI: 10.1002/jor.25177

[185] M. M. Rahman, P. N. Watton, C. P. Neu, and D. M. Pierce, "Predicting the heterogeneous chemo-mechano-biological degeneration of cartilage using 3-d biphasic finite elements," *Computer Methods and Programs in Biomedicine*, p. 108 902, Jun. 25, 2025, ISSN: 0169-2607. DOI: 10.1016/j.cmpb.2025.108902

[186] S. M. Hosseini, W. Wilson, K. Ito, and C. C. van Donkelaar, "A numerical model to study mechanically induced initiation and progression of damage in articular cartilage," *Osteoarthritis and Cartilage*, vol. 22, no. 1, pp. 95–103, Jan. 1, 2014, ISSN: 1063-4584, 1522-9653. DOI: 10.1016/j.joca.2013.10.010

[187] J. M. Párraga Quiroga, W. Wilson, K. Ito, and C. C. van Donkelaar, "The effect of loading rate on the development of early damage in articular cartilage," *Biomechanics and Modeling in Mechanobiology*, vol. 16, no. 1, pp. 263–273, Feb. 1, 2017, ISSN: 1617-7940. DOI: 10.1007/s10237-016-0815-0

[188] M. E. Mononen, P. Tanska, H. Isaksson, and R. K. Korhonen, "New algorithm for simulation of proteoglycan loss and collagen degeneration in the knee joint: Data from the osteoarthritis initiative," *Journal of Orthopaedic Research®*, vol. 36, no. 6, pp. 1673–1683, Jun. 2018, ISSN: 07360266. DOI: 10.1002/jor.23811

[189] S. A. Elahi et al., "Contribution of collagen degradation and proteoglycan depletion to cartilage degeneration in primary and secondary osteoarthritis: An in silico study," *Osteoarthritis and Cartilage*, vol. 31, no. 6, pp. 741–752, Jun. 1, 2023, ISSN: 1063-4584, 1522-9653. DOI: 10.1016/j.joca.2023.01.004 PMID: 36669584.

[190] G. A. Holzapfel and B. Fereidoonnezhad, "Chapter 5 - modeling of damage in soft biological tissues," in *Biomechanics of Living Organs*, ser. Translational Epigenetics, Y. Payan and J. Ohayon, Eds., vol. 1, Oxford: Academic Press, Jan. 1, 2017, pp. 101–123. DOI: 10.1016/B978-0-12-804009-6.00005-5

[191] A. J. Mueller, M. J. Peffers, C. J. Proctor, and P. D. Clegg, "Systems approaches in osteoarthritis: Identifying routes to novel diagnostic and therapeutic strategies: Systems approaches in osteoarthritis," *Journal of Orthopaedic Research*, vol. 35, no. 8, pp. 1573–1588, Aug. 2017, ISSN: 07360266. DOI: 10.1002/jor.23563

[192] R. Shumnalieva, G. Kotov, and S. Monov, "Obesity-related knee osteoarthritis—current concepts," *Life*, vol. 13, no. 8, p. 1650, Jul. 28, 2023, ISSN: 2075-1729. DOI: 10.3390/life13081650

[193] D. Park et al., "Association of general and central obesity, and their changes with risk of knee osteoarthritis: A nationwide population-based cohort study," *Scientific Reports*, vol. 13, no. 1, p. 3796, Mar. 7, 2023, ISSN: 2045-2322. DOI: 10.1038/s41598-023-30727-4

[194] T. P. Andriacchi, A. Mündermann, R. L. Smith, E. J. Alexander, C. O. Dyrby, and S. Koo, "A framework for the in vivo pathomechanics of osteoarthritis at the knee," *Annals of Biomedical Engineering*, vol. 32, no. 3, pp. 447–457, Mar. 2004, ISSN: 0090-6964. DOI: 10.1023/B:ABME.0000017541.82498.37

[195] S. L. Kolasinski et al., "2019 american college of rheumatology/arthritis foundation guideline for the management of osteoarthritis of the hand, hip, and knee," *Arthritis Care & Research*, vol. 72, no. 2, pp. 149–162, Feb. 2020, ISSN: 2151-464X, 2151-4658. DOI: 10.1002/acr.24131

[196] R. Bannuru et al., "Oarsi guidelines for the non-surgical management of knee, hip, and polyarticular osteoarthritis," *Osteoarthritis and Cartilage*, vol. 27, no. 11, pp. 1578–1589, Nov. 2019, ISSN: 10634584. DOI: 10.1016/j.joca.2019.06.011

[197] S. P. Messier et al., "Effects of intensive diet and exercise on knee joint loads, inflammation, and clinical outcomes among overweight and obese adults with knee osteoarthritis: The idea randomized clinical trial," *JAMA*, vol. 310, no. 12, p. 1263, Sep. 25, 2013, ISSN: 0098-7484. DOI: 10.1001/jama.2013.277669

[198] S. Masouros, A. Bull, and A. Amis, "(i) biomechanics of the knee joint," *Orthopaedics and Trauma*, vol. 24, no. 2, pp. 84–91, Apr. 2010, ISSN: 18771327. DOI: 10.1016/j.mporth.2010.03.005

[199] D. Thompson, F. Karpe, M. Lafontan, and K. Frayn, "Physical activity and exercise in the regulation of human adipose tissue physiology," *Physiological Reviews*, vol. 92, no. 1, pp. 157–191, Jan. 2012, ISSN: 0031-9333, 1522-1210. DOI: 10.1152/physrev.00012.2011

[200] F. Rocha and S. Ali, "Soluble biomarkers in osteoarthritis in 2022: Year in review," *Osteoarthritis and Cartilage*, vol. 31, no. 2, pp. 167–176, Feb. 2023, ISSN: 10634584. DOI: 10.1016/j.joca.2022.09.005

[201] S. K. Papadopoulou et al., "Exercise and nutrition impact on osteoporosis and sarcopenia—the incidence of osteosarcopenia: A narrative review," *Nutrients*, vol. 13, no. 12, p. 4499, Dec. 16, 2021, ISSN: 2072-6643. DOI: 10.3390/nu13124499

[202] K. Kuettner and A. Cole, "Cartilage degeneration in different human joints," *Osteoarthritis and Cartilage*, vol. 13, no. 2, pp. 93–103, Feb. 2005, ISSN: 10634584. DOI: 10.1016/j.joca.2004.11.006

[203] K. Muldrew, "Osteoarthritis as an inevitable consequence of the structure of articular cartilage," *Medical Hypotheses*, vol. 59, no. 4, pp. 389–397, Oct. 2002, ISSN: 03069877. DOI: 10.1016/S0306-9877(02)00122-6

[204] P. Burrage S., "Matrix metalloproteinases: Role in arthritis," *Frontiers in Bioscience*, vol. 11, no. 1, p. 529, 2006, ISSN: 10939946, 10934715. DOI: 10.2741/1817

[205] S. Pérez-García et al., "Profile of matrix-remodeling proteinases in osteoarthritis: Impact of fibronectin," *Cells*, vol. 9, no. 1, p. 40, Dec. 22, 2019, ISSN: 2073-4409. DOI: 10.3390/cells9010040

[206] R. Lesage, M. N. Ferrao Blanco, R. Narcisi, T. Welting, G. J. V. M. van Osch, and L. Geris, "An integrated in silico-in vitro approach for identifying therapeutic targets against osteoarthritis," *BMC Biology*, vol. 20, no. 1, p. 253, Nov. 9, 2022, ISSN: 1741-7007. DOI: 10.1186/s12915-022-01451-8

[207] M. N. Ferrao Blanco et al., "A multi-model approach identifies alw-ii-41-27 as a promising therapy for osteoarthritis-associated inflammation and endochondral ossification," *Heliyon*, vol. 10, no. 23, e40871, Dec. 2024, ISSN: 24058440. DOI: 10.1016/j.heliyon.2024.e40871

[208] C. Liu, D. Chu, K. Kalantar-Zadeh, J. George, H. A. Young, and G. Liu, "Cytokines: From clinical significance to quantification," *Advanced Science*, vol. 8, no. 15, p. 2 004 433, Aug. 2021, ISSN: 2198-3844, 2198-3844. DOI: 10.1002/advs.202004433

[209] M. Santillán, "On the use of the hill functions in mathematical models of gene regulatory networks," *Mathematical Modelling of Natural Phenomena*, vol. 3, no. 2, pp. 85–97, 2008, ISSN: 0973-5348. DOI: 10.1051/mmnp:2008056

[210] K. L. Spalding et al., "Dynamics of fat cell turnover in humans," *Nature*, vol. 453, no. 7196, pp. 783–787, Jun. 2008, ISSN: 0028-0836, 1476-4687. DOI: 10.1038/nature06902

[211] I. Palacios-Marin, D. Serra, J. Jimenez-Chillarón, L. Herrero, and M. Todor e-vi , "Adipose tissue dynamics: Cellular and lipid turnover in health and disease," *Nutrients*, vol. 15, no. 18, p. 3968, Sep. 14, 2023, ISSN: 2072-6643. DOI: 10.3390/nu15183968

[212] G. A. Brooks, N. F. Butte, W. M. Rand, J.-P. Flatt, and B. Caballero, "Chronicle of the institute of medicine physical activity recommendation: How a physical activity recommendation came to be among dietary recommendations," *The American Journal of Clinical Nutrition*, vol. 79, no. 5, 921S–930S, May 2004, ISSN: 00029165. DOI: 10.1093/ajcn/79.5.921S

[213] G. Hawker et al., "Understanding the pain experience in hip and knee osteoarthritis – an oarsi/omeract initiative," *Osteoarthritis and Cartilage*, vol. 16, no. 4, pp. 415–422, Apr. 2008, ISSN: 10634584. DOI: 10.1016/j.joca.2007.12.017

[214] L. Herrero-Manley, A. Alabajos-Cea, L. Suso-Martí, and E. Viosca-Herrero, "Classification criteria for early knee osteoarthritis: A review article," *Aktuelle Rheumatologie*, a-2173–1607, Oct. 24, 2023, ISSN: 0341-051X, 1438-9940. DOI: 10.1055/a-2173-1607

[215] D. Felson, "Osteoarthritis as a disease of mechanics," *Osteoarthritis and Cartilage*, vol. 21, no. 1, pp. 10–15, Jan. 2013, ISSN: 10634584. DOI: 10.1016/j.joca.2012.09.012

[216] F. Berenbaum and J. Sellam, "Obesity and osteoarthritis: What are the links?" *Joint Bone Spine*, vol. 75, no. 6, pp. 667–668, Dec. 2008, ISSN: 1297319X. DOI: 10.1016/j.jbspin.2008.07.006

[217] M. Blüher, "Obesity: Global epidemiology and pathogenesis," *Nature Reviews Endocrinology*, vol. 15, no. 5, pp. 288–298, May 2019, ISSN: 1759-5037. DOI: 10.1038/s41574-019-0176-8

[218] V. P. Leifer, J. N. Katz, and E. Losina, "The burden of oa-health services and economics," *Osteoarthritis and Cartilage*, vol. 30, no. 1, pp. 10–16, Jan. 1, 2022, ISSN: 1063-4584. DOI: 10.1016/j.joca.2021.05.007

[219] E. W. Orlowsky and V. B. Kraus, "The role of innate immunity in osteoarthritis: When our first line of defense goes on the offensive," *The Journal of Rheumatology*, vol. 42, no. 3, pp. 363–371, Mar. 1, 2015, ISSN: 0315-162X, 1499-2752. DOI: 10.3899/jrheum.140382 PMID: 25593231.

[220] T. A. Nees et al., "Synovial cytokines significantly correlate with osteoarthritis-related knee pain and disability: Inflammatory mediators of potential clinical relevance," *Journal of Clinical Medicine*, vol. 8, no. 9, p. 1343, Aug. 29, 2019, ISSN: 2077-0383. DOI: 10.3390/jcm8091343 PMID: 31470613.

[221] T. M. Griffin, J. L. Huebner, V. B. Kraus, Z. Yan, and F. Guilak, "Induction of osteoarthritis and metabolic inflammation by a very high-fat diet in mice: Effects of short-term exercise," *Arthritis & Rheumatism*, vol. 64, no. 2, pp. 443–453, 2012, ISSN: 1529-0131. DOI: 10.1002/art.33332

[222] T. M. Griffin, A. Batushansky, J. Hudson, and E. B. P. Lopes, "Correlation network analysis shows divergent effects of a long-term, high-fat diet and exercise on early stage osteoarthritis phenotypes in mice," *Journal of Sport and Health Science*, vol. 9, no. 2, pp. 119–131, Mar. 1, 2020, ISSN: 2095-2546. DOI: 10.1016/j.jshs.2019.05.008

[223] S. P. Messier et al., "Exercise and dietary weight loss in overweight and obese older adults with knee osteoarthritis: The arthritis, diet, and activity promotion trial," *Arthritis & Rheumatism*, vol. 50, no. 5, pp. 1501–1510, 2004, ISSN: 1529-0131. DOI: 10.1002/art.20256

[224] J. Sakamoto et al., "Regular walking exercise prior to knee osteoarthritis reduces joint pain in an animal model," *PLOS ONE*, vol. 18, no. 8, T. Grubi Kezele, Ed., e0289765, Aug. 10, 2023, ISSN: 1932-6203. DOI: 10.1371/journal.pone.0289765

[225] A. K. Hahn, A. Batushansky, R. A. Rawle, E. B. P. Lopes, R. K. June, and T. M. Griffin, "Effects of long-term exercise and a high-fat diet on synovial fluid metabolomics and joint structural phenotypes in mice: An integrated network analysis," *Osteoarthritis and Cartilage*, vol. 29, no. 11, pp. 1549–1563, Nov. 1, 2021, ISSN: 1063-4584, 1522-9653. DOI: 10.1016/j.joca.2021.08.008 PMID: 34461226.

[226] Y.-L. Hsieh and C.-C. Yang, "Early intervention of swimming exercises attenuate articular cartilage destruction in a rat model of anterior cruciate ligament and meniscus knee injuries," *Life Sciences*, vol. 212, pp. 267–274, Nov. 1, 2018, ISSN: 0024-3205. DOI: 10.1016/j.lfs.2018.10.013

[227] P. Castrogiovanni et al., "Moderate physical activity as a prevention method for knee osteoarthritis and the role of synoviocytes as biological key," *International Journal of Molecular Sciences*, vol. 20, no. 3, p. 511, 3 Jan. 2019, ISSN: 1422-0067. DOI: 10.3390/ijms20030511

[228] C. Huesa et al., "Moderate exercise protects against joint disease in a murine model of osteoarthritis," *Frontiers in Physiology*, vol. 13, Dec. 5, 2022, ISSN: 1664-042X. DOI: 10.3389/fphys.2022.1065278

[229] J. Runhaar et al., "Inflammatory cytokines mediate the effects of diet and exercise on pain and function in knee osteoarthritis independent of bmi," *Osteoarthritis and Cartilage*, vol. 27, no. 8, pp. 1118–1123, Aug. 1, 2019, ISSN: 1063-4584. DOI: 10.1016/j.joca.2019.04.009

[230] H. Kong, X.-Q. Wang, and X.-A. Zhang, "Exercise for osteoarthritis: A literature review of pathology and mechanism," *Frontiers in Aging Neuroscience*, vol. 14, May 3, 2022, ISSN: 1663-4365. DOI: 10.3389/fnagi.2022.854026

[231] C. Drenowatz, G. A. Hand, M. Sagner, R. P. Shook, S. Burgess, and S. N. Blair, "The prospective association between different types of exercise and body composition," *Medicine & Science in Sports & Exercise*, vol. 47, no. 12, pp. 2535–2541, Dec. 2015, ISSN: 0195-9131. DOI: 10.1249/MSS.0000000000000701

[232] A. Saeidi et al., "The effects of physical activity on adipokines in individuals with overweight/obesity across the lifespan: A narrative review," *Obesity Reviews*, vol. 22, no. 1, e13090, Jan. 2021, ISSN: 1467-7881, 1467-789X. DOI: 10.1111/obr.13090

[233] E. M. Roos and N. K. Arden, "Strategies for the prevention of knee osteoarthritis," *Nature Reviews Rheumatology*, vol. 12, no. 2, pp. 92–101, Feb. 2016, ISSN: 1759-4804. DOI: 10.1038/nrrheum.2015.135

[234] D. R. Barrow et al., "Exercise prescription for weight management in obese adults at risk for osteoarthritis: Synthesis from a systematic review," *BMC Musculoskeletal Disorders*, vol. 20, no. 1, p. 610, Dec. 20, 2019, ISSN: 1471-2474. DOI: 10.1186/s12891-019-3004-3

[235] S. T. Skou, B. K. Pedersen, J. H. Abbott, B. Patterson, and C. Barton, "Physical activity and exercise therapy benefit more than just symptoms and impairments in people with hip and knee osteoarthritis," *Journal of Orthopaedic & Sports Physical Therapy*, vol. 48, no. 6, pp. 439–447, Jun. 2018, ISSN: 0190-6011. DOI: 10.2519/jospt.2018.7877

[236] K. F. Huffman, K. R. Ambrose, A. E. Nelson, K. D. Allen, Y. M. Golightly, and L. F. Callahan, "The critical role of physical activity and weight management in knee and hip osteoarthritis: A narrative review," *The Journal of Rheumatology*, vol. 51, no. 3, pp. 224–233, Mar. 1, 2024, ISSN: 0315-162X, 1499-2752. DOI: 10.3899/jrheum.2023-0819 PMID: 38101914.

[237] J. Lai and D. Lacroix, "Mathematical modelling of inflammatory process and obesity in osteoarthritis," *PLOS ONE*, vol. 20, no. 6, e0323258, Jun. 2, 2025, ISSN: 1932-6203. DOI: 10.1371/journal.pone.0323258

[238] S. Klein, S. W. Coppack, V. Mohamed-Ali, and M. Landt, "Adipose tissue leptin production and plasma leptin kinetics in humans," *Diabetes*, vol. 45, no. 7, pp. 984–987, Jul. 1, 1996, ISSN: 0012-1797. DOI: 10.2337/diab.45.7.984

[239] G. A. Homandberg, C. Wen, and F. Hui, "Cartilage damaging activities of fibronectin fragments derived from cartilage and synovial fluid," *Osteoarthritis and Cartilage*, vol. 6, no. 4, pp. 231–244, Jul. 1998, ISSN: 10634584. DOI: 10.1053/joca.1998.0116

[240] S. Marino, I. B. Hogue, C. J. Ray, and D. E. Kirschner, "A methodology for performing global uncertainty and sensitivity analysis in systems biology," *Journal of Theoretical Biology*, vol. 254, no. 1, pp. 178–196, Sep. 2008, ISSN: 00225193. DOI: 10.1016/j.jtbi.2008.04.011

[241] G. D. Miller, B. J. Nicklas, and R. F. Loeser, "Inflammatory biomarkers and physical function in older, obese adults with knee pain and self-reported osteoarthritis after intensive weight-loss therapy," *Journal of the American Geriatrics Society*, vol. 56, no. 4, pp. 644–651, 2008, ISSN: 1532-5415. DOI: 10.1111/j.1532-5415.2007.01636.x

[242] S. Vasilic-Brasnjevic et al., "Association of body mass index and waist circumference with severity of knee osteoarthritis," *Acta reumatologica portuguesa*, vol. 2016, pp. 226–231, Mar. 23, 2016.

[243] J. Runhaar, M. Kloppenburg, M. Boers, J. W. J. Bijlsma, S. M. A. Bierma-Zeinstra, and and the CREDO expert group, "Towards developing diagnostic criteria for early knee osteoarthritis: Data from the check study," *Rheumatology*, vol. 60, no. 5, pp. 2448–2455, May 1, 2021, ISSN: 1462-0324. DOI: 10.1093/rheumatology/keaa643

[244] Q. Wang, J. Runhaar, M. Kloppenburg, M. Boers, J. W. J. Bijlsma, and S. M. A. Bierma-Zeinstra, "Diagnosis for early stage knee osteoarthritis: Probability stratification, internal and external validation; data from the check and oai cohorts," *Seminars in Arthritis and Rheumatism*, vol. 55, p. 152 007, Aug. 1, 2022, ISSN: 0049-0172. DOI: 10.1016/j.semarthrit.2022.152007

[245] X. Li, F. W. Roemer, F. Cicuttini, J. W. MacKay, T. Turmezei, and T. M. Link, "Early knee oa definition-what do we know at this stage? an imaging perspective," *Therapeutic Advances in Musculoskeletal Disease*, vol. 15, p. 1759720X231158204, Jan. 1, 2023, ISSN: 1759-720X. DOI: 10.1177/1759720X231158204

[246] S. M. Brooke, H.-S. An, S.-K. Kang, J. M. Noble, K. E. Berg, and J.-M. Lee, "Concurrent validity of wearable activity trackers under free-living conditions," *The Journal of Strength & Conditioning Research*, vol. 31, no. 4, p. 1097, Apr. 2017, ISSN: 1064-8011. DOI: 10.1519/JSC.0000000000001571

[247] R. L. Bailey, "Overview of dietary assessment methods for measuring intakes of foods, beverages, and dietary supplements in research studies," *Current Opinion in Biotechnology*, vol. 70, pp. 91–96, Aug. 1, 2021, ISSN: 0958-1669. DOI: 10.1016/j.copbio.2021.02.007

[248] S. Zheng et al., "The cross-sectional and longitudinal associations of dietary patterns with knee symptoms and mri detected structure in patients with knee osteoarthritis," *Osteoarthritis and Cartilage*, vol. 29, no. 4, pp. 527–535, Apr. 1, 2021, ISSN: 1063-4584. DOI: 10.1016/j.joca.2020.12.023

[249] R. J. Cooper et al., *Three subject-specific human tibiofemoral joint finite element models: Complete three-dimensional imaging (ct & mr), experimental validation and modelling dataset.* University of Leeds, 2023. DOI: 10.5518/981

[250] A. T. Collins et al., "Obesity alters the in vivo mechanical response and biochemical properties of cartilage as measured by mri," *Arthritis Research & Therapy*, vol. 20, no. 1, p. 232, Oct. 17, 2018, ISSN: 1478-6362. DOI: 10.1186/s13075-018-1727-4

[251] G. B. Joseph et al., "Weight cycling and knee joint degeneration in individuals with overweight or obesity: Four-year magnetic resonance imaging data from the osteoarthritis initiative," *Obesity*, vol. 29, no. 5, pp. 909–918, 2021, ISSN: 1930-739X. DOI: 10.1002/oby.23129

[252] H. B. Sun, "Mechanical loading, cartilage degradation, and arthritis," *Annals of the New York Academy of Sciences*, vol. 1211, no. 1, pp. 37–50, Nov. 2010, ISSN: 0077-8923, 1749-6632. DOI: 10.1111/j.1749-6632.2010.05808.x

[253] P. E. Riemenschneider, M. D. Rose, M. Giordani, and S. M. McNary, "Compressive fatigue and endurance of juvenile bovine articular cartilage explants," *Journal of Biomechanics*, vol. 95, p. 109 304, Oct. 11, 2019, ISSN: 0021-9290. DOI: 10.1016/j.jbiomech.2019.07.048

[254] K. J. Vazquez, J. T. Andreae, and C. R. Henak, "Cartilage-on-cartilage cyclic loading induces mechanical and structural damage," *Journal of the Mechanical Behavior of Biomedical Materials*, vol. 98, pp. 262–267, Oct. 1, 2019, ISSN: 1751-6161. DOI: 10.1016/j.jmbbm.2019.06.023

[255] R. Case, E. Thomas, E. Clarke, and G. Peat, "Prodromal symptoms in knee osteoarthritis: A nested case–control study using data from the osteoarthritis initiative," *Osteoarthritis and Cartilage*, vol. 23, no. 7, pp. 1083–1089, Jul. 1, 2015, ISSN: 1063-4584, 1522-9653. DOI: 10.1016/j.joca.2014.12.026 PMID: 25843364.

[256] A. Eitner, G. O. Hofmann, and H.-G. Schaible, "Mechanisms of osteoarthritic pain. studies in humans and experimental models," *Frontiers in Molecular Neuroscience*, vol. 10, Nov. 3, 2017, ISSN: 1662-5099. DOI: 10.3389/fnmol.2017.00349

[257] M. D. Kohn, A. A. Sassoon, and N. D. Fernando, "Classifications in brief: Kellgren-lawrence classification of osteoarthritis," *Clinical Orthopaedics and Related Research®*, vol. 474, no. 8, pp. 1886–1893, Aug. 1, 2016, ISSN: 1528-1132. DOI: 10.1007/s11999-016-4732-4

[258] R. D. Altman and G. E. Gold, "Atlas of individual radiographic features in osteoarthritis, revised," *Osteoarthritis and Cartilage*, Radiographic Atlas for Osteoarthritis of the Hand, Hip and Knee, vol. 15, A1–A56, Jan. 1, 2007, ISSN: 1063-4584. DOI: 10.1016/j.joca.2006.11.009

[259] F. W. Roemer, A. Guermazi, S. Demehri, W. Wirth, and R. Kijowski, "Imaging in osteoarthritis," *Osteoarthritis and Cartilage*, vol. 30, no. 7, pp. 913–934, Jul. 1, 2022, ISSN: 1063-4584, 1522-9653. DOI: 10.1016/j.joca.2021.04.018 PMID: 34560261.

[260] J. Sanchez-Adams, H. A. Leddy, A. L. McNulty, C. J. O'Conor, and F. Guilak, "The mechanobiology of articular cartilage: Bearing the burden of osteoarthritis," *Current Rheumatology Reports*, vol. 16, no. 10, p. 451, Sep. 3, 2014, ISSN: 1534-6307. DOI: 10.1007/s11926-014-0451-6

[261] H. M. Ismail, K. Yamamoto, T. L. Vincent, H. Nagase, L. Troeberg, and J. Saklatvala, "Interleukin-1 acts via the jnk-2 signaling pathway to induce aggrecan degradation by human chondrocytes," *Arthritis & Rheumatology*, vol. 67, no. 7, pp. 1826–1836, 2015, ISSN: 2326-5205. DOI: 10.1002/art.39099

[262] Q. T. Nguyen, T. D. Jacobsen, and N. Chahine, "Effects of inflammation on multiscale biomechanical properties of cartilaginous cells and tissues," *ACS Biomaterials Science & Engineering*, vol. 3, no. 11, pp. 2644–2656, Nov. 13, 2017, ISSN: 2373-9878, 2373-9878. DOI: 10.1021/acsbiomaterials.6b00671

[263] H. M. Ismail, A. Didangelos, T. L. Vincent, and J. Saklatvala, "Rapid activation of transforming growth factor β–activated kinase 1 in chondrocytes by phosphorylation and k63-linked polyubiquitination upon injury to animal articular cartilage," *Arthritis & Rheumatology*, vol. 69, no. 3, pp. 565–575, 2017, ISSN: 2326-5205. DOI: 10.1002/art.39965

[264] M. Nickien, A. Thambyah, and N. D. Broom, "How a decreased fibrillar interconnectivity influences stiffness and swelling properties during early cartilage degeneration," *Journal of the Mechanical Behavior of Biomedical Materials*, vol. 75, pp. 390–398, Nov. 1, 2017, ISSN: 1751-6161. DOI: 10.1016/j.jmbbm.2017.07.042

[265] Z. Peng et al., "The regulation of cartilage extracellular matrix homeostasis in joint cartilage degeneration and regeneration," *Biomaterials*, vol. 268, p. 120 555, Jan. 1, 2021, ISSN: 0142-9612. DOI: 10.1016/j.biomaterials.2020.120555

[266] J. Song, X. Zeng, C. Li, H. Yin, S. Mao, and D. Ren, "Alteration in cartilage matrix stiffness as an indicator and modulator of osteoarthritis," *Bioscience Reports*, vol. 44, no. 1, BSR20231730, Jan. 12, 2024, ISSN: 0144-8463. DOI: 10.1042/BSR20231730

[267] B. B. Seedhom, "Conditioning of cartilage during normal activities is an important factor in the development of osteoarthritis," *Rheumatology*, vol. 45, no. 2, pp. 146–149, Feb. 1, 2006, ISSN: 1462-0324. DOI: 10.1093/rheumatology/kei197

[268] T. L. Vincent and A. K. T. Wann, "Mechanoadaptation: Articular cartilage through thick and thin," *The Journal of Physiology*, vol. 597, no. 5, pp. 1271–1281, 2019, ISSN: 1469-7793. DOI: 10.1113/JP275451

[269] L. Chen et al., "Horizontal fissuring at the osteochondral interface: A novel and unique pathological feature in patients with obesity-related osteoarthritis," *Annals of the Rheumatic Diseases*, vol. 79, no. 6, pp. 811–818, Jun. 1, 2020, ISSN: 0003-4967. DOI: 10.1136/annrheumdis-2020-216942

[270] N. Reina et al., "Bmi-related microstructural changes in the tibial subchondral trabecular bone of patients with knee osteoarthritis," *Journal of Orthopaedic Research*, vol. 35, no. 8, pp. 1653–1660, 2017, ISSN: 1554-527X. DOI: 10.1002/jor.23459

[271] W. Wilson, C. C. van Donkelaar, B. van Rietbergen, K. Ito, and R. Huiskes, "Stresses in the local collagen network of articular cartilage: A poroviscoelastic fibril-reinforced finite element study," *Journal of Biomechanics*, vol. 37, no. 3, pp. 357–366, Mar. 1, 2004, ISSN: 0021-9290. DOI: 10.1016/S0021-9290(03)00267-7

[272] J. Sun et al., "Finite element analysis of the valgus knee joint of an obese child," *BioMedical Engineering OnLine*, vol. 15, no. 2, p. 158, Dec. 28, 2016, ISSN: 1475-925X. DOI: 10.1186/s12938-016-0253-3

[273] M. Imeni, B. Seyfi, N. Fatouraee, and A. Samani, "Constitutive modeling of menisci tissue: A critical review of analytical and numerical approaches," *Biomechanics and Modeling in Mechanobiology*, vol. 19, no. 6, pp. 1979–1996, Dec. 2020, ISSN: 1617-7959, 1617-7940. DOI: 10.1007/s10237-020-01352-1

[274] H. Orava et al., "Changes in subchondral bone structure and mechanical properties do not substantially affect cartilage mechanical responses – a finite element study," *Journal of the Mechanical Behavior of Biomedical Materials*, vol. 128, p. 105 129, Apr. 1, 2022, ISSN: 1751-6161. DOI: 10.1016/j.jmbbm.2022.105129

[275] J. Yao et al., "Effect of meniscus modelling assumptions in a static tibiofemoral finite element model: Importance of geometry over material," *Biomechanics and Modeling in Mechanobiology*, vol. 23, no. 3, pp. 1055–1065, Jun. 2024, ISSN: 1617-7959, 1617-7940. DOI: 10.1007/s10237-024-01822-w

[276] Y. J. Hu et al., "Mechanical and structural properties of articular cartilage and subchondral bone in human osteoarthritic knees," *Journal of Bone and Mineral Research*, vol. 39, no. 8, pp. 1120–1131, Aug. 1, 2024, ISSN: 0884-0431. DOI: 10.1093/jbmr/zjae094

[277] R. J. Cooper et al., "The role of high-resolution cartilage thickness distribution for contact mechanics predictions in the tibiofemoral joint," *Proceedings of the Institution of Mechanical Engineers, Part H: Journal of Engineering in Medicine*, vol. 239, no. 1, pp. 18–28, Jan. 1, 2025, ISSN: 0954-4119. DOI: 10.1177/09544119241307793

[278] M. E. Stender, R. D. Carpenter, R. A. Regueiro, and V. L. Ferguson, "An evolutionary model of osteoarthritis including articular cartilage damage, and bone remodeling in a computational study," *Journal of Biomechanics*, vol. 49, no. 14, pp. 3502–3508, Oct. 2016, ISSN: 00219290. DOI: 10.1016/j.jbiomech.2016.09.024

[279] M. E. Mononen, M. K. Liukkonen, and R. K. Korhonen, "Utilizing atlas-based modeling to predict knee joint cartilage degeneration: Data from the osteoarthritis initiative," *Annals of Biomedical Engineering*, vol. 47, no. 3, pp. 813–825, Mar. 2019, ISSN: 0090-6964, 1573-9686. DOI: 10.1007/s10439-018-02184-y

[280] M. E. Stender, R. A. Regueiro, and V. L. Ferguson, "A poroelastic finite element model of the bone–cartilage unit to determine the effects of changes in permeability with osteoarthritis," *Computer Methods in Biomechanics and Biomedical Engineering*, vol. 20, no. 3, pp. 319–331, Feb. 17, 2017, ISSN: 1025-5842, 1476-8259. DOI: 10.1080/10255842.2016.1233326

[281] D. Yue et al., "Time-dependently appeared microenvironmental changes and mechanism after cartilage or joint damage and the influences on cartilage regeneration," *Organogenesis*, vol. 17, no. 3–4, pp. 85–99, Oct. 2, 2021, ISSN: 1547-6278. DOI: 10.1080/15476278.2021.1991199 PMID: 34806543.

[282] D. M. Findlay and J. S. Kuliwaba, "Bone–cartilage crosstalk: A conversation for understanding osteoarthritis," *Bone Research*, vol. 4, no. 1, p. 16 028, Dec. 2016, ISSN: 2095-6231. DOI: 10.1038/boneres.2016.28

[283] S. Lee, T.-N. Kim, and S.-H. Kim, "Sarcopenic obesity is more closely associated with knee osteoarthritis than is nonsarcopenic obesity: A cross-sectional study," *Arthritis & Rheumatism*, vol. 64, no. 12, pp. 3947–3954, 2012, ISSN: 1529-0131. DOI: 10.1002/art.37696

[284] A. S. A. Eskelinen et al., "Time-dependent computational model of post-traumatic osteoarthritis to estimate how mechanoinflammatory mechanisms impact cartilage aggrecan content," *PLOS Computational Biology*, vol. 21, no. 10, e1013641, Oct. 31, 2025, ISSN: 1553-7358. DOI: 10.1371/journal.pcbi.1013641

[285] W. Wilson, C. van Burken, C. van Donkelaar, P. Buma, B. van Rietbergen, and R. Huiskes, "Causes of mechanically induced collagen damage in articular cartilage," *Journal of Orthopaedic Research*, vol. 24, no. 2, pp. 220–228, 2006, ISSN: 1554-527X. DOI: 10.1002/jor.20027

[286] S. Saarakkala, P. Julkunen, P. Kiviranta, J. Mäkitalo, J. S. Jurvelin, and R. K. Korhonen, "Depth-wise progression of osteoarthritis in human articular cartilage: Investigation of composition, structure and biomechanics," *Osteoarthritis and Cartilage*, vol. 18, no. 1, pp. 73–81, Jan. 1, 2010, ISSN: 1063-4584. DOI: 10.1016/j.joca.2009.08.003

[287] F. Eckstein, A. E. Wluka, W. Wirth, and F. Cicuttini, "30 years of mri-based cartilage & bone morphometry in knee osteoarthritis: From correlation to clinical trials," *Osteoarthritis and Cartilage*, vol. 32, no. 4, pp. 439–451, Apr. 1, 2024, ISSN: 1063-4584, 1522-9653. DOI: 10.1016/j.joca.2024.02.002 PMID: 38331162.

[288] F. Cicuttini, C. Ding, A. Wluka, S. Davis, P. R. Ebeling, and G. Jones, "Association of cartilage defects with loss of knee cartilage in healthy, middle-age adults: A prospective study," *Arthritis & Rheumatism*, vol. 52, no. 7, pp. 2033–2039, 2005, ISSN: 1529-0131. DOI: 10.1002/art.21148

[289] S. S. J. Pragasam and V. Venkatesan, "Metabolic syndrome predisposes to osteoarthritis: Lessons from model system," *CARTILAGE*, vol. 13, 1598S–1609S, 1_suppl Dec. 2021, ISSN: 1947-6035, 1947-6043. DOI: 10.1177/1947603520980161

[290] M. J. Wood, R. E. Miller, and A.-M. Malfait, "The genesis of pain in osteoarthritis: Inflammation as a mediator of osteoarthritis pain," *Clinics in geriatric medicine*, vol. 38, no. 2, pp. 221–238, May 2022, ISSN: 0749-0690. DOI: 10.1016/j.cger.2021.11.013 PMID: 35410677.

[291] P. Kaukinen et al., “Associations between mri-defined structural pathology and generalized and localized knee pain – the oulu knee osteoarthritis study,” *Osteoarthritis and Cartilage*, vol. 24, no. 9, pp. 1565–1576, Sep. 1, 2016, ISSN: 1063-4584, 1522-9653. DOI: 10.1016/j.joca.2016.05.001 PMID: 27174007.